

Dag Anders Moldestad

Some Aspects of Ski Base Sliding Friction and Ski Base Structure

Dr.ing. thesis

Department of Structural Engineering
Norwegian University of Science and Technology
N-7491 Trondheim
Norway

December 1999

Abstract

The present work highlights some aspects of ski base sliding friction and ski base structure. Ski base structure causes speed differences that range from negligible to almost 10 % of the skier speed. The great speed difference under some snow conditions makes the choice of the best structure an important issue for competition skiers and an interesting aspect to understand the physical processes that control friction against snow.

The thesis discusses and explains ski base sliding friction by use of tribology, impact and compaction resistances, electrical charging and electrostatic pressures. The optimum ski base structure roughness varies under different snow conditions according to the generated frictional water film thickness under the ski and the roughness of the snow surface. Thick water films correspond to coarse ski base structures, while it is advantageous to use finer ski base structures and increase the water film thickness when the water film is thin. The possible increase of water film thickness along the ski implies an increase of the ski base structure roughness along the ski. Impact and compaction resistances are important when the snow hardness is below a certain limit, and when the water film thickness is low relative to the roughness of the ski base structure and the snow surface. The dry friction process is dominated and characterised electrically by accumulation of electrostatic charge in the ski base contact points. The frictional water film initiates discharge of potential differences between ski and snow due to the much higher electrical conductivity of water relative to snow. When the air gap volumes between the water film and the ski base structure, and the water film and the snow surface get small, the electrostatic pressures in the air gaps increase, and suction or drag may start occurring. The wet friction process is characterised electrically by electrolytic behaviour. Further research is necessary in order to increase the knowledge and understanding of the simultaneous processes of mass, impulse, energy, electrical and chemical balances between the two interacting surfaces in relative motion during friction.

A Ski base Structure Analyser (SSA) utilising laser technology has been developed to analyse the detailed structure of a stone-ground ski base. The SSA displays the measured surface as an image with 739×570 pixels, where each pixel can have a grey level value from 0 to 255. The value of each pixel is proportional to the height at the corresponding point of the measured surface. In the period between 1995 and 1998 almost 1700 ski base structure measurements were performed on more than 350 skis. It was found that ski pairs ground with the "same" structure at two different times are not necessarily equal if no quality control of the ski base structure and the stone grinding process has been performed. On several competition ski pairs higher structure roughness (up to 84 %) was revealed on the forebody than the afterbody of the ski. The work has resulted in development of ski base structures with increased roughness along the ski, development and extreme optimisation of the best structures, and improvement of the grinding diamonds used to set the grinding stone. Further, it has given ski technicians and competition skiers confidence in that optimum structures and skis are used in competitions under different snow and weather conditions, and that the best structures can be reproduced. The ski base structure roughness can be divided into four categories: fine (arithmetic mean roughness 1-4 μm), medium (arithmetic mean roughness 4-7 μm), coarse (arithmetic mean roughness 7-10 μm) and very coarse (arithmetic mean roughness higher than 10 μm) that correspond to dry to moist, moist, moist to wet, and wet to very wet snow conditions, respectively.

A structure test series consisting of ten ski pairs with eight different structures has been ground and quality-controlled. Accurate sliding tests showed that ski pairs with arithmetic mean structure roughness $\leq 5.4 \mu\text{m}$ were best under snow conditions with snow humidity $\leq 0.6 \%$, snow temperatures below zero and new snow. A ski pair with arithmetic mean structure roughness equal to $9.3 \mu\text{m}$ was best under snow conditions with snow humidity between approximately 0.3 and 4.0 %, snow hardness higher than $4.1 \times 10^4 \text{ Pa}$ and transformed snow types. Under snow conditions with snow humidity higher than approximately 4 %, a structure with arithmetic mean roughness $12.7 \mu\text{m}$ was best. Coarser structures were relatively better than finer structures at high speeds compared to low speeds, thus implying an increase in the water film thickness and optimum structure roughness with speed. A decrease of the structure roughness along the ski was unfortunate under most snow conditions.

Various snow parameters have been registered during measurement campaigns in ski tracks in Norway (1995-98), Hakuba/Japan (1996-98) and Sundance/USA (1999). Specific attention has been paid to snow hardness, snow humidity, snow density, snow grain structure and electrolytic conductivity. Snow hardness between 10^4 and 10^6 Pa is most common in ski tracks, and snow hardness below 10^5 Pa is likely to be present 60 % of the time. The mean density of snow in ski tracks (0.50 g/cm^3) is considerably higher than typical densities of seasonal snow covers ($0.26\text{-}0.38 \text{ g/cm}^3$) and higher for transformed snow types ($0.51\text{-}0.59 \text{ g/cm}^3$) than new snow types ($0.39\text{-}0.43 \text{ g/cm}^3$). The snow humidity in a ski track typically ranges between 0 and 12.5 %. It is typically less than 2 % for snow temperatures below -2°C and less than 1 % for snow temperatures below -7°C . Snow humidities exceeding 4 % have only been registered at air temperatures above $+1^\circ\text{C}$. High electrolytic conductivities ($61.7 \mu\text{S/cm}$ and $94.5 \mu\text{S/cm}$, respectively) and high levels of Na^+ - and Cl^- -ions have been registered in melted snow samples from Trondheim and Sundance/Heber due to salt being a major agent during snow nucleation in the snowfalls. These values are approximately 3 times higher than the maximum values found for snow samples from Hakuba ($21.9 \mu\text{S/cm}$). The electrolytic conductivity of a melted snow sample may indicate the rate of ions introduced to the interface between snow and ski by frictional melting and thereby the rate and ease of discharge between ski and snow through the frictional water film during skiing.

Acknowledgements

I would like to express my gratitude to main supervisor Professor S. Løset, Department of Structural Engineering, for valuable advice, continuous encouragement and active participation throughout my study. The collaboration during these years has been a pleasure. The support of supervisor Professor O. Egeland, Department of Cybernetics, is also sincerely appreciated.

This work was made possible by financial support from the Norwegian Olympic Committee and Confederation of Sports (Olympiatoppen), Madshus A/S and The Research Council of Norway (VARP). Madshus A/S has also supported the project with test skis, and given me access to register mechanical ski parameters with the *Madshus Compuflex System*. Special thanks are given to Racing Manager T. Fardal for continuous support and commitment, co-operation during grinding of test structures and participation in sliding tests, and Technical Manager G. Bjertnæs for useful assistance during surveys of ski material parameters and ski literature. Olympiatoppen has given financial support to perform sliding tests and snow and weather measurements in different parts of the world, e.g. Japan and the USA. My appreciation goes to Director of Research A. Lier for always having confidence and belief in our ideas and research. I would also like to extend my appreciation to participators in the Olympiatoppen collaboration project "Gliprosjektet" in the period between 1996 and 1999: G. Tufto, K. Skjelbreid, E. K. Mikkelsplass, J. E. Bjørn, V. Granheim, P. K. Aaland, O. Stuveseth, R. Helgesen, T. Langli, J. E. Berger, I. M. Ulekleiv, M. Dalen, M. Myrmo, T. O. Seim, F. M. Hagen, E. Bråthen and Å. Skinstad. Their contribution through co-operation in measurement campaigns and sliding tests, open-minded fruitful discussions on ski base sliding friction and ski base structure, and stepwise development of the best ski base structures the world has seen, can not be overrated.

Acknowledgements are also given to T. Oxaas (Department of Production and Quality Engineering) for assistance during profilometer measurements of ski base structures, and T. Kolås, J. K. Hansen, Dr. E. Vikhagen and Dr. S. Winther (SINTEF Applied Physics) for co-operation during the development of the SSA measurement technology. Further, thanks are given to Salomon for supporting us with ski bindings and SWIX for supporting us with glide wax. I. Dahl, H. Holden, J. A. Skjetne, O. J. Sande, A. Løset, L. O. Valøen and G. Kjestveit deserve credit for assistance with ski preparation, sliding tests and ski base structure measurements, and Dr. K. Sand and A. Harby (SINTEF Water Resources) for good advice on snow measurement technology. Moreover, credits are given to Professor Å. Killingtveit and B. J. Kirksæther (Department of Hydraulic and Environmental Engineering) for giving me access to their meteorological data from Granåsen and Trondheim, and Hego Timing System A/S for releasing time measurements from the Nordic World Championships'97.

Finally, I gratefully thank my family and friends for their support, encouragement and patience.

Table of contents

Abstract	i
Acknowledgements	iii
Table of contents	v
1. Introduction	1
1.1. General remarks	1
1.2. Objectives, scope and organisation of the thesis	2
1.3. Readership	3
2. Basics of ski base sliding friction	5
Notation	5
2.1. Friction against a moving skier	7
2.1.1. Air resistance	7
2.1.2. Ski base sliding friction	9
2.1.3. Air resistance and ski base sliding friction estimated as a function of speed	11
2.2. How does ski base sliding friction work?	13
2.2.1. Tribology and ski base sliding friction	15
2.2.2. The lubricant (water film)	16
2.2.3. The sliding surface (snow)	19
2.2.4. The slider (ski base)	20
2.2.5. Ski base sliding friction theory	27
2.3. References	36
3. The ski base structure analyser - SSA	41
Notation	41
3.1. Introduction	43
3.2. Basic theory of the SSA instrumentation and measurement technology	45
3.3. Basic theory of the SSA characterisation of ski base structure topography	50
3.4. An SSA example	57
3.5. References	59

4. Ski base structure measurements	61
Notation	61
4.1. Introduction	62
4.2. Measurement methods and procedures	62
4.3. Results	63
4.3.1. Structure types	63
4.3.2. Finer structure along the ski	67
4.3.3. Rilling	70
4.3.4. Plane grinding	75
4.3.5. Test skis	77
4.3.6. Competition skis	78
4.4. Discussion	85
4.5. Conclusions	86
4.6. References	87
5. Characterisation of snow structure in a cross-country race ski track	89
Notation	89
5.1. Introduction	90
5.2. Measurement methods and procedures	95
5.2.1. Snow temperature	95
5.2.2. Snow hardness	95
5.2.3. Snow humidity and snow density	98
5.2.4. Snow type and snow grain structure	100
5.2.5. Electrolytic conductivity	102
5.2.6. Air temperature	102
5.2.7. Relative humidity	103
5.2.8. Net radiation and cloudiness	103
5.3. Results	104
5.3.1. Snow hardness	104
5.3.2. Snow humidity and snow density	111
5.3.3. Snow type and snow grain structure	115
5.3.4. Electrolytic conductivity	127
5.4. Discussion	133
5.4.1. Snow hardness	133
5.4.2. Snow humidity and snow density	134
5.4.3. Snow type and snow grain structure	135
5.4.4. Electrolytic conductivity	135
5.5. Conclusions	140

5.6. References	142
6. Searching for the optimum cross-country ski base structure	151
Notation	151
6.1. Introduction	152
6.2. Hypotheses of low ski base sliding friction and ski base structures	153
6.3. Experimental setup	154
6.4. Results	156
6.5. Discussion	166
6.6. Conclusions and recommendations	169
6.6.1. Conclusions	169
6.6.2. Recommendations	170
7. The effect of electrical charging and electrostatic pressure on ski base sliding friction	171
Notation	171
7.1. Introduction	173
7.2. The effect of electrical charging and electrostatic pressure on ski base sliding friction	173
7.3. Summary and recommendations	187
7.3.1. Interpretation of friction	187
7.3.2. Minimisation of ski base sliding friction	189
7.3.3. Epilogue	190
7.4. References	190
8. Summary, conclusions and recommendations for further work	193
8.1. Summary and conclusions	193
8.2. Recommendations for further work	197

1. Introduction

1.1 *General remarks*

The low friction coefficient of ski base sliding friction is primarily caused by the development of a tiny water film between ski base and snow due to frictional heating. The development of this water film is regarded as favourable for below zero snow temperatures i.e. snow with low initial liquid content. Under wet snow conditions the water film may cause suction or viscous drag and thereby increase the friction coefficient. The ski base sliding friction and water film development depends on the speed and weight of the skier, and ski and snow parameters.

The most important ski parameters are the tension or pressure distribution, structure, base material quality and wax. Given otherwise equal skis, i.e. skis with the same pressure distribution, base material quality and ski wax, manipulation of the structure can to some extent be used to control the ski base sliding friction. The importance of the manipulation of the structure depends on skier speed and snow conditions. Measured skier speed differences caused by structure ranges from negligible to almost 10 % of the skier speed. The great speed difference under some snow conditions makes the choice of the best structure an important issue for competition skiers and an interesting aspect to understand the physical processes that control friction against snow. The literature in the field is in addition very insufficient. The structure of the ski can be handmade, made by a stone grinding machine or made combining the two processes. Stone grinding of cross-country ski bases has been widely used since the end of the 1980s. Nowadays it is common that skis have factory finished base structures intended for different snow conditions. Skis are in addition often restructured due to structure wear or a wish of improving the original structure. Local stone grinders mostly do this.

Unfortunately the stone grinding process is not highly automated and reliable. Different inaccuracies in the process result in equal adjustment of the stone grinding machine parameters not necessarily giving the same structure from time to time. It is also difficult for the human eye to distinguish small structure quality variations that can have practical importance to the ski base sliding friction, due to the fact that structure groove depths vary from approximately 5 μm for fine structures to 100 μm for coarse structures. In order to evolve the understanding of the ski base structure sliding process against snow, it is therefore necessary to measure and characterise the structure qualitatively in a proper way.

It is also equally important to measure and characterise snow structure and weather parameters in-situ in the cross-country race track during accurate sliding tests. Human caused and nature caused snow and snow friction processes are important in several physical processes on Earth, often in combination with ice processes. Knowledge of this is important when working with matters like:

- Friction between different vehicles and snow/ice
- Avalanche prediction and forecasts
- Glacier and ice sheet advance and retreat as an indicator of climate change
- Hydrological processes and construction and control of hydroelectric plants in areas with snow accumulation and/or glaciers
- Tracking of pollution spreading
- Cold region structural engineering

It is also needed in order to increase the knowledge about these processes and improve existing snow and snow friction models to develop snow measurement technology, do in-situ snow measurements and characterisation and thereby develop snow experience databases.

1.2 Objectives, scope and organisation of the thesis

The intent of this thesis has been to evolve the understanding of factors that affect ski base sliding friction. It can also be viewed as case study of a frictional process against snow. In addressing these matters, the overall objectives of the present study were:

- To evolve the understanding of the physical processes that control ski base structure sliding against snow and develop models that expresses the relation between structure, tension or pressure distribution and sliding properties of cross-country skis.
- To develop a PC-based instrument for non-contact measurement of the ski base structure.
- To execute accurate sliding tests that can verify theory and contribute to an optimum shape of a cross-country ski in addition to making and proposing new ski base structures.

With these items in mind, the thesis consists of seven chapters in addition to the introduction chapter. The thesis is organised as follows:

Chapter 2 reviews ski base sliding friction theories and experiments and discusses how ski base sliding friction works. The chapter focuses on tribology and impact and compaction resistances.

Chapter 3 introduces the ski base structure analyser (SSA). The basic theory behind the SSA instrumentation and measurement technology is given, as well as SSA characterisation of ski base topography.

Chapter 4 presents some of the results from the ski base structure measurement experiments between 1995 and 1998. In this period almost 1700 measurements were taken of more than 350 skis. This unique collection of structure measurements included characterisation of 8 Olympic and 6 World Championship gold medal winning skis. Due to respect for the ski technicians and stone grinding experts that have been co-operating on this project and the knowledge this collaboration has given, some of the results from the measurements are given restricted access until 30 July 2002. These are not presented here.

Chapter 5 describes different measurement methods and procedures for characterisation of snow structure and weather parameters in a cross-country race ski track. Results from different measurement experiments are given and discussed.

Chapter 6 is called searching for the optimum structure. This chapter briefly presents some hypotheses for low ski base sliding friction and ski base structures, together with results from in-situ experiments of skis made with structures according to the hypotheses. An evaluation of the hypotheses in light of the structure series experiment and ski base structure measurements is also given.

Chapter 7 discusses the effect of electrical charging and electrostatic pressures on ski base sliding friction. A present interpretation of friction is suggested that combines knowledge of tribology, electrical charging and electrostatic pressures and uses ski base sliding friction as a case study. A summary of the processes that must be accounted for in order to minimise ski base sliding friction in different friction regimes is also given. Chapter 8 concludes the study and makes recommendations for further work within the realm of ski base sliding friction and ski base structure.

1.3 Readership

This study of ski base sliding friction has been highly multi-disciplinary and involved many fields of science. In order to understand the basic physics and tribology between ski and snow, different tools from applied computer science and instrumentation, image processing, interferometry, snow and ice science and basic mathematics have been used. The primary readership targeted by the thesis consists of:

- Ski and stone grinding technicians, ski engineers, ski and stone grinding manufacturers, ski federation authorities, competition and recreational skiers and others involved and interested in skiing.
- Scientists, research engineers, lecturers, students and engineers employed in companies dealing with snow friction or snow and cold regions related problems.
- Physicists and tribologists dealing with friction.

Besides scientists, research engineers, lecturers, students and others interested in such fields as interferometry, image processing and measurement, characterisation and quality control of surface topography may read chapter 3 as an example of exploiting these disciplines in applied physics.

2. Basics of ski base sliding friction

Notation

A	wind blocking area, m ²
A_d	actual dry contact area, m ²
A_n	nominal contact area between ski and snow, m ²
A_w	wet contact area, m ²
C_d	air drag coefficient
F_{air}	viscous air drag force against a body moving with relative speed v , N
F_c	compaction resistance, N
F_d	dry friction (adhesion), N
F_i	impact resistance, N
F_{sn}	ski base sliding friction, N
F_w	wet friction (viscous drag), N
g	acceleration due to gravity, 9.81 m/s ²
h	height difference between the beginning and the end of the test length, m
h_b	height of the body of the skier, m
$h_{min,wf}$	minimum water film thickness between a specific area on the ski and snow at a specific time during skiing, μm
h_{wf}	water film thickness, m
i	index

l	ski length in contact with snow surface i.e. effective ski length, m
l_1	half nominal contact length on the forebody of a ski ($l_1 = l_f/2$), m
l_2	half nominal contact length on the afterbody of a ski ($l_2 = l_a/2$), m
l_a	nominal contact length on the afterbody of the ski, m
l_f	nominal contact length on the forebody of the ski, m
m	mass of skier and skis, kg
m_b	mass of the body of the skier, kg
N	normal load from skier, N
N	number of registrations in Eqs. (2.12) - (2.14)
p_{air}	dry air pressure, Pa
$p_n(x)$	nominal pressure distribution along the ski in the x -direction, Pa
R	ideal gas constant, 8.314 J/mol·K
R_a	arithmetic mean surface roughness, μm
R_q	root mean square (rms) roughness, μm
$R_{q,\text{sbs}}$	root mean square roughness of the ski base structure surface in a specific area on the ski, μm
$R_{q,\text{sn}}$	root mean square roughness of snow surface, μm
R_t	maximum peak-to-valley height, μm
s	distance, m
S	test length in a ski test track, m
T_0	air temperature at sea level, K
T_{air}	air temperature, K
T_{sn}	snow temperature, K or $^{\circ}\text{C}$
v	speed, m/s
v_f	final speed of the skier at the end of the test length, m/s
v_i	initial speed of the skier at the beginning of the test length, m/s
w	width of the ski, m
w_a	nominal contact width on the afterbody of the ski, m
w_f	nominal contact width on the forebody of the ski, m
W_{tot}	work over the test length S , J
x	direction along the ski
y	direction across the ski
z	height above sea level, m
z_i	surface height registrations on a surface profile across the ski, where the surface heights refer to a reference line which gives a mean value of zero for z_i , μm
Δz	vertical snow compaction distance, m
α	inclination of the test length S in the ski test track, $^{\circ}$
γ_c	surface pattern parameter
η_{wf}	absolute viscosity of the water film, Pa·s
Λ	film parameter
λ_x	autocorrelation length in the x -direction, i.e. the direction along the ski, mm
λ_y	autocorrelation length in the y -direction, i.e. the direction across the ski, mm
μ	sliding friction coefficient
μ_d	dry friction coefficient
ρ_0	air density at sea level, kg/m^3
ρ_{air}	air density, kg/m^3

$\rho_{\text{sn},i}$	initial snow density before compaction under the ski, kg/m^3
σ	unconfined compression strength of snow, Pa
τ	shear strength of the softest material in the interfacial contact between snow and ski (i.e. snow or glide wax or powder), Pa
$\Phi(x)$	total nominal pressure distribution function for a ski
$\Phi_1(x)$	total nominal pressure distribution function for the forebody of a ski
$\Phi_2(x)$	total nominal pressure distribution function for the afterbody of a ski

2.1. Friction against a moving skier

The friction against a moving skier consists of two parts:

- Air resistance
- Ski base sliding friction

Air resistance and ski base sliding friction are briefly introduced in the following section. The next section fully concentrates on ski base sliding friction.

2.1.1. Air resistance

The viscous air drag force, F_{air} , against a body moving with relative speed, v , is given by:

$$F_{\text{air}} = \frac{1}{2} \rho_{\text{air}} C_d A v^2 \quad (2.1)$$

where:

- ρ_{air} - air density, kg/m^3
- C_d - air drag coefficient
- A - wind blocking area, m^2

According to Nørstrud (1997) the drag area of a skier $C_d A$ reads:

$$\begin{aligned} C_d A &= 0.2029 \cdot 0.35^2 \cdot m_b^{0.425} \cdot h_b^{0.725} \\ &\approx 0.025 \cdot m_b^{0.4} \cdot h_b^{0.7} \end{aligned} \quad (2.2)$$

where:

- m_b - mass of the body of the skier, kg
- h_b - height of the body of the skier, m

Typical values for the drag area C_dA of a cross-country skier are given in Table 2.1. The drag area is known to be dependent on the shape and speed of the skier and the quality of his or her clothing (Spring et al., 1988; Erkkilä et al., 1985). It is normally assumed constant when analysing results from ski base sliding friction experiments (Leino and Spring, 1984; Leino et al., 1983).

Table 2.1. Typical values for the drag area C_dA of a cross-country skier.

Posture	C_dA (m ²)	Experiment	Reference
Competition skier (weight 75 kg, height 1.80 m) with competition suit in a semi-squatting posture	≈ 0.23 (0.21-0.24)	Deduced from Eq. (2.2)	Nørstrud (1997)
Average size skier (weight 80 kg, height 1.75 m) with tight-fitting ski suit in semi-squatting posture	0.27 ± 0.03	Determined from retardation of cross-country skiers when gliding on roller-skis over a horizontal smooth asphalt surface in a subway	Spring et al. (1988)
Average size skier (weight 80 kg, height 1.75 m) with tight-fitting ski suit in upright posture	0.65 ± 0.05	„	„
Average size skier (weight 80 kg, height 1.75 m) with tight-fitting ski suit in semi-squatting posture pacing up with skier ahead also gliding in semi-squatting posture 2-3 m ahead	0.21 ± 0.03	„	„

By applying the ideal gas law for dry air:

$$p_{\text{air}} = \rho_{\text{air}} RT_{\text{air}} \quad (2.3)$$

where:

- p_{air} - dry air pressure, Pa
- R - ideal gas constant, 8.314 J/mol·K
- T_{air} - air temperature, K

and further assuming isothermal conditions (Hess, 1959), the following equation is obtained:

$$\rho_{\text{air}}(z, T_{\text{air}}) = \rho_0 \frac{T_0}{T_{\text{air}}} e^{-\frac{z}{8000}} \quad (2.4)$$

where:

- z - height above sea level, m
- ρ_0 - air density at sea level, kg/m³
- T_0 - air temperature at sea level, K

It follows from Eq. (2.4) that the air resistance against a moving skier in principle is reduced by height above sea level. We also see that at the same altitude the influence is largest at low air temperatures. It can furthermore be calculated that at the same speed the air resistance is approximately 15 % less at

1000 m above sea level than at sea level. Air resistance contributes therefore more to the total friction (air resistance and ski base sliding friction) against a moving skier in lowlands than in more elevated regions. More details can be found in Løset et al. (1995).

2.1.2. Ski base sliding friction

The ski base sliding friction, F_{sn} , can be expressed as:

$$F_{sn} = \mu N \quad (2.5)$$

where:

- μ - sliding friction coefficient
- N - normal load from skier, N

The sliding friction coefficient is known to vary with speed. Fig. 2.1 shows measured values of the sliding friction coefficient on snow as a function of speed. The values from Kuroiwa (1977) and Spring (1988) were measured using skis gliding on snow, while the values from Shimbo (1961) were measured in laboratory using a rotational friction instrument consisting of a rotational disk and a snow pan. The observed values range from 0.02 to 0.11. The sliding friction coefficient decreases below the static value at the onset of motion because of lubrication by frictional melting (Colbeck, 1992). It then reaches an optimum point where it has its minimum value. After passing through this optimum point, friction increases with speed. Notice that friction increases rapidly already at low speeds under wet snow conditions (curve a), while under dry cold snow conditions (curve c) it almost remains constant. This can be explained by wet friction (suction or viscous drag) taking place at a much earlier stage under wet snow conditions than under dry cold snow conditions. Under dry cold snow conditions it takes much higher speeds to form thick water films and thereby introduce wet friction under the skis. The kinetic friction coefficient between metal and ice has a typical value of 0.01 (Løset et al., 1995). This value can be considered as a lower limit for the sliding friction coefficient during skiing and may be possible to attain under extremely icy conditions.

The average sliding friction coefficient, μ , for a skier gliding over a test length, S , in a ski test track can be found experimentally. The work, W_{tot} , over the test length S can be assumed to be given by:

$$W_{tot} = \int_0^S (F_{sn} + F_{air}) ds \quad (2.6)$$

where air resistance, F_{air} , is given by Eqs. (2.1) and (2.4), and ski base sliding friction, F_{sn} , is given by:

$$F_{sn} = \mu mg \cos \alpha \quad (2.7)$$

where:

- m - mass of skier and skis, kg
 g - acceleration due to gravity, 9.81 m/s^2
 α - inclination of the test length S in the ski test track, °

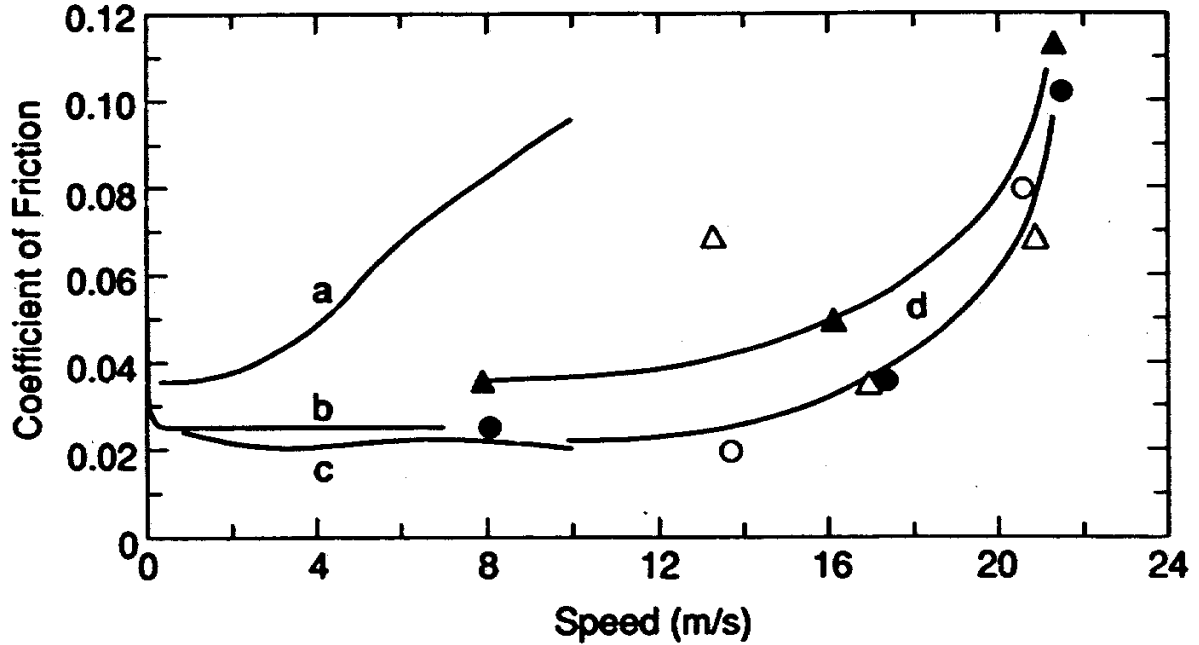


Fig. 2.1. Measured values of the sliding friction coefficient as a function of speed (Colbeck, 1992). a) Old grainy wet snow with 20% snow humidity (Spring, 1988). b) P.T.F.E. on wet snow (Shimbo, 1961). c) Old grainy dry snow with 0 % snow humidity at -7.5°C (Spring, 1988). d) Waxed (circles) and unwaxed (triangles) polyethylene on dry (solid circles and triangles) snow at -2.5 to -1.6°C and on wet (open circles and triangles) snow (Kuroiwa, 1977).

From energy considerations for a skier (and skis) with mass, m , Eq. (2.6) takes the following form:

$$\begin{aligned}
 \frac{1}{2}mv_i^2 + mgh &= \frac{1}{2}mv_f^2 + F_{\text{sn}}S + F_{\text{air}}S \\
 &= \frac{1}{2}mv_f^2 + \mu mgS \cos \alpha + F_{\text{air}}S
 \end{aligned} \tag{2.8}$$

where:

- v_i - initial speed of the skier at the beginning of the test length, m/s
 v_f - final speed of the skier at the end of the test length, m/s
 h - height difference between the beginning and the end of the test length, m

From Eq. (2.8) the average sliding friction coefficient, μ , can be obtained as:

$$\mu = \frac{1}{g \cos \alpha} \left(\frac{v_i^2 - v_f^2}{2S} - \frac{F_{\text{air}}}{m} + \frac{gh}{S} \right) \tag{2.9}$$

By measuring α , v_i , v_f , S , h , m , z and T_{air} (the last two parameters come from Eq. (2.4)) during sliding tests, and further assuming $C_d A \approx 0.23 \text{ m}^2$, the average sliding friction coefficient, μ , can be estimated for different ski pairs of a skier under different snow and weather conditions. In Table 2.2 an example of sliding friction coefficients estimated from Eq. (2.9) is given. The coefficients were registered during two different in-situ sliding tests of waxed and unwaxed new-ground cross-country skis under different snow and weather conditions (Moldestad, 1995). The sliding friction coefficients were much higher under the wet snow conditions (0.062-0.069) than when the snow temperature was below zero (0.048-0.051), although the skis were unwaxed in the second case.

Table 2.2. Example of sliding friction coefficients estimated from Eq. (2.9). The coefficients were registered during two different in-situ sliding tests of waxed and unwaxed new-ground cross-country skis under different snow and weather conditions (Moldestad, 1995). The mass of the skier and the skis were the same in both tests (82.5 kg). Snow hardness is termed according to Colbeck et al. (1990).

Parameter	Value/Remark		
Sliding friction coefficient	0.048-0.051 0.062-0.069		
Skis	New-ground country skis	unwaxed	cross- country skis
Speed	8.19-8.44 m/s 6.99-7.61 m/s		
Weather	Cloudy Cloudy and high relative humidity. A bit rainy at the end of the test.		
Snow type	Combination of new and transformed snow, mainly new snow. (Ski track: Dry new snow with some ice underneath, during the test the track turned a bit glassy).		
Snow surface temperature	-4.2 to -2.7°C 0°C		
0.5-m air temperature	-0.7 to 0.4°C 5.5 to 4.9°C		
Snow hardness	5.4×10 ⁵ -3.0×10 ⁵ Pa 0.24×10 ⁵ -0.36×10 ⁵ Pa		
	High: R4 Medium: R3		

The sliding friction coefficient can to some extent be described and explained by:

- Tribology
- Impact and compaction resistances
- Electrostatic charging effects

The two first items are outlined in Section 2.2. The electrostatic charging effects are described in Chapter 7.

2.1.3. Air resistance and ski base sliding friction estimated as a function of speed

Fig. 2.2 shows air resistance and ski base sliding friction estimated as a function of speed. Ski base sliding friction is estimated from the sliding friction coefficient values given by Spring (1988) for a skier of mass 75 kg. The air resistance is estimated at different heights above sea level at zero air

temperature for a skier with $C_dA = 0.23 \text{ m}^2$. In the air resistance calculations ρ_0 has been set to 1.2928 kg/m^3 according to Perry (1984). From Fig. 2.2 it can be deduced that ski base sliding friction dominates over air resistance at dry, dense snow at -7.5°C , when the speed of the skier is less than approximately 10 m/s. The influence of the air resistance takes over when the speed of the skier exceeds this value. When the speed of the skier is 10 m/s at dense, wet snow, the ski base sliding friction is almost 4 times higher than the value at dry, dense snow. Given a drag area of 0.23 m^2 , it seems likely to assume that ski base sliding friction dominates over air resistance under these conditions, when the speed of the skier is less than approximately 25 m/s. At higher altitudes ski base sliding friction probably exceeds air resistance also at even higher speeds. It is difficult to execute accurate in-situ sliding tests at such high speeds, due to the large influence of possible changes in the skier's drag area during a test ski run.

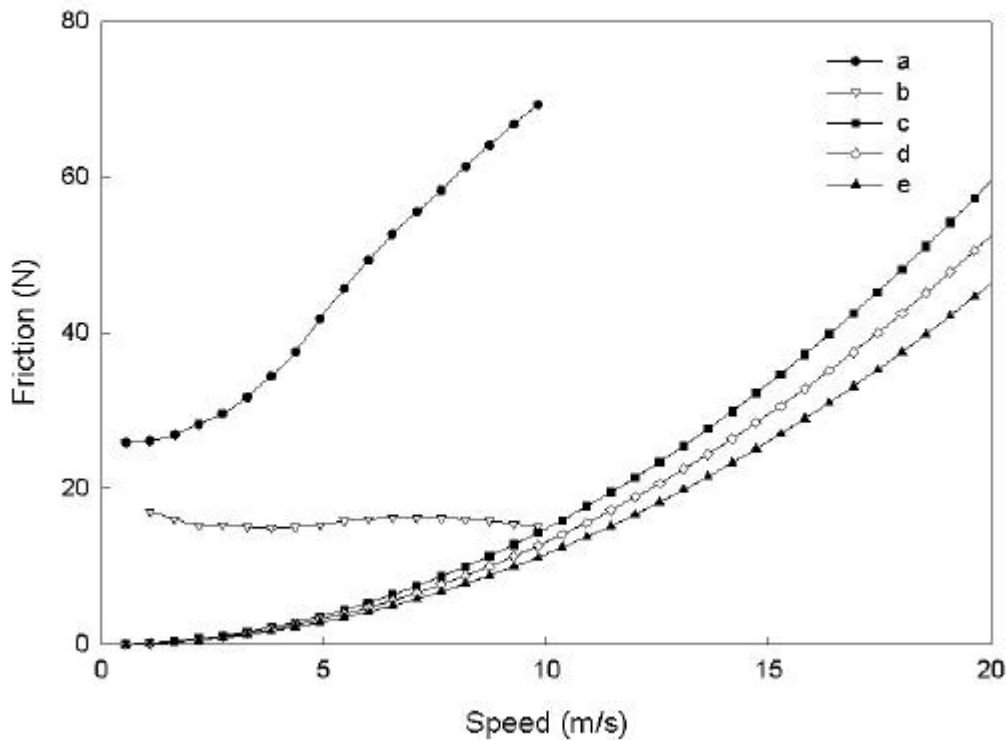


Fig. 2.2. Air resistance and ski base sliding friction estimated as a function of speed. a) Ski base sliding friction for a skier with mass 75 kg at old grainy wet snow (sliding friction coefficient values from Spring, 1988). b) Ski base sliding friction for a skier with mass 75 kg at old grainy dry snow at -7.5°C (sliding friction coefficient values from Spring, 1988). c) Air resistance estimated for a skier with $C_dA = 0.23 \text{ m}^2$ at sea level and zero air temperature. d) Air resistance estimated for a skier with $C_dA = 0.23 \text{ m}^2$ at 1000 m and zero air temperature. e) Air resistance estimated for a skier with $C_dA = 0.23 \text{ m}^2$ at 2000 m and zero air temperature.

2.2. How does ski base sliding friction work?

The low ski base sliding friction can be explained with lubrication by a thin water film created between ski and snow during skiing. Creation of water film under the ski is considered positive for minimum ski base sliding friction at cold snow temperatures. For snow close to or at the freezing point and containing a considerable amount of initial liquid content, water film creation may increase ski base sliding friction due to suction or viscous drag.

Reynolds (1901) suggested that the water film was created by pressure melting, i.e. lowering of the freezing point due to high pressure. It can be shown that the pressure from a slider against snow or ice is insufficient to lower the freezing point significantly in most sliding situations. Mayr (1979) estimated that the freezing point was lowered by 0.00021°C for a 75-kg skier with a ski contact surface of 2700 cm^2 . Løset et al. (1995) calculated that the freezing point could be lowered by 0.74°C for a 90 kg ice skater with skate blades of 1.1 mm width and 80 mm contact length. Colbeck (1995a) pointed out that the pressure needed to reach melting temperature would be approximately $2.7 \times 10^8\text{ Pa}$, i.e. 2700 times atmospheric pressure, at -20°C , thus implying a contact area of 2.3 mm^2 for a typical ski in order to introduce pressure melting at that temperature. A contact area of that size order is much less than observed contact areas (Colbeck, 1994a). It is therefore unlikely that the pressure melting theory should be the main explanation for the low ski base sliding friction.

Bowden and Hughes (1939) were the first to suggest the friction melting theory. They meant that frictional heating created the water film between slider and snow. The friction melting theory has been supported experimentally by e.g. Evans et al. (1976), Ambach and Mayr (1981), Warren et al. (1989) and Colbeck et al. (1997). Ambach and Mayr (1981) used a capacitor probe in the ski to estimate water film thickness under the ski during skiing (See Section 2.2.2). They found increased film thickness as the snow temperature rose, thus implying the importance and effect of snow temperature, frictional heating and heat loss on water film generation.

Warren et al. (1989) installed thermocouples in an alpine ski base and measured a large thermal response from frictional heating. The temperature rise of the moving ski base increased with lower snow temperature due to more heat production caused by less water film development and higher sliding friction coefficient. It also increased with heavier loads. Long ski runs showed steady-state temperatures at the ski base that increased with snow temperature. Warren et al. (1989) also found that heat generation was more uniformly distributed when the snow was soft and could conform to the shape of the ski. Colbeck (1994b) performed a similar experiment for skating skis and Colbeck et al. (1997) for ice skates. Colbeck (1994b) found that the greatest temperature response at the ski base of a skating ski was just behind the foot, where the ski is heavily loaded. He also experienced increasing temperatures along the length of the ski. Further theoretical arguments for the friction melting theory have been provided by e.g. Oksanen (1980), Oksanen and Keinonen (1982) and Colbeck (1995a).

Reviews of ski base sliding friction mechanisms have been given by e.g. Glenne (1987), Balakin and Pereverzeva (1991), Colbeck (1992 and 1994a) and Lind and Sanders (1996). Perla and Glenne and Glenne addressed respectively skiing and the mechanics of skiing in *Handbook of Snow* (Gray and Male, 1981). Performance and properties of alpine skis have been specifically discussed by e.g. Schultes (1980), K2 (1996), Lind and Sanders (1996) and Glenne et al. (1997). Studies of friction

against snow or ice have also been performed by e.g. Shimbo (1971), Kuroiwa (1977), Slotfeldt-Ellingsen and Torgersen (1983), Hensvold (1985), Hämäläinen and Spring (1986), Pikhala and Spring (1986), Spring (1989), Lehtovaara (1989), Petrenko (1994), Petrenko and Colbeck (1995) and Sahashi and Ichino (1998). The electrical charging of skis gliding on snow has been examined by Colbeck (1995b). These results are further discussed in Chapter 7.

The influence of high-quality ski base structures on ski base sliding friction has been paid very little attention to in the literature. Slotfeldt-Ellingsen and Torgersen (1982) studied sliding properties of different polyethylene ski bases and the effect of different ski base grinding techniques. Their studies mainly considered manual grinding techniques and band grinding, but initial testing with stone grinding was also performed. Stone grinding of competition skis has been revolutionised since their study. Slotfeldt-Ellingsen and Torgersen reported stone-ground grooves with depths of 3 to 5 μm . Nowadays a ski base structure with such characteristics would have been characterised as very fine and almost plane. Groove depths of up to 100 μm have been made with present ski base grinding machinery. Slotfeldt-Ellingsen and Torgersen pointed out that the optimum glide was established with coarse and deep grooves under wet conditions and fine and shallow grooves under cold conditions. A wrong structure was referred to give 5-10% less glide than an optimum structure.

Mathia et al. (1989) and Mathia et al. (1992) reported the development of a 3D profilometer for systematic study of micro- and macro-topography of ski bases. Their research had concentrated on non-dimensional parameterisation of ski bases and wear mechanisms associated with alpine skiing. The measurements of 60 areas on ski base surfaces for two manufacturing processes were reported to give skewness between -0.6 and 1.2 and kurtosis between 2.2 and 4.8 for wheel grinding, and skewness between -1.5 and 1 and kurtosis between 2.2 and 5 for belt grinding (Mathia et al., 1992). Skewness and kurtosis are defined as the normalised third and fourth central moments of the probability density function of the height distribution of an analysed surface. Measurements of skewness and kurtosis at different wear stages for a ski base during a whole ski season in the Alps were also shown in Mathia et al. (1992). Mathia et al. did not characterise different types of ski base structures in their papers. Neither did they study the effect of different ski base structures on ski base sliding friction. Mathia et al. claimed that the sliding friction coefficient remains constant at a value of 0.05 in the range of bump heights from 10 to 30 μm referring to McConica (1950) and Midol and Mathia (1985). For phenolic resins Shimbo (1971) similarly reported that the kinetic sliding friction coefficient remained constant in the range of bump heights from 15 to 35 μm at an air temperature of 3°C and snow temperature of 0°C. These results can not be generalised for ski base structures. An assumption that ski base structures with bump heights from 10 to 30 μm , i.e. arithmetic mean surface roughness from approximately 1.4 to 4.3 μm , should have constant and equal sliding properties, is completely meaningless and wrong from my point of view and experiences with characterisation and testing of ski base structures. A complete definition of the arithmetic mean surface roughness is given together with a few other roughness parameter definitions in Section 2.2.4.

Both Shimbo (1971) and Mathia et al. (1992) referred an abnormal increase of the sliding friction coefficient to 0.10 for smooth surfaces. Shimbo also commented that most of the roughened surfaces gave kinetic sliding friction coefficients between 0.02 and 0.05. K2 (1996) has stated that polyethylene surface structures on alpine skis should have an arithmetic mean surface roughness of approximately 1.5-1.9 μm . Such a claim is indeed questionable for different snow conditions. Colbeck (1996)

presented a simple theoretical model of a two-dimensional grooved polyethylene surface adhering to ice. This model was not based on measurements of actual ski base structures. Moldestad (1995) has shown that visual interpretation of ski base structure characteristics is insufficient to characterise ski base structures. Colbeck (1997) further explored capillary bonding of wet surfaces and the effects of contact angle and surface roughness.

2.2.1. Tribology and ski base sliding friction

Tribology is defined as the science and technology of interacting surfaces in relative motion and of the practices related thereto (Hamrock, 1994). A tribological system consists of three parts:

- Upper surface i.e. moving ski with structure, pressure distribution, glide wax and base properties.
- Lubricant i.e. microscopic water film created by frictional melting and free water content in the snow.
- Lower surface i.e. snow.

By describing the three parts the frictional regime of the sliding friction coefficient, μ , can be found and determined. Fig. 2.3 shows the lubricant conditions for different frictional regimes. The left part of Fig 2.3 shows the conditions when dry friction dominates. Such conditions can exist under the ski when skiing on dry snow at cold snow temperatures, at least at the start of the forward contact line between ski and snow. The middle part of Fig 2.3 indicates the conditions when both dry and wet friction are significant. The conditions when wet friction dominates are shown in the right part of Fig. 2.3. This is typically achieved when the snow contains a high free water content.

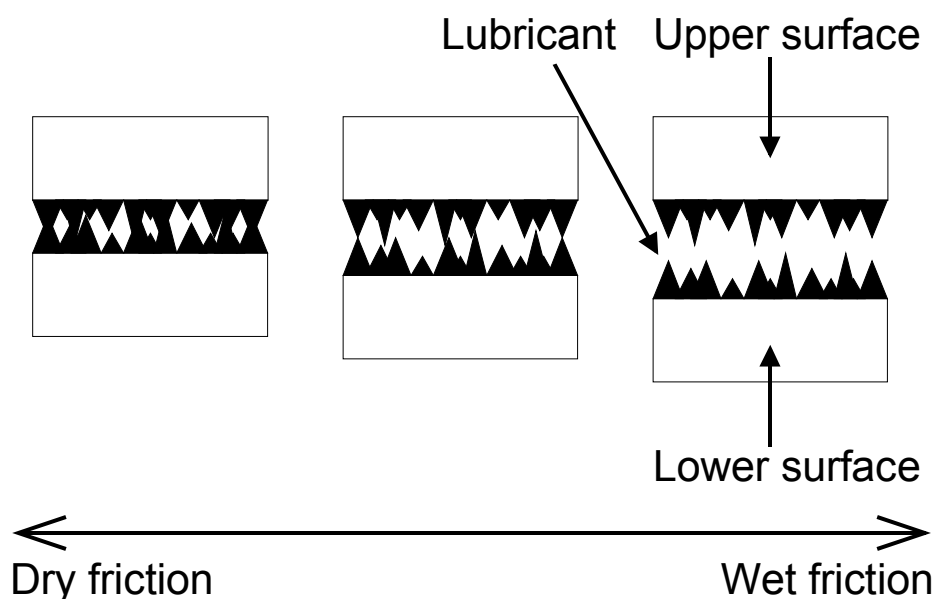


Fig. 2.3. Lubricant conditions showed for different friction regimes.

2.2.2. The lubricant (water film)

Ambach and Mayr (1981) were the first to publish measurements of water film thickness under a moving ski. Their measurements were performed with a comb-shaped capacitor with a surface of $10 \times 10 \text{ mm}^2$, installed in the sliding surface of an alpine ski. The capacitor was used to measure the relative permittivity (dielectric constant) in the contact zone between ski and snow during skiing. The measurement frequency was 100 kHz. High values of the relative permittivity corresponded to thick water films under the ski, since the relative permittivity of water is known to be high compared with that of snow and ice at the frequency of 100 kHz. A special calibration procedure and calibration curve was used to convert measured voltage signal, i.e. change in capacitance of the probe due to relative permittivity changes in the contact zone between ski and snow, to water film thickness. Thus, Colbeck (1992) commented that the reported values of water film thicknesses were necessarily not exact, but certainly of the right order of magnitude. The relative permittivity of snow is known to be a function of snow density and snow wetness, see e.g. Tiuri et al. (1984).

Fig. 2.4 shows the water film development under the ski during two comparable test runs at different snow and air temperatures, but otherwise equal conditions. In Test Run 1, at the highest air and snow temperatures, the water film thickness increases quickly after start and approaches an approximately constant value during the first half of the test run. In Test Run 2, at lower air and snow temperatures, the water film thickness shows almost no increase during the first two-thirds of the test run, but increases quickly during the last third of the run, when the speed is getting higher.

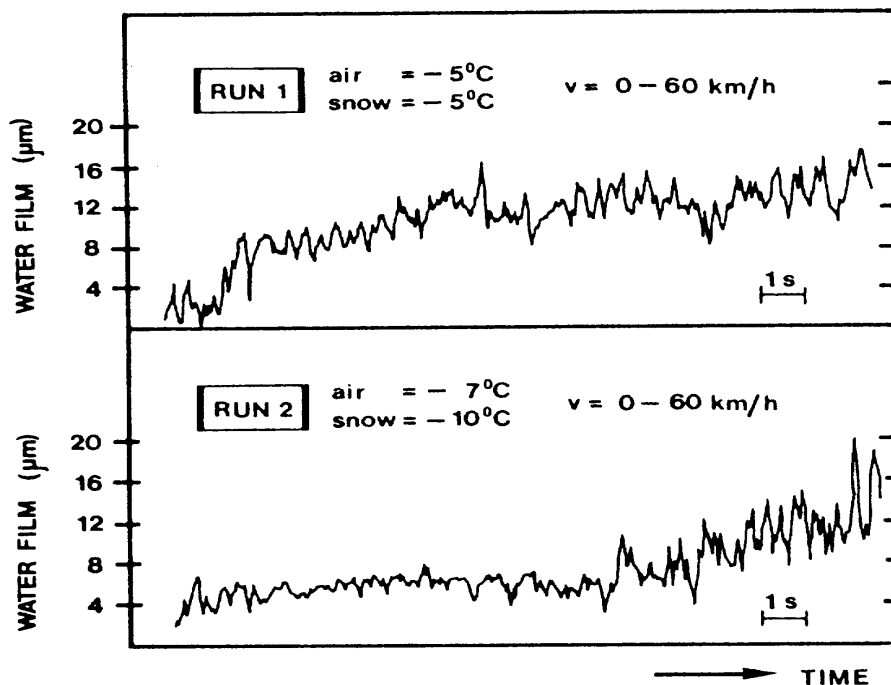


Fig. 2.4. Water film development under the ski during test runs in the same course at different snow and air temperatures (Ambach and Mayr, 1981). Run 1: Air temperature -5°C , snow temperature -5°C . Run 2: Air temperature -7°C , snow temperature -10°C . The speed development in the two runs was equal.

Mean values of the water film thickness measured at nearly constant speed up to 20 km/h and different snow and air temperatures are given in Table 2.3. Ambach and Mayr performed too few measurements to find quantitative relations, but it is easy to see from their results that the developed water film thickness decreases as the snow temperature decreases.

Table 2.3. Mean values of water film thickness at different snow and air temperatures at speeds up to 20 km/h (Ambach and Mayr, 1981).

Snow temperature (°C)	Air temperature (°C)	Water film thickness (µm)
0.0	+3.0	13.5
0.0	-0.7	10.6
-1.0	-2.0	6.5
-1.0	-3.0	6.0
-1.3	-2.5	5.7
-4.0	-4.5	5.0

Fig. 2.5 shows test results from a ski run that alternated between skiing in prepared piste and deep snow at constant speed. Ambach and Mayr claimed that the difference in the shape of the curve was caused by a more constant contact with the surface in deep snow compared to a prepared piste. In the prepared piste bumps in the piste caused lifting of the ski and measurement probe and fluctuations in the measured signal. Ambach and Mayr meant that the difference in measured water film thickness between prepared piste and deep snow was due to slight distinctions in snow temperature. In addition Mayr (1979) pointed out that the difference in free water content of the snow could play a part. The difference could also have been caused by the increased snow compression that takes place in deep snow compared to in a piste and thereby possible percolation of water on the ski base if the deep snow contains some free water.

The water film development for three different glide waxes at different snow and air temperatures is depicted in Fig. 2.6. The glide waxes used belonged to the *Toko System 4* series. According to the manufacturer, an optimum glide should be obtained by yellow wax at temperatures down to -2°C , by red wax at temperatures down to -5°C and by green wax at temperatures below -5°C . The green wax produced most water film at air temperatures below -7°C . Above -6°C red wax produced most water film. The yellow wax produced least water film, which was natural since its given optimum temperature area was outside the tested temperature area. Ambach and Mayr concluded that at least for temperatures below -5°C , the optimum glide is performed with the glide wax that produces most water film. They also stated that the results could not be generalised, since wet snow and high speeds can give opposite effects with poorer glide behaviour for thicker water films.

Ambach and Mayr also performed two test series with ski bases with different roughness. These tests were done on a medium hard test course at a snow temperature of -7°C . The ski base in the first test series had been smoothed between the ski tip and the sensor with a sharp smoothing knife. In the second test series the same part of the sliding surface had been roughened with a special ski-grinding machine. The test series gave no difference in water film development. The two series give a too fragile basis and too little information to decide the effect of ski base roughness on water film development.

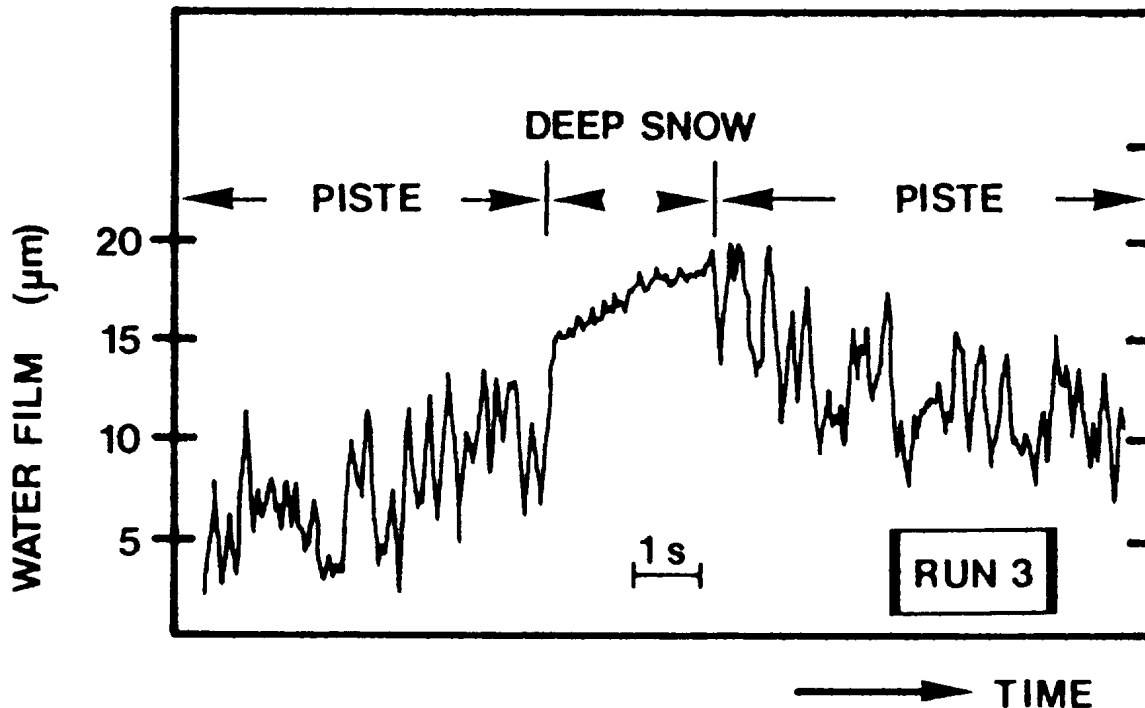


Fig. 2.5. Estimated water film thickness for a test run in deep snow and prepared piste at constant speed (Ambach and Mayr, 1981).

The paper of Ambach and Mayr (1981) is based on the thesis written by Mayr (1979). In his thesis Mayr also described results from some other tests e.g.:

- A test performed with two ski runs with two different speeds, 15 km/h and 25 km/h, at the same course under otherwise equal conditions. When the speed was 15 km/h, a mean water film thickness of 5.7 μm was produced, while a mean water film thickness of 12.5 μm was produced when the speed was 25 km/h. This addresses the speed dependency of water film development and ski base sliding friction.
- A test performed with two subsequent ski runs in the same track. In the first run 3 cm of new-fallen snow was lying in the track. The second run was taken in the exact same track as the first run. The second run gave almost two times the water film thickness of the first at high speeds. This addresses the importance of snow compaction and snow hardness on water film development and ski base sliding friction.

More details can be found in Mayr (1979).

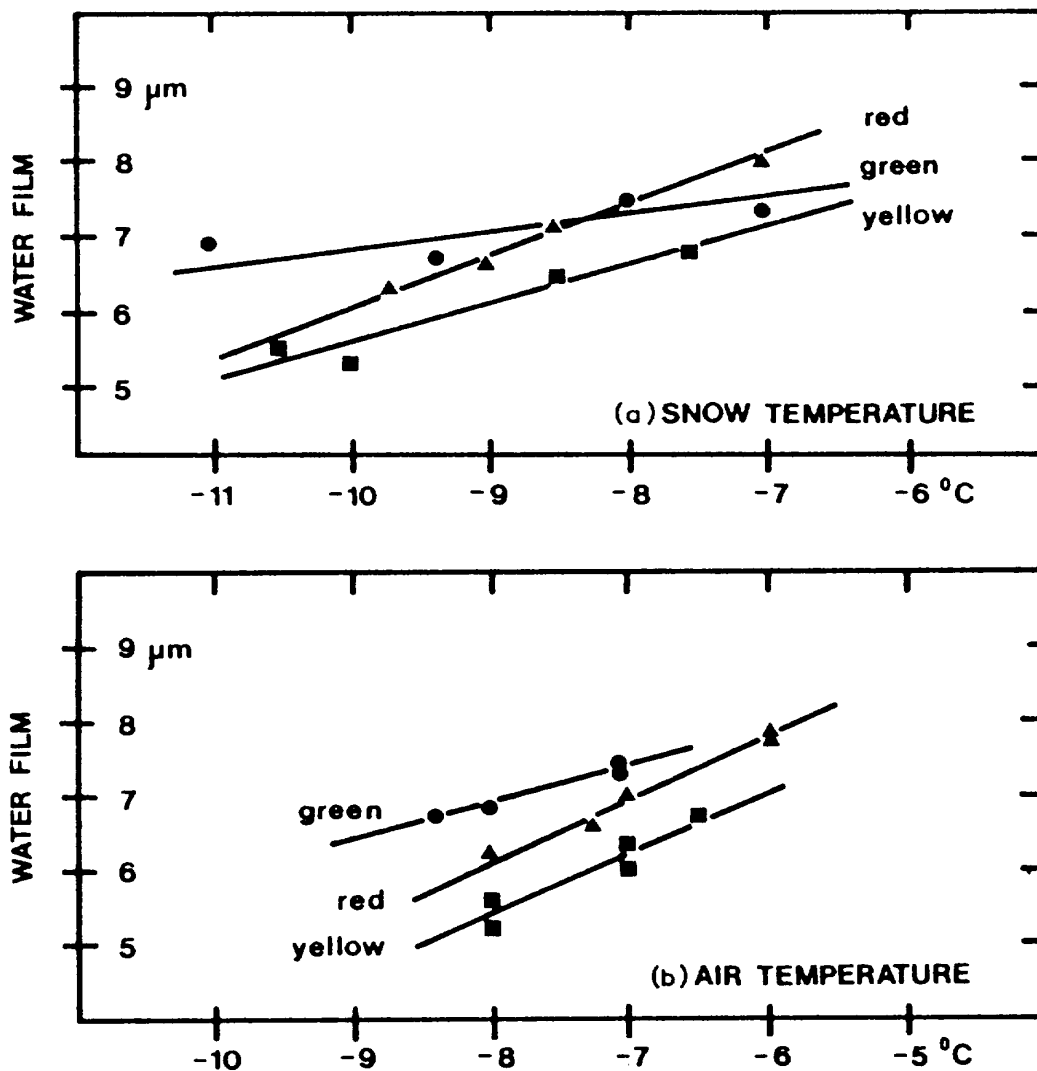


Fig. 2.6. Water film development for different glide waxes at: (a) different snow temperatures and (b) different air temperatures (Ambach and Mayr, 1981).

2.2.3. The sliding surface (snow)

The most important snow parameters for ski base sliding friction are:

- Snow temperature
- Snow humidity
- Snow density
- Snow hardness
- Snow type and snow grain structure
- Thermal conductivity of snow
- Electrical conductivity of snow and electrolytic conductivity of meltwater
- Pollution in the snow
- Snow roughness

The characterisation of snow temperature, snow humidity, snow density, snow hardness, snow type and snow grain structure in a cross-country race ski track is described in Chapter 5. The characterisation of electrolytic conductivity of melted snow samples from ski tracks is also found there. The electrical conductivity of ice has been measured by e.g. Petrenko and Colbeck (1995).

Snow consists of ice, water and air. The thermal conductivity of snow may therefore be regarded as a combination of the thermal conductivities for ice (2.21 W/mK at 0 K), water (0.55 W/mK at 0 K) and air (0.025 W/mK at 0 K). Sturm et al. (1997) have performed an extensive study on the thermal conductivity of snow.

Two other interesting snow parameters when dealing with ski base sliding friction or other types of snow (or ice) friction, are the specific heat capacity of snow (2.09 J/gK) and the latent heat of fusion of snow (334 J/g). From the values of these two parameters it can be deduced that it takes approximately 160 times the energy to melt 1 g snow compared to increase the temperature of 1 g snow by 1°C. This indicates that the frictional conditions at -5°C and -15°C do necessarily not have to be very different given otherwise equal snow conditions, since the main part of the frictional energy at both temperatures has to be used to melt the snow, not to increase the snow temperature.

When doing in-situ sliding tests weather parameters such as air temperature, relative humidity, cloudiness and net radiation also have to be characterised in addition to the snow parameters. It is important to notice that input of energy in the energy balance under the ski during skiing also can be contributed from solar radiation in addition to frictional energy. The total amount of energy is decisive for snowmelt under the ski and thereby water film creation during skiing. Some of the energy is conducted away in the snow and in the ski and thereby heats the ski and the snow under the water film developed. This addresses the importance of the thermal conductivity of the snow and the ski base. Colbeck (1992) stated that when the ski base is black and receiving intense solar radiation, it can absorb nearly as much heat at the base due to diffusion from the underlying snow, as it produces by friction. He further claimed that when heat absorption at the sides and top were considered in addition, solar radiation could control the heat balance under the ski under such conditions. Colbeck (1994b) showed in his measurements of bottom temperatures of skating skis on snow that solar radiation absorption heated the ski base directly and raised the temperature of the ski base considerably.

When modelling ski base sliding friction some authors use snow parameters e.g. Lehtovaara (1989) and Balakin and Pereverzeva (1991), while others use water parameters e.g. Warren et al. (1989). We find it natural to use water parameters given for 0°C for the water film and snow parameters for the snow underneath in a ski base sliding friction model. Presently an exactly correct ski base sliding friction model is extremely difficult to present due to the uncertainties in how the contact behaviour between ski base and snow/water film is in reality during friction.

2.2.4. The slider (ski base)

The most essential ski parameters for ski base sliding friction are:

- The pressure distribution of the ski

- The ski base material and quality
- The glide wax or powder applied at the ski base
- The ski base surface structure
- The speed of the ski

The contact between the ski and the sliding surface is from a macroscopic point of view given by:

- The pressure distribution of the ski
- The snow hardness i.e. the bearing strength of the snow

These parameters indicate the nominal contact between the ski and the sliding surface, i.e. the area on the ski where the contact between the ski and the sliding surface possibly can exist, when a given weight is applied on the ski. The real contact between the ski and the sliding surface is found from a microscopic point of view and is given by:

- The ski base structure with applied ski wax or powder
- The snow roughness and the orientation, size and hardness of the snow grains
- The free water content in the snow and the development of frictional water film along the ski

Research on measurement of mechanical properties of skis has been performed in Norway since 1969 (Stemsrud and Brun, 1976). The *Madshus Compuflex System* is a result of this research. This unique system measures e.g. the camber and kick zone of any ski along its entire length, thereby helping to identify the proper ski design for each type of *Madshus* ski. The ideal flex patterns for each *Madshus* model can therefore be developed and reproduced. Figs. 2.7 and 2.8 show the pressure (or load) distribution for two types of dry snow skating skis measured by the *Madshus Compuflex System*. The half skier weight has been applied 8 cm behind the balance point on both skis. Fig. 2.9 shows the cumulative pressure distributions for the same skating skis. The pressure distribution of a Nordic ski is characterised by two main peaks respectively on the forebody and afterbody of the ski. Ski preparation with glide wax or powder is therefore of course most important and effective in the areas under the two peaks, at least under hard packed snow conditions. Glenne (1981), Glenne et al. (1997) and K2 (1996) have shown that an alpine ski typically has a big pressure (or load) peak under the foot and nominal peaks at the end of the ski. The *Madshus 234 WC Supraflex Skate Dry* skating ski in Fig. 2.7 is specially designed for loose and uneven track conditions. The ski is said to perform better the softer the snow conditions are. This is natural due to:

- The soft pressures in the tip and tail sections of the pressure distribution of the ski in Fig. 2.7.
- The late pressure increase in the tip section and the early pressure decrease in the tail section in the cumulative pressure distribution of the ski in Fig. 2.9.

Impact and compaction resistances against the ski are therefore minimised, and the ski does not bury down into the snow. Due to the influence of such resistances a stiffer ski may have less glide in soft, loose snow and under some soft wet snow conditions where suction occurs. The *Madshus 134 WC Supraflex Skate Hard Packed Dry* skating ski in Fig. 2.8 is specially designed for firm and well-

packed tracks. This ski has higher torsion stiffness than the softer ski in Fig. 2.7 and is said to have more "life", sensitivity and power than softer skis in hard packed courses. It is characterised by:

- Relatively hard pressures in the tip and tail sections of the pressure distribution in Fig. 2.8.
- Early pressure increase in the tip section and late pressure decrease in the tail section in the cumulative pressure distribution in Fig. 2.9.

The early pressure increase in the tip section in the cumulative pressure distribution is favourable for early water film development and minimum dry friction length on the ski under cold snow conditions.

The contact area between ski and snow vary with ski properties, snow conditions and ski course preparation. Pikhala and Spring (1986) found a contact area of 5-15 % of the ski base area between ski and snow for old, dry, grainy snow with temperature below or at -5°C and a snow density of $520\text{-}580\text{ kg/m}^3$ in their experiments. Old, wet, grainy snow close to 0°C with 12 % free water content and 600 kg/m^3 snow density, gave a contact area of 45-50 %. A contact area of 90-100% was reached when the same snow had a free water content of 28 % and snow density of 620 kg/m^3 . Lehtovaara (1989) has pointed out that the contact at the afterbody of the ski can be only approximately 20 cm in icy tracks, while the contact length can consist of almost the whole ski length on newly fallen snow. The nominal contact area between ski and snow, A_n , can be defined as:

$$A_n = l_f w_f + l_a w_a \quad (2.10)$$

where:

- l_f - nominal contact length on the forebody of the ski, m
- w_f - nominal contact width on the forebody of the ski, m
- l_a - nominal contact length on the afterbody of the ski, m
- w_a - nominal contact width on the afterbody of the ski, m

The nominal pressure distribution $p_n(x)$ along the ski in the x -direction can then be defined as (after Lehtovaara, 1989):

$$p_n(x) = \frac{N}{A_n} \Phi(x),$$

$$\frac{1}{2(l_1 + l_2)} \left[\int_{-l_1}^{l_1} \Phi_1(x) dx + \int_{-l_2}^{l_2} \Phi_2(x) dx \right] = 1 \quad (2.11)$$

where:

- N - normal load on the ski from skier, N
- $\Phi(x)$ - total nominal pressure distribution function for a ski
- $\Phi_1(x)$ - total nominal pressure distribution function for the forebody of a ski
- $\Phi_2(x)$ - total nominal pressure distribution function for the afterbody of a ski

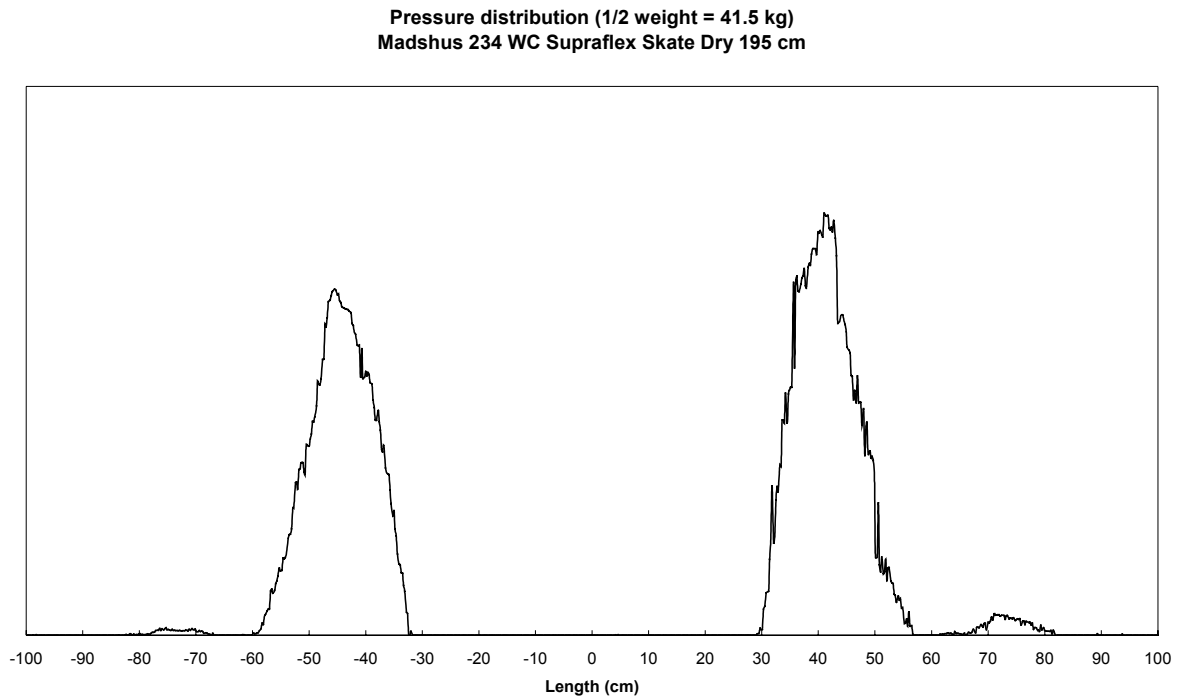


Fig. 2.7. Pressure (or load) distribution for a *Madshus 234 WC Supraflex Skate Dry* skating ski measured by the *Madshus Compuflex System*. Half skier weight (41.5 kg) has been applied 8 cm behind the balance point of the 195 cm long skating ski. The balance point is the zero point of the length axis.

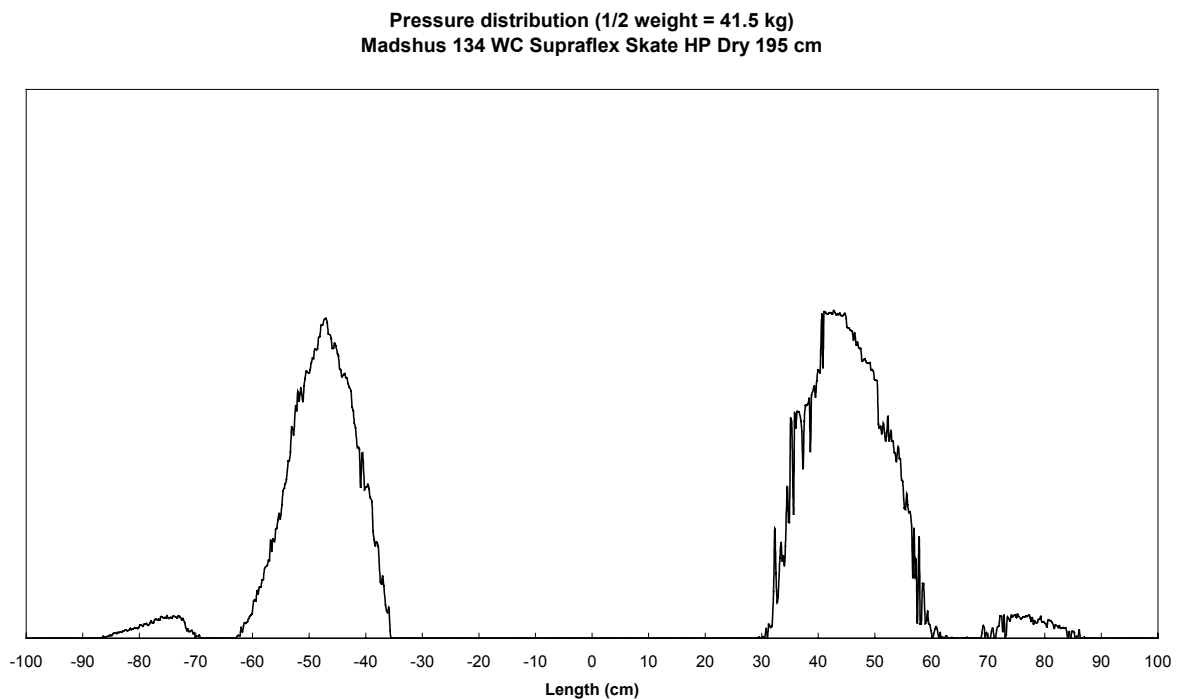


Fig. 2.8. Pressure (or load) distribution for a *Madshus 134 WC Supraflex Skate Hard Packed Dry* skating ski measured by the *Madshus Compuflex System*. Half skier weight (41.5 kg) has been applied 8 cm behind the balance point of the 195 cm long skating ski. The balance point is the zero point of the length axis.

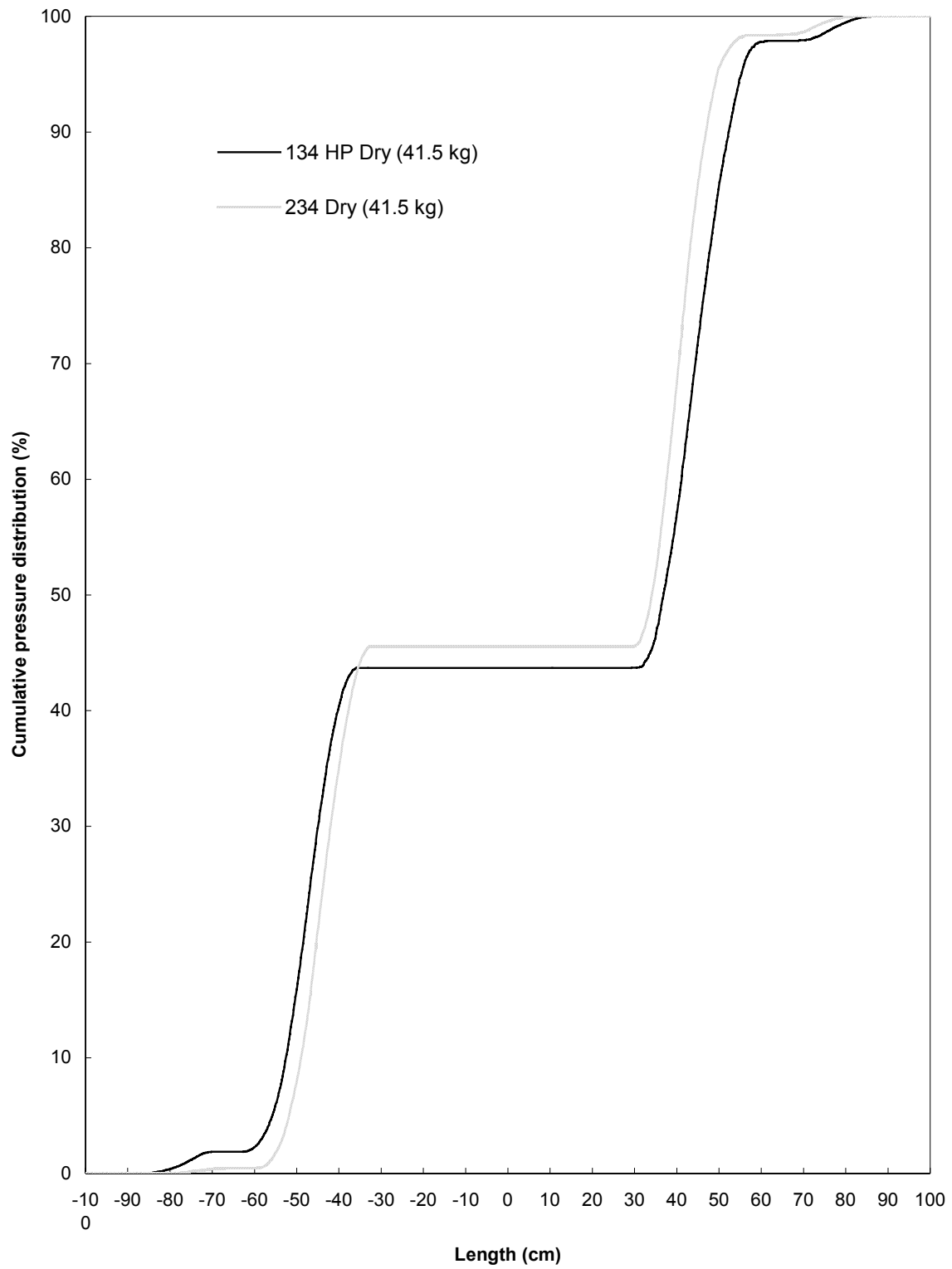


Fig. 2.9. Cumulative pressure distributions for the *Madshus 234 WC Supraflex Skate Dry* and *Madshus 134 WC Supraflex Skate Hard Packed Dry* skating skis in Figs. 2.7 and 2.8.

- l_1 - half nominal contact length on the forebody of a ski ($l_1 = l_f/2$), m
 l_2 - half nominal contact length on the afterbody of a ski ($l_2 = l_a/2$), m

The most important ski base material parameters are:

- Thermal conductivity
- Electrical conductivity
- Graphite content
- Molecular weight
- Density
- Hydrophobicity (contact angle)
- Glide wax and powder absorption
- Colour (absorption of solar radiation)
- Hardness
- Elasticity
- Abrasion resistance
- Oxidation resistance
- UV radiation resistance
- Amount of hairs in the ski base surface

High quality ski bases are normally made of sintered ultrahighmolecular-weight and high-density polyethylene (UHDPE). The UHDPE is modified with graphite (carbon black) and/or other additives. Some manufacturers use e.g. fluorocarbon additives in their top model ski bases. The graphite content of the ski base influences both the thermal and electrical conductivity.

Table 2.4 shows the density and thermal conductivity for some specific ski bases and ski base materials. Notice the high thermal conductivity values for steel and graphite compared to polyethylene. Warren et al. (1989) observed both in field measurements and finite element models of alpine skis that steel edges increase the heat flow out the sides of the skis and thereby reduce the frictional melting under the skis. Graphite wax can also lead heat away from the frictional interface (Colbeck, 1992). Pikhala and Spring (1986) have reported thermal conductivities of 0.15-0.23 W/mK for ski bases, 0.18-0.24 W/mK for ski waxes and 0.13-0.25 W/mK for snow registered with their thermal conductivity meter.

Table 2.4. Density and thermal conductivity for some specific ski bases and ski base materials.

Material	Density (g/cm ³)	Thermal conductivity (W/mK)	Reference
P-tex 2000 Clear	0.937	0.4	Geisbühler (1995)
P-tex 2000 Electra	0.99	0.45	„
P-tex 4000 Electra	0.99	?	„
Polyethylene	0.95	0.4	Warren et al. (1989)
Steel	7.8	50	„
Graphite, high strength	1.7	125	Hamrock (1994)

Polyethylene is an electrical isolator with an electrical conductivity in the order of 10^{-10} $\mu\text{S}/\text{cm}$ (deduced from the electrical resistivity value given for moulded/extruded HDPE by MatWeb, 1998). Graphite on the other hand is an electrical conductor with electrical conductivity of size order 10^8 $\mu\text{S}/\text{cm}$ (deduced from the electrical resistivity value given for graphite in CRC, 1977). The graphite content of the ski base is therefore highly decisive for the electrical conductivity of the ski base. The electrical conductivity of P-tex 2000 has a measured value ≥ 0.1 $\mu\text{S}/\text{cm}$ (IMS Kunststoff AG, 1998). The same can be stated for the electrolytic conductivity of melted snow samples from ski tracks. The electrolytic conductivity of melted snow samples from ski tracks is further discussed in Chapters 5 and 7. The electrical conductivity of the ski base and the ski wax applied at the ski base is important for electrostatic charging of the ski base and drainage of electrostatic charges. The effect of electrical charging on ski base sliding friction is further discussed in Chapter 7.

Ski base material and quality are not the objective of this thesis and are therefore not discussed any further here. More information on the subject can be found in e.g. Slotfeldt-Ellingsen and Torgersen (1982) and K2 (1996). Skis from the same production series have always been used in our ski base structure sliding tests. The sole quality of the skis in the production series has been quality controlled. Ski base material parameters and ski base quality have therefore been assumed constant for the used ski pairs.

Glide wax or powder are neither the objective of this thesis and are therefore not discussed. Information on the subject can be found in e.g. Slotfeldt-Ellingsen and Torgersen (1982), Torgersen (1983), Street and Tsui (1987), Lind and Sanders (1996) or material published by wax manufacturers e.g. SWIX (1996).

The structure of a ski base can be characterised in many different ways. From the discrete set of surface height registrations of a surface profile across the ski (z_1, z_2, \dots, z_N), three different surface or structure parameters may for instant be computed:

Arithmetic mean roughness, R_a , defined by:

$$R_a = \frac{1}{N} \sum_{i=1}^N |z_i| \quad (2.12)$$

, root mean square (rms) roughness, R_q given by:

$$R_q = \sqrt{\frac{1}{N} \sum_{i=1}^N z_i^2} \quad (2.13)$$

and the maximum peak-to-valley height, denoted R_t :

$$R_t = \max(z) - \min(z) \quad (2.14)$$

All discrete height registrations (z_1, z_2, \dots, z_N) of the surface profile refer to a reference line. The reference lines used in this thesis and by the SSA (Ski base Surface Analyser) give a mean value of zero for z_i .

Many surfaces have a roughness that is directionally oriented. This can be described by the surface pattern parameter γ_c , introduced by Peklenik (1968) as:

$$\gamma_c = \frac{\lambda_x}{\lambda_y} \quad (2.15)$$

where:

- λ_x - autocorrelation length in the x -direction, i.e. the direction along the ski, mm
- λ_y - autocorrelation length in the y -direction, i.e. the direction across the ski, mm

The characterisation of ski base structures is further described in Chapter 3.

2.2.5. Ski base sliding friction theory

According to Glenne (1987) the ski base sliding friction can be divided into 4 parts:

1. Dry friction (adhesion), F_d
2. Wet friction (viscous drag), F_w
3. Impact resistance, F_i
4. Compaction resistance, F_c

Dry friction, F_d , can be expressed by:

$$\begin{aligned} F_d &= A_d \tau \\ &= \frac{N}{\sigma} \tau = \mu_d N \end{aligned} \quad (2.16)$$

where:

- A_d - actual dry contact area, m^2
- τ - shear strength of the softest material in the interfacial contact between snow and ski (i.e. snow or glide wax or powder), Pa
- σ - unconfined compression strength of the snow, Pa
- μ_d - dry friction coefficient

The unconfined compression strength of snow is assumed to be a function of snow density, snow temperature and structure and size of snow grains (Mellor, 1964). Notice that the last expression in Eq.

(2.16) is almost similar to the general expression for ski base sliding friction given by Eq. (2.5) in Section 2.1.2.

Wet friction, F_w , can be expressed by:

$$F_w = \frac{\eta_{wf} v A_w}{h_{wf}} \quad (2.17)$$

where:

- η_{wf} - absolute viscosity of the water film, Pa·s
- A_w - wet contact area, m²
- h_{wf} - water film thickness, m

A resistance against the ski base due to snow compression may occur under soft snow conditions. This compaction resistance, F_c , can be expressed by:

$$F_c = \frac{\Delta z}{l} N \quad (2.18)$$

where:

- Δz - vertical snow compaction distance, m
- l - ski length in contact with snow surface i.e. effective ski length, m

An impact resistance occurs at the front of the ski when skiing under soft snow conditions. This resistance, F_i , can be obtained as:

$$F_i = \rho_{sn,i} w \Delta z v^2 \quad (2.19)$$

where:

- $\rho_{sn,i}$ - initial snow density before compaction under the ski, kg/m³
- w - width of the ski, m

Hämäläinen and Spring (1986) studied the influence of snow hardness on ski friction. In their experiments they used a miniature ski and a circular shaped friction meter placed in a freezer. A general observation was that the kinetic friction coefficients decreased when snow hardness increased at ski speeds of 1 and 4 m/s. Glide wax coated skis had almost constant friction coefficients at snow hardness above $\approx 0.4 \times 10^5$ Pa and a ski speed of 4 m/s.

A skating track has lower snow hardness than a classic track under most snow conditions and can often be soft and loose. The vertical compaction distance, Δz , is therefore often significant during skating, thus leading to significant compaction and impact resistances. This is important to account for

when designing, testing and selecting skis and ski base structures for respectively skate and classic skiing.

From the science of fluid-film lubrication the sliding friction coefficient, μ , between two interacting surfaces in relative motion, is known to vary with the film parameter, Λ . For skiing the non-dimensional film parameter, Λ , can be defined as:

$$\Lambda = \frac{h_{\min, wf}}{\sqrt{R_{q, sbs}^2 + R_{q, sn}^2}} \quad (2.20)$$

where:

- $h_{\min, wf}$ - minimum water film thickness between a specific area on the ski and snow at a specific time during skiing, μm
- $R_{q, sbs}$ - root mean square roughness of the ski base structure surface in the specific area, μm
- $R_{q, sn}$ - root mean square roughness of the snow surface, μm

The characteristic dependence between μ and Λ is shown in Fig. 2.10 (based on a figure in Hamrock and Dowson, 1981). Under snow conditions where impact and compaction resistance contributions are negligible or small due to Δz approaching zero, i.e. the snow surface has snow hardness above a certain threshold level, the friction situation in an area under the ski at a given time during skiing is possible to approach by exploiting the knowledge of Eq. (2.20) and Fig. 2.10. The dry and wet friction parts can then be treated by one tribological framework, instead of a theoretical division into two frictional parts.

From Fig. 2.10 it can be deduced that the optimum glide, i.e. minimum sliding friction coefficient, arise when $\Lambda \approx 8-10$. A classic ski should therefore seek to have $\Lambda \approx 8-10$ in the sliding phase and $\Lambda \approx 0$ in the kick phase in order to have both optimum sliding and grip properties.

It is favourable to increase Λ when $\Lambda < 8$. Such frictional sliding conditions can possibly exist for instance under cold snow conditions where the free water content is small. Λ can then be increased by:

- Water film generation, i.e. increase of water film thickness $h_{\min, wf}$.
- Decrease of $R_{q, sbs}$, i.e. use of a finer ski base structure with less roughness. A finer structure has little effect if $R_{q, sbs}$ is small compared to $R_{q, sn}$, i.e. snow surface roughness.

Oksanen and Keinonen (1982) showed that the dynamic sliding friction coefficient decreased with increased speed at cold snow temperatures ($T_{sn} = -15^\circ\text{C}$, $0.5 \leq v \leq 3$ m/s), thus indicating:

- The positive contribution of increased frictional melting, water film thickness $h_{\min, wf}$ and film parameter Λ for better glide with increased speeds at cold snow temperatures.
- The movement from the left side of the minimum point of the graph in Fig. 2.10 towards the optimum point with increased speeds at cold snow temperatures.

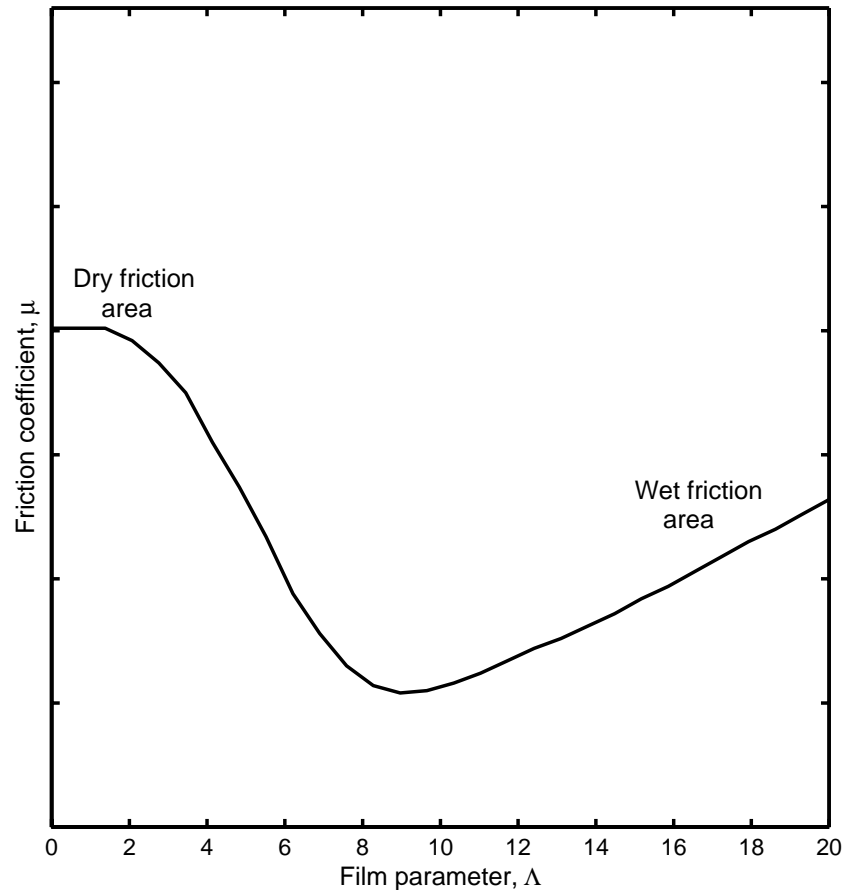


Fig. 2.10. Variation of friction coefficient, μ , with film parameter Λ (after figure in Hamrock and Dowson, 1981).

It is favourable to decrease Λ when $\Lambda > 10$. Such wet friction sliding conditions can possibly exist for instance when the snow contains a considerable amount of free water content. Λ can then be decreased by:

- Water film dilution, i.e. decrease of water film thickness $h_{\min, wf}$.
- Increase of $R_{q, sbs}$, i.e. use of a coarser ski base structure with higher roughness.

The free water content of the snow or snow humidity which is possible to register in-situ by means of snow humidity measurement equipment can be viewed as:

- An indicator of initial water film thickness under the ski.
- A potential start point for estimation of generated water film thickness under the ski during skiing at different speeds.

Oksanen and Keinonen (1982) showed that the dynamic sliding friction coefficient increased with increased speed at near zero snow temperatures ($T_{sn} > -1^\circ\text{C}$, $0.5 \leq v \leq 3 \text{ m/s}$), thus indicating:

- The negative contribution of increased water film thickness $h_{\min, wf}$ and film parameter Λ on the sliding properties of a flat surface when sliding with increased speeds at near zero snow temperatures.

- Movement towards the right side of the graph in Fig. 2.10, i.e. wet friction area, with increased speeds at near zero snow temperatures, at least for flat surfaces.

Fig. 2.10 indicates that a ski base structure should be coarser, i.e. have higher roughness, when the water film thickness under the ski is large, compared to situations when the water film thickness is small. Moore (1975) stated that friction between a ski and ice quite probably is dominated by solid friction in the front, surface tension in the middle and viscous drag at the rear. This indicates that the ski base structure ought to be different in the length direction of the ski. Thus, a fine structure that effectively induces and increases the water film production ought to be used at the front part of the forebody of the ski, at least for cold snow and snow with negligible free water content. As the water film development possibly increases along the ski, structure with regularly higher roughness should be applied in order to stay in the optimum point of Fig. 2.10 all along the ski. The increased bottom temperatures found along the length of skating skis during skiing by Colbeck (1994b), support the hypothesis of increased water film thickness along the ski. In spite of this it is very difficult at present to assume and predict water film thickness development along the ski under different snow, weather and skiing conditions. Another important issue is that the water film development should be a function of the weight of the skier and the ski length. Given equal ski length, heavier skiers should tend to have coarser structures.

Cann et al. (1994) have criticised the lambda ratio defined in Eq. (2.20) for not:

- Describing theoretically the collapse of a lubricant film and determining when a lubricated rough surface in contact with another surface can come into solid contact through the lubricant film.
- Accounting for the fact that the film thickness needed to separate two lubricated surfaces is strongly dependent on the structure of the surface roughness, not only the values of different surface roughness parameters.

Cann et al. also stated that using Λ as a measure of how well surfaces are separated by a film, underestimates how well smooth surfaces are lubricated compared with rough surfaces. They further claimed that smooth surfaces not only need proportionally thinner films for good lubrication, but that also the optimum Λ can be decreased. This indicates that a smooth surface can be favourable for maintaining lubrication under cold snow conditions compared to a rougher surface with the same roughness value. Furthermore a non-smooth surface should have better functionality than a smooth surface with the same roughness value under wet friction conditions. Colbeck (1992) has observed that melt films can slide along the base of the slider if the slider base is smooth and hydrophobic.

Patir and Cheng (1978) developed an average flow model for determining effects of roughness with arbitrary surface pattern parameter γ_c (defined in Eq. (2.15)) on film thickness. They found that longitudinally oriented surfaces tend to decrease the film thickness, while transversely oriented surfaces tend to increase the film thickness. Colbeck (1992) concluded from this that a transverse structure should be beneficial at low temperatures, while a longitudinal structure should be better at high temperatures. He also commented the positive effect of frequent resurfacing of sliders on roughness orientation and optimum sliding performance. Fig. 2.11 shows typical flow patterns and

contact area configurations for surfaces that are longitudinally oriented, Fig. 2.11a ($\gamma_c = 6$), isotropic, Fig. 2.11b ($\gamma_c = 1$) and transversely oriented, Fig. 2.11c ($\gamma_c = 1/6$).

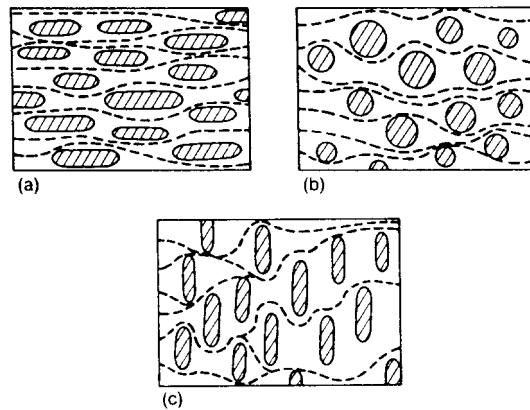


Fig. 2.11. Typical flow patterns and contact area configurations for surfaces with: (a) longitudinally oriented ($\gamma_c = 6$), (b) isotropic ($\gamma_c = 1$) and (c) transversely oriented ($\gamma_c = 1/6$) roughness (Patir and Cheng, 1978).

Guha and Roy Chowdhuri (1996) found that the surface temperature increased monotonically with roughness when 45 % carbon steel discs with different roughness slid against a sapphire pin in a pin-on-disc apparatus. This observation was physically explained by a rougher surface having the total frictional heat only distributed over a small number of asperity peaks, thus causing an increase in the individual maximum peak temperature as well as average surface temperature. This indicates that a too large structure contact area can be poor for initial frictional heat generation and water film production under cold snow conditions. Itagaki et al. (1989) experienced experimentally that rough metal runners with transverse grooves sometimes gave lower friction than smooth metal runners on cold ice (-10°C).

Williamson (1984) stated that surfaces with mixed structures can be designed for particular combinations of properties which can not be obtained with a single surface treatment, e.g. can:

- One process make a structure on the slider surface that causes wide interfacial gaps relative to the sliding surface in order to facilitate lubricant access.
- Another process makes shallow-domed plateaus that can carry the load with very little deformation and wear.

Mixed structures are interesting e.g. under soft and wet snow conditions where dilution of water film and sufficient bearing area capabilities must be combined at the same time. Relatively low snow hardness is quite normal under wet snow conditions.

To minimise the friction between snow and ski when the frictional sliding situation in an area under the ski at a given time is on the left side of the minimum point of the graph in Fig. 2.10, i.e. dry friction area, several aspects must be taken into account at the same time by means of structure, base, skier weight distribution given by the tension of the ski and glide product used on the ski:

- Creation of water film and increase of water film thickness under the ski in order to optimise the film parameter Λ given by Eq. (2.20) according to Fig. 2.10. It might not be possible to produce enough water film and reach an optimum water film thickness under all snow conditions, for instance when the snow is extremely cold.
- Optimisation of the structure roughness along the ski in order to optimise the film parameter Λ given by Eq. (2.20) according to Fig. 2.10.

These aspects highlight the means of e.g.:

- A pressure distribution due to ski tension that induce higher pressure at the start of the contact area on the forebody of the ski and thereby decrease dry friction length and induce water film development quickly. The same effect might also be possible to provoke by e.g. mounting the ski binding some centimetres in front of the balance point or the skier adjusting her/his downhill position, but this can cause poorer ski performance.
- A fine ski base structure and structure roughness in order to increase the film parameter Λ when optimum film parameter can not or is not reached. At the same time the ski base structure must seek to optimise the contact pressure, frictional heat generation and water film production, at least at the beginning of the contact length of the ski. Transversal structure patterns tend to thicken the water film, but give resistance to water flow. Longitudinal structure patterns tend to dilute the water film. It might be a good idea to have a special pattern on the first centimetres of the contact area on the forebody of the ski under hard, cold snow conditions in order to provoke friction, frictional heat and water film generation. This may induce less friction on the rest of the contact length and less total friction. The dry friction length has great influence on the total ski base sliding friction due to the sliding friction coefficient being higher in the dry friction area than all other friction regimes (Fig. 2.10). The dry friction length should furthermore decrease with increased snow density and skier speed according to Colbeck (1992). A smooth surface can be favourable for maintaining lubrication along the ski under cold snow conditions compared to a rougher surface with the same roughness as discussed and mentioned earlier.
- A coarser ski base structure and higher structure roughness with ski length in order to optimise the film parameter Λ along the ski as mentioned and discussed earlier.
- The wear of applied glide wax or powder due to significant direct contact between ski base and snow asperities when the surfaces are not fully lubricated. The impact of applied glide product on ski base sliding friction is not the objective of this thesis, but some important aspects are mentioned in Chapter 7.

To minimise friction between snow and ski when the frictional sliding situation in an area under the ski at a given time is on the right side of the minimum point of the graph in Fig. 2.10, i.e. wet friction area, several aspects must be taken care of at the same time by means of structure, base, skier weight distribution given by the tension of the ski and the glide product used on the ski:

- Dilution of water film and decrease of water film thickness under the ski in order to optimise the film parameter Λ given by Eq. (2.20) according to Fig. 2.10.
- Optimisation of structure roughness along the ski in order to optimise the film parameter Λ given by Eq. (2.20) according to Fig. 2.10.

- Minimisation of the capillary forces in the contact points between ski base and water film or snow and in air gaps between ski base and water film or snow.

These aspects highlight that:

- An increased water film thickness $h_{\min, wf}$ requires increased ski base surface roughness $R_{q, sbs}$. The water film thickness increases with the speed of the skier (Ambach and Mayr, 1981) and most likely also along the ski.
- Longitudinal structure patterns tend to dilute and disrupt the water film. What values do the characteristics, i.e. frequency, depth, width and length, of optimum structure grooves have under different wet snow conditions?
- The ski base structure must work favourable with so-called capillary forces. Capillary bonding occurs when the water film is in a state of tension, i.e. the pressure of the water film is below atmospheric pressure (Colbeck, 1997). What is the characteristics of the structure patterns that give less drag surface under different wet snow conditions? Colbeck (1997) commented that coarser structures can lead to greater wetted areas, instead of the intentional decrease of wetted area. The steepness of the grooves and the size of flat area plateaus also seem to be important for capillary bonding. Colbeck (1996) stated theoretically that adhesion could be minimised if the grooves were cut square rather than in a vee shape. This theory does not necessarily hold in real in-situ capillary contact situations during ski base sliding friction. Squared cut grooves increase the exposed surface area compared to vee grooves. In some practical contact situations snow grains can be smaller than the groove widths. Broad square-cut grooves might then be filled up with small snow grains, thereby increasing surface wetted area and capillary forces compared to vee grooves.
- A pressure distribution that cause the main pressure to be induced softly and late on the contact area on the forebody of the ski, may start suction late and have suction over a shorter total ski length. This influences the choice of ski tension, binding placement and skier weight distribution under wet snow conditions. The influence of suction is greatest when the snow is fresh and wet because of smaller and more numerous pores (Colbeck, 1992). The suction in a pore increases inversely with pore size, i.e. fresh, fine-grained snow has smaller pores.
- The wear of ski base and glide wax due to dry contact between ski base and snow occurs infrequently under wet snow conditions compared to dry snow conditions. Softer glide waxes can therefore be applied. Hydrophobicity and minimisation of attachment of dirt on the ski base are more important parameters, when choosing glide wax or powder for wet snow.

In addition minimisation of macroscopic (mainly given by tension) and microscopic (mainly given by structure) impact and compaction resistances on the ski by optimisation of ski base bearing area might have to be taken care of both in the dry and wet friction area of Fig. 2.10. This addresses the importance of aspects such as e.g.:

- Structure roughness and hairs in the ski base surface that can cause the ski base to cut deep into the snow and increase the effective contact area with the snow surface. This can for instance be a problem when the snow is cold and new-fallen and has very fine snow grains and low snow hardness.

- High early pressure on the forebody of the ski that can cause the skis to bury down into the snow. Relations between snow type, hardness and grain size, point pressures under the skis (given by load/pressure distribution of the skier and ski base structure characteristics such as e.g. typical groove and plateau widths and lengths, some points are load-supporting, while others are not) and the buoyancy of the skis probably exist. Colbeck (1992) has stated that polished ice grains respond elastically due to their flat surfaces, while virgin ice grains (fresh new-fallen snow) behave plastically or fracture. The eventual elasticity at the interface between a snow and a ski base surface will be a function of their surface slopes and hardness as well as pressure from the skier. Hirano and Tada (1996) have stated that an edged ski creates a snow impacting force when the snow is soft, while a snow cutting force occurs when the snow is hard.

Electrostatic charging effects on the ski base sliding friction are described in Chapter 7.

According to the measurements of Ambach and Mayr (1981) in Table 2.3, mean water film thicknesses of 5.0 and 13.5 μm were generated during alpine skiing at constant speed of 20 km/h at snow temperatures of -4.0 and 0°C respectively. Assuming that optimum Λ equals 8 and ignoring snow roughness, the optimum ski base roughness $R_{q,\text{sbs}}$ under those conditions should be 0.63 and 1.69 μm , respectively. These optimum roughness values seem underestimated according to our experiences with cross-country ski base structures. An optimum ski base roughness $R_{q,\text{sbs}}$ of 11 μm is for instance not abnormal under wet snow conditions, thus indicating a possible water film thickness of approximately 90 μm , if $\Lambda \approx 8$ is assumed optimum under such conditions. If the measurements of Ambach and Mayr are assumed exact correct and the width of alpine skis relative cross-country skis is accounted for, Λ -values of 5-7 seem reasonable to assume as optimum for sliding friction of cross-country skis. The qualitative model of ski base sliding friction vs. water film thickness shown in Colbeck (1992) and based on the empirical model of Colbeck (1988) predicts an optimum water film thickness of 8 μm for ski base sliding friction. This prediction seems reasonable for flat sliders with ski base roughness $R_{q,\text{sbs}}$ of 1-2 μm .

This section has described the nature of ski base sliding friction in light of existing theories. The hope is that the rest of this thesis can cast even more light on this nature. In spite of this it is obvious that most issues presented here need more research in order to be fully solved. The main goal of the research so far has been to optimise the ski base structures for relative broad ranges of speeds and snow conditions in order to find robust structures that works good throughout a whole ski race.

In snow friction tests described in the literature, full-scale in-situ measurement and characterisation of snow have never been performed. In order to evolve the understanding of friction against snow the most important snow and weather parameters have to be measured in-situ during accurate sliding tests. The measurement and characterisation of snow in cross-country ski tracks are described in Chapter 5, while search of optimum cross-country ski base structures by means of accurate sliding tests is handled in Chapter 6.

2.3. References

- Ambach, W. and B. Mayr (1981): Ski gliding and water film. *Cold Regions Science and Technology*, Vol. 5, pp. 59-65.
- Balakin, V. A. and O. V. Pereverzeva (1991): Friction against ice and snow. *Soviet Journal of Friction and Wear*, Vol. 12, No. 3, pp. 132-143.
- Bowden, F. P. and T.P. Hughes (1939): The mechanism of sliding on ice and snow. *Proceedings of the Royal Society of London, Series A172*, pp. 280-298.
- Cann, P., E. Ioannides, B. Jacobsen and A. A. Lubrecht (1994): The lambda ratio - a critical re-examination. *Wear*, Vol. 175, pp. 177-188.
- Colbeck, S. C. (1988): Kinetic friction of snow. *Journal of Glaciology*, Vol. 34, No. 116, pp. 78-86.
- Colbeck, S. C., E. Akitaya, R. Armstrong, H. Gubler, J. Lafeuille, K. Lied, D. McClung and E. Morris (1990): International classification for seasonal snow on the ground. *International Commission for Snow and Ice, World Data Center for Glaciology, University of Colorado, Boulder, Colorado*, 23 p.
- Colbeck, S. C. (1992): A review of the processes that control snow friction. *CRREL Monograph 92-2*, 49 p.
- Colbeck, S. C. (1994a): A review of the friction of snow skis. *Journal of Sports Sciences*, Vol. 12, pp. 285-295.
- Colbeck, S. C. (1994b): Bottom temperatures of skating skis on snow. *Medicine and Science in Sports and Exercise*, Vol. 26, No. 2, pp. 258-262.
- Colbeck, S. C. (1995a): Pressure melting and ice skating. *American Journal of Physics*, Vol. 63, No. 10, pp. 888-890.
- Colbeck, S. C. (1995b): Electrical charging of skis gliding on snow. *Medicine and Science in Sports and Exercise*, Vol. 27, No. 1, pp. 136-141.
- Colbeck, S. C. (1996): Capillary bonding of wet surfaces. *Surface and Coatings Technology*. Vol. 81, No. 2-3, pp. 209-214.
- Colbeck, S. C. (1997): Capillary bonding of wet surfaces - the effects of contact angle and surface roughness. *Journal of Adhesion Science Technology*, Vol. 11, No. 3, pp. 359-371.
- Colbeck, S. C., L. Najarian and H. B. Smith (1997): Sliding temperatures of ice skates. *American Journal of Physics*, Vol. 65, No. 6, pp. 488-492.
- CRC (1977): *CRC handbook of chemistry and physics* (R. C. Weast, Ed.). CRC Press, Cleveland, Ohio, pp. D-53.
- Erkkilä, J. , T. Hämäläinen, P. Pihkala, S. Savolainen and E. Spring (1985): A cinematographic method for determination of the kinetic friction of skis on snow. *Report Series in Geophysics, University of Helsinki*, Vol. 21, pp. 1-15.
- Evans, D. C. B., J. F. Nye and K. J. Cheeseman (1976): The kinetic friction of ice. *Proceedings of the Royal Society of London, Series A347*, pp. 493-512.
- Geisbühler, U. (1995, personal communication): Ski base characteristics from IMS Kunststoff AG, Ittigen, Switzerland.
- Glenne, B. (1981): Mechanics of skis. In *Handbook of Snow. Principles, Processes, Management and Use* (D. M. Gray and D. H. Male, Ed.), Pergamon press, Toronto, pp. 741-756.
- Glenne, B. (1987): Sliding friction and boundary lubrication of snow. *Journal of Tribology, Transactions of the ASME*, Vol. 109, No. 4, pp. 614-617.
- Glenne, B., A. DeRocco and J. Vandergrift (1997): The modern alpine ski. *Cold Regions Science and Technology*, Vol. 26, pp. 35-38.

- Gray, D. M. and D. H. Male (1981): Handbook of snow. Principles, processes, management and use. Pergamon press, Toronto, 776 p.
- Guha, D. and S. K. Roy Chowdhuri (1996): The effect of surface roughness on the temperature at the contact between sliding bodies. *Wear*, Vol. 197, No. 1-2, pp. 63-73.
- Hämäläinen, T. and E. Spring (1986): Influence of snow hardness on ski friction. *Commentationes Physico-Mathematicae*, Vol. 76, 17 p.
- Hamrock, B.J. and D. Dowson (1981): Ball bearing lubrication - The elastohydrodynamics of elliptical contacts. Wiley-Interscience, New York, pp.121.
- Hamrock, B. J. (1994): Fundamentals of fluid film lubrication. McGraw-Hill, New York, 690 p.
- Hensvold, E. (1985): Metod for fältmässig mätning av friktion och glidmotstånd mot snö och is. Tekniska Högskolan i Luleå, Avdelning for Transportteknikk. In *Proceedings of Winter Knowledge and Winter Data Conference*, 26.-28. March, Örnsköldsvik, Sverige. Cooperative for Vehicle Field Research, SFM Meddelande, No. 35 (in Swedish), pp. 291-300.
- Hess, S. L. (1959): Introduction to theoretical meteorology. Holt, Rinehart and Winston, New York, 362 p.
- Hirano, Y. and N. Tada (1996): Numerical simulation of a turning alpine ski during recreational skiing. *Medicine and Science in Sports and Exercise*, Vol. 28, No. 9, pp. 1209-1213.
- IMS Kunststoff AG (1998): Data Sheet, P-tex 2000 Electra. IMS Kunststoff AG, Ittigen, Switzerland, 1 p.
- Itagaki, K., N. P. Huber and G. E. Lemieux (1989): Dynamic friction of a metal runner on ice. I. Model sled test. CRREL Report 89-14, 23 p.
- K2 (1996): K2 SkiBook. K2 Corporation, Vashon Island, Washington, 40 p.
- Kuroiwa, D. (1977): Kinetic friction on snow and ice. *Journal of Glaciology*, Vol. 19, No. 81, pp. 141-152.
- Lehtovaara, A. (1989): Kinetic friction between ski and snow. *Acta Polytechnica Scandinavica, Mechanical Engineering Series*, No. 93, Helsinki, 52 p.
- Leino, M. A. H., E. Spring and H. Suominen (1983): Methods for the simultaneous determination of air resistance to a skier and the coefficient of friction of his skis on the snow. *Wear*, Vol. 86, pp. 101-104.
- Leino, M. A. H. and E. Spring (1984): Determination of the coefficient of kinetic friction between ski and snow from the gliding velocity of a skier. *Report Series in Geophysics, University of Helsinki*, Vol. 19, pp. 1-11.
- Lind, D. and S. P. Sanders (1996): The physics of skiing: skiing at the triple point. Springer Verlag, New York, 268 p.
- Løset, S., T. Carstens, E. Hammer and J.E. Stokkan (1995): Is i Vikingskipet - Del I. SINTEF, NHL, Report No. STF60 A058 (in Norwegian), 24 p.
- Mathia, T. G., A. Midol, P. Lanteri and R. Longerey (1989): Topography, physico-chemistry and wear in sliding of ski soles in regard to rheology of snow. In *Proceedings of Eurotrib 89*, Elsevier, Amsterdam, pp. 253-260.
- Mathia, T. G., H. Zahouani and A. Midol (1992): Topography, wear, and sliding functions of skis. *International Journal of Machine Tools Manufacturing*, Vol. 32, No. 1/2, pp. 263-266.
- MatWeb (1998): Electrical properties of polyethylene, high density; moulded/extruded. <http://www.matweb.com>.
- Mayr, B. (1979): Ein Beitrag zur Physik des Schigleitens: Elektronische Messung des Wasserfilms beim Gleitvorgang. Dissertation zur Erlangung des Doktorgrades an der Naturwissenschaftlichen Fakultät der Leopold-Franzens-Universität Innsbruck (in German), 152 p.

- McConica, T. H. (1950) Sliding on ice and snow. American Ski Co. Technical Report, 46 p.
- Mellor, M. (1964): Properties of snow. CRREL Monograph III-A1, 105 p.
- Midol, A. and T. G. Mathia (1985): Actes de Colloque Sport, un Enjau Technologique, Paris, *La glisse 1985*. Ed., Sporettec-Lyon.
- Moldestad, D. A. (1995): PC-basert system for måling og valg av sålestruktur på langrennsski. The Norwegian Institute of Technology, Department of Engineering Cybernetics, Thesis (in Norwegian), 82 p.
- Moore, D. F. (1975): Principles and applications of tribology, Pergamon Press, Oxford, United Kingdom, 388 p.
- Nørstrud H. (1997): Skihopp og aerodynamikk, Gunnerus-forelesning, Det Kgl. Norske Videnskabers Selskabs Forhandling 1997 (in Norwegian), 12 p.
- Oksanen, P. (1980): Coefficient of friction between ice and some construction materials, plastics and coatings. Laboratory of Structural Engineering, Espoo, Report 7, 73 p.
- Oksanen, P. and J. Keinonen (1982): The mechanism of friction of ice. *Journal of Wear*, Vol. 78, pp. 315-324.
- Patir, N. and Cheng, H. S. (1978): Effect of surface roughness on the central film thickness in EHD contacts. *Elastohydrodynamics and Related Topics. Proceedings of the Fifth Leeds-Lyon Symposium on Tribology*, Institution of Mechanical Engineers, London, pp. 15-21.
- Peklenik, J. (1968): New developments in surface characterization and measurements by means of random process analysis. *Properties and Metrology of Surfaces. Proc. Inst. Mech. Eng.*, London, Vol. 182, Part 3K, pp. 108-114.
- Perla, R. and B. Glenne (1981): Skiing. In *Handbook of Snow. Principles, Processes, Management and Use* (D. M. Gray and D. H. Male, Ed.), Pergamon press, Toronto, pp. 709-740.
- Perry, R. H. and D. W. Green (1984): Perry's chemical engineers' handbook sixth edition. McGraw-Hill, New York, pp. 3-78.
- Petrenko, V. F. (1994): The effect of static electric fields on ice friction. *Journal of Applied Physics*, Vol. 76, No. 2, pp. 1216-1219.
- Petrenko, V. F. and S. C. Colbeck (1995): Generation of electric fields by ice and snow friction. *Journal of Applied Physics*, Vol. 77, No. 9, pp. 4518-4521.
- Pikhala, P. and E. Spring (1986): Determination of the contact area between ski and snow using a simple thermal conductivity meter. Helsinki University, Department of Geophysics, Geophysics Report Series, No. 22, 12 p.
- Reynolds, O. (1901): Papers on mechanical and physical Subjects, Vol. 2. Cambridge University Press, pp. 734-738.
- Sahashi, T. and S. Ichino (1998): Coefficient of kinetic friction of snow skis during turning descents. *Japanese Journal of Applied Physics*, Part 1, Vol. 37, No. 2, pp. 720-727.
- Schultes, H. (1980): The alpine ski (R. Gammons, Ed.). Olin ski company, Middletown, Connecticut. Printed by Horton Printing, Meriden, Connecticut, 165 p.
- Shimbo, M. (1961): Mechanism of sliding on snow. In *General Assembly of Helsinki*, International Association of Scientific Hydrology Publication No. 54, Gentbrugge, Belgium, pp. 101-106.
- Shimbo, M. (1971): Friction on snow of ski soles, unwaxed and waxed. In *Scientific Study of Skiing in Japan* (The Society of Ski Science, Ed.). Tokyo: Hitachi, Ltd., pp. 99-112.
- Slotfeldt-Ellingsen, D. and L. Torgersen (1982): Glienskaper til skisåler i polyetylen. Report No. 820113-2 (in Norwegian), SI, Oslo, 64 p.
- Slotfeldt-Ellingsen, D. and L. Torgersen (1983): Water in ice: influence on friction. *Journal of Physics D: Applied Physics*, Vol. 16, pp. 1715-1719.

- Spring, E. (1988): A method for testing the gliding quality of skis. *Tribologia*, Vol. 7, No. 1, pp. 9-14.
- Spring, E., S. Savolainen, J. Erkkilä, T. Hämäläinen and P. Pihkala (1988): Drag Area of a Cross-Country Skier. *International Journal of Sport Biomechanics*, Vol. 4, pp. 103-113.
- Spring, E. (1989): Ski tribology. *Acta Polytechnica Scandinavica*, No. 64, pp. 108-119.
- Stemsrud, F. and H. Brun (1976): Skiforskning ved Norges Landbrukshøgskole og Sentralinstitutt for Industriell forskning. Note from SI, Oslo, Norway (in Norwegian).
- Street, G. M. and P. Tsui (1987): Composition of glide waxes used in cross country skiing. Biomechanics Laboratory, Pennsylvania State University, College Station, Pennsylvania.
- Sturm, M., J. Holmgren, M. König and K. Morris (1997): The thermal conductivity of seasonal snow. *Journal of Glaciology*, Vol. 43, No. 143, pp. 26-41.
- SWIX (1996): Alpine Ski Preparation Tech Manual, PR 952 N, SWIX SPORT, Lillehammer, Norway, 38 p.
- Tiuri, M., A. Sihvola, E. Nyfors and M. Hallikainen (1984): The complex dielectric constant of snow at microwave frequencies. *IEEE Journal of Oceanic Engineering*, Vol. OE-9, No. 5, pp. 377-382.
- Torgersen, L. (1983): Good Glide. Human Kinetics, Champaign, Illinois.
- Warren, G. C., S. C. Colbeck and F. E. Kennedy (1989): Thermal response of downhill skis. CRREL Report 89-23, 43 p.
- Williamson, J. B. P. (1984): The shape of surfaces. In *CRC Handbook of Lubrication. Theory and Practice of Tribology. Volume II. Theory and Design* (E. R. Booser, Ed.). CRC Press Inc., Boca Raton, Florida, pp. 3-16.

3. The ski base structure analyser - SSA

Notation

a	angle between projection from optical unit and measurement surface, radians or °
dz	equidistance, e.g. 45 μm
$G(u,v)$	2-D Fourier transform of a measured surface image, i.e. a height matrix $z(x,y)$ transformed to e.g. an 8-bit image
$g(x,y)$	grey level value of a pixel in a measured surface image, i.e. a height matrix $z(x,y)$ transformed to e.g. an 8-bit image
g_{max}	maximum value of the grey scale
i	index
$I(u,v)$	imaginary part of the 2-D Fourier transform of a measured surface image, i.e. a height matrix $z(x,y)$ transformed to e.g. an 8-bit image
$I_a(x,y)$	modulation amplitude in an image pixel for the stripe pattern that the optical unit 11 projects
$I_0(x,y)$	intensity of an image pixel without projection from the optical unit 11
$I_1(x,y)$	intensity of an image pixel when the piezoelectric transducer has given the reference beams an optical phase shift, $0 < \alpha = \alpha_1 < 90^\circ$, with respect to the object beams
$I_2(x,y)$	intensity of an image pixel when the piezoelectric transducer has given the reference beams an optical phase shift, $\alpha_1 + 90^\circ$, with respect to the object beams
$I_3(x,y)$	intensity of an image pixel when the piezoelectric transducer has given the reference beams an optical phase shift, $\alpha_1 + 180^\circ$, with respect to the object beams
$I_4(x,y)$	intensity of an image pixel when the piezoelectric transducer has given the reference beams an optical phase shift, $\alpha_1 + 270^\circ$, with respect to the object beams
j	$\sqrt{-1}$
l^*	bearing length of a surface profile, mm
M	number of sampled points in the x -direction, i.e. number of columns in the measured surface image

n	number of peaks above a given level parallel and above the mean line of a surface profile
N	number of registrations in Eq. (3.8)
N	number of sampled points in the y -direction, i.e. number of rows in the measured surface image in Eqs. (3.10) and (3.14)
$O_{\alpha}(x,y)$	phase matrix for the object
$R(u,v)$	real part of the 2-D Fourier transform of a measured surface image, i.e. a height matrix $z(x,y)$ transformed to e.g. an 8-bit image
R_a	the arithmetic mean of a surface profile, μm
$R_{a,2D}$	R_a for a surface relative to a reference plane parallel with the xy plane, μm
$\bar{R}_{a,x}$	mean of the R_a of the rows in a measured surface image, i.e. along the ski, when each row has an individual reference line parallel to the x -axis, μm
$\bar{R}_{a,xs}$	mean of the R_a of the rows in a measured surface image, i.e. along the ski, when each row has an individual possibly sloping reference line relative to the x -axis, μm
$\bar{R}_{a,y}$	mean of the R_a of the columns in a measured surface image, i.e. across the ski, when each column has an individual reference line parallel to the y -axis, μm
$\bar{R}_{a,ys}$	mean of the R_a of the columns in a measured surface image, i.e. across the ski, when each column has an individual possibly sloping reference line relative to the y -axis, μm
R_q	the root mean square (rms) of a surface profile, μm
$R_{q,2D}$	R_q for a surface relative to a reference plane parallel with the xy plane, μm
$\bar{R}_{q,x}$	mean of the R_q of the rows in a measured surface image, i.e. along the ski, when each row has an individual reference line parallel to the x -axis, μm
$\bar{R}_{q,y}$	mean of the R_q of the columns in a measured surface image, i.e. across the ski, when each column has an individual reference line parallel to the y -axis, μm
R_t	maximum peak-to-valley height for a surface profile, μm
$R_{t,2D}$	R_t for a surface, μm
$\bar{R}_{t,x}$	mean of the R_t of the rows in a measured surface image, i.e. along the ski, when each row has an individual reference line parallel to the x -axis, μm
$\bar{R}_{t,y}$	mean of the R_t of the columns in a measured surface image, i.e. across the ski, when each column has an individual reference line parallel to the y -axis, μm
$R_{\alpha}(x,y)$	phase matrix for a plane reference surface
T	characteristic period perpendicular to the characteristic direction for a measured surface, mm
u	frequency variable in the x -direction, $u = 0, 1, 2, \dots, M - 1$
v	frequency variable in the y -direction, $v = 0, 1, 2, \dots, N - 1$
x	direction along the ski
(x,y)	position of an image pixel
x_c	x -coordinate relative to the origin for a bright point in the 2D Fourier spectrum of a measured surface image, pixels
x_r	resolution in the x -direction for the measured surface image, mm/pixel
y	direction across the ski
y_c	y -coordinate relative to the origin for a bright point in the 2D Fourier spectrum of a measured surface image, pixels
y_r	resolution in the y -direction for the measured surface image, mm/pixel
z	profile height, μm

$z(x,y)$	height matrix, μm
z^*	distance of the mean value of z from the value chosen as the origin of the height axis, z^* equals zero if the mean line of the profile is set as the origin of the height axis, μm
z_i	surface height registrations on a surface profile, μm
α	optical phase shift angle between reference beams and object beams, radians or $^\circ$
α_1	initial optical phase shift angle between reference beams and object beams, radians or $^\circ$
$\alpha'(x,y)$	phase difference between the object beams and the phase shifted reference beams in an image pixel, radians or $^\circ$
$\beta(x,y)$	phase difference caused by the texture of the measured object, radians or $^\circ$
γ_c	surface pattern parameter
δ	angle relative to the x -axis for a vector from the origin to the bright point in the 2D Fourier spectrum of a measured surface image, the angle must be adjusted accordingly if the resolution of the measured surface image is different in the x - and y -direction, radians
Δ	sample interval, mm
θ	phase angle between two light beams emitted from the same source (Mercer and Beheim, 1992), radians or $^\circ$
λ_x	autocorrelation length in the x -direction, i.e. the direction along the ski, mm
λ_y	autocorrelation length in the y -direction, i.e. the direction across the ski, mm
$\tilde{\rho}_k$	autocorrelation parameter
$\bar{\sigma}$	standard deviation of the profile given by R_q , see Eq. (3.6), μm
ϕ	characteristic angle relative to the x -axis for a measured surface, radians
$\tilde{\psi}$	probability density function of the height distribution of a profile

3.1. Introduction

For skis applied in competitions the requirements to the sliding surfaces are high. One of the major ski parameters is the ski base structure. The ski base structure contains grooves aligned along the ski that is in the order of 10^{-1} mm wide and 10^{-2} - 10^{-1} mm deep. It is important to be able to characterise the surface topography and roughness of this structure, for instance in order to select competition skis with optimum sliding properties under different snow conditions.

Systematic measurements of high-quality ski base structures have been paid very little attention to in literature. However, Mathia et al. (1989 and 1992) have reported the development of a 3D profilometer for systematic study of micro and macro topography of ski bases, but they did not characterise different types of ski base structures or study the effect of different ski base structures on ski base sliding friction in their papers. Surface topography has important implications for wear, friction, lubrication, fatigue, sealing, painting and bearing surfaces, and related measurement problems exists in metals, plastics as well as electronics industry.

Grinding of ski bases is performed with a stone grinding machine. The primary components of the stone grinding machine are the stone and the diamond. The diamond can be positioned on the stone surface transversally to the rotational direction of the stone. Moving the diamond transversally over

the surface while the stone rotates provides grooves on the stone surface (Fig. 3.1). During grinding the groove pattern on the stone surface produces and decides the structure of the ski base. The roughness of the ski base structure is varied by the transversal speed of the diamond over the stone surface. If the transversal speed is low, the structure will be shallow, since the diamond in that case will grind a lot of the stone.

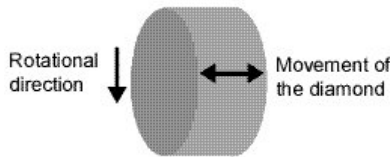


Fig. 3.1. Principle sketch of stone grinding.

The minerals in the stone surface get blunt during ski grinding, and after that a couple of dozens of ski pairs have been ground, the stone loses the ability to provide sharp grooves in the ski base. The pattern in the stone surface must then be restructured. The diamond is also worn during use, and must be changed from time to time.

When setting the surface of the stone, the rotational speed of the stone is typically 1300 rotations per minute. The rotational speed of the stone is lower when grinding the skis, but a constant speed is used also then. This speed can be adjusted, but a low speed is preferable in order to avoid frictional heating of the ski base and thereby a burnt ski base.

By moving the diamond back and forth over the stone, a cross structure is produced in the ski base. On the contrary, if the diamond is moved only one way, a line structure is produced.

Both non-contact and contact methods are used for measuring the surface structure of an object. The contact method is based on a sensor head that traverses the surface while in contact. Normally the sensor head or stylus has a tip radius of about $2\ \mu\text{m}$ and a static load of less than $0.0007\ \text{N}$ (Hamrock, 1994). Such a sensor head would not give a correct measurement result if the object material is soft, or the movement of the sensor head is obstructed during the measurement. This may be a problem for ski bases of polyethylene prepared with glider products based on fluor or hydrocarbons. Non-contact measurement methods are therefore preferable in that case.

It is well known to use phase-measurement interference (PMI) techniques to detect surface characteristics, see e.g. Creath (1988). However, no appropriate portable method/instrumentation has so far existed for performing rapid, repeatable and non-destructive measurements of 3-D surface textures of sliding surfaces, i.e. skis, snow boards or similar equipment made for sliding on snow.

Mercer and Beheim (1992) described a system for surface topography measurement based on phase shifting, projected fringes and use of fibre optics. A projected fringe interferometer designed for measuring the topography of an object shifts stepwise and periodically the phase angle θ between two light beams emitted from the same source. The steps are $\pi/2$ radians (90°) apart, and at each step a video image of the fringes is registered and stored. Photo detectors measure either the phase angle θ of the beams or 2θ , and one of these angles is used to control one of the light beams so that the $90^\circ - \theta$

angle is accurately maintained. A camera, computer, phase modulator and phase controller establish closed-loop control of θ . A calibration reference is found by measuring the phase matrix of a plane surface.

The phase controller described by Mercer and Beheim gives a precise phase shift, but do require specially designed electronics (Fig. 2 in Mercer and Beheim, 1992) that hampers a flexible integration with present portable computers. A D/A card and a framegrabber card can easily control our measurement system. Thereby a compact and portable system can be obtained, where:

- A piezoelectric transducer controls the phase shift between the object beams and the reference beams by adjusting the position of a mirror in the path of the reference beams.
- A D/A-card in a portable computer controls the piezoelectric transducer.

3.2. Basic theory of the SSA instrumentation and measurement technology

The purpose of the development of the SSA (Ski base Structure Analyser) has been to provide a portable measurement device that can give rapid, precise, repeatable and non-destructive 3-D measurements of surface topography. Furthermore the device was intended to execute the measurements statically, i.e. without relative movement between the device and the object.

The SSA applies a method and instrumentation that is specifically designed for measuring texture and roughness of black ski base surfaces, but measurements can also be performed on other one-coloured, dim surfaces. By measuring several test fields on the ski base surface, a sufficient precise estimate of the roughness characteristics of the total ski base surface can be given. The instrumentation of the SSA is designed to be compact and easily portable in order to be able to do measurements independent of special laboratory facilities. Furthermore the SSA has a physical design that allows different dimensions and flexible positioning of the sliding surfaces that shall be measured.

The SSA measurement provides both a graphical presentation (see Fig. 3.2) and a numerical characterisation (surface roughness or texture) of the measured surface. Characterisation of ski base structure topography by the SSA is further described in Section 3.3.

The SSA measurement technology is in the following described by referring to Figs. 3.2 - 3.5, where:

- Fig. 3.2 depicts a principle sketch of the SSA technology and a graphical presentation of the measured surface.
- Fig. 3.3 shows the major elements of the SSA technology and how it interacts with the measurement object.
- Fig. 3.4 shows a block diagram of the optical unit (interferometer) that transforms the laser beam to projected fringes.
- Fig. 3.5 shows a sketch of the arrangement of the compact SSA instrument construction.

In Fig. 3.3 we see the optical unit 11 project an area of the ski base 13 with an interference pattern in form of projected fringes. The optical unit 11 is designed as described in Fig. 3.4. The projection 12,

which is further described below, is emitted by the optical unit 11 at an angle α to the surface 13. The structure of the measurement surface deflects the interference pattern in form of projected fringes, and the measurement surface with deflected pattern is registered at different phase shifts (see also the explanation of Figs. 3.4 and 3.5) with the camera lens 14 of the CCD-camera 15. The CCD-camera 15 is connected to a framegrabber in a portable computer where further registration and processing of data are performed as described below.

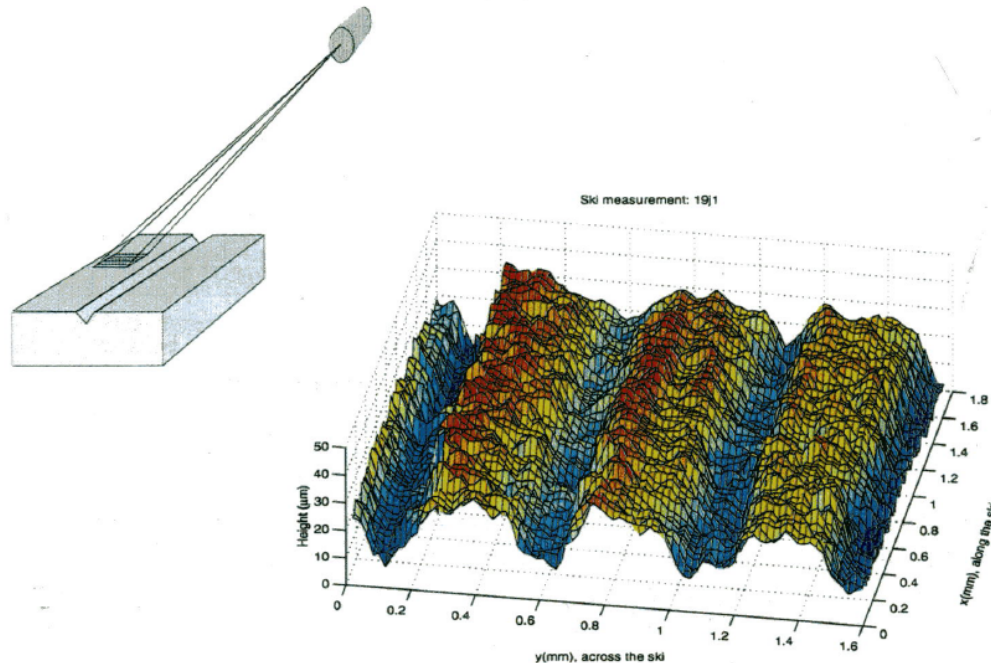


Fig. 3.2. Principle sketch of the SSA measurement technology and graphical presentation of the measurement result.

The CCD-camera 15 with camera lens 14 register images from a defined area of a surface 13, e.g. an area of approximately 11×15 mm or larger. Normally this will provide sufficient amount of data to characterise the surface area of interest accurately. A sliding surface may well have different roughness at different test areas on the surface, e.g. on the forebody and the afterbody of the ski. Thus measurements should be provided from different areas of the sliding surface in order to obtain optimum characteristics and knowledge on the sliding surface.

Fig. 3.4 shows a possible flow chart for an optical unit 11 (interferometer) that transforms a laser beam to projected fringes. A laser 16 emits a beam 17 to a microscope objective 18 where the beam is scattered 19. The scattered beams enter the beam splitter 20 that splits the beams into two parts, object beams 21 and reference beams 20. The two parts have the same intensity. The reference beams 22 are phase shifted in a systematic manner relative to the object beams 21 by a piezoelectric transducer 23 that is controlled by a D/A-card in a portable computer. The setup in the portable computer is not shown. The optical phase shift angle α can start between 0 and 90° (α_1) and then be increased in steps, e.g. by 90, 180 and 270° .

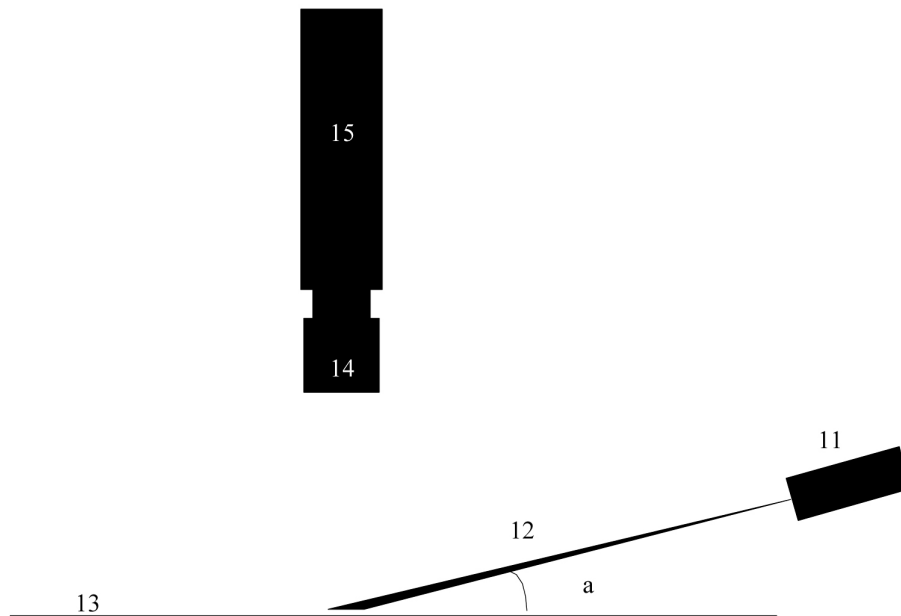


Fig. 3.3. Major elements of the SSA technology.

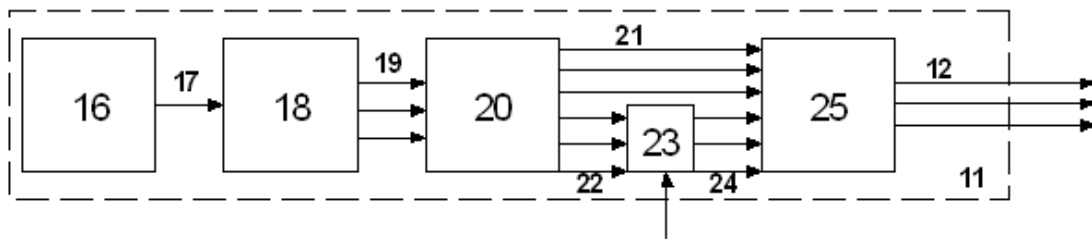


Fig. 3.4. Possible flow chart for an optical unit (interferometer) that transforms a laser beam to projected fringes.

The object beams 21 and the phase shifted reference beams 24 are then combined in a beam combiner 25 where they interfere after having propagated different distances. This causes an interference pattern in form of projected fringes 12 on the surface 13. The intensity of a pixel in the image registered by the CCD-camera (15), is given by:

$$I_1(x, y) = I_0(x, y) + I_a(x, y) \cos(\alpha'(x, y)) \quad (3.1)$$

where:

- $I_1(x,y)$ - intensity of an image pixel when the piezoelectric transducer has given the reference beams an optical phase shift, $0 < \alpha = \alpha_1 < 90^\circ$, with respect to the object beams
- $I_0(x,y)$ - intensity of an image pixel without projection from the optical unit 11
- $I_a(x,y)$ - modulation amplitude in an image pixel for the stripe pattern that the optical unit 11 projects

- $\alpha'(x,y)$ - phase difference between the object beams 21 and the phase shifted reference beams 24 in an image pixel, radians or $^\circ$
- (x,y) - position of an image pixel

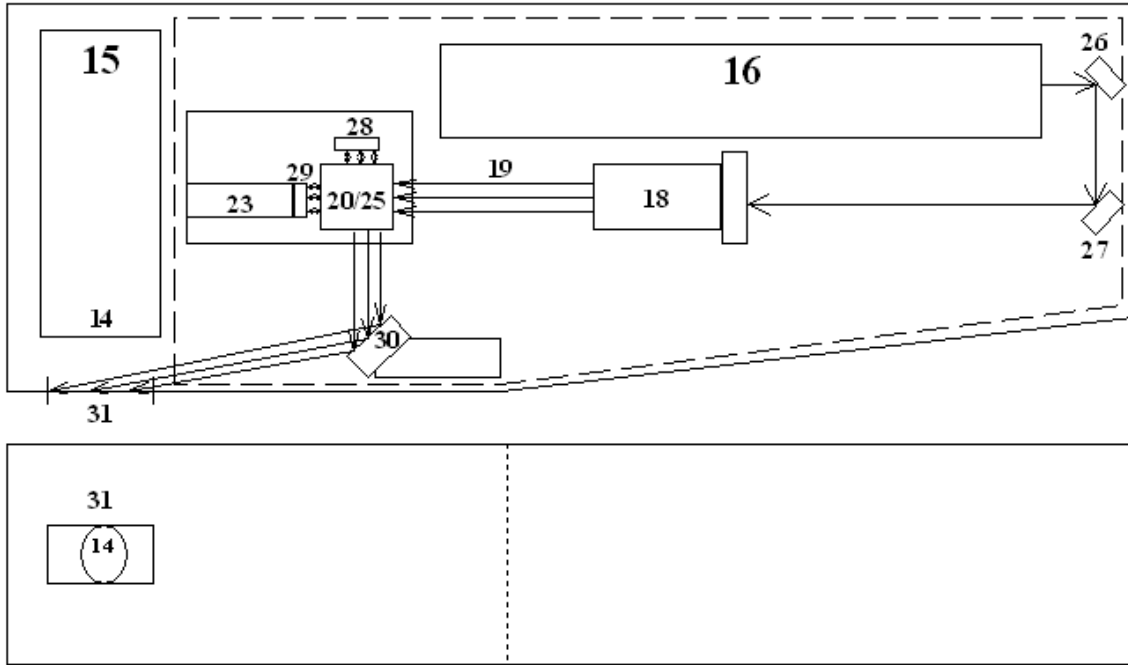


Fig. 3.5. Sketch of the arrangement of the compact SSA instrument construction.

The phase shift α can for instance be increased stepwise by 90° in such a way that four images with different intensities $I_1(x,y)$, $I_2(x,y)$, $I_3(x,y)$ and $I_4(x,y)$ are registered with the camera (15). From these images a computer can calculate the phase difference $\alpha'(x,y)$ between the object and phase shifted reference beams in each image pixel:

$$\alpha'(x,y) = \arctan \left[\frac{I_3(x,y) - I_1(x,y)}{I_2(x,y) - I_4(x,y)} \right] \quad (3.2)$$

This method for calculating the phase difference $\alpha'(x,y)$ is called a 4-step technique (Creath, 1988). The phase difference can also be estimated by a 3-step technique. For more details, see e.g. Creath (1988).

Eq. (3.2) gives the phase difference $\alpha'(x,y)$ in the different image pixels values between $-\pi$ and π . For $\alpha'(x,y) < 0$, 2π is added, thus $\alpha'(x,y)$ is assigned values between 0 and 2π . The system then transforms the adjusted $\alpha'(x,y)$ linearly to image pixel values between 0 and the maximum value of the grey scale, g_{\max} . The phase matrix of the object $O_\alpha(x,y)$ is then found as:

$$O_\alpha(x,y) = \alpha'(x,y) \left(\frac{g_{\max}}{2\pi} \right) \quad (3.3)$$

For a system with an 8-bit grey tone scale, g_{\max} equals 255.

The phase matrix of the object, $O_\alpha(x,y)$, is compared with the phase matrix of a plane reference surface, $R_\alpha(x,y)$, that is found with the same procedure as $O_\alpha(x,y)$. $R_\alpha(x,y)$ is stored in advance in the computer program that controls the measurement procedure. The program user can therefore choose between generating a new phase matrix for a plane reference surface or using the stored phase matrix from an earlier calibration of a plane reference surface. The height matrix, $z(x,y)$, is obtained in the following way:

$$\beta(x, y) = \left(\frac{2\pi}{g_{\max}} \right) (O_\alpha(x, y) - R_\alpha(x, y)) \quad (3.4a)$$

$$z(x, y) = \beta(x, y) \frac{dz}{2\pi} \quad (3.4b)$$

where:

- $\beta(x,y)$ - phase difference caused by the texture of the measured object, radians or $^\circ$
- dz - equidistance, e.g. 45 μm

The equidistance dz is found from a calibration procedure where the user moves an object manually in the z -direction with a micrometer system, while a new image is registered after each movement. When the image repeats itself after the projected fringes have moved one period in the image, the displacement in the z -direction can be read on the micrometer system, and the equidistance dz can be found. This calibration procedure is performed initially for a new instrument and later say once a year. The value of dz is stored in the computer program that controls the measuring device. In the prototype dz is set to 45 μm . Surface topography of sliding surfaces will normally be in the range 0-45 μm .

$O_\alpha(x,y)$ and $R_\alpha(x,y)$ in Eq. (3.4a) is assumed to take on values between 0 and g_{\max} . Thus the quadrants must be considered in the subtraction of the phase matrices, i.e. for $\beta(x,y) < 0$ in Eq. (3.4a), 2π must be added.

In order to reconstruct the surface topography of the measured object correctly, $z(x,y)$ needs to be unwrapped. This is performed by correcting $\beta(x,y)$ when the phase difference between adjacent pixels is larger than π . More details can be found in e.g. Creath (1988), Section 3.7. After $z(x,y)$ has been unwrapped, the surface topography of the sliding surface can be displayed in 3D as e.g. shown in Fig. 3.2. The ski base structure topography can also be characterised numerically. This is as mentioned earlier further described in Section 3.3.

Fig. 3.5 shows the arrangement of the compact SSA instrument construction. A He-Ne laser 16 emits a beam to a microscope objective 18 via the mirrors 26 and 27. The microscope objective scatters the beam prior to the input of unit 20/25, which is a combined beam splitter and beam combiner. Here the scattered beams are split into two parts with equal intensity, the parts enter mirrors 28 and 29 respectively. The mirrors reflect the beam parts and return them to unit 20/25 where they again are combined (interfered) before entering mirror 30 and thereafter being projected out the camera opening 31. By means of the piezoelectric transducer 23 that is controlled by a D/A-card in a portable computer, mirror 29 can be adjusted in such a way that the distance to unit 20/25 can be controlled.

This means that a phase shift can be introduced between the two beam parts that propagate 20/25-28-20/25 and 20/25-29-20/25, respectively. By putting the measurement surface 13 against the opening of the camera 31, fringes are projected on the measurement surface 13. Images at different phase shifts are then easy to register by the camera lens 14 of the CCD-camera 15, and the structure and roughness of the measurement surface 13 can be found. In Fig. 3.6 the SSA is shown in use.



Fig. 3.6. The SSA shown in use.

3.3. Basic theory of the SSA characterisation of ski base structure topography

A number of different parameters can be used to characterise the surface topography. Some of the most common are described in this section. Most of the parameters are described for two dimensions, i.e. a row or a column of the height matrix $z(x,y)$ or a submatrix of $z(x,y)$. Parameters that are extended to three dimensions, i.e. the whole height matrix $z(x,y)$ or a submatrix of $z(x,y)$, are calculated according to the same principles as for two dimensions.

The geometric characteristics, or texture, of a surface as shown in Fig. 3.7, can typically be divided into three main categories:

- Error of form
- Waviness
- Roughness

Most measurement methods concentrate on roughness when characterising the surface.

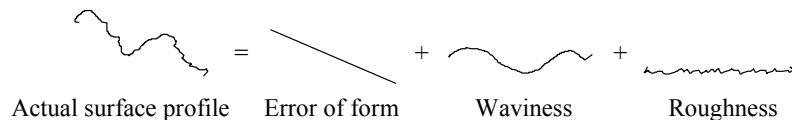


Fig. 3.7. Geometric characteristics of a surface.

There are several ways of characterising the texture of a surface from a surface profile. In most of the methods a reference line is defined (see Fig. 3.8). All the discrete height measurements z_i , $i = 1, 2, \dots, N$, refer to this reference line that can be chosen by means of:

- a) The mean line method (M-method) is a method where the reference line is the centroid of the profile (the areas above and below the line are equal). The method provides a horizontal reference, which does not consider the slope of the profile (see Fig. 3.8a).
- b) The ten-point-mean method is based on finding the five highest peaks and the five lowest valleys. The mean of these 10 points provides the reference line (see Fig. 3.8b).
- c) The least squares method is based on a sloping reference line instead of a horizontal reference line as is the case for the M-method. Thus this method can compensate for the tilt (linear error of form) of the profile (see Fig. 3.8c).

Reference lines based on the M-method or the least squares method give a mean value of z_i equal to 0. The three different surface parameters R_a (arithmetic mean roughness), R_q (root mean square roughness) and R_t (maximum peak-to-valley height) may be calculated from a discrete set of height measurements z_1, z_2, \dots, z_N . Definitions of these parameters have already been given in Eqs. (2.12)-(2.14) in Chapter 2. If a Gaussian height distribution is assumed, R_q will be equal to the standard deviation of the height profile. Normally $R_a \leq R_q \leq R_t$.

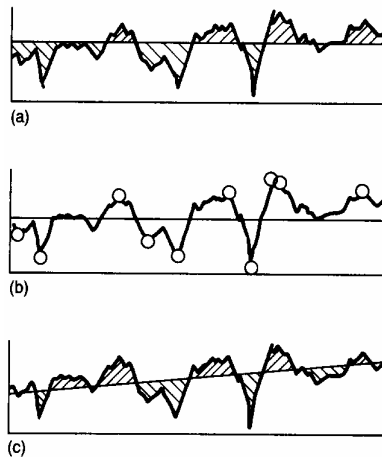


Fig. 3.8. Comparison of three types of reference lines: a) The M-method, b) the ten-point-mean, and c) the least squares method (Hamrock, 1994).

Fig. 3.9 shows six different surface profiles with the same R_a -values. This demonstrates that there can be major differences between surfaces with equal R_a -values. The R_a -, R_q - and R_t -values depend on the profile heights, but are independent of the distances between the heights.

The bearing length l^* can be used to characterise the length of the peaks of a surface. The bearing length of a surface profile is determined by cutting the profile peaks with a line on a given level above and in parallel with the mean line (Fig. 3.10). The bearing length is defined as:

$$l^* = l_1^* + l_2^* + \dots + l_n^* \quad (3.5)$$

The profile bearing length ratio, t_p , is given by:

$$t_p = \frac{l^*}{l} \quad (3.6)$$

where:

l - profile length, mm

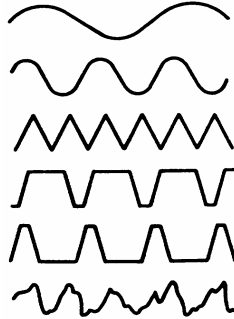


Fig. 3.9. Geometric profiles with the same R_a -values (Halling, 1976).

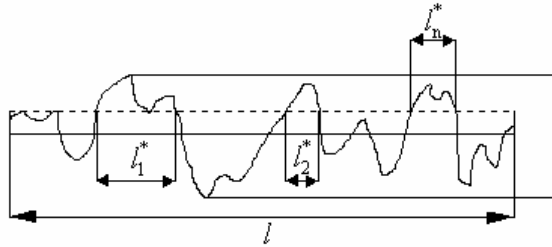


Fig. 3.10. Surface profile showing bearing length.

Abbott and Firestone (1933), the founders of profilometry, have defined the so-called Abbott curve. The profile is then divided into levels that are parallel with the mean line and lie between the maximum point and the minimum point of the profile. By measuring the percentage of the sample length that is above the different levels, the Abbott curve can be deduced. Fig. 3.11 shows how the Abbott curve is derived.

The probability density function of the height distribution of a profile, $\tilde{\psi}$, can be found by assuming a Gaussian height distribution and is given by:

$$\tilde{\psi} = \frac{1}{\bar{\sigma}\sqrt{2\pi}} \exp\left[-\frac{(z - z^*)^2}{2\bar{\sigma}^2}\right] \quad (3.7)$$

where:

z - profile height, μm

$\bar{\sigma}$ - standard deviation of the profile given by R_q , see Eq. (3.6), μm

- z^* - distance of mean value of z from the value chosen as the origin of the height axis, z^* equals zero if the mean line of the profile is set as the origin of the height axis, μm

The probability density function indicates the same as the histogram of a surface or profile.

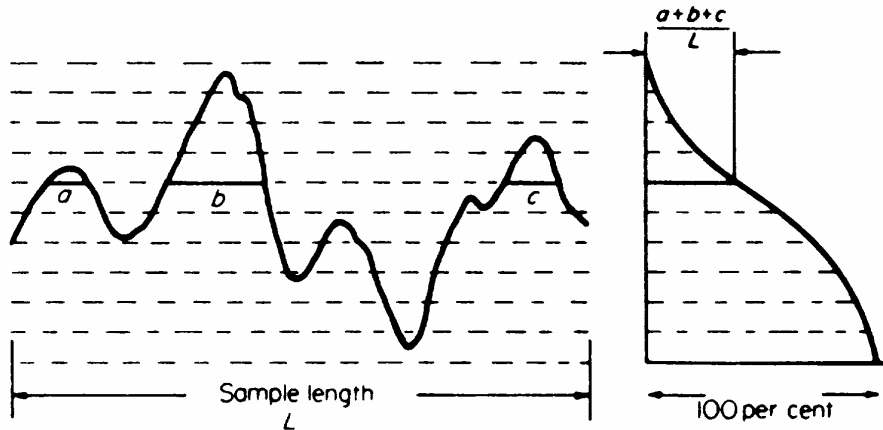


Fig. 3.11. Derivation of the Abbott curve (Halling, 1975).

The autocorrelation parameter, $\tilde{\rho}_k$, incorporates the distance between heights and is found by multiplying the individual profile heights with the heights of points at a fixed horizontal distance further along the profile. The autocorrelation parameter is defined as:

$$\tilde{\rho}_k = \frac{1}{R_q^2(N-k)} \sum_{i=1}^{N-k} z_i z_{i+k} \tag{3.8}$$

The autocorrelation parameter depends on k and is a measure of the similarity of heights separated by a distance $k\Delta$ (where Δ is the sample interval and assumed to be constant). Fig. 3.12 shows a plot of the autocorrelation functions and the probability density functions for two different profiles. The oscillating component of the autocorrelation function indicates the periodicity of the profile as shown in Fig. 3.12a. The general decrease of the autocorrelation function as $k\Delta$, increase indicates the noise component of the profile as shown in Fig. 3.12b.

Many surfaces have a roughness that is directionally oriented. This can be described by e.g. the surface pattern parameter γ_c , that has already been defined in Eq. (2.15) in Chapter 2. The correlation lengths at which the autocorrelation function of the profile is 50 % of the value at the origin, can be used as values for λ_x and λ_y in Eq. (2.15) respectively (CRC, 1984). γ_c may also be interpreted as the length-to-width ratio of a typical contact point between the characterised surface and another plane surface. A simplified way of obtaining γ_c is then given by:

$$\gamma_c \approx \frac{HSC_y}{HSC_x} \tag{3.9}$$

where:

HSC_x – high spot counts in the x -direction, i.e. the direction along the ski

HSC_y – high spot counts in the y -direction, i.e. the direction across the ski

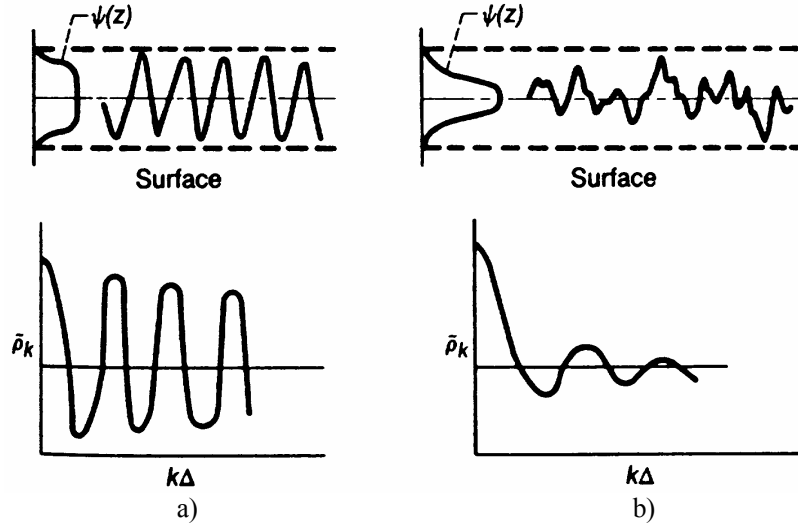


Fig. 3.12. Two different surfaces and their autocorrelation functions. a) Profile with a periodic autocorrelation function. b) Profile with a decreasing autocorrelation function (Halling, 1975).

The directional orientation of the surface roughness can also be found by computing the 2-D Fourier transform of the measured surface image:

$$G(u, v) = \frac{1}{MN} \sum_{x=0}^{M-1} \sum_{y=0}^{N-1} g(x, y) \exp \left[-j2\pi \left(\frac{ux}{M} + \frac{vy}{N} \right) \right] \quad (3.10)$$

where:

- $g(x, y)$ - grey level value of a pixel in the measured surface image, i.e. the height matrix $z(x, y)$ from the SSA measurement transformed to an 8-bit image
- M - number of sampled points in the x -direction, i.e. number of columns in the measured surface image
- N - number of sampled points in the y -direction, i.e. number of rows in the measured surface image
- u - frequency variable in the x -direction, $u = 0, 1, 2, \dots, M - 1$
- v - frequency variable in the y -direction, $v = 0, 1, 2, \dots, N - 1$
- j - $\sqrt{-1}$

and subsequently the spectrum of the 2-D Fourier transform:

$$|G(u, v)| = |R^2(u, v) + I^2(u, v)| \quad (3.11)$$

where:

$$G(u, v) = R(u, v) + jI(u, v) \quad (3.12)$$

Fig. 3.13 shows an imaginary surface image where the heights at the different surface points are described by the grey tones in the corresponding surface image pixels. Light grey tones indicate high points, while dark grey tones indicate low points. The surface illustrated in Fig. 3.13 has a texture with a characteristic direction of -45° relative to the x -axis and a characteristic period of $2\sqrt{2}$ pixels perpendicular to the characteristic direction, if the resolution in the x - and y -direction of the surface image is assumed equal. Fig. 3.14 shows the spectrum of the 2-D Fourier transform for the surface image in Fig. 3.13. We see that the surface image in Fig. 3.13 gives rise to three points in the spectrum shown in Fig. 3.14. The point in the middle of the spectrum, from now on entitled the origin, corresponds to the static component or the background of the measured surface. The two other points, which actually is one point due to the symmetry round the origin in a centred 2-D Fourier transform spectrum, can be used to find the characteristic direction and the characteristic period perpendicular to the characteristic direction for the surface.

A real surface can be interpreted as a collection of surfaces with different characteristic directions, characteristic periods perpendicular to characteristic directions and strengths. Bright points, i.e. points with high values, found in the 2-D Fourier spectrum of a measured surface image often indicate interesting properties distinctive for the measured surface. The characteristic direction of the bright point in the spectrum is related to the characteristic angle ϕ relative to the x -axis for the measured surface. The characteristic angle ϕ indicates the characteristic direction for the measured surface. If the bright point is located in the first (and third) quadrant relative to the origin in the spectrum, ϕ is given by:

$$\phi = \delta - \frac{\pi}{2} \quad (3.13a)$$

where:

- δ - angle relative to the x -axis for a vector from the origin to the bright point in the 2D Fourier spectrum of a measured surface image, the angle must be adjusted accordingly if the resolution of the measured surface image is different in the x - and y -direction, radians

If the bright point is located in the fourth (and second) quadrant relative to the origin in the spectrum, ϕ is given by:

$$\phi = \frac{\pi}{2} - \delta \quad (3.13b)$$

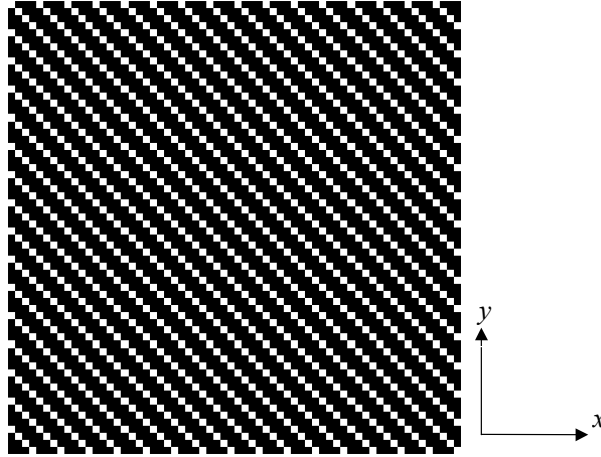


Fig. 3.13. Imaginary surface image where heights at different surface points are described by grey tones in corresponding surface image pixels.

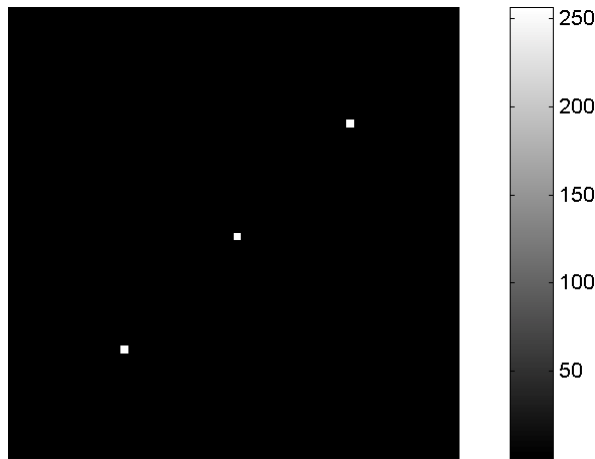


Fig. 3.14. Spectrum of the 2-D Fourier transform of the imaginary surface image in Fig. 3.13.

The characteristic period perpendicular to the characteristic direction for the measured surface, T (mm), is given by:

$$T = \frac{1}{\sqrt{\left(\frac{x_c}{Nx_r}\right)^2 + \left(\frac{y_c}{My_r}\right)^2}} \quad (3.14)$$

where:

- x_r - resolution in the x -direction, mm/pixel
- y_r - resolution in the y -direction, mm/pixel
- x_c - x -coordinate relative to the origin for a bright point in the 2D Fourier spectrum of a measured surface image, pixels
- y_c - y -coordinate relative to the origin for a bright point in the 2D Fourier spectrum of a measured surface image, pixels

3.4. An SSA example

A SSA-measured surface image has 739×570 pixels. Let us consider a part of such an image consisting of 128×128 pixels. A 3-D plot of this surface is shown in Fig. 3.15. Fig. 3.16 displays the same surface as a grey level image, while the histogram of the surface is shown in Fig. 3.17. The spectrum of the 2-D Fourier-transform of the surface is depicted in Fig. 3.18. The bright point in the first (and third) quadrant of the spectrum in Fig. 3.18 is used to find the characteristic angle ϕ and the characteristic period T of the surface. These two parameters can be found in Table 3.1 together with the maximum strength of the bright point in the spectrum, $\log(|G(u,v)|)$, and different variants of the surface parameters R_q , R_a and R_t .

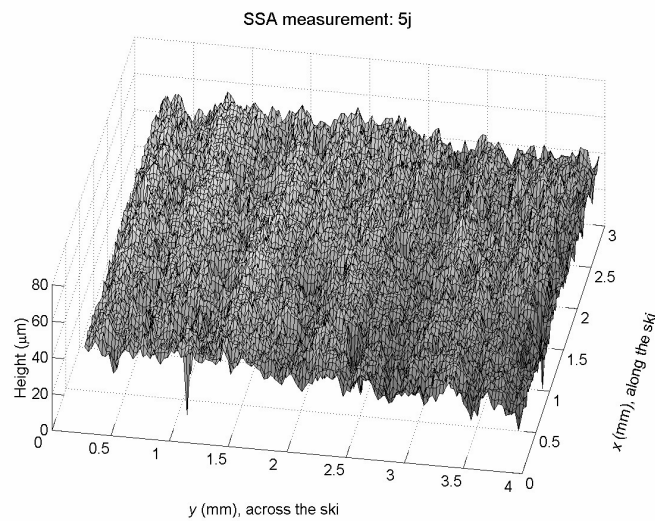


Fig. 3.15. 3-D plot of a part of a SSA-measured surface image consisting of 128×128 pixels.

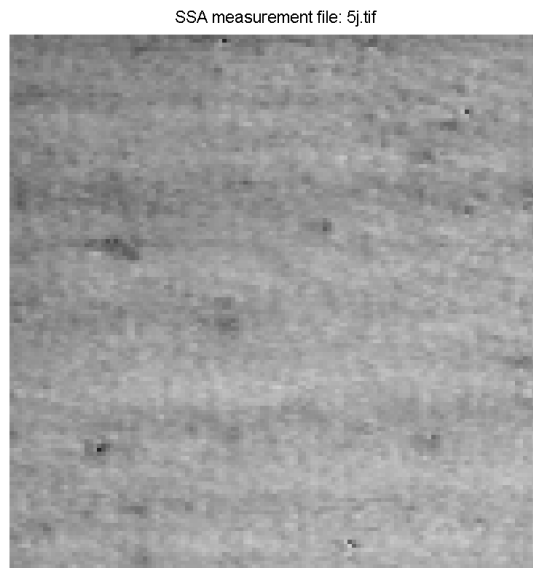


Fig. 3.16. The surface in Fig. 3.15 shown as a grey level image.

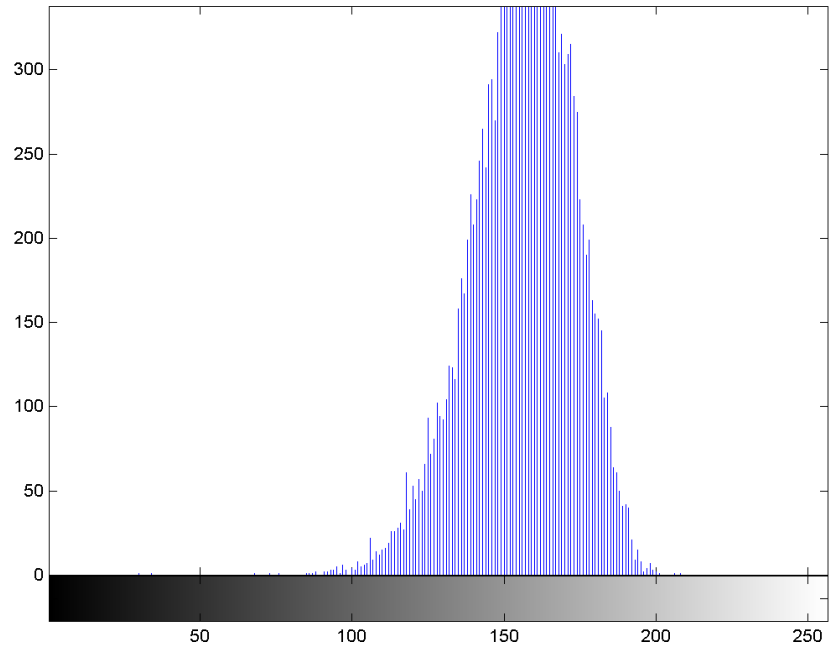


Fig. 3.17. The histogram of the surface in Fig. 3.16. The grey tones are indicated on the x -axis, while the number of image pixels with different grey tones are given on the y -axis.

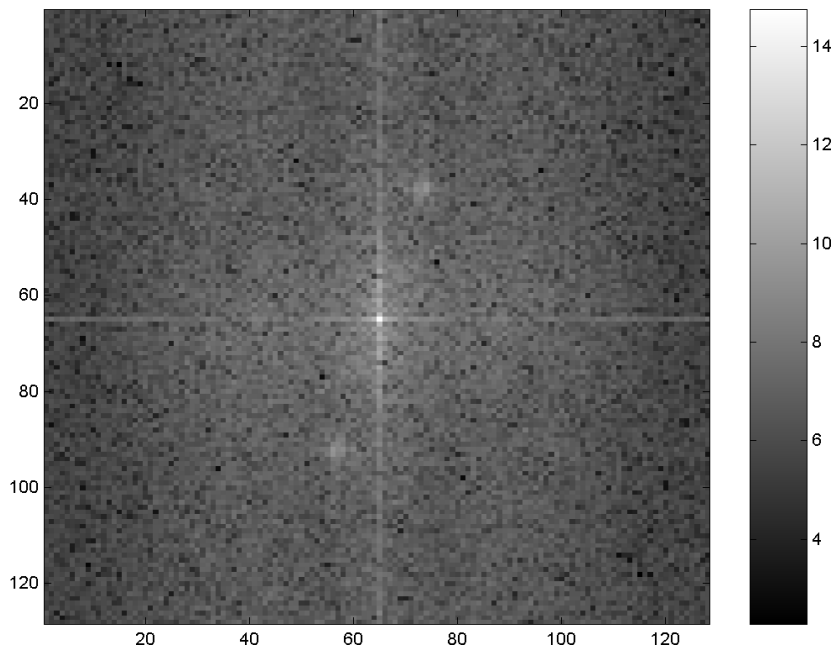


Fig. 3.18. The spectrum of the 2-D Fourier transform of the surface in Fig. 3.16.

Table 3.1. Calculated surface parameters for the measured surface in Fig. 3.15.

Surface parameter	Value
Characteristic angle ϕ for the measured surface (found by using the bright point of the 2-D Fourier spectrum of the surface)	-0.1707 radians
Characteristic period T for the measured surface (found by using the bright point of the 2-D Fourier spectrum of the surface)	0.1260 mm
Maximum strength of the bright point in the 2-D Fourier spectrum of the surface, $\log(G(u,v))$	8.2918
R_q for the whole surface relative to a reference plane parallel with the xy plane, $R_{q,2D}$	6.53 μm
Mean of the R_q for the columns in the measured surface image, i.e. across the ski, when each column has an individual reference line parallel to the y -axis, $\bar{R}_{q,y}$	5.88 μm
Mean of the R_q for the rows in the measured surface image, i.e. along the ski, when each row has an individual reference line parallel to the x -axis, $\bar{R}_{q,x}$	4.78 μm
R_a for the whole surface relative to a reference plane parallel with the xy plane, $R_{a,2D}$	5.20 μm
Mean of the R_a for the columns in the measured surface image, i.e. across the ski, when each column has an individual reference line parallel to the y -axis, $\bar{R}_{a,y}$	4.68 μm
Mean of the R_a for the columns in the measured surface image, i.e. across the ski, when each column has an individual possibly sloping reference line relative to the y -axis, $\bar{R}_{a,ys}$	3.61 μm
Mean of the R_a for the rows in the measured surface image, i.e. along the ski, when each row has an individual reference line parallel to the x -axis, $\bar{R}_{a,x}$	3.79 μm
Mean of the R_a for the rows in the measured surface image, i.e. along the ski, when each row has an individual possibly sloping reference line relative to the x -axis, $\bar{R}_{a,xs}$	3.02 μm
R_t for the whole surface, $R_{t,2D}$	69 μm
Mean of the R_t for the columns in the measured surface image, i.e. across the ski, when each column has an individual reference line parallel to the y -axis, $\bar{R}_{t,y}$	31 μm
Mean of the R_t for the rows in the measured surface image, i.e. along the ski, when each row has an individual reference line parallel to the x -axis, $\bar{R}_{t,x}$	25 μm

3.5. References

- Abbott, E. J. and F. A. Firestone (1933): Specifying surface quality. *Journal of Mechanical Engineering*, Vol. 55, No. 9, pp. 569-572.
- CRC (1984): *CRC handbook of lubrication. Theory and practice of tribology. Volume II. Theory and design.* (E. R. Booser, Ed.). CRC Press, Inc., Boca Raton, Florida, USA, pp. 153.
- Creath, K. (1988): Phase-measurement interferometry techniques. In *Progress in Optics XXVI* (E. Wolf, Ed.), Elsevier Science Publishers B.V., s. 349-393.
- Halling, J. (1975): *Principles of tribology.* Macmillan Press, London and Basingstoke, 401 p.
- Halling, J. (1976): *Introduction to tribology.* Wykeham Publications, London, 157 p.
- Hamrock, B. J. (1994): *Fundamentals of fluid film lubrication,* McGraw-Hill, New York, 690 p.
- Mathia, T. G., A. Midol, P. Lanteri and R. Longerey (1989): Topography, physico-chemistry and wear in sliding of ski soles in regard to rheology of snow. In *Proceedings of Eurotrib 89,* Elsevier, Amsterdam, pp. 253-260.

Mathia, T. G., H. Zahouani and A. Midol (1992): Topography, wear, and sliding functions of skis. *International Journal of Machine Tools Manufacturing*, Vol. 32, No. 1/2, pp. 263-266.

Mercer, C. R. and G. Beheim (1992): Phase-stepping fiber-optic projected fringe system for surface topography measurements. U.S. Patent No. 5,146,293, 6 p.

4. Ski base structure measurements

Notation

\bar{d}	mean of d_j for the n_g snow grains with distinguishable boundaries in a microscope image of a snow surface, mm
d_j	length of the largest 2D diagonal for snow grain surface number j in a microscope image of a snow surface, mm
H	snow hardness, N/m ² or Pa
n_g	number of snow grains with distinguishable boundaries in a microscope image of a snow surface
p_y	typical period between grooves in the y -direction, i.e. across the ski
R_a	arithmetic mean surface roughness, μm
$\bar{R}_{a,y}$	mean of the R_a of the columns in a measured surface image, i.e. across the ski, when each column has an individual reference line parallel to the y -axis, μm
$\bar{R}_{a,ya}$	mean of $\bar{R}_{a,y}$ for the afterbody of the ski, μm
$\bar{R}_{a,yas}$	mean of $\bar{R}_{a,ys}$ for the afterbody of the ski, μm
$\bar{R}_{a,yf}$	mean of $\bar{R}_{a,y}$ for the forebody of the ski, μm
$\bar{R}_{a,yfs}$	mean of $\bar{R}_{a,ys}$ for the forebody of the ski, μm
$\bar{R}_{a,ys}$	mean of the R_a of the columns in a measured surface image, i.e. across the ski, when each column has an individual possibly sloping reference line relative to the y -axis, μm
$\bar{R}_{a,yw}$	mean of $\bar{R}_{a,y}$ for the whole ski, μm
$\bar{R}_{a,yws}$	mean of $\bar{R}_{a,ys}$ for the whole ski, μm
R_t	maximum peak-to-valley height, μm

$\bar{R}_{t,y}$	mean of the R_t of the columns in a measured surface image, i.e. across the ski, when each column has an individual reference line parallel to the y -axis, μm
$\bar{R}_{t,yw}$	mean of $\bar{R}_{t,y}$ for the whole ski, μm
T_s	snow temperature 2 cm below the snow surface, $^{\circ}\text{C}$
x	co-ordinate along the ski, mm
y	co-ordinate across the ski, mm
z_i	surface height registrations on a surface profile, μm
$W_{\text{vol},\%}$	volume per cent liquid water content in the snow, %
δ_d	standard deviation of d_j for the n_g snow grains with distinguishable boundaries in a microscope image of a snow surface, mm
δ_{Raya}	standard deviation of $\bar{R}_{a,ya}$, μm
δ_{Rayas}	standard deviation of $\bar{R}_{a,yas}$, μm
δ_{Rayf}	standard deviation of $\bar{R}_{a,yf}$, μm
δ_{Rayfs}	standard deviation of $\bar{R}_{a,yfs}$, μm
δ_{Rayw}	standard deviation of $\bar{R}_{a,yw}$, μm
δ_{Rayws}	standard deviation of $\bar{R}_{a,yws}$, μm
δ_{Rtyw}	standard deviation of $\bar{R}_{t,yw}$, μm
ρ	density of snow, g/cm^3

4.1. Introduction

This section presents some of the results from the ski base structure measurement experiments between 1995 and 1998. In this period almost 1700 measurements were taken of more than 350 skis. This unique collection of structure measurements included characterisation of 8 Olympic and 6 World Championship gold medal winning skis. Due to respect for the ski technicians and stone grinding experts that have been co-operating on this project and the knowledge this collaboration has given, some of the results from the measurements are given restricted access until 30 July 2002. These are not presented here.

4.2. Measurement methods and procedures

Ski base structure measurements have been performed with a *Taylor Hobson Talysurf 4* profilometer and the Ski base Surface Analyser (SSA) described in Chapter 3. Measurement points along the skis have been chosen according to typical pressure distributions for cross-country skating skis and classic skis. A typical measurement procedure for one ski has involved six measurements along the ski, three on the forebody and three on the afterbody. The measurements have been taken:

- 65-70 cm in front of the balance point of the ski
- 50 cm in front of the balance point of the ski

- 40 cm in front of the balance point of the ski
- 25-30 cm behind the balance point of the ski
- 35-40 cm behind the balance point of the ski
- 45-50 cm behind the balance point of the ski

From these measurements different roughness parameters can be calculated. The roughness parameter definitions used in this chapter are given in the notation list. Notice that $\bar{R}_{a,y}$ is defined according to individual reference lines parallel to the y -axis, while $\bar{R}_{a,ys}$ is defined according to individual possibly sloping reference lines relative to the y -axis. Typically $\bar{R}_{a,y}$ equals $\bar{R}_{a,ys}$ for skis that are properly plane ground before the ski base structure is set, while $\bar{R}_{a,y}$ can be considerably higher than $\bar{R}_{a,ys}$ for non-plane ski bases.

4.3. Results

4.3.1. Structure types

The ski base structure roughness can be divided into four categories:

- Fine: $\bar{R}_{a,ys} = 1-4 \mu\text{m}$
- Medium: $\bar{R}_{a,ys} = 4-7 \mu\text{m}$
- Coarse: $\bar{R}_{a,ys} = 7-10 \mu\text{m}$
- Very coarse: $\bar{R}_{a,ys} > 10 \mu\text{m}$

Structures with a fine roughness are typically used under dry to moist snow conditions, while medium structures are best under moist snow conditions. For classic skis coarse structures are normally used under moist to wet snow conditions, while very coarse structures can be used under wet to very wet snow conditions. The optimum structures on skating skis tend to be finer than the optimum structures on classic skis under similar snow and weather conditions. The reason is that impact and compaction resistances often have more influence on the total ski base sliding friction in a skating track compared to a classic track due to lower snow hardness in the skating track.

Roughness statistics for examples of fine, medium, coarse and very coarse structures are listed in Table 4.1. Surface profiles across the ski and contour plots of the surface topography for the fine, medium and coarse structures in Table 4.1 are shown in Figs. 4.1-4.6, while surface profile and contour plot for the very coarse structure are depicted in Figs. 6.8 and 6.9 in Chapter 6.

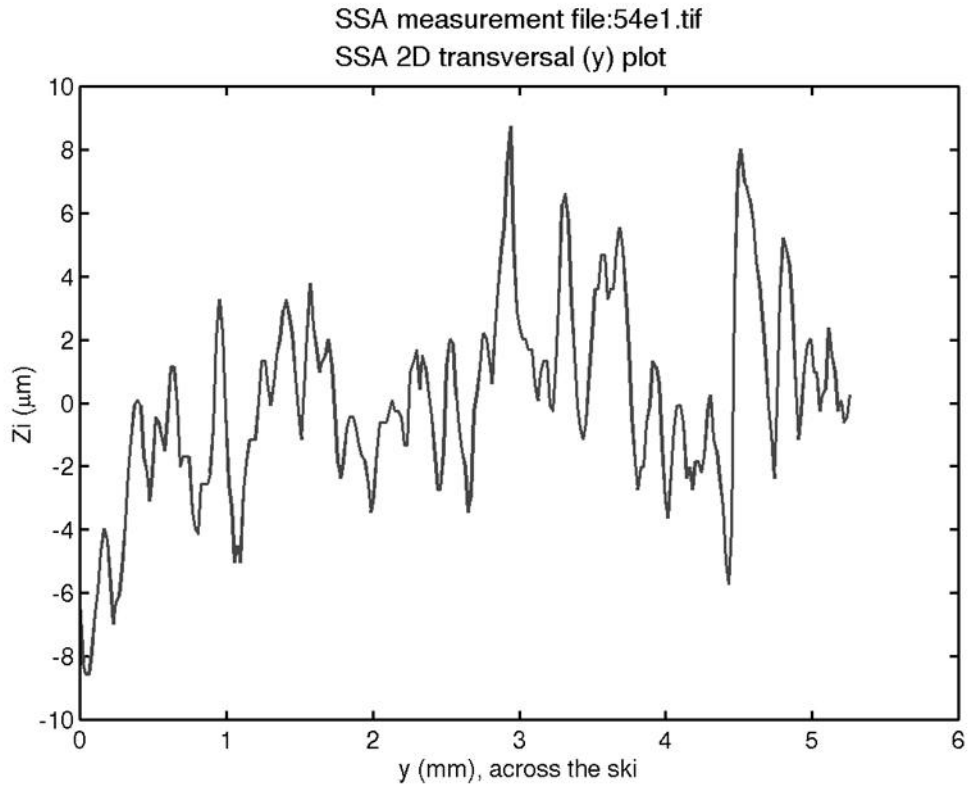


Fig. 4.1. Example of a surface profile across the ski for the fine structure in Table 4.1.

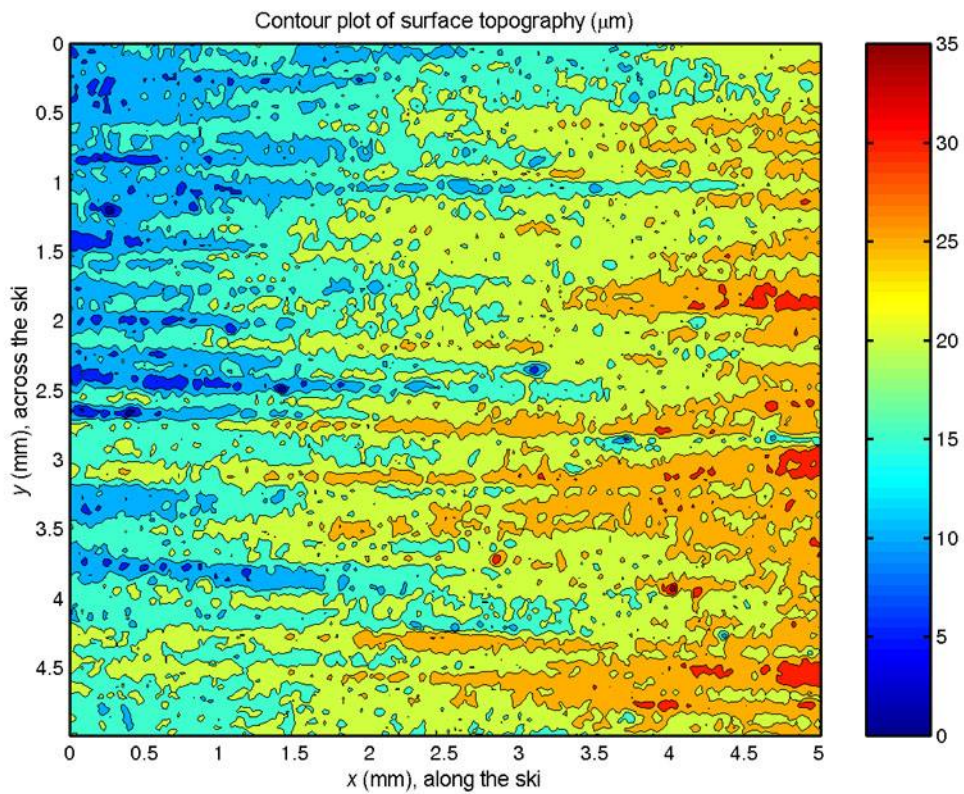


Fig. 4.2. Contour plot of the surface topography of the fine structure in Table 4.1.

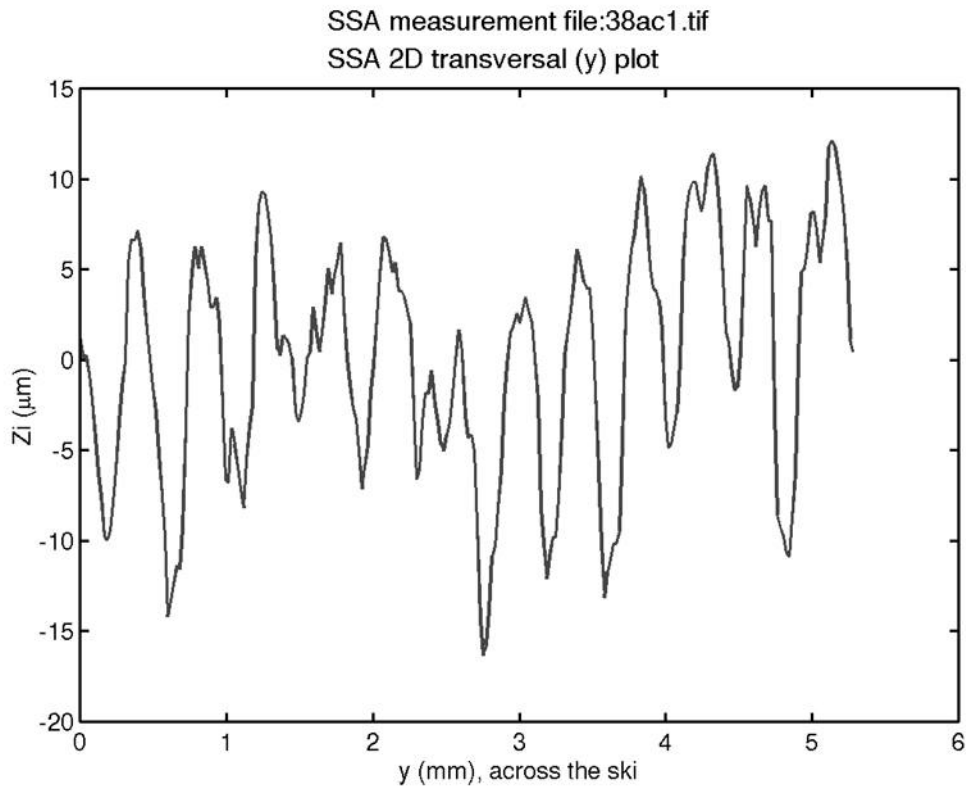


Fig. 4.3. Example of a surface profile across the ski for the medium structure in Table 4.1.

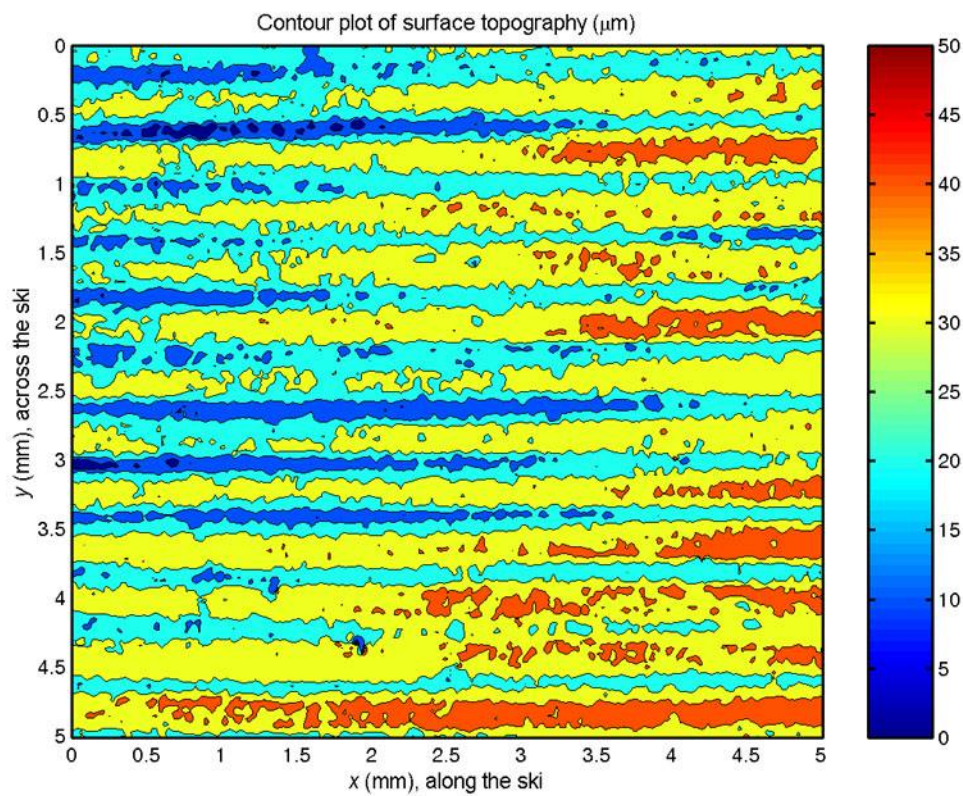


Fig. 4.4. Contour plot of the surface topography of the medium structure in Table 4.1.

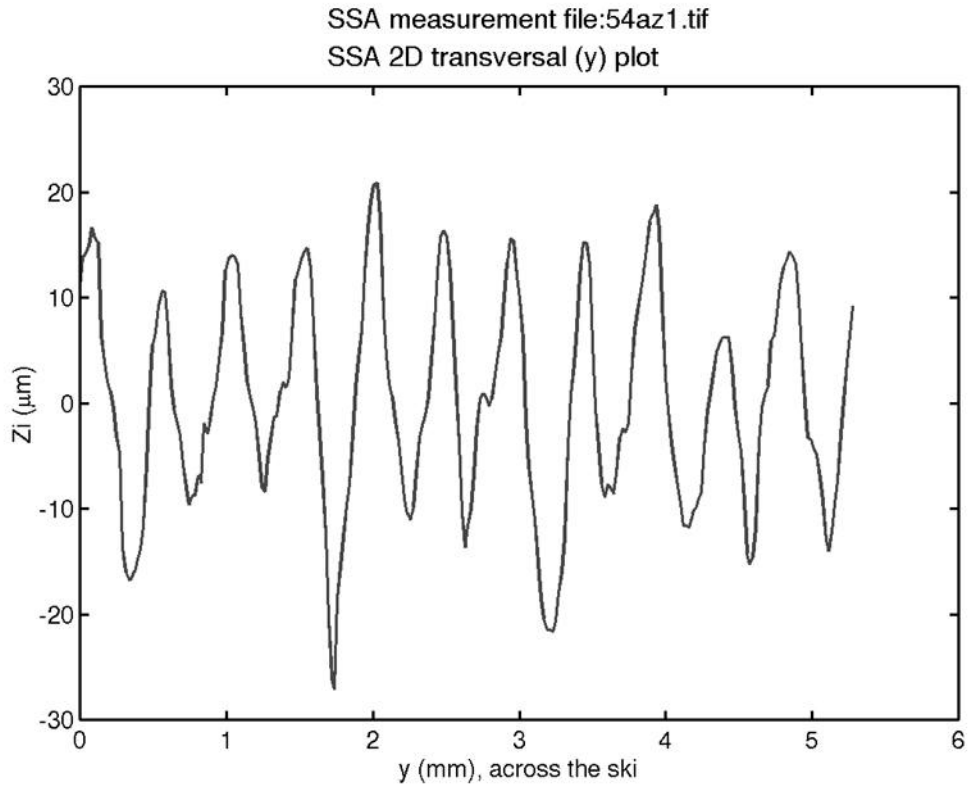


Fig. 4.5. Example of a surface profile across the ski for the coarse structure in Table 4.1.

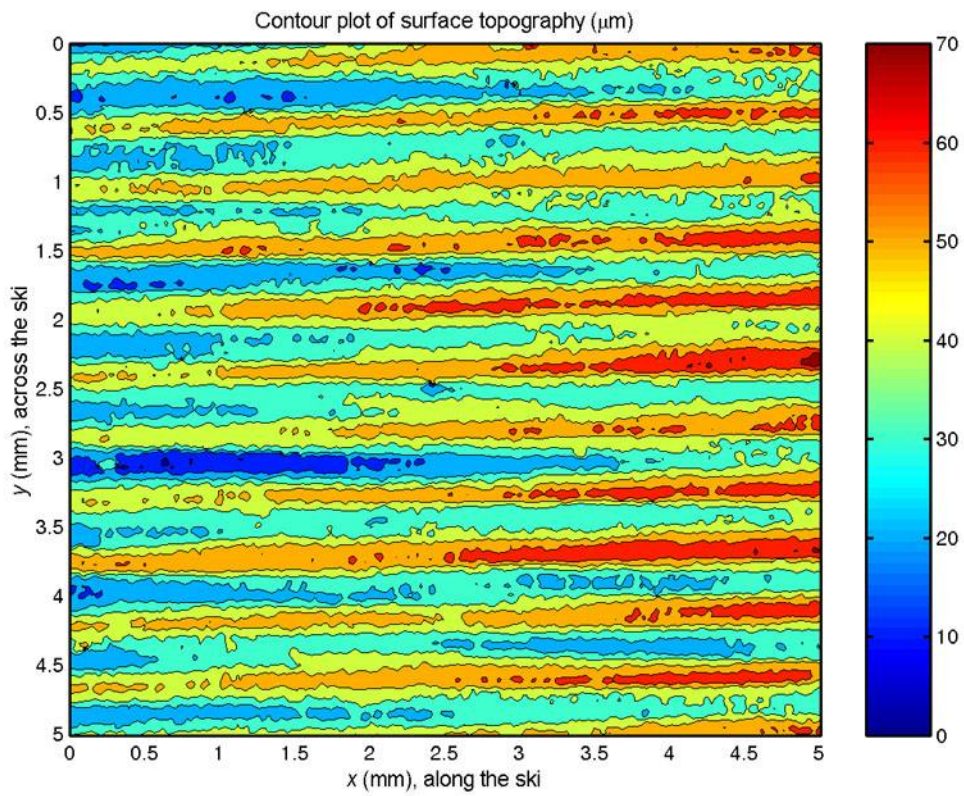


Fig. 4.6. Contour plot of the surface topography of the coarse structure in Table 4.1.

Table 4.1. Roughness statistics for examples of fine, medium, coarse and very coarse structures.

Structure type	$\bar{R}_{a,yws} \pm \delta_{Rayws}$ (μm)	p_y (mm)	Continuity
Fine	2.5 ± 0.2	0.20	Discontinuous
Medium	5.0 ± 0.5	0.42	Continuous
Coarse	8.9 ± 1.1	0.48	„
Very coarse	12.7 ± 1.2	0.55	„

4.3.2. Finer structure along the ski

This section presents ski base structure measurements that have revealed finer structure along the ski. Roughness statistics for various ski pairs with finer structure along the ski are listed in Table 4.2, while surface profiles and 3-D surface plots of the forebody and afterbody of the skis are given in Figs. 4.7-4.14.

Table 4.2. Roughness statistics for various ski pairs with finer structure along the ski.

Ski	$\bar{R}_{a,yw} \pm \delta_{Rayw}$ (μm)	$\bar{R}_{a,yf} \pm \delta_{Rayf}$ (μm)	$\bar{R}_{a,ya} \pm \delta_{Raya}$ (μm)
CSP4	3.6	4.6	2.5
CSP11	3.9 ± 1.2	5.0 ± 0.2	2.8 ± 0.5
CSP14	7.2 ± 2.2	9.1 ± 0.9	5.2 ± 0.7
TSP19E	5.5	6.5	4.4

The first ski base structure measurement of a competition ski pair was performed in June 1995 (Moldestad, 1995). This ski pair, CSP4, belonged to Bjørn Dæhlie and had been used in two competitions where he had won gold and bronze medals (15 and 50 km free technique) during the Nordic World Championships'93 in Falun (Sweden). Since then the ski pair had been reground with the "same" structure, but the ski technicians claimed that the glide properties of the ski pair had been better during the World Championships'93 than it was during the 1995 season. Ski base structure measurements revealed that the roughness $\bar{R}_{a,yf}$ on the forebody of ski pair CSP4 was $4.6 \mu\text{m}$, while the roughness on the afterbody $\bar{R}_{a,ya}$ was $2.5 \mu\text{m}$, i.e. 84 % higher structure roughness on the forebody of the ski pair relative to the afterbody. The difference in structure roughness along the ski is easy to see from the surface profiles across the forebody and afterbody of the ski shown in Figs. 4.7 and 4.8, respectively. The decrease in structure roughness along the ski had not been made on purpose during stone grinding. Neither had anybody believed nor paid attention to the fact that stone-ground skis could have decreased structure roughness along the ski. According to the assumption that the water film thickness increases along the ski, it should be favourable with increased structure roughness along the ski according to the theories described by Eq. (2.20) and Fig. 2.10 in Chapter 2. This was exactly opposite to what was the case for ski pair CSP4. It was therefore suggested to regrind ski pair CSP4 in order to improve the structure roughness along the ski. Furthermore, the measurements highlighted that quality control of ski base structures was important and an extensive structure measurement program was started.

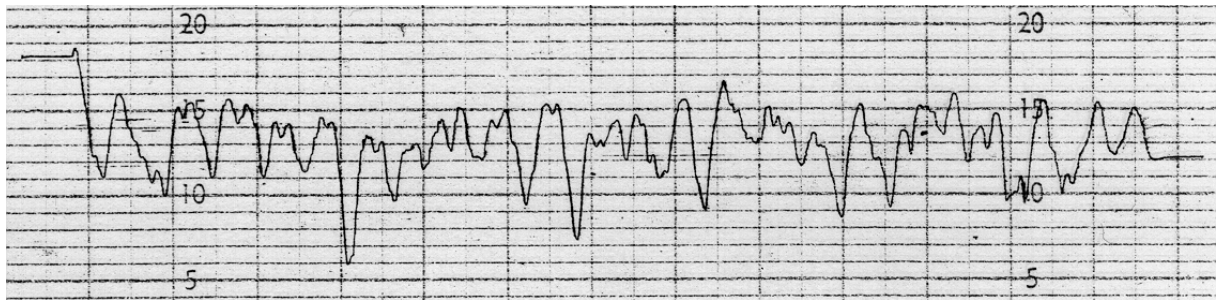


Fig. 4.7. Example of a surface profile across the forebody of ski pair CSP4. The distance between the horizontal grid lines is 2 μm , while it is 500 μm between the vertical grid lines.

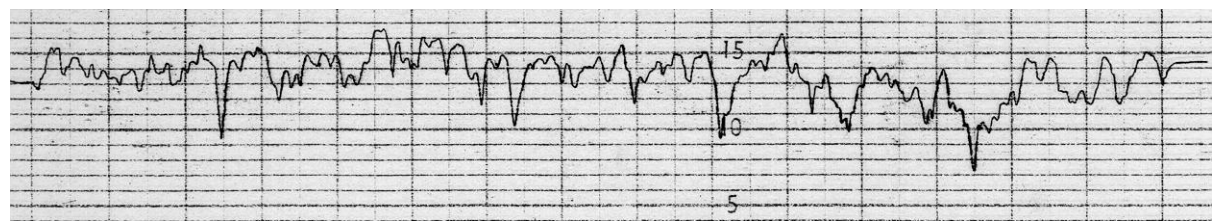


Fig. 4.8. Example of a surface profile across the afterbody of ski pair CSP4. The distance between the horizontal grid lines is 2 μm , while it is 500 μm between the vertical grid lines.

Figs. 4.9 and 4.10 show surface profiles across the forebody and afterbody of ski pair CSP11. This ski pair was measured prior to a competition during the Nordic World Championships'97 in Trondheim. The measurements showed that the roughness $\bar{R}_{a,yf}$ on the forebody of ski pair CS11 was 5.0 μm , while the roughness on the afterbody $\bar{R}_{a,ya}$ was 2.8 μm , i.e. 79 % higher structure roughness on the forebody of the ski pair relative to the afterbody. As a consequence the ski pair was reground before the competition, and caution was taken in order to avoid decreased structure roughness along the competition skis during the rest of the championships.

Figs. 4.11 and 4.12 depict surface profiles across the forebody and afterbody of another competition ski pair with decreased structure roughness along the ski, namely CSP14. Structure measurements revealed that the roughness $\bar{R}_{a,yf}$ on the forebody of this ski pair was 9.1 μm , while the roughness on the afterbody $\bar{R}_{a,ya}$ was 5.2 μm , i.e. 75 % higher structure roughness on the forebody of the ski pair relative to the afterbody. A 1 mm riller had been used in addition to stone grinding to make the ski base structure of this ski pair.

Three-dimensional surface plots of the forebody and afterbody of ski pair TSP19E are shown in Figs. 4.13 and 4.14. This measurement was performed in order to characterise a structure produced by a new grinding machine. It can be seen from Table 4.2 that the roughness $\bar{R}_{a,yf}$ on the forebody of ski pair TSP19E was 6.5 μm , while the roughness on the afterbody $\bar{R}_{a,ya}$ was 4.4 μm , i.e. 48 % higher structure roughness on the forebody of the ski pair relative to the afterbody. These findings led to development and improvement of the grinding diamonds used to set the grinding stone.

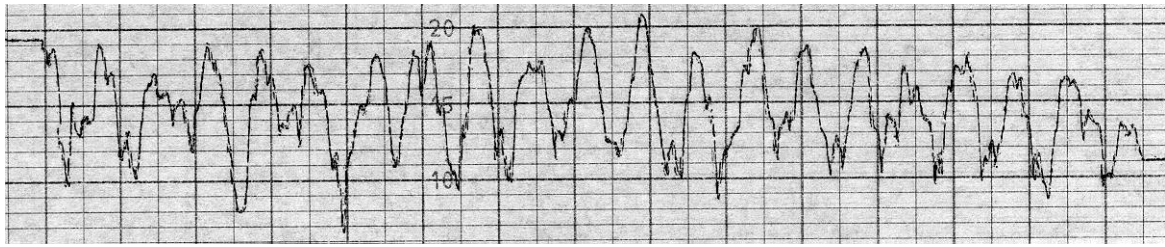


Fig. 4.9. Example of a surface profile across the forebody of ski pair CSP11. The distance between the horizontal grid lines is $2\ \mu\text{m}$, while it is $500\ \mu\text{m}$ between the vertical grid lines.

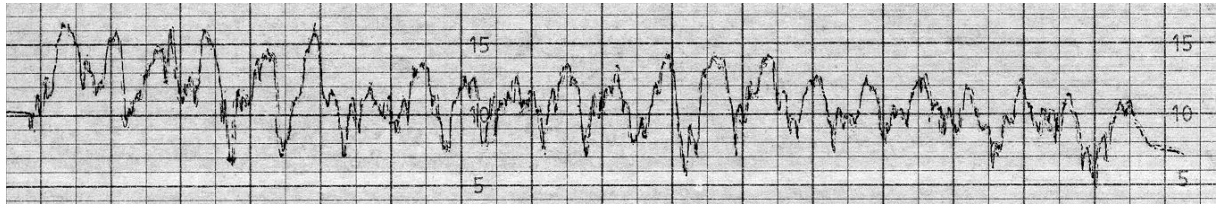


Fig. 4.10. Example of a surface profile across the afterbody of ski pair CSP11. The distance between the horizontal grid lines is $2\ \mu\text{m}$, while it is $500\ \mu\text{m}$ between the vertical grid lines.

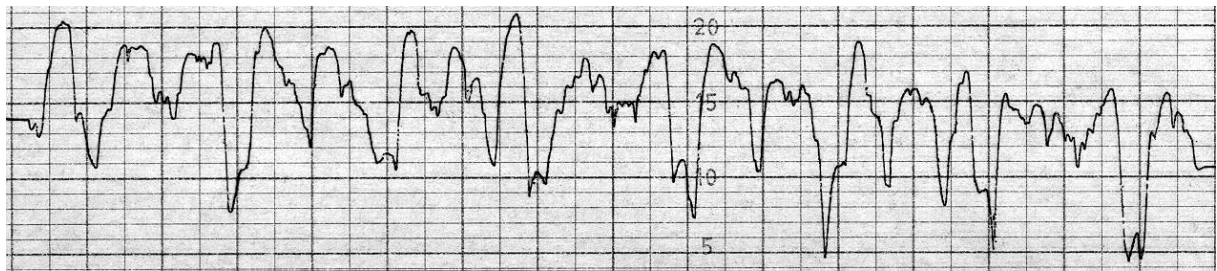


Fig. 4.11. Example of a surface profile across the forebody of ski pair CSP14. The distance between the horizontal grid lines is $4\ \mu\text{m}$, while it is $500\ \mu\text{m}$ between the vertical grid lines.

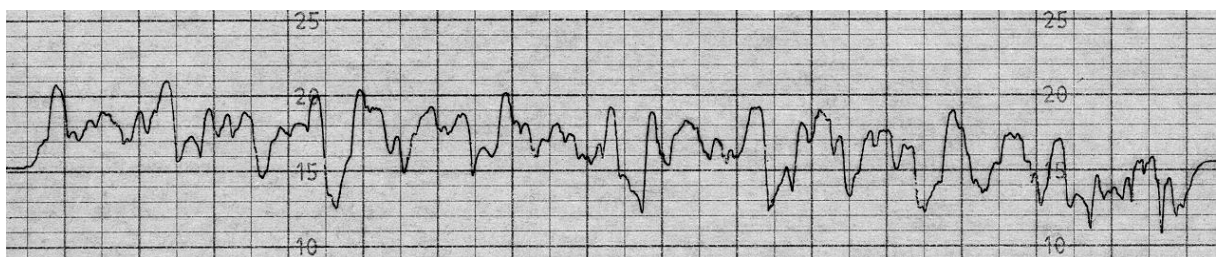


Fig. 4.12. Example of a surface profile across the afterbody of ski pair CSP14. The distance between the horizontal grid lines is $4\ \mu\text{m}$, while it is $500\ \mu\text{m}$ between the vertical grid lines.

At present the best stone grinders usually manage to produce structures with similar roughness along the ski. It is believed that differences in structure roughness along the ski mainly are caused by pressure variations along the ski during stone grinding. Other causes can be:

- Ski base hardness variations along the ski
- Poor grinding diamonds

- Poor grinding stone
- Shaky manual treatment of the ski during stone grinding

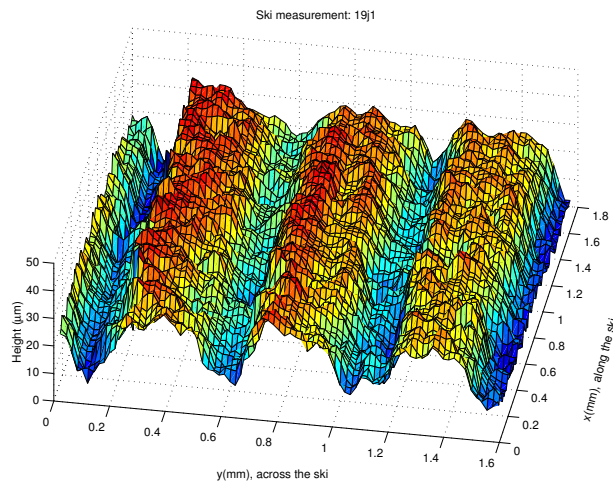


Fig. 4.13. 3-D surface plot of the forebody of ski pair TSP19E.

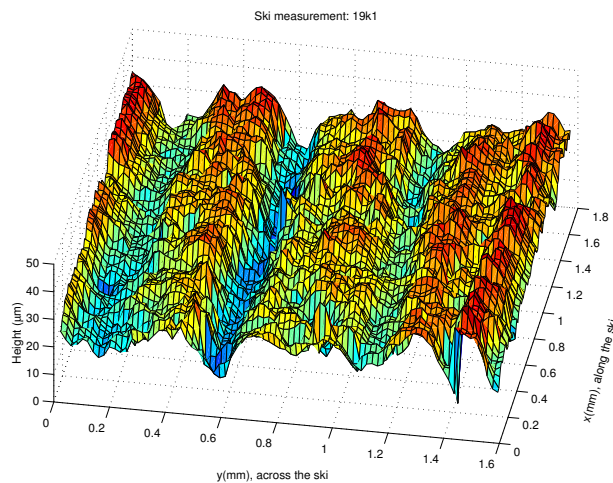


Fig. 4.14. 3-D surface plot of the afterbody of ski pair TSP19E.

4.3.3. Rilling

In June 1998 a measurement experiment was performed in order to study the effect of handmade structures produced by rilling. An experienced ski technician made "rilling" structures by applying ten different SWIX rillers on ten skis. Table 4.3 lists the structure roughness statistics for the various SWIX rillers. Figs. 4.15, 4.17 and 4.19 show examples of surface profiles across the afterbody of the ski for 0.35, 1.0 and 3.0 mm rillers. Contour plots of the surface topography on the afterbody of the ski are given for the 0.35, 1.0 and 3.0 mm rillers in Figs. 4.16, 4.18 and 4.20, respectively.

It can be seen from Table 4.3 that rilling caused higher structure roughness on the afterbody of the ski than the forebody of the ski for all rillers except the 0.16 mm and 0.5 mm rillers in this experiment.

The increase in roughness along the ski varied between 18 (2.0 mm) and 91 % (0.25 mm) for the eight other rillers.

Table 4.3. Structure roughness statistics for different *SWIX* rillers.

Riller width (mm)	$\bar{R}_{a,yws} \pm \delta_{Rayws}$ (μm)	$\bar{R}_{a,yfs} \pm \delta_{Rayfs}$ (μm)	$\bar{R}_{a,yas} \pm \delta_{Rayas}$ (μm)
0.16	3.3 ± 0.3	3.5 ± 0.2	3.0 ± 0.2
0.25	6.2 ± 2.3	4.3 ± 1.6	8.2 ± 0.2
0.35	7.3 ± 1.8	5.7 ± 0.9	8.8 ± 0.1
0.5	4.0 ± 0.3	4.2 ± 0.4	3.8 ± 0.1
0.75	4.1 ± 0.5	3.7 ± 0.2	4.5 ± 0.5
1.0	4.9 ± 1.1	4.0 ± 0.3	5.8 ± 0.7
1.5	7.7 ± 1.0	6.9 ± 0.4	8.5 ± 0.7
2.0	5.1 ± 0.4	4.8 ± 0.5	5.3 ± 0.2
2.5	5.3 ± 0.8	4.7 ± 0.3	5.9 ± 0.6
3.0	4.6 ± 0.7	4.2 ± 0.5	5.1 ± 0.6

The structure roughness did not increase with the riller width. The highest structure roughness was registered for the 0.35 and 1.5 mm rillers. These rillers gave $\bar{R}_{a,yws}$ equal to 7.3 and 7.7 μm , respectively. The lowest structure roughness was produced by the 0.16 mm riller. This riller had $\bar{R}_{a,yws}$ equal to 3.3 μm .

Ski base mass is replaced during rilling, while it is removed during stone grinding. This effect can be studied by examining the surface profiles and contour plots in Figs. 4.15-4.20. The base mass is pushed up at the sides of a rilling groove and small tops are created relative to the plateaus between the grooves. This is very clear for the 1.0 and 3.0 mm rillers depicted in Figs. 4.17-4.20, but the tendency can also be seen in the surface profile for the 0.35 mm riller in Fig. 4.15. No such effects are present in the surface profiles and contour plots of stone-ground structures shown in Figs. 4.1-4.8.

It is possible to combine stone grinding and rilling in order to make an optimum ski base structure for a specific snow condition. Fig. 4.21 shows an example of a surface profile across the ski for a competition ski pair, CSP15, with such a mixed structure. The mixed structure was made by combining stone grinding and rilling with a 3.0 mm *SWIX* riller. The ski pair had a structure roughness $\bar{R}_{a,yw}$ equal to 8.8 μm and showed very good sliding properties under a competition with:

- Snow type 5
- Snow humidity $W_{vol,\%} = 1.2$ to 1.5 %
- Snow grain size $\bar{d} \pm \delta_d = 1.32 \pm 0.50$ mm
- Snow hardness $H = 2.2 \times 10^4$ to 6.6×10^4 Pa
- Snow density $\rho = 0.41$ to 0.52 g/cm^3
- Snow temperature $T_s = -0.9$ to -0.4 °C

Full definitions of snow parameters and snow measurement procedures are given in Chapter 5.

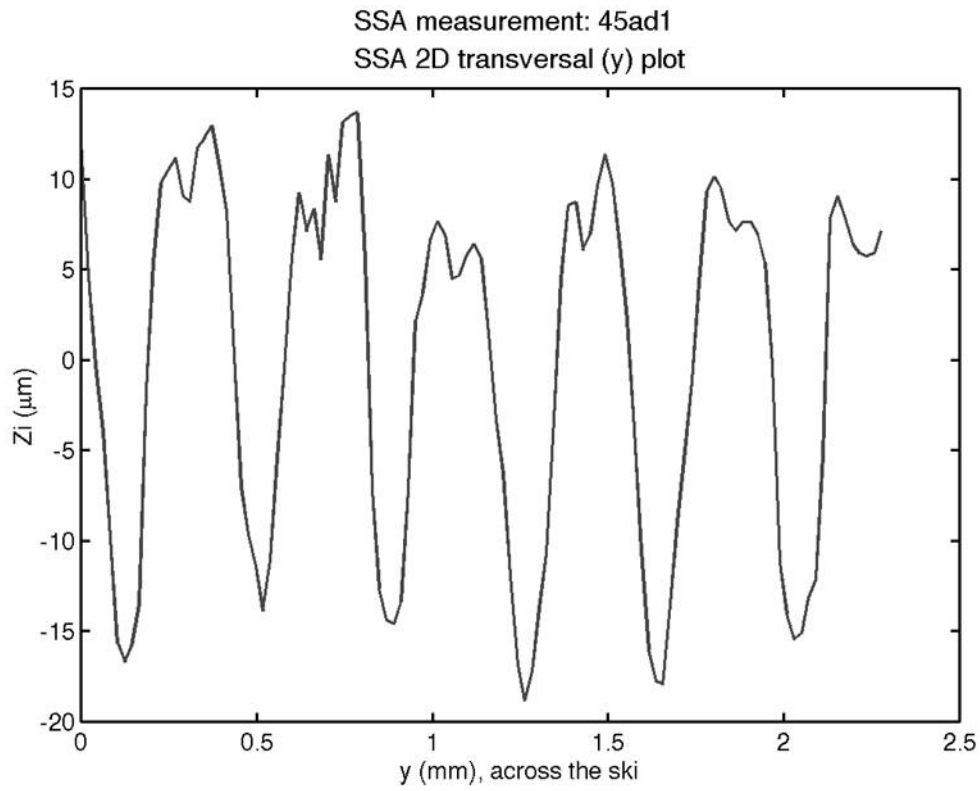


Fig. 4.15. Example of a surface profile across the afterbody of the ski for the 0.35 mm riller in Table 4.3.

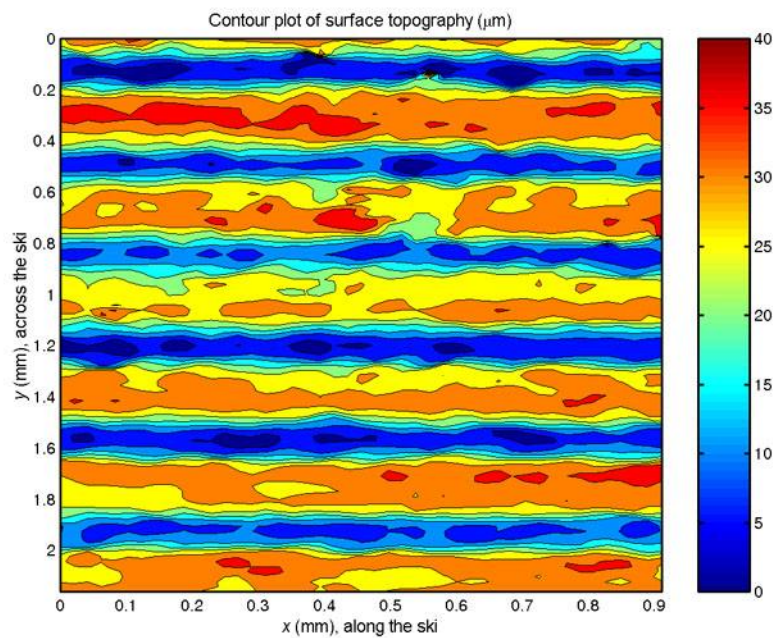


Fig. 4.16. Contour plot of the surface topography on the afterbody of the ski for the 0.35 mm riller in Table 4.3.

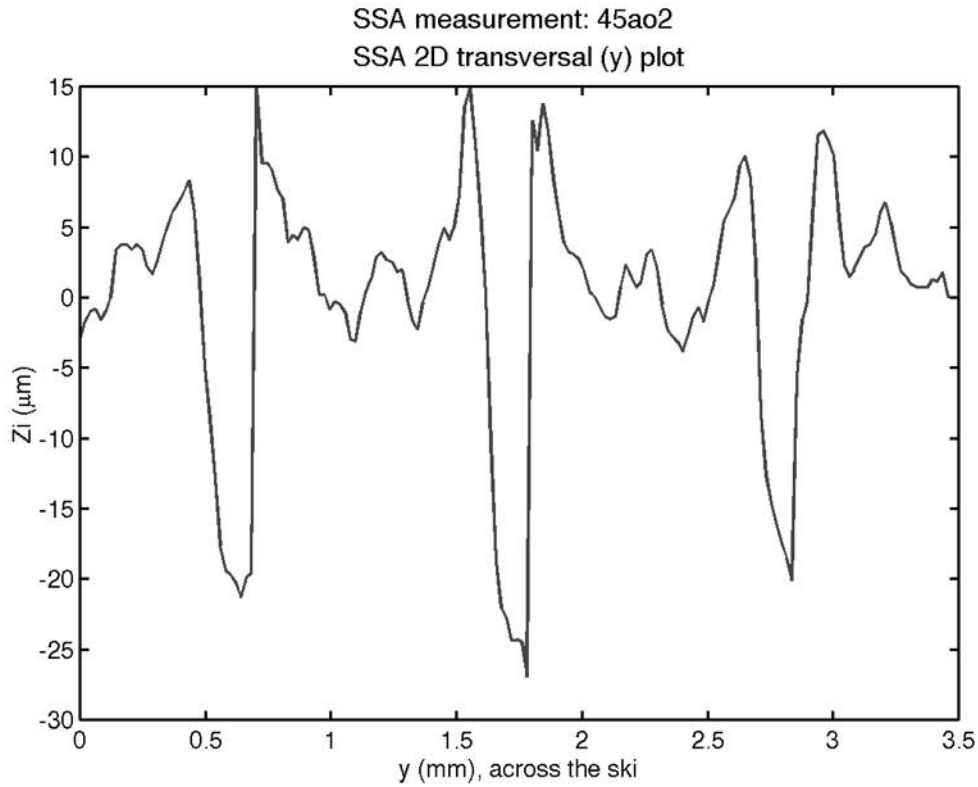


Fig. 4.17. Example of a surface profile across the afterbody of the ski for the 1.0 mm SWIX riller in Table 4.3.

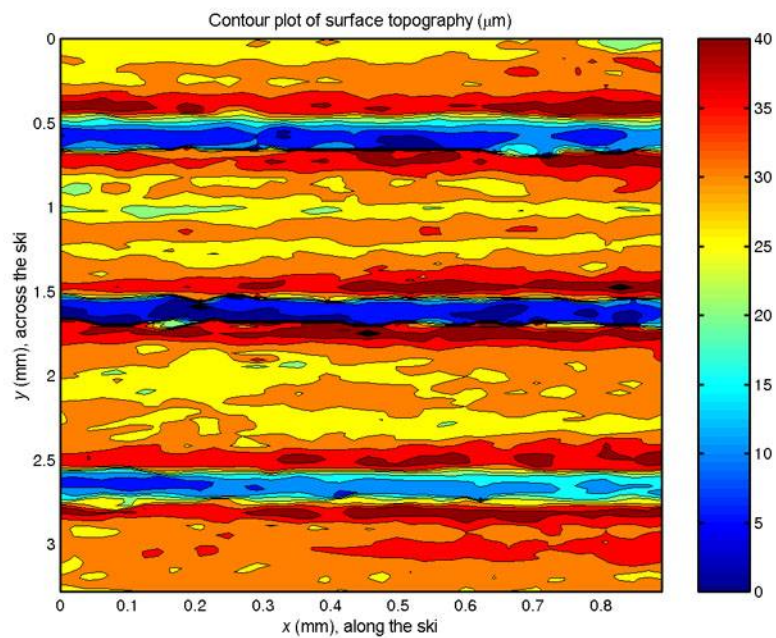


Fig. 4.18. Contour plot of the surface topography of the afterbody of the ski for the 1.0 mm SWIX riller in Table 4.3.

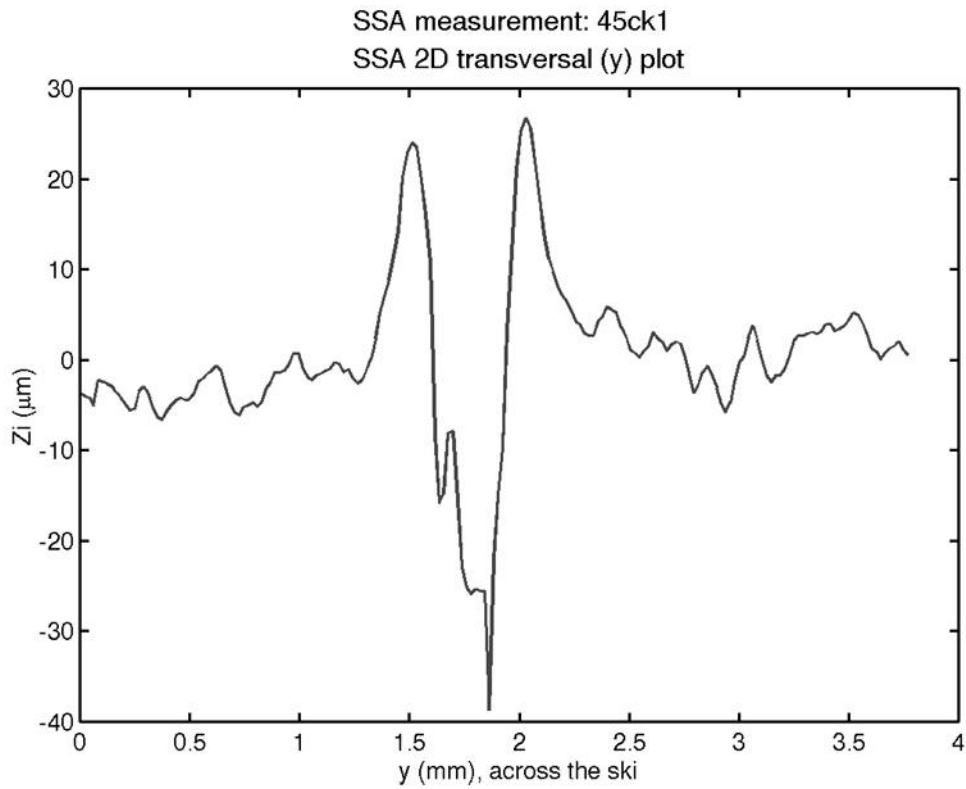


Fig. 4.19. Example of a surface profile across the afterbody of the ski for the 3.0 mm *SWIX* riller in Table 4.3.

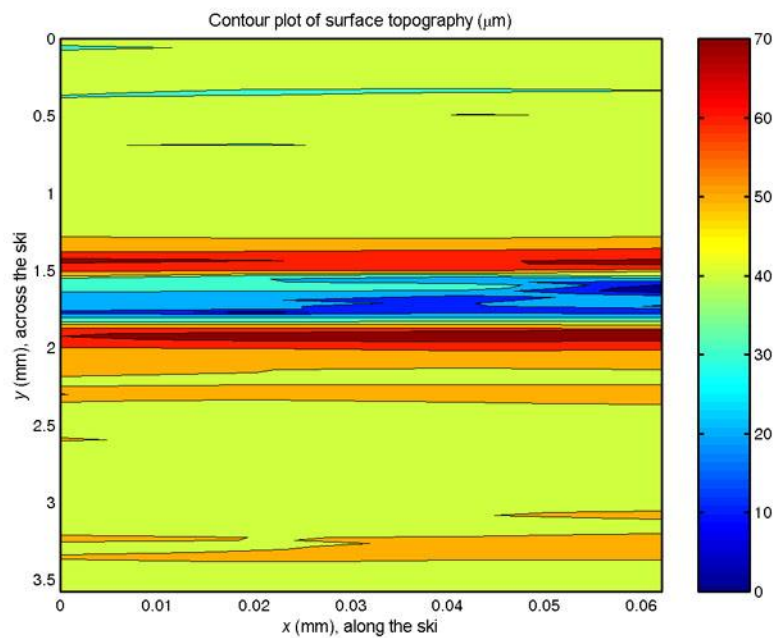


Fig. 4.20. Contour plot of the surface topography of the afterbody of the ski for the 3.0 mm *SWIX* riller in Table 4.3.

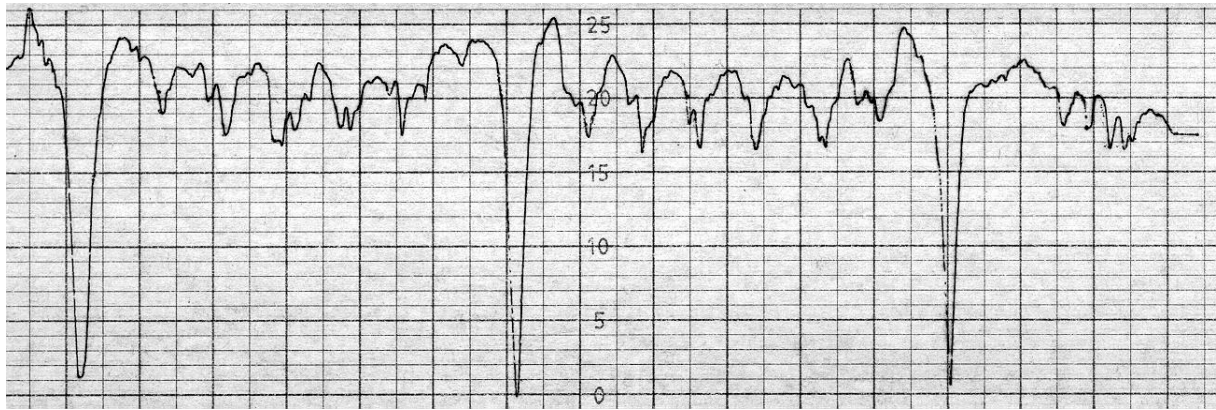


Fig. 4.21. Example of a surface profile across the ski for ski pair CSP15. The distance between the horizontal grid lines is 4 μm , while it is 500 μm between the vertical grid lines.

Ski technicians have experienced when mixing stone-ground structures and rilling that:

- Rounded worn structures need deeper rill grooves than new-ground structures.
- Optimum rill groove width and depth are related to the snow grain size. Deeper and wider rill grooves are needed for larger snow grain sizes.

4.3.4. Plane grinding

In order to attain optimum structure quality by means of stone grinding the ski base surface has to be plane ground thoroughly before the structure is ground on the ski. Figs. 4.22 and 4.23 show a surface profile across the ski and a contour plot of the surface topography for the test ski pair TSP52A. It is easy to see from Fig 4.22 and 4.23 that this ski pair has not been plane ground properly. The SSA characterisation established that the roughness parameters $\bar{R}_{a,yws}$ and $\bar{R}_{a,yw}$ were equal to 3.5 and 5.8 μm for ski pair TSP52A. The large difference between the $\bar{R}_{a,yws}$ - and $\bar{R}_{a,yw}$ -values also indicates that the ski base surface is not plane. Properly plane ground test skis with similar structure roughness as TSP52A have shown up to 3 % higher sliding speeds than TSP52A in sliding tests under snow conditions with snow temperatures below zero.

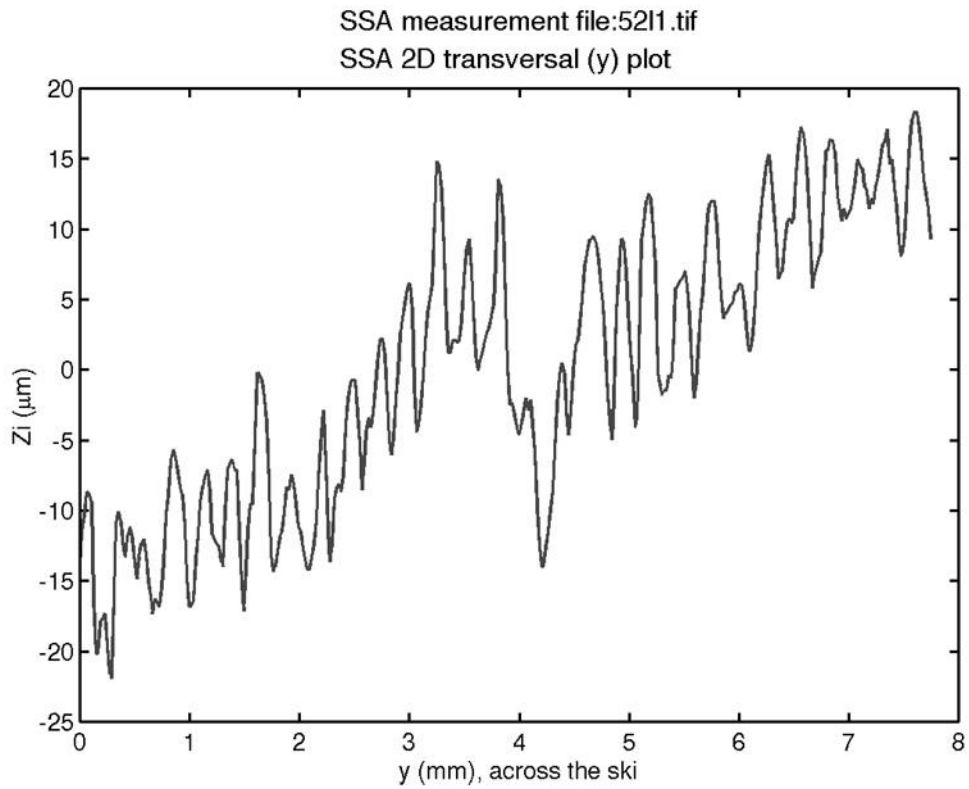


Fig. 4.22. Example of a surface profile across the afterbody of the test ski pair TSP52A.

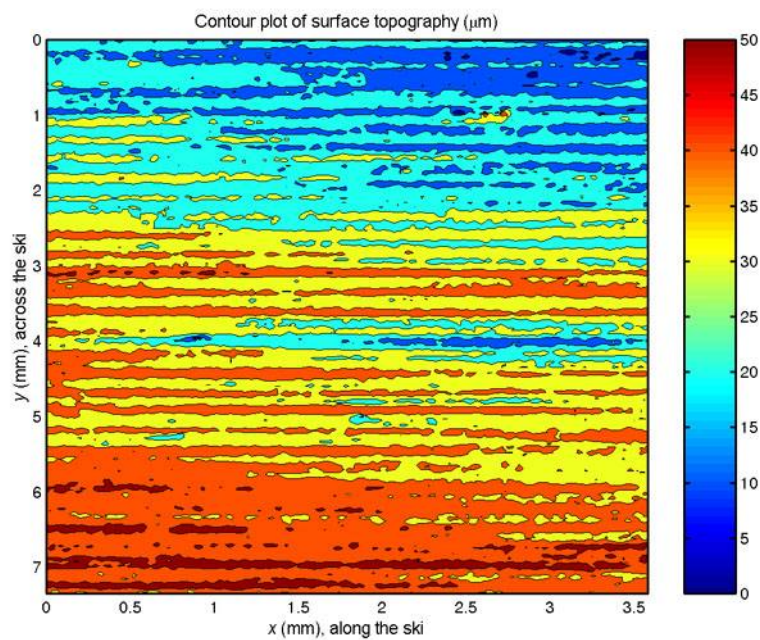


Fig. 4.23. Contour plot of the surface topography of the afterbody of the test ski pair TSP52A.

4.3.5. Test skis

During sliding tests of a structure test series it was experienced that two ski pairs that had been ground with the "same" structure at two different times, showed completely different sliding properties. Ski pair TSP8B was better than ski pair TSP8A when the air temperature was above zero and considerably better under conditions with falling or new-fallen, glazed snow. The average sliding speed of ski pair TSP8B was typically 3 to 6 % higher than the sliding speed of ski pair TSP8A under such conditions. Ski pair TSP8A was best under conditions with below zero air temperatures. TSP8A had for instance 1 % higher average sliding speed than ski pair TSP8B in a sliding test where the snow temperature varied between -8 and -10°C.

Figs. 4.24 and 4.25 show examples of surface profiles across the ski for the two test ski pairs TSP8A and TSP8B, while Table 4.4 lists structure roughness statistics. It is easy to see from Figs. 4.24 and 4.25 that ski pair TSP8B has considerably coarser and sharper structure relative to ski pair TSP8A. This can also be established from the structure roughness statistics in Table 4.4. Ski pair TSP8B has $\bar{R}_{a,yw}$ equal to 4.9 μm and $\bar{R}_{t,yw}$ equal to 30 μm , while $\bar{R}_{a,yw}$ and $\bar{R}_{t,yw}$ equals 3.8 and 26 μm for ski pair TSP8A. According to the theories described by Fig. 2.10 and Eq. (2.20) in Chapter 2 it was natural that ski pair TSP8B showed better sliding properties than TSP8A at above zero air temperatures (higher water film thickness) and TSP8A best under conditions with below zero air temperatures (lower water film thickness). The findings resulted in further development and extreme optimisation of the structure that was ground on ski pair TSP8B. Measurement of good and poor structures on test and competition skis has together with snow parameters like e.g. snow humidity been an important tool for optimising the ski base structures and increasing the knowledge on the effect of ski base structure on ski base sliding friction.

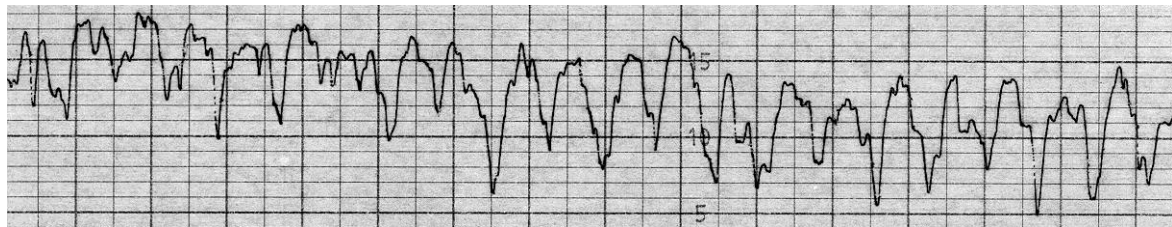


Fig. 4.24. Example of a surface profile across the ski for test ski pair TSP8A. The distance between the horizontal grid lines is 2 μm , while it is 500 μm between the vertical grid lines.

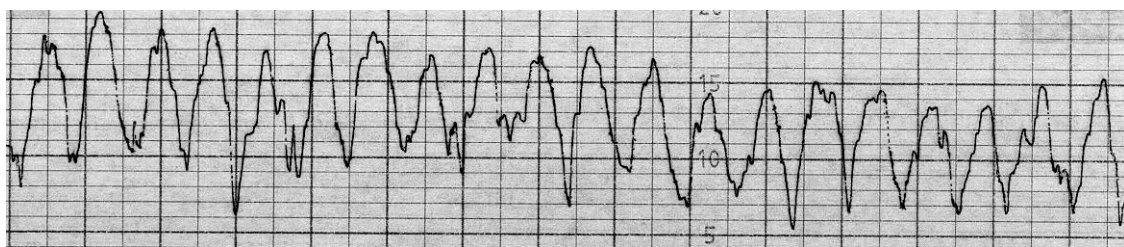


Fig. 4.25. Example of a surface profile across the ski for test ski pair TSP8B. The distance between the horizontal grid lines is 2 μm , while it is 500 μm between the vertical grid lines.

Table 4.4. Roughness statistics for the test ski pairs TSP8A and TSP8B.

Ski pair	$\bar{R}_{a,yw} \pm \delta_{Rayw}$ (μm)	$\bar{R}_{t,yw} \pm \delta_{Rtyw}$ (μm)
TSP8A	3.8 ± 0.5	26 ± 4
TSP8B	4.9 ± 0.5	30 ± 2

4.3.6. Competition skis

During a 30 km free technique competition that consisted of two rounds á 15 km, sliding times were registered in a downhill between 13.8 and 15 km on both rounds. Fig. 4.26 shows the elevation profile of the 15 km course together with markings of the test distance between 13.8 and 15 km. The competition took place under snow conditions with:

- Snow type 5
- Snow humidity $W_{\text{vol},\%} = 0.3$ to 1.0 %
- Snow grain size $\bar{d} \pm \delta_d = 0.93 \pm 0.33$ mm
- Snow hardness $H = 2.6 \times 10^4$ to 5.6×10^4 Pa
- Snow density $\rho = 0.48$ to 0.65 g/cm³
- Snow temperature $T_s = -8.4$ to -6.2 °C

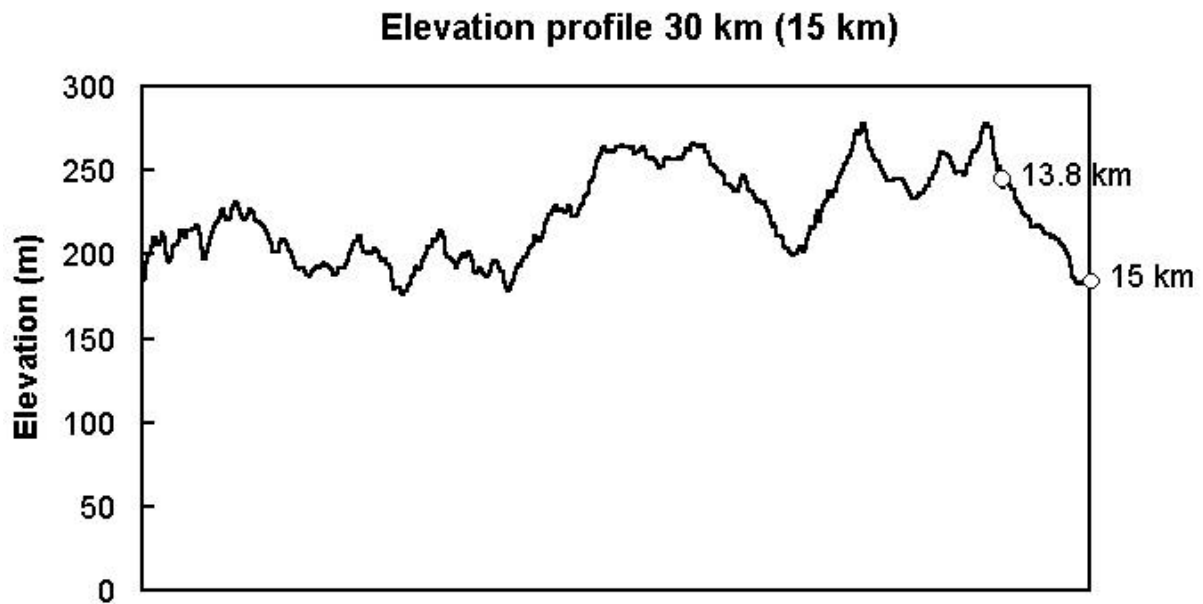


Fig. 4.26. Elevation profile of the 15 km course that was skied two times during the 30 km free technique competition. Sliding times were registered on both rounds in the downhill between 13.8 and 15 km.

Table 4.5 lists the registered sliding times during the 30 km free technique competition. It is easy to see from Table 4.5 that skier NSK4 had considerably poorer glide than the fastest skiers. Skier NSK4 spent 8.6 % more time on sliding down the downhill between 13.8 and 15 km on the first round than the fastest skier and 9.1 % more time on the second round. Although this skier ended up on a 26th

place in the competition, it was not natural that he should ski so slowly in the downhill (Rank 53 and 54 on the two rounds).

Table 4.5. Registered sliding times during the 30 km free technique competition. The sliding times are given in minutes, seconds and tenths of a second.

Round 1 (13.8 - 15 km)			Round 2 (28.8 - 30 km)		
Rank	Skier	Sliding time (Rank 30 km)	Rank	Skier	Sliding time (Rank 30 km)
1	SK4	2.26.3 (4)	1	SK7	2.24.2 (7)
2	SK24	2.27.3 (24)	2	SK39	2.24.7 (39)
3	SK23	2.28.6 (23)	3	NSK2	2.25.5 (3)
4	SK1	2.29.2 (1)	3	SK33	2.25.5 (33)
4	SK27	2.29.2 (27)	5	NSK3	2.25.6 (8)
14	NSK1	2.31.4 (2)	14	NSK1	2.28.3 (2)
15	NSK3	2.31.5 (8)	53	NSK4	2.37.3 (26)
21	NSK2	2.32.4 (4)			
54	NSK4	2.38.9 (26)	?	SK4	? (4)

The structures of the ski pairs of skier NSK1, NSK2 and NSK4 were measured and characterised after the 30 km competition. The roughness statistics for these measurements are given in Table 4.6. Figs. 4.27-4.32 show surface profiles across the forebody and afterbody for the various ski pairs. Notice that the distance between the horizontal grid lines is 4 μm in Fig. 4.32, while it is 2 μm in Figs. 4.27-4.31.

Although the structure roughness statistics seem quite good for the different ski pairs, it is easy to see from Fig. 4.32 that there is something wrong with the afterbody of the left ski of skier NSK4. It is clear from Fig 4.32 that this part of the ski is not plane. The left ski is in fact warped. This highlights the importance of having a plane ski base surface before the structure is ground and having a ski base surface where the water film can develop along the ski without fading away at snow temperatures below zero.

Table 4.6. Roughness statistics for the ski pairs of skier NSK1, NSK2 and NSK4.

Skier	$\bar{R}_{a,yw} \pm \delta_{Rayw}$ (μm)	$\bar{R}_{a,yf} \pm \delta_{Rayf}$ (μm)	$\bar{R}_{a,ya} \pm \delta_{Raya}$ (μm)
NSK1	2.2 ± 0.3	2.1 ± 0.1	2.3 ± 0.4
NSK2	2.6 ± 0.4	2.4 ± 0.3	2.8 ± 0.5
NSK4	2.8 ± 0.7	2.4 ± 0.5	3.3 ± 0.6

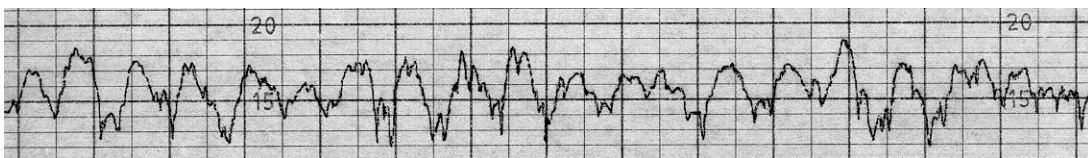


Fig. 4.27. Example of a surface profile across the forebody of the ski pair of skier NSK1. The distance between the horizontal grid lines is 2 μm , while it is 500 μm between the vertical grid lines.

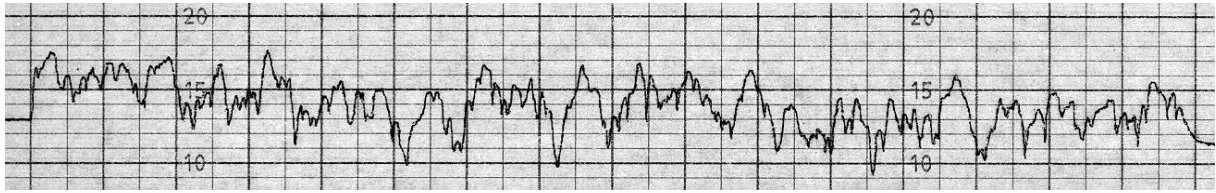


Fig. 4.28. Example of a surface profile across the afterbody of the ski pair of skier NSK1. The distance between the horizontal grid lines is $2\ \mu\text{m}$, while it is $500\ \mu\text{m}$ between the vertical grid lines.

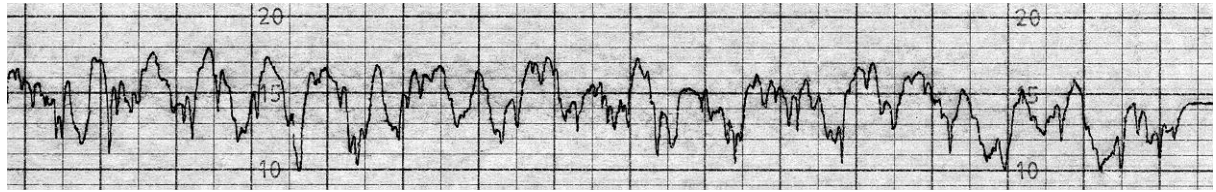


Fig. 4.29. Example of a surface profile across the forebody of the ski pair of skier NSK2. The distance between the horizontal grid lines is $2\ \mu\text{m}$, while it is $500\ \mu\text{m}$ between the vertical grid lines.

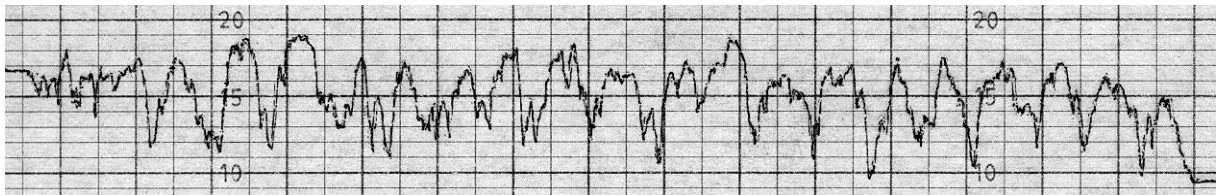


Fig. 4.30. Example of a surface profile across the afterbody of the ski pair of skier NSK2. The distance between the horizontal grid lines is $2\ \mu\text{m}$, while it is $500\ \mu\text{m}$ between the vertical grid lines.

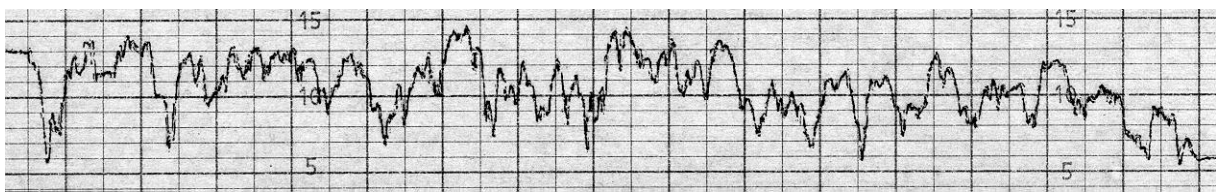


Fig. 4.31. Example of a surface profile across the forebody of the ski pair of skier NSK4. The distance between the horizontal grid lines is $2\ \mu\text{m}$, while it is $500\ \mu\text{m}$ between the vertical grid lines.

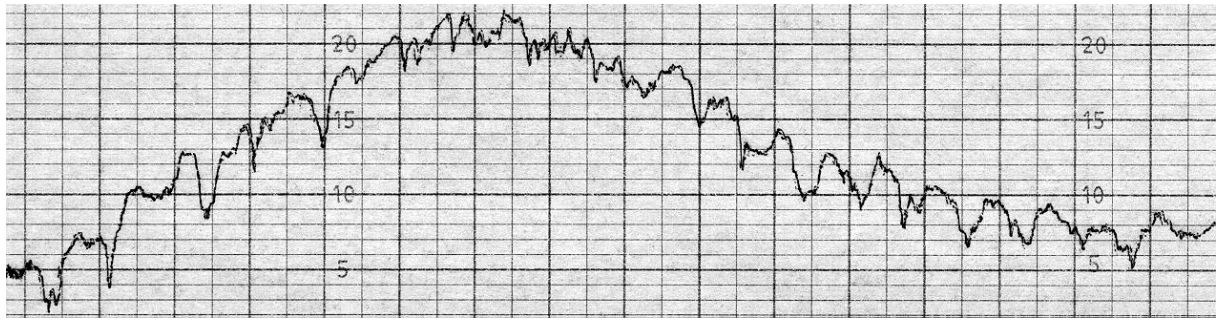


Fig. 4.32. Surface profile across the afterbody of the left ski of skier NSK4. The measurement is taken 36 cm behind the balance point of the ski. Notice that the distance between the horizontal grid lines is 4 μm , while it is 500 μm between the vertical grid lines.

Table 4.7 lists roughness statistics for two competition ski pairs with increased structure roughness along the ski. Ski pair CSP1 showed very good sliding properties under a competition with:

- Snow type 5
- Snow humidity $W_{\text{vol},\%} = 0.8$ to 1.4%
- Snow grain size $\bar{d} \pm \delta_d = 1.56 \pm 0.53$ mm
- Snow hardness $H = 8.8 \times 10^3$ to 1.9×10^4 Pa
- Snow density $\rho = 0.49$ to 0.55 g/cm³
- Snow temperature $T_s = -2.4$ to -1.7°C

The structure roughness $\bar{R}_{a,yf}$ on the forebody of this ski pair was equal to 3.2 μm , while the structure roughness $\bar{R}_{a,ya}$ on the afterbody was equal to 5.9 μm . Figs. 4.33-4.36 depict surface profiles and contour plots of the forebody and afterbody of ski pair CSP1.

Table 4.7. Roughness statistics for the competition ski pairs CSP1 and CSP2.

Ski pair	$\bar{R}_{a,yw} \pm \delta_{\text{Rayw}}$ (μm)	$\bar{R}_{a,yf} \pm \delta_{\text{Rayf}}$ (μm)	$\bar{R}_{a,ya} \pm \delta_{\text{Raya}}$ (μm)
CSP1	4.5 ± 1.5	3.2 ± 0.5	5.9 ± 0.4
CSP2	8.3 ± 1.7	6.9 ± 1.1	9.7 ± 0.6

Ski pair CSP2 has been very good on transformed and wet snow. The structure roughness $\bar{R}_{a,yf}$ on the forebody of this ski pair equals 6.9 μm , while the structure roughness $\bar{R}_{a,ya}$ on the afterbody equals 9.7 μm . Figs. 4.37 and 4.38 show surface profiles across the forebody and afterbody of ski pair CSP2.

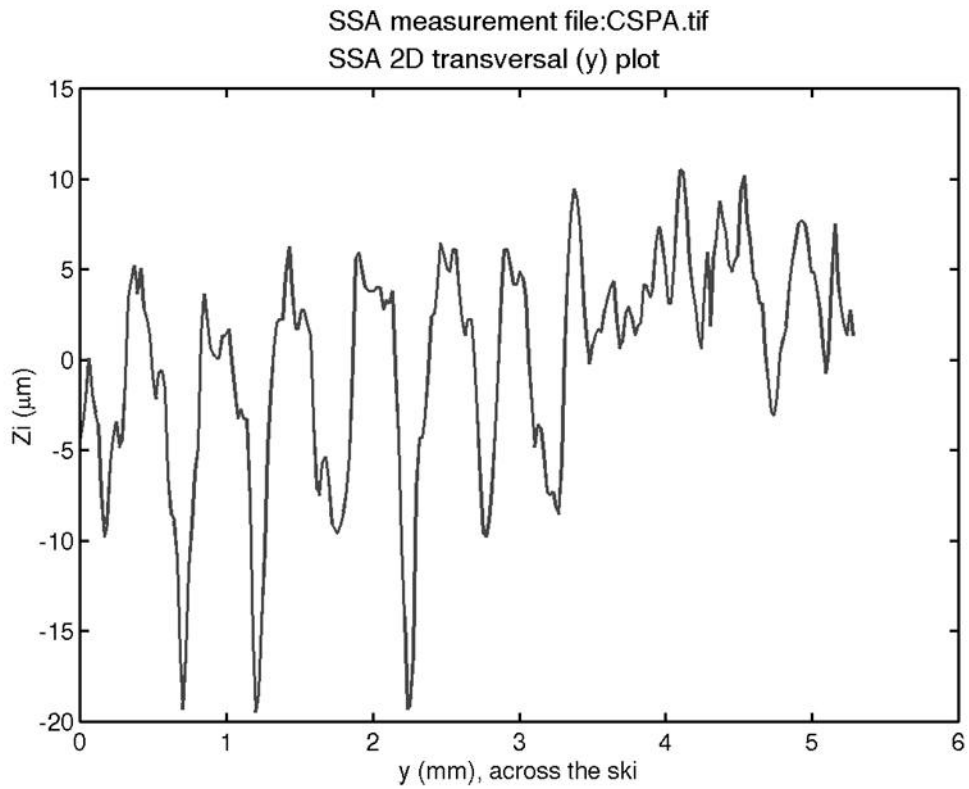


Fig. 4.33. Example of a surface profile across the forebody of the competition ski pair CSP1.

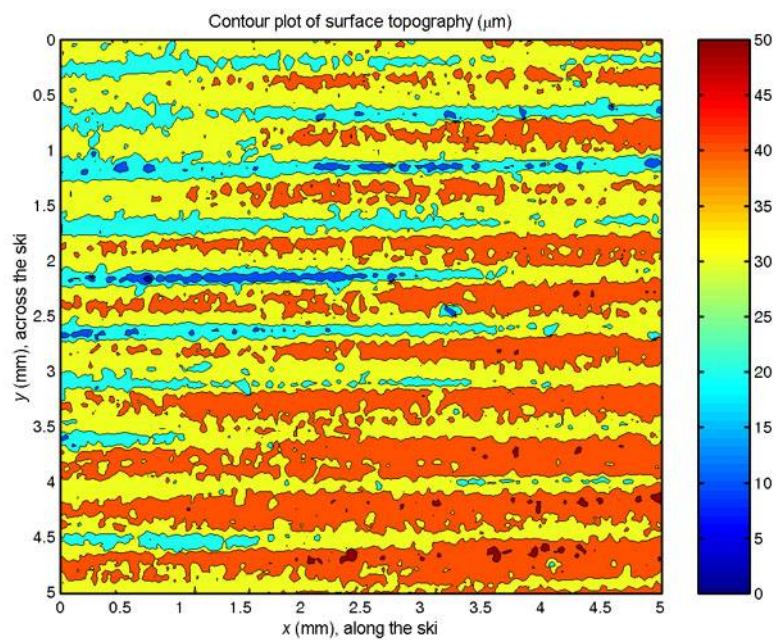


Fig. 4.34. Contour plot of the surface topography of the forebody of the competition ski pair CSP1.

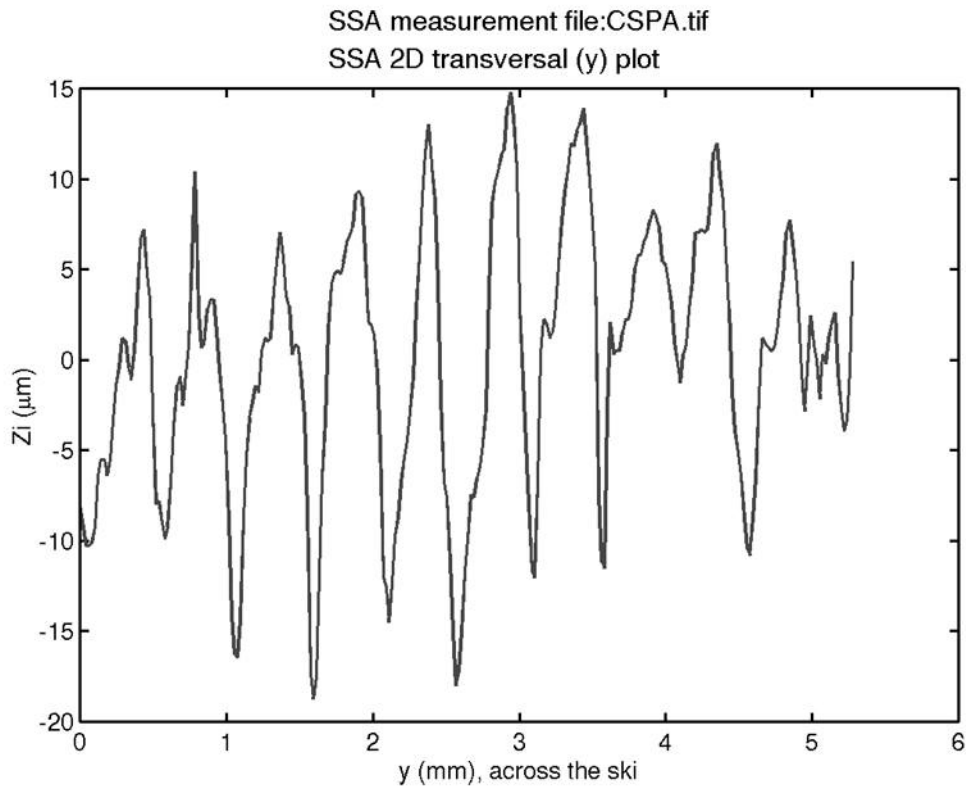


Fig. 4.35. Example of a surface profile across the afterbody of the competition ski pair CSP1.

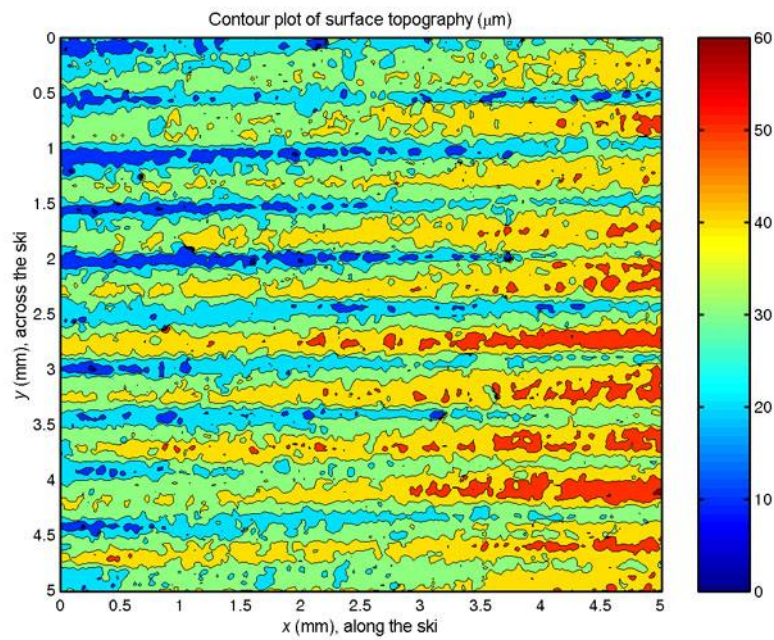


Fig. 4.36. Contour plot of the surface topography of the afterbody of the competition ski pair CSP1.

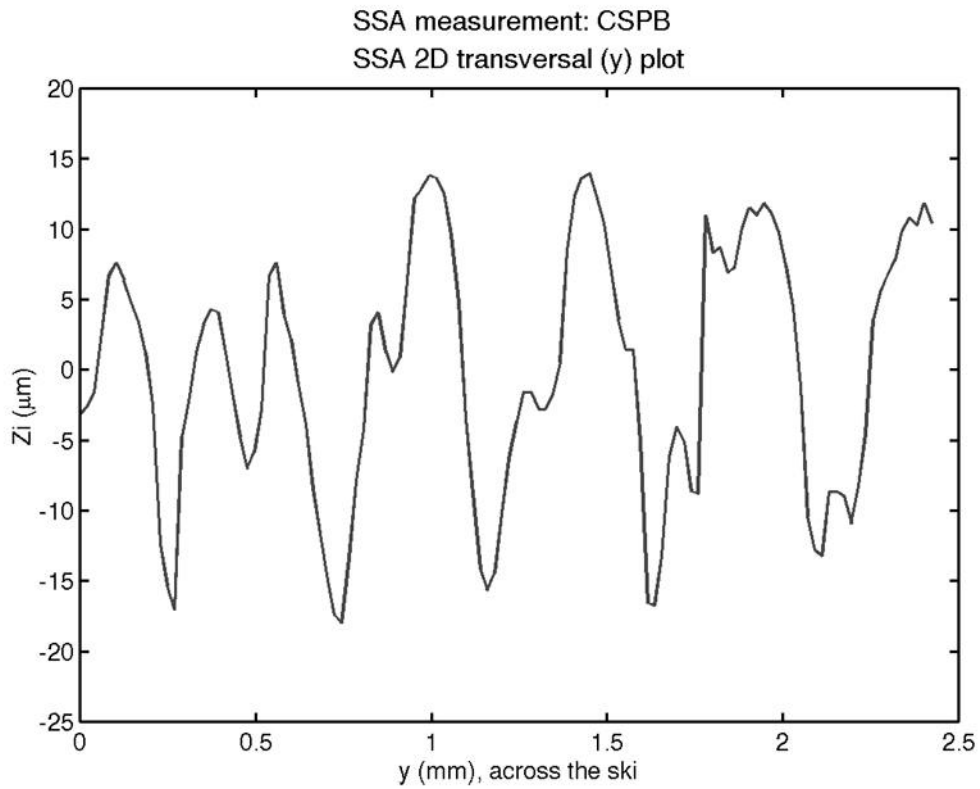


Fig. 4.37. Example of a surface profile across the forebody of the competition ski pair CSP2.

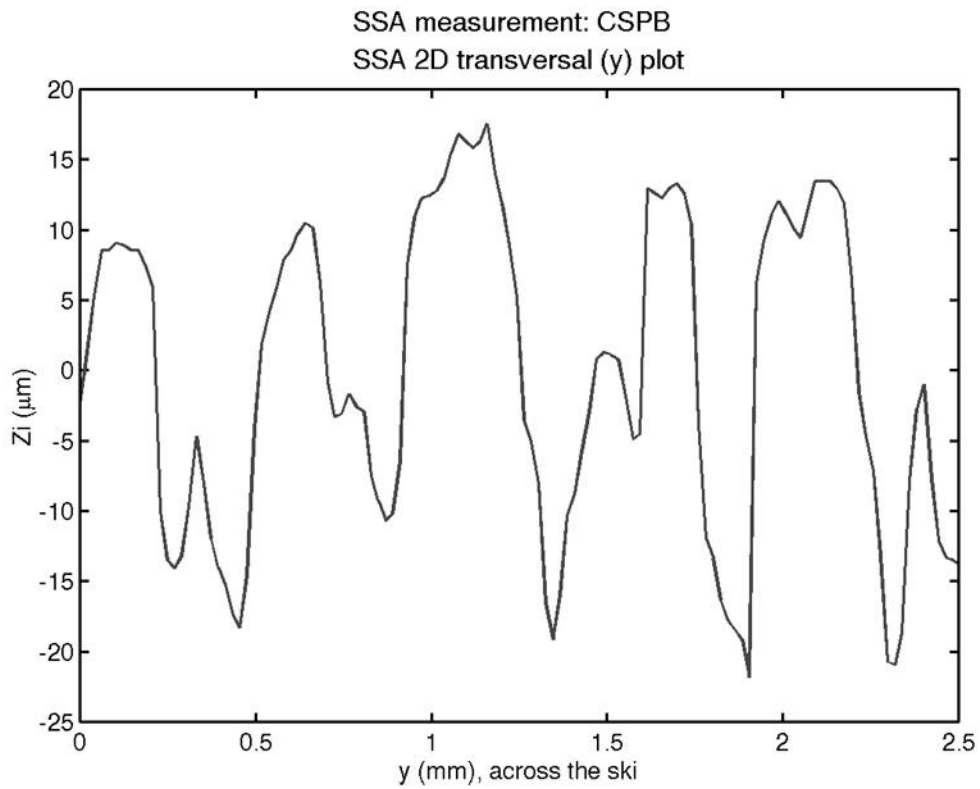


Fig. 4.38. Example of a surface profile across the afterbody of the competition ski pair CSP2.

4.4. Discussion

In Section 4.3.3 it was shown that rilling gave structure roughness that mainly increased along the ski. This can be explained from the fact that it is natural to increase the pressure on the rilling tool during rilling from the tip to the tail of the ski. It also highlights that manual rilling is a more unstable process than high-quality stone grinding.

Further, it was shown in Section 4.3.3 that structure roughness did not increase with the riller width. This can be explained from:

- Manual pressure instability during rilling.
- Increased riller width causing larger flat plateaus between the rilling grooves.

An example of a competition ski pair with mixed structure CSP15 was depicted in Section 4.3.3. This ski pair had shown very good gliding properties under moist snow conditions with relatively low snow hardness i.e. under conditions where dilution of water film and sufficient bearing area capabilities had to be combined at the same time. It was referred to in Chapter 2 that surfaces with mixed structures can be designed for particular combinations of properties which can not be obtained with a single surface treatment (Williamson, 1984), e.g. can

- One process make a structure on the slider surface that causes wide interfacial gaps relative to the sliding surface in order to facilitate lubricant access.
- Another process makes shallow-domed plateaus that can carry the load with very little deformation and wear.

The experiences with CSP15 show that such structure design criteria also are efficient for ski base structures.

It was referred to in Section 4.3.4 that properly plane ground test skis could have up to 3 % higher sliding speeds than non-plane test skis with similar structure roughness in sliding tests under snow conditions with snow temperatures below zero. Similar experiences were described in Section 4.3.6 for the skier NSK4 with a non-plane warped competition ski. This can be explained from the fact that it is more likely that generated water film fade away along the ski for a non-plane ski than a plane ski. Thus, it is also more likely that water film generation must start from scratch at more points along the ski for a non-plane ski. This means that a non-plane ski will have larger contact areas between ski and snow with pure dry friction relative to a plane ski during skiing under snow conditions with snow temperatures below zero. According to Fig. 2.10 and Eq. (2.20) in Chapter 2, this should cause a higher ski base sliding friction coefficient.

It was shown in Section 4.3.5 that a test ski pair TSP8B with $\bar{R}_{a,yw}$ and $\bar{R}_{t,yw}$ equal to 4.9 and 30 μm typically had 3 to 6 % higher average sliding speeds than a test ski pair TSP8A with $\bar{R}_{a,yw}$ and $\bar{R}_{t,yw}$ equal to 3.8 and 26 μm under conditions with above zero air temperatures. This shows that the assumption that the sliding friction coefficient remains constant at a value of 0.05 in the range of bump heights from 10 to 30 μm (McConica, 1950; Midol and Mathia, 1985; Mathia et al., 1992) does not hold.

It was referred to in Section 4.3.6 that increased structure roughness along the ski has shown very good results under some snow conditions. This is very sensible since it is assumed that the water film thickness increase along the ski under most snow conditions. Further development of ski base structures with increased structure roughness along the ski seems very promising for the future.

4.5. Conclusions

In the period between 1995 and 1998 almost 1700 ski base structure measurements were performed on more than 350 skis. Among these were 8 Olympic and 6 World Championship gold medal winning skis. The ski base structure measurement experiments gave the following findings:

- The ski base structure roughness can be divided into four categories: fine ($\bar{R}_{a,ys} = 1-4 \mu\text{m}$), medium ($\bar{R}_{a,ys} = 4-7 \mu\text{m}$), coarse ($\bar{R}_{a,ys} = 7-10 \mu\text{m}$) and very coarse ($\bar{R}_{a,ys} > 10 \mu\text{m}$) that correspond to dry to moist, moist, moist to wet, and wet to very wet snow conditions, respectively.
- The optimum structures on skating skis tend to be finer than the optimum structures on classic skis under similar snow and weather conditions due to impact and compaction resistances often having more influence on the total ski base sliding friction in a skating track compared to a classic track.
- Higher structure roughness on the forebody than the afterbody of the ski (up to 84 %) has been revealed on several competition ski pairs and led to adjustment and regrinding of the ski pairs in order to improve the structure roughness along the ski. Increased structure roughness along the ski is assumed as favourable for minimising ski base sliding friction according to the assumption that the water film thickness increases along the ski.
- Eight of ten rillers gave higher structure roughness on the afterbody of the ski (18 to 91 %) than the forebody of the ski in an experiment with ten different rillers. This was explained by increased pressure on the rilling tool during rilling from the tip to the tail of the ski and highlighted that manual rilling is a more unstable process than high-quality stone grinding. The experiment also showed that structure roughness not necessarily increases with riller width.
- Mixed structures where one process (rilling) make a structure on the slider surface that causes wide interfacial gaps relative to the sliding surface in order to facilitate lubricant access, and another process (stone grinding) makes shallow-domed plateaus that can carry the load with very little deformation and wear (Williamson, 1984), have proved to be efficient also for minimising ski base sliding friction.
- Properly plane ground test skis have shown up to 3 % higher sliding speeds than non-plane test skis with similar structure roughness under snow conditions with snow temperatures below zero. It has also been experienced that a skier with a non-plane warped competition ski spent 8.6 to 9.1 % more time on sliding down a 1.2 km downhill during a 30 km competition than the fastest skier. These variations can be explained from the fact that it is more likely that the generated water film fade away along the ski for a non-plane ski than a plane ski.
- Ski pairs ground with the "same" structure at two different times are not necessarily equal if no quality control of the ski base structure and the stone grinding process has been performed.

In an experiment with two test ski pairs that were assumed to have the "same" structure, sliding speed differences typically ranged between 3 and 6 % in sliding tests under conditions with above zero air temperatures. Ski base structure measurements showed that the best ski pair had $\bar{R}_{a,yw}$ and $\bar{R}_{t,yw}$ equal to 4.9 and 30 μm , while the other ski pair had $\bar{R}_{a,yw}$ and $\bar{R}_{t,yw}$ equal to 3.8 and 26 μm . It can be concluded from these sliding test results and ski base structure measurements that the assumption that the sliding friction coefficient remains constant at a value of 0.05 in the range of bump heights from 10 to 30 μm (McConica, 1950; Midol and Mathia, 1985; Mathia et al., 1992) does not hold.

The ski base structure measurements have also resulted in:

- Focus on the importance of quality control of ski base structures.
- Improvement of the stone grinding procedure, e.g. development and improvement of the grinding diamonds used to set the grinding stone.
- Avoidance of decreased structure roughness along competition skis and test skis.
- Development and extreme optimisation of the best ski base structures.
- Development of ski base structures with increased roughness along the ski.
- Confidence for ski technicians and competition skiers that the best structures can be reproduced.
- Confidence for ski technicians and competition skiers that optimum structures and skis are used in competitions under different snow and weather conditions.
- Investigation and visualisation of the effect of ski base mass being replaced during rilling, while being removed during stone grinding.
- Increased knowledge of the effect of ski base structure on ski base sliding friction.

4.6. References

- Mathia, T. G., H. Zahouani and A. Midol (1992): Topography, wear, and sliding functions of skis. *International Journal of Machine Tools Manufacturing*, Vol. 32, No. 1/2, pp. 263-266.
- McConica, T. H. (1950) Sliding on ice and snow. American Ski Co. Technical Report, 46 p.
- Midol, A. and T. G. Mathia (1985): Actes de Colloque Sport, un Enjau Technologique, Paris, *La glisse 1985*. Ed., Sporettec-Lyon.
- Moldestad, D. A. (1995): PC-basert system for måling og valg av sålestruktur på langrennsski. The Norwegian Institute of Technology, Department of Engineering Cybernetics, Thesis (in Norwegian), 82 p.
- Williamson, J. B. P. (1984): The shape of surfaces. In *CRC Handbook of Lubrication. Theory and Practice of Tribology. Volume II. Theory and Design* (E. R. Booser, Ed.). CRC Press Inc., Boca Raton, Florida, pp. 3-16.

5. Characterisation of snow structure in a cross-country race ski track

Notation

B_m	measured bandwidth of the <i>Snow Fork</i> resonance curve when the <i>Snow Fork</i> is put in snow, MHz
B_{wl}	bandwidth of the <i>Snow Fork</i> resonance curve at the frequency f_m for a material without loss, MHz
C	cloudiness in octoparts, $C = 0 \Rightarrow$ clear sky, $C = 8 \Rightarrow$ complete cloud cover
\bar{d}	mean of d_j for the n_g snow grains with distinguishable boundaries in a microscope image of a snow surface, mm
d_{ba}	diameter of steel ball, 4×10^{-2} m
d_j	length of the largest 2D diagonal for snow grain surface number j in a microscope image of a snow surface, mm
d_{sn}	indentation diameter of the dropped steel ball in the snow, m
f_{air}	measured resonant frequency when the <i>Snow Fork</i> is in air, MHz
f_m	measured resonant frequency when the <i>Snow Fork</i> is put in snow, MHz
F	momentary resistance of the snow relative to the dropped steel ball, N
\bar{F}_{sn}	mean resistance of the snow relative to the dropped steel ball, N
g	acceleration due to gravity, 9.81 m/s^2

H	snow hardness, N/m ² or Pa
\bar{H}	mean snow hardness for a snow type, Pa
H_{\max}	maximum snow hardness for a snow type, Pa
H_{\min}	minimum snow hardness for a snow type, Pa
H_{50}	median snow hardness for a snow type, Pa
h_{ba}	drop height of the steel ball through the plastic tube, h_{ba} has been varied from 6.47×10^{-2} m for soft snow to 44.1×10^{-2} m for hard snow
h_{sn}	indentation depth of the dropped steel ball in the snow, m
j	snow grain surface number in a microscope image of a snow surface
m_{ba}	mass of steel ball, 0.265 kg
n_g	number of snow grains with distinguishable boundaries in a microscope image of a snow surface
n_H	number of hardness measurements for a given snow type
n_p	number of density measurements for a given snow type
q_{net}	net radiation 50 cm above the snow surface, W/m ²
Rh	relative humidity 50 cm above the snow surface, %
S	surface contact area of the steel ball with snow, m ²
T_a	air temperature 50 cm above the snow surface, °C
T_s	snow temperature 2 cm below the snow surface, °C
$W_{\text{vol},\%}$	volume per cent liquid water content in the snow, %
$W_{\text{wgt},\%}$	weight per cent liquid water content of snow, %
δ_d	standard deviation of d_j for the n_g snow grains with distinguishable boundaries in a microscope image of a snow surface, mm
δ_H	standard deviation of \bar{H} , Pa
δ_p	standard deviation of $\bar{\rho}$, g/cm ³
ϵ'	real part of the relative permittivity of the snow
ϵ''	imaginary part of the relative permittivity of the snow
ρ	density of snow, g/cm ³
$\bar{\rho}$	mean snow density for a snow type, g/cm ³
ρ_{\max}	maximum snow density for a snow type, g/cm ³
ρ_{\min}	minimum snow density for a snow type, g/cm ³
ρ_w	density of water, 1 g/cm ³
ρ_{50}	median snow density for a snow type, g/cm ³
σ_{mss}	electrolytic conductivity of snow collected from the snow surface, i.e. electrolytic conductivity of a melted snow sample from the snow surface, $\mu\text{S}/\text{cm}$

5.1. Introduction

This chapter describes the methods and procedures we have used when measuring and characterising the different snow and weather parameters. Furthermore results from measurement and characterisation of snow are referred and discussed.

Characterisation of the sliding surface, i.e. the snow surface in the cross-country ski track, is necessary in order to understand ski base sliding friction and results from ski base sliding friction tests. It is therefore important to register essential snow parameters when performing accurate ski base sliding friction tests in-situ. In our research we have registered and characterised the following snow parameters:

- Snow temperature at depths -5, -2 and 0 cm relative to the snow surface
- Snow hardness
- Snow humidity and snow density
- Snow type and snow grain structure
- Electrolytic conductivity and water chemistry of melted snow samples

In addition the following weather parameters have been registered:

- Air temperature (50 cm above the snow surface)
- Relative humidity (50 cm)
- Net radiation (50 cm)

Knowledge on the matter of snow is essential for scientists (and others) working with e.g.:

- Friction between different vehicles and snow or ice
- Snow avalanche safety
- Glacier and ice sheet advance and retreat
- Climate modelling and meteorology
- Remote sensing of seasonal snowcovers
- Snow hydrology
- Tracking of pollution spreading
- Structural engineering in cold regions
- Snow mechanics
- Snow physics

Due to the variety of physical processes involving snow, the published material on the subject is quite comprehensive. In spite of this fact it has been pointed out that "the properties of snow are not yet well enough known for use with a high degree of confidence" (Brown, 1989). This highlights the importance of further measurements and characterisation of snow parameters and generation of knowledge databases on snow.

It is neither the scope of this chapter nor thesis to review or refer to most published material on snow. Instead this section briefly gives an account of some chosen works on measurement and characterisation of different snow parameters and some general works on snow. A further study of snow measurements and characterisation of snow parameters should be possible to accomplish by reading the references.

Gray and Male (1981) gave an extensive survey of snow in the *Handbook of Snow*. This book presented snow topics such as the impact and interaction of snow with living things, climate and

agriculture, snowfall formation, snow cover distribution, measurement of snow, physics and properties of snowcovers, snow drifting, snowcover ablation and runoff, avalanches, snow engineering and skiing. A review of progress in snow and ice research in the quadrennial between 1987 and 1990 was given by Richter-Menge et al. (1991). Their review focused on the influence of layers in seasonal snow covers, research in ice mechanics on freshwater and sea ice, and remote sensing of polar ice sheets. Bales and Harrington evaluated recent progress in snow hydrology in 1995.

The latest classification of seasonal snow on the ground was given by Colbeck et al. (1990). This included classification of features of deposited snow such as:

- Snow density
- Grain shape
- Grain size
- Liquid water content of the snow (snow humidity)
- Impurities in the snow
- Snow strength
- Snow hardness
- Snow temperature
- Snow layer thickness

The terms used in Colbeck et al. (1990) for classification of grain shape, grain size, liquid water content and hardness have been applied in this chapter. More details on classification of these snow parameters are given in Section 5.2. A classification system for seasonal snow covers with six classes; tundra, taiga, alpine, maritime, prairie and ephemeral has been proposed by Sturm et al. (1995). Falling snowflakes are normally classified according to the system of Magano and Lee (1966). Their system was based on the work of Nakaya (1954).

Colbeck (1997) reviewed sintering in seasonal snow. He has also given a review of the metamorphism and classification of seasonal snow cover crystals (Colbeck, 1987) and evaluated the basic ideas behind snow metamorphism (Colbeck, 1996). Arons and Colbeck (1995) have reviewed theories and experiments involving geometry of heat and mass transport in dry snow. Davis (1991) discussed links between snow metamorphism, water flow and solute transport through a snowpack. Ionic elution through a snowpack has furthermore been studied by e.g. Davies et al. (1982 and 1987), Tsiouris et al. (1985), Brimblecombe et al. (1985 and 1987), Tranter et al. (1986), Bales et al. (1989), Hewitt et al. (1989 and 1991), Cragin et al. (1993), Raben and Theakstone (1994, 1997 and 1998) and Davis et al. (1995). Davidson et al. (1996) evaluated atmospheric deposition of chemical species to polar snow. Hewitt and Cragin (1994) have investigated chemical composition of snow crystals.

Measurements and characterisation of snow morphology have usually been destructive to the original state of the snow surface. A normal measurement procedure (see e.g. Coléou and Lesaffre, 1998) has been to:

- Remove snow grains from the snow surface or snow sample.
- Put the snow grains on a glass slide or plate that has been ruled in millimetres.
- Observe the snow grains through a microscope.

- Capture microscope images with a camera that is connected to the microscope.
- Analyse the registered snow microscope images with some sort of image analysis system.

Another method has been to use planar sections of snow, i.e. flat face cuts through specimen of snow (Arons and Colbeck, 1995). Planar sections have been preserved by use of special conservation techniques and analysed indoor at a later stage using transmitted or reflected light, for more details see e.g. Fuchs (1956), Kinoshita and Wakahama (1960), Perla et al. (1986) and Good (1987; 1989). A new method for in-situ photography of snow slabs using transmitted light was reported by Good et al. (1991). According to Arons and Colbeck (1995) this method seemed to be well suited for analyses of large delicate snow structures that would not survive sample collection and transport. In our research we have used a stereomicroscope (max. 40× magnification) to observe the snow surface directly in-situ in the ski track.

Snow structure in natural ski fields have been evaluated by e.g. Seligman (1936), Yosida (1971), and Perla and Glenne (1981), but to our knowledge no authors have so far performed a proper systematic microscope examination of the snow surfaces that exists in-situ in ski tracks. Warren et al. (1989) have depicted a snow grain with melt cap from a snow surface where a slider had passed over.

Studies of snow grain structure have taken place since the mid 1930's e.g. by Bader et al. (1939), de Quervain (1948; 1958), Eugster (1952), Kinoshita (1960a), Yosida (1963) and Wakahama (1968). These studies were followed by works in the late 1960's and 1970's by LaChapelle (1969), Narita (1969; 1971), Sommerfeld and LaChapelle (1970), Akitaya (1974), Kry (1975), Good (1975), Gubler (1978), and Raymond and Tusima (1979). The 1980's introduced papers by e.g. Good (1980; 1982; 1987), Perla (1985), Perla and Ommanney (1985), Colbeck (1986; 1987), Hansen and Brown (1986) and Dozier et al. (1987). More recent work have been presented by e.g. Colbeck et al. (1990), Hewitt et al. (1991), Davis (1991), Edens and Brown (1991), Cragin et al. (1993), Takahashi et al. (1996), Colbeck (1997) and Wiesmann et al. (1998). Specific snow grain image analysis systems have been described by e.g. Brun et al. (1987), Good (1987; 1989) and Lesaffre et al. (1998). Studies of the relationship between permeability, density and snow structure have been performed by e.g. Shimizu (1970), Buser and Good (1987), and Arons and Colbeck (1995).

Because shear and tensile tests are both time consuming and difficult to make, hardness is often used as an index of the strength of snow (Schaerer, 1981). Hardness is defined as the resistance of the snow to penetration by a specified object and is related to the tensile, shear and compressive strengths of snow. Field measurements of snow hardness can be performed by e.g. the Swiss Rammsonde, the Russian AARI penetrometer, the Canadian gauge, a Kinoshita-type hardness meter (Kinoshita, 1960b), a flat plate penetrometer (Kragelski, 1949), a thin-walled hollow cylinder penetrometer (Shapiro et al., 1997) and the blade penetration test (Fukue, 1979). Recently a handheld, digital load-gauge (push-pull gauge) has also been developed for snow hardness measurements (Takeuchi et al., 1998). In our study we have estimated the snow hardness of the surface of a track from the indentation diameter a steel ball with known mass and diameter gives in the snow surface when being dropped from a known height through a plastic tube (more details in Section 5.2.2).

Hardness measurements made systematically for evaluating ski performance have been performed by e.g. Kinoshita (1960b), Yosida (1971), Kuroiwa and LaChapelle (1972), and Hämäläinen and Spring (1986). Bader and Kuroiwa (1962), Mellor (1964; 1975; 1977), Gubler (1975), Salm (1982) and

Shapiro et al. (1997) have presented reviews on snow mechanics. Johnson (1998) has examined the micromechanics of snow compaction. Snow compaction or snow densification have also been studied by e.g. Anderson and Benson (1963), Yosida (1963), Kojima (1967) and Gow (1968). In the 1970's studies were performed by e.g. Gray et al. (1970), Grant and Rhea (1974), Abele and Gow (1975; 1976), Voitkovsky et al. (1975), Wakahama (1975) and Colbeck et al. (1978). In the last two decades works have been presented by e.g. Goodison et al. (1981), Maeno and Ebinuma (1983), Alley (1987), Ebinuma and Maeno (1987), Wilkinson (1988), Johnson et al. (1993), and Frolov and Fedyukin (1998).

Several measurement methods can be used for determining the snow humidity or liquid water content in a snowpack:

- Melting (hot) calorimetry, see e.g. Yosida (1940; 1960), and Hansen and Jellenik (1957).
- Freezing (cold) calorimetry, see e.g. Jones et al. (1983).
- Alcohol calorimetry, see e.g. Fisk (1986).
- Dilution measurements, see e.g. Davis et al. (1985).
- Centrifugal measurements, see e.g. Kuroda and Hurukawa (1954), and Kuroiwa (1954).
- Dielectric measurements, see e.g. Ambach and Denoth (1975), Aebischer and Mätzler (1983), Denoth et al. (1984), Sihvola and Tiuri (1986), Bergman (1986; 1987), Kendra et al. (1994), Denoth (1997) and Stein et al. (1997).

Calorimetry, dilution and centrifugal measurements are destructive methods. Freezing calorimetry is accepted as a standard field measurement method and is used to calibrate non-destructive methods (Stein et al., 1997). Dielectric measurements are faster to perform than the other measurement methods (Boyne and Fisk, 1987) and suitable for in-situ non-destructive measurements. The *Snow Fork* instrument (Sihvola and Tiuri, 1986) has been used for measuring snow humidity and density in the work of this thesis.

Measurements of the liquid water content of snow have not been made systematically to a great extent in in-situ ski studies. Spring (1988) presented kinetic friction coefficients for skis gliding with speeds up to 10 m/s on old grainy snow with 0 and 20 % snow humidity. Slotfeldt-Ellingsen and Torgersen (1983) published laboratory friction tests on crushed ice with various liquid water contents, but these tests were performed with too small slider speed (0.3 m/s) to be of great relevance for typical ski base sliding friction situations. Non-destructive in-situ measurements of liquid water content in snow have been presented by e.g. Sihvola and Tiuri (1986), Toikka (1992), Kendra et al. (1994), Denoth (1997) and Stein et al. (1997).

Measurements of electrical conductivity and chemical properties of snow and melted snow samples have to the author's knowledge not been paid any attention to in in-situ ski studies. Petrenko (1994) presented static electrical conductivity values for ice used in friction tests in laboratory at -10 (10^{-3} $\mu\text{S}/\text{cm}$) and -30°C (10^{-5} $\mu\text{S}/\text{cm}$). The electrical static conductivity of snow was evaluated by Kopp (1962) for different snow densities, snow temperatures and snow types. Norwegian snow chemistry was studied in the 1970's by e.g. Elgmork et al. (1973), Hagen and Langeland (1973), Johannesen et al. (1975), Johannesen and Henriksen (1978), Wright and Dovland (1978), and Skartveit and Gjessing (1979). The last two decades have introduced works by e.g. Davies et al. (1982), Tsiouris et al. (1985),

Storrø (1990), He and Theakstone (1994), Raben and Theakstone (1994, 1997; 1998) and Reimann et al. (1996). Annual records of long range-transported pollutants in precipitation in Norway can be retrieved from the Norwegian Institute for Air Research.

5.2. Measurement methods and procedures

This section describes briefly the measurement methods and procedures used in the thesis work.

5.2.1. Snow temperature

Snow temperature has been measured using a *STAR HD 8901 Hygrometer-Thermometer* with a snow probe with a small temperature sensor in the tip. The instrument has an accuracy of $\pm 0.1\%$ of registered value $\pm 0.2^\circ\text{C}$ (STAR, 1995). Snow temperature measurements have been taken at three different levels in the race ski track:

- 5 cm below the surface of the track
- 2 cm below the surface of the track
- In the surface of the track

It can be difficult to perform qualitatively good measurements of snow surface temperature due to potential influence from air temperature, precipitation and solar radiation on the snow temperature sensor. Direct sunlight on the sensor has been avoided by using the body of the person that holds the probe, to shade for the sun when necessary.

Different measurement levels have been chosen in order to get consistent snow temperature measurements and obtain information about the temperature gradient in the snow. Throughout this chapter the snow temperature 2 cm below the surface of the track is referred to as the snow temperature T_s .

5.2.2. Snow hardness

Snow hardness has been estimated from the indentation diameter, d_{sn} , a steel ball with mass, $m_{\text{ba}} = 0.265$ kg, and diameter, $d_{\text{ba}} = 4.0 \times 10^{-2}$ m, gives in the snow surface when being dropped from a known height, h_{ba} , through a plastic tube. The measurement procedure is shown in Fig. 5.1. Fig. 5.1a shows the setup before the steel ball is dropped through the plastic tube from a known height. The drop height is adjusted according to the snow conditions. Under soft snow conditions smaller drop heights are used than under hard snow conditions. Fig. 5.1b shows the situation after the steel ball has been dropped, and an indentation in the snow surface has been made. In Fig 5.1c the indentation diameter of the dropped steel ball is measured with a slide gauge. The snow hardness is estimated from the measured indentation diameter.

The mean resistance of the snow relative to the dropped steel ball, \bar{F}_{sn} , is given from the following energy considerations:

$$m_{ba}g(h_{ba} + h_{sn}) = \int_0^{h_{sn}} F_{sn} dh = \bar{F}_{sn} h_{sn} \quad (5.1)$$

$$\bar{F}_{sn} = m_{ba}g \left(1 + \frac{h_{ba}}{h_{sn}} \right)$$

where:

- F_{sn} - momentary resistance of the snow relative to the dropped steel ball, N
- g - acceleration due to gravity, 9.81 m/s²
- h_{sn} - indentation depth of the dropped steel ball in the snow, m

The indentation depth of the dropped steel ball in the snow, h_{sn} , may be obtained from the measured indentation diameter of the steel ball in the snow, d_{sn} :

$$h_{sn} = \frac{d_{ba}}{2} - \sqrt{\left(\frac{d_{ba}}{2}\right)^2 - \left(\frac{d_{sn}}{2}\right)^2} \quad (5.2)$$

The snow hardness, H , is defined as:

$$H = \frac{\bar{F}_{sn}}{S} \quad (5.3)$$

where the surface contact area of the steel ball with snow, S , is given by:

$$S = \pi \left[\left(\frac{d_{sn}}{2}\right)^2 + h_{sn}^2 \right] \quad (5.4)$$

The snow hardness measurements have an accuracy of approximately $\pm 5\%$ of the measured value. The classification of snow hardness has been performed according to Colbeck et al. (1990), see Table 5.1.

Table 5.1. Classification of snow hardness according to Colbeck et al. (1990).

Term	H (Pa)	Hand test	Symbol
Very low	0 - 10 ³	fist	R1
Low	10 ³ - 10 ⁴	4 fingers	R2
Medium	10 ⁴ - 10 ⁵	1 finger	R3
High	10 ⁵ - 10 ⁶	pencil	R4
Very high	> 10 ⁶	knife blade	R5
Ice			R6

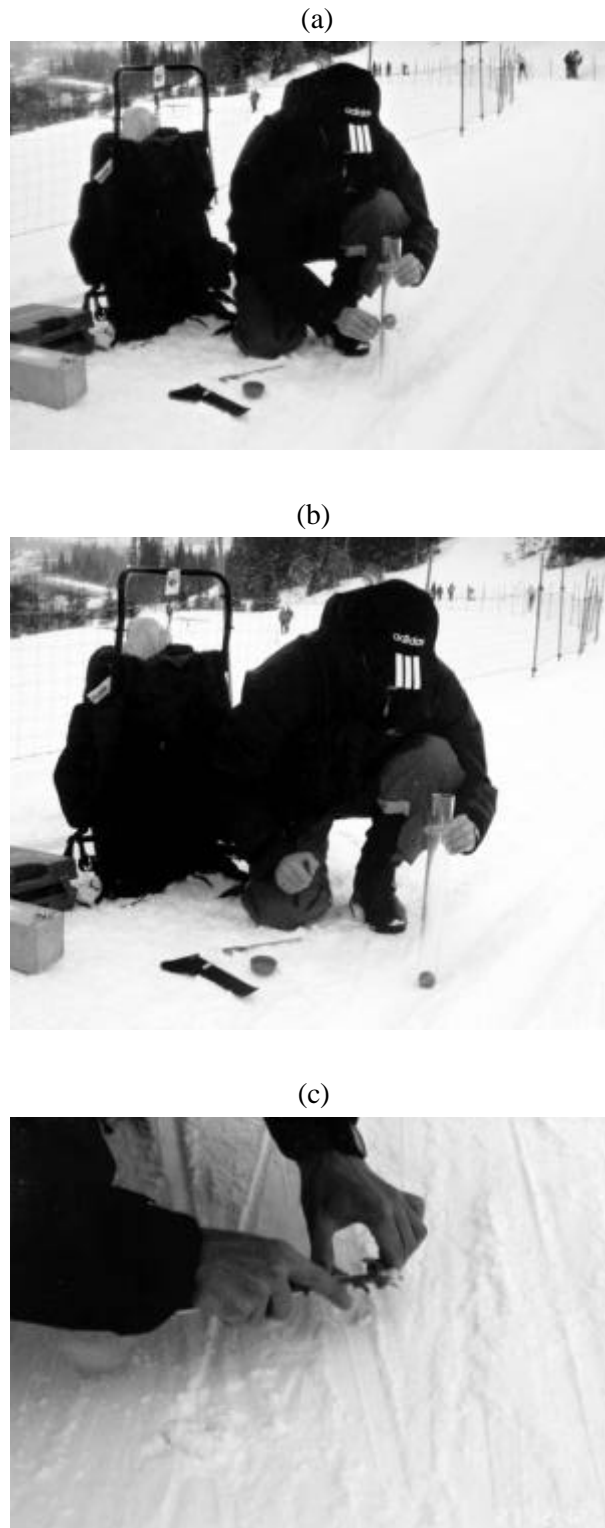


Fig. 5.1. The snow hardness measurement procedure: (a) The steel ball is about to be dropped through the plastic tube from a known height. (b) The steel ball has been dropped, and an indentation in the snow surface has been made. (c) The indentation diameter of the dropped steel ball is measured. The snow hardness is estimated from the measured indentation diameter.

5.2.3. Snow humidity and snow density

The snow humidity and snow density have been measured with the *Snow Fork* instrument (Sihvola and Tiuri, 1986). The *Snow Fork* is a steel fork used as microwave resonator which operates in the resonance frequency range 500 to 1000 MHz and measures the resonance frequency, attenuation and 3-dB bandwidth of a snow volume. From these electrical parameters the complex dielectric permittivity of the snow can be calculated as well as the density and liquid water content of the snow. The real part of the relative permittivity of the snow, ϵ' , is given from a *Snow Fork* measurement by (Toikka, 1998):

$$\epsilon' = \left(\frac{f_{\text{air}}}{f_m} \right)^2 \quad (5.5)$$

where:

f_m - measured resonant frequency when the *Snow Fork* is put in snow, MHz

f_{air} - measured resonant frequency when the *Snow Fork* is in air, MHz

The imaginary part of the relative permittivity of the snow, ϵ'' , is calculated from the equation (Toikka, 1998):

$$\epsilon'' = \left(\frac{B_m - B_{\text{wl}}}{f_m} \right) \epsilon' \quad (5.6)$$

where the bandwidth of the *Snow Fork* resonance curve at the frequency f_m for a material without loss, B_{wl} , is given in MHz by:

$$B_{\text{wl}} = 0.03 \times (f_m - 183) \quad (5.7)$$

where:

B_m - measured bandwidth of the *Snow Fork* resonance curve when the *Snow Fork* is put in snow, MHz

The volume per cent liquid water content in the snow, $W_{\text{vol},\%}$, may be deduced from the values of ϵ'' and f_m by using the equation (Toikka, 1998):

$$W_{\text{vol},\%} = 100 \times \left[-0.06 + \sqrt{0.06^2 + \frac{\epsilon''}{0.0075 f_m}} \right] \quad (5.8)$$

Further, the density of the snow in g/cm^3 , ρ , reads (Toikka, 1998):

$$\rho = -1.2142857 + \sqrt{1.2142857^2 - \frac{1 + 8.7 \times \left| \frac{W_{\text{vol},\%}}{100} \right| + 70 \times \left| \frac{W_{\text{vol},\%}}{100} \right|^2 - \varepsilon'}{0.7}} + \left| \frac{W_{\text{vol},\%}}{100} \right| \quad (5.9)$$

The weight per cent liquid water content of snow, $W_{\text{wt},\%}$, can be deduced from the values of $W_{\text{vol},\%}$ and ρ (Toikka, 1998):

$$W_{\text{wt},\%} = \frac{W_{\text{vol},\%}}{r/r_w} \quad (5.10)$$

where:

$$\rho_w - \text{density of water, } 1 \text{ g/cm}^3$$

The *Snow Fork* is designed for measuring liquid water content between 0 and 10 % with an accuracy of ± 0.3 % (Toikka, 1996). The measurement of snow density has an accuracy of $\pm 0.005 \text{ g/cm}^3$. The *Snow Fork* is primarily designed for measuring snow density below 0.6 g/cm^3 , but is also usable for measuring higher snow densities.

Normally when measuring the snow humidity and snow density, the *Snow Fork* is pushed horizontally into the snow pack. In order to measure the snow humidity and snow density as close as possible to the snow surface, the *Snow Fork* has been put into the snow surface with an angle of approximately 30° relative to the snow surface. The measurement setup is shown in Fig. 5.2. When the *Snow Fork* measurements are performed at an angle of 30° to the snow surface, a small part of the measurement volume will contain air instead of snow. It is important to adjust the humidity and density results accordingly. This can be performed quite simply by using the fact that the spikes of the *Snow Fork* are 75 mm long, and the width is 20 mm. Assuming that the *Snow Fork* measurement volume consists of a 75 mm long cylinder with 10 mm radius, it can be found that approximately 6 % of the measurement volume is air when the *Snow Fork* is put into the snow at a 30° angle relative to the snow surface. The calculated density and snow humidity must therefore be multiplied by the factor:

$$\frac{75}{75 - \frac{\sqrt{300}}{4}} = 1.0612726 \approx 1.06$$

If a 45° angle to the snow surface is used in the measurements instead of a 30° angle, the multiplication factor will be approximately 1.034. Half-space measurements (Sihvola and Tiuri, 1986) where the *Snow Fork* lies at the snow surface have also been tested in our research. This setup has not given reliable results.

Classification of the snow humidity or liquid water content of the snow according to Colbeck et al. (1990) is shown in Table 5.2. Snow with liquid water content less than 0.5 % has been approximated as dry in our measurements.



Fig. 5.2. Setup for snow surface measurements with the *Snow Fork*.

Table 5.2. Classification of the snow humidity or liquid water content of the snow according to Colbeck et al. (1990).

Term	$W_{\text{vol.},\%}$ (%)
Dry	0
Moist	< 3
Wet	3 - 8
Very wet	8 - 15
Slush	> 15

5.2.4. Snow type and snow grain structure

To avoid damage of the original structure of the snow surface in the track, we chose to use a measurement procedure that did not involve movement of snow from the track. A *LEICA MS5* stereomicroscope (max. 40 \times magnification) was used to observe the snow surface directly in-situ in the track. Microscope images of the snow surface were captured with a *Nikon F70D* camera connected to the microscope through a phototube. The setup without camera connected to the phototube is shown in Fig. 5.3. At a later stage (indoor) the captured images were converted to digital form by a scanner, and analysed and characterised digitally using the general image processing program *Adobe Photoshop 5.0* (Adobe, 1998).

The in-situ measurement procedure has proved to be very efficient for ski tracks with snow surface grains larger than approximately 0.1-0.2 mm. For smaller snow surface grains it has been difficult to capture microscope images with sufficient quality.

The 2D snow grain surfaces in microscope images have been characterised using the following definitions:

- j - snow grain surface number in a microscope image of a snow surface
- d_j - length of the largest 2D diagonal for snow grain surface number j in a microscope image of a snow surface, mm
- n_g - number of snow grains with distinguishable boundaries in a microscope image of a snow surface

- \bar{d} - mean of d_j for the n_g snow grains with distinguishable boundaries in a microscope image of a snow surface, mm
- δ_d - standard deviation of d_j for the n_g snow grains with distinguishable boundaries in a microscope image of a snow surface, mm

\bar{d} has also been classified according to the classification of grain size given in Colbeck et al. (1990), see Table 5.3.

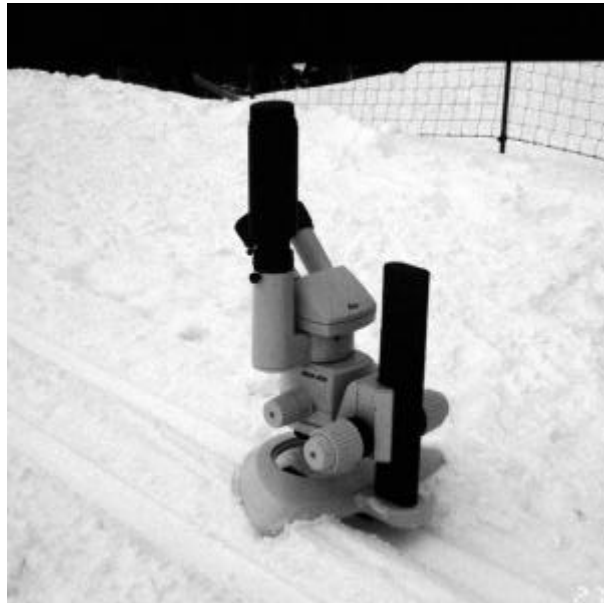


Fig. 5.3. Snow microscopy setup without camera connected to the phototube. The camera is used to take the setup picture.

Table 5.3. Classification of \bar{d} according to the classification of grain size given in Colbeck et al. (1990).

Term	\bar{d} (mm)
Very fine	< 0.2
Fine	0.2 - 0.5
Medium	0.5 - 1.0
Coarse	1.0 - 2.0
Very coarse	2.0 - 5.0
Extreme	> 5.0

Further, the snow type in the track has roughly been classified according to the following snow type categories:

1. Falling new snow
2. New snow
3. Combination of new snow and transformed snow, mainly new snow
4. Combination of new snow and transformed snow, mainly transformed snow.

5. Transformed snow
6. Artificial snow

The grain shape of the snow has furthermore been classified according to Colbeck et al. (1990), see Table 5.4.

Table 5.4. Classification of the grain shape of the snow according to Colbeck et al. (1990).

Basic classification	Graphic symbol
Precipitation particles	+
Decomposing and fragmented precipitation particles	/
Rounded grains (monocrystals)	●
Faceted crystals	□
Cup-shaped crystals and depth hoar	^
Wet grains	○
Feathery crystals	∨
Ice masses	■
Surface deposits and crusts	∇

5.2.5. Electrolytic conductivity

Snow from the surface of the ski tracks has been collected in 500 ml plastic bottles and analysed in laboratory for electrolytic conductivity i.e. electrical conductivity of the melted snow sample. In addition, the content of Cl^- , Na^+ , K^+ , Ca^{2+} , SO_4^{2-} , Mg^{2+} , NO_3^- and F^- ions have been registered for some chosen melted snow samples.

Electrolytic conductivity, σ_{mss} , was registered with the stationary *WTW Microprocessor Conductivity Meter LF537* instrument in 1996-1998 and the portable *testo 240* instrument in 1999. All measurements were performed at 25°C, and the accuracy was typically ± 1 % of the measured value. The ionic content of Na^+ , K^+ , Ca^{2+} and Mg^{2+} has been found by using atomic absorption after the NS (Norwegian Standard) 470 procedure. Ion chromatography has been applied in order to find the ionic content of NO_3^- , F^- , SO_4^{2-} and Cl^- .

5.2.6 Air temperature

Air temperature, T_a , has been measured by using an air probe on the *STAR HD 8901 Hygrometer-Thermometer*. The measurement of air temperature has the same precision as the snow temperature measurements (STAR, 1995). The measurements have been performed 50 cm above the snow surface.

5.2.7. Relative humidity

Relative humidity has been registered 50 cm above the snow surface with the same air probe as in the air temperature measurements. The measurement of relative humidity has a precision of ± 2 % for relative humidities between 5 and 90 % and $+4/-2.5$ % for relative humidities between 90 and 98 %. The relative humidity, Rh , is defined as the ratio between the amount of vapour present in the air considered and the amount that air at the same temperature could contain if it was saturated. Air is defined as saturated when it in these determined conditions of temperature, air and pressure, has absorbed the greatest possible amount of vapour.

5.2.8 Net radiation and cloudiness

Net radiation, q_{net} , is the difference between incoming and outgoing radiation at the surface of the earth. Modelling of net short wave and long wave radiation has been performed by e.g. Male and Gray (1981), and Løset (1992).

Net radiation has been registered 50 cm above the snow surface with the *Anderaa Instruments net radiation sensor 2811* instrument. This sensor measures both sunlight and infrared radiation. The measurement range of the instrument is ± 2000 W/m², and the accuracy ± 1 % of full scale.

Cloudiness, C , has roughly been characterised in octoparts ($0 < C < 8$). A complete cloud cover is expressed as $C = 8$, while $C = 0$ indicates a clear cloud cover.

5.3. Results

This section presents major results from measurements of different snow parameters in 152 cross-country race ski tracks. The presented measurement results are based on measurement campaigns in Norway, 1995-98, Hakuba/Japan, 1996-98 and Sundance/USA, 1999. Some measurements have also been performed in the jumping ski track of the jumping hill in Granåsen, Trondheim, Norway, 1997-98. In addition an analysis of the electrolytic conductivity and ionic content of artificial Continental snow has been made.

The snow temperature in the campaigns has ranged from 0 to -22.1°C (Granåsen, 26.01.1996), while the air temperature has ranged from +14.2 (Hakuba, 14.02.1996) to -14.6°C (Granåsen, 26.01.1996). The relative humidity has varied from 18 % in dry sunny Sundance (03.03.1999) to 100 % during snow events in Trondheim (winter 1996). A maximum net radiation of 816 W/m² has been registered in Hakuba at 36°N (27.01.1998).

Specific attention is not given to parameters such as snow temperature, air temperature, relative humidity, cloudiness and net radiation in the following. Instead the rest of this chapter focuses on snow hardness, snow humidity, snow density, snow grain structure and electrolytic conductivity in the presentation and discussion of the results.

5.3.1. Snow hardness

The cumulative distribution of our snow hardness measurements is shown in Fig. 5.4. It can be seen that medium and high snow hardness, i.e. hardness values between 10⁴ and 10⁶ Pa, are most common in ski tracks. Snow hardness statistics for different snow types in cross-country race ski tracks are given in Table 5.5. The following definitions are used:

\bar{H}	mean snow hardness for a snow type, Pa
δ_H	standard deviation of \bar{H} , Pa
H_{\max}	maximum snow hardness for a snow type, Pa
H_{\min}	minimum snow hardness for a snow type, Pa
H_{50}	median snow hardness for a snow type, Pa
n_H	number of hardness measurements for a given snow type

Table 5.5 shows that the snow hardness values have ranged between 4.3×10³ Pa and 2.8×10⁶ Pa in our 143 measurements. The maximum hardness was measured in the jumping ski track of the jumping hill in Granåsen in Trondheim, but very high snow hardness has also been registered on transformed snow types in cross-country ski tracks e.g. in the morning after cold, clear nights. In race ski tracks passed by more than 20 skiers, low snow hardness has been registered on both falling new snow and transformed snow. Very low snow hardness had probably also been obtained if hardness tests had been performed on new-fallen virgin snow in ski tracks. The lowest registered hardness value was obtained in a very wet jumping ski track ($W_{\text{vol.,\%}} = 8.4 \%$).

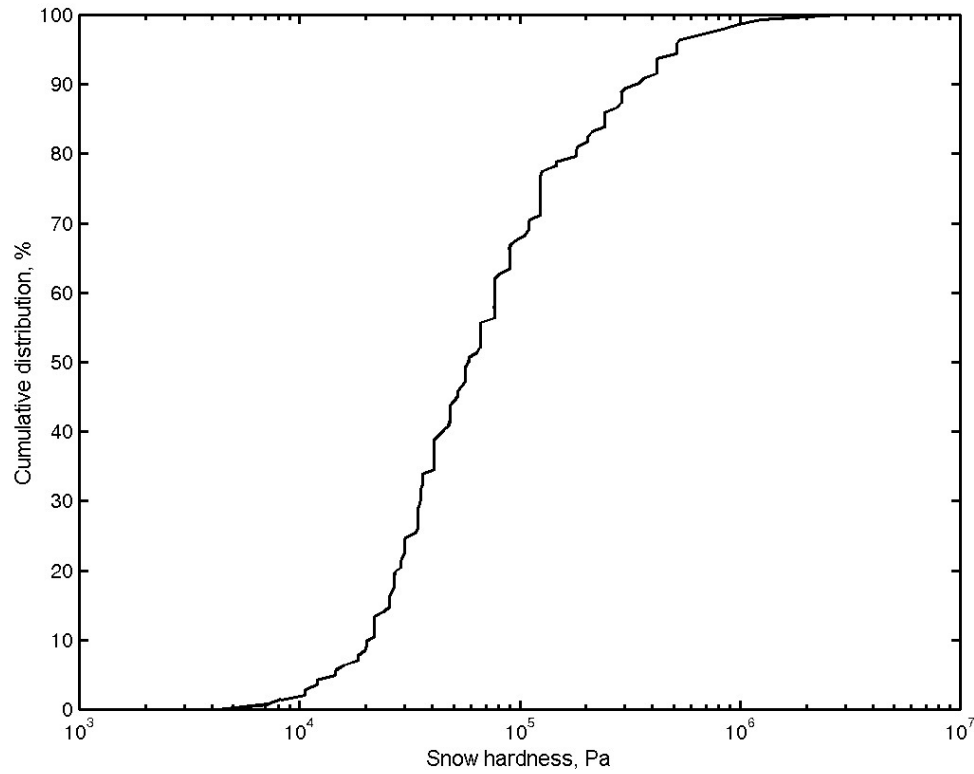


Fig. 5.4. Cumulative distribution of the 143 snow hardness measurements.

Table 5.5. Snow hardness statistics for different snow types in cross-country race ski tracks.

Snow type	\bar{H} (Pa)	δ_H (Pa)	H_{\max} (Pa)	H_{\min} (Pa)	H_{50} (Pa)	n_H
All	1.5×10^5	2.9×10^5	2.8×10^6	4.3×10^3	5.9×10^4	143
	High		Very high	Low	Medium	
1	6.8×10^4	4.8×10^4	1.5×10^5	7.2×10^3	5.9×10^4	17
	Medium		High	Low	Medium	
2	1.3×10^5	1.3×10^5	5.1×10^5	2.7×10^4	6.6×10^4	45
	High		High	Medium	Medium	
3	1.8×10^5	1.9×10^5	6.6×10^5	2.2×10^4	9.0×10^4	15
	High		High	Medium	Medium	
4	1.6×10^5	3.1×10^5	9.8×10^5	1.2×10^4	4.1×10^4	9
	High		High	Medium	Medium	
5	1.7×10^5	4.2×10^5	2.8×10^6	4.3×10^3	4.1×10^4	55
	High		Very high	Low	Medium	

The mean hardness of the measurements, \bar{H} , is equal to 1.5×10^5 Pa. Since the snow hardness is found to vary by almost three orders of magnitude, the median hardness, H_{50} , might be a better measure for the typical snow hardness in a ski track. H_{50} is equal to 5.9×10^4 Pa in our measurements. Snow type 3, i.e. a combination of new snow and transformed snow where new snow dominates, has the highest median and mean snow hardness ($H_{50} = 9.0 \times 10^4$ Pa and $\bar{H} = 1.8 \times 10^5$ Pa). Snow type 5, i.e.

transformed snow, has the highest standard deviation ($\delta_H = 4.2 \times 10^5$ Pa), i.e. the highest variation. The variation in snow hardness is generally lower for Snow types 1 and 2, i.e. falling new snow and new snow, than for the other snow types.

Fig. 5.5 shows snow hardness as a function of snow density for different snow types. There seems to be no apparent relationship between the snow hardness and snow density, except for perhaps Snow type 1 that tends to have an increased snow hardness with an increased snow density. The snow hardness has large variance for the most common snow densities between 0.3 and 0.6 kg/m³.

Fig. 5.6 shows snow hardness as a function of snow humidity for different snow types. It can be seen from the figure that ski tracks with snow humidity above 5 % tend to have lower mean values and less variance in snow hardness. Both the highest and lowest snow hardness values seem to decrease when the snow humidity is above approximately 3 %.

Fig. 5.7 shows snow hardness as a function of snow temperature for different snow types, while Fig. 5.8 displays snow hardness as a function of snow temperature for Snow types 1 and 2. It can be seen from Fig. 5.7 that the minimum snow hardness tends to increase with decreasing snow temperature. The hardest conditions for newer snow types, i.e. Snow types 1 and 2, are found at snow temperatures below -3°C. The best-fit relationship for H (Pa) for Snow type 1 is:

$$H = -22000T_s + 13000 \quad (5.11a)$$

while the best-fit relationship for Snow type 2 is:

$$H = -11000T_s + 79000 \quad (5.11b)$$

Fig. 5.9 shows a contour plot of the logarithm of H versus snow humidity and snow temperature for our measurements. The highest hardness values in the measurements are found for moist snow with snow temperature between -1 and -4°C and dry snow with snow temperature below -2°C. The snow hardness and the bonding between the snow grains seem to be dependent on both the snow temperature and the snow humidity.

Fig. 5.10 illustrates snow hardness as a function of grain size, i.e. \bar{d} , for different snow types, while Fig. 5.11 displays a contour plot of the logarithm of H versus grain size and snow temperature. As shown in the figures there seem to be relatively little correlation between snow hardness and grain size in the analysed snow temperature range. Differences in hardness of almost three orders of magnitude are found for snow with medium and coarse grain sizes ($0.5 \text{ mm} < \bar{d} < 2 \text{ mm}$).

Snow hardness statistics for different snow types in cross-country classic ski tracks and skating ski tracks are given in Table 5.6. All the tests in the skating and classic tracks have been performed as a set of experiments, thus separated in time by just a few minutes. The average snow hardness for new snow types, i.e. Snow types 1 and 2, is approximately three times higher in classic ski tracks than in skating ski tracks. The few measurements performed on transformed snow have indicated less difference in snow hardness between classic and skating ski tracks. The snow hardness in skating ski tracks have ranged from 73 to 142 % of the hardness in classic ski tracks under such conditions.

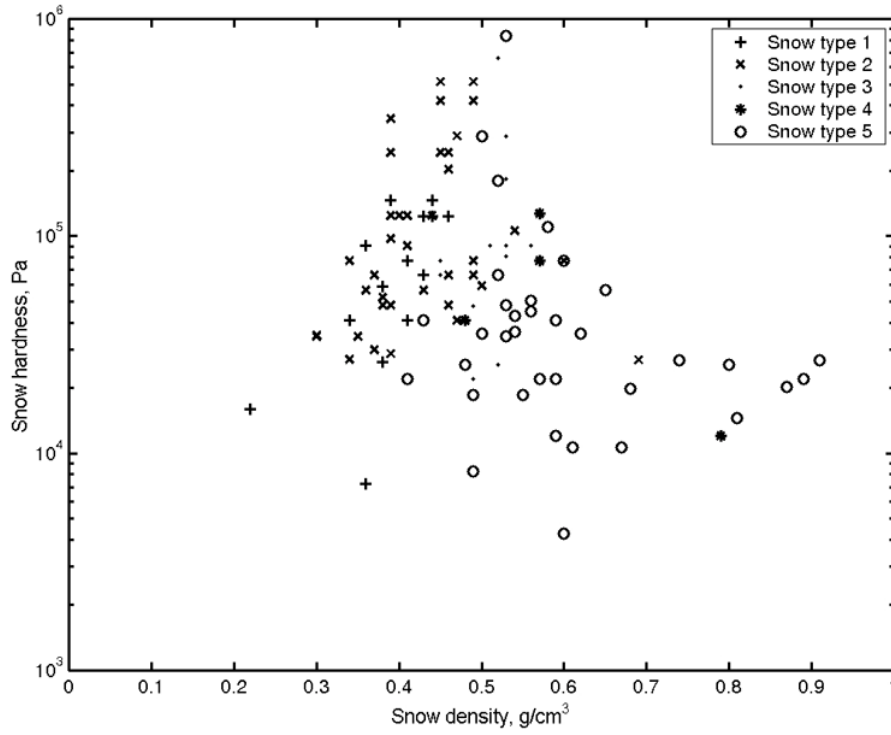


Fig. 5.5. Snow hardness as a function of snow density for different snow types.

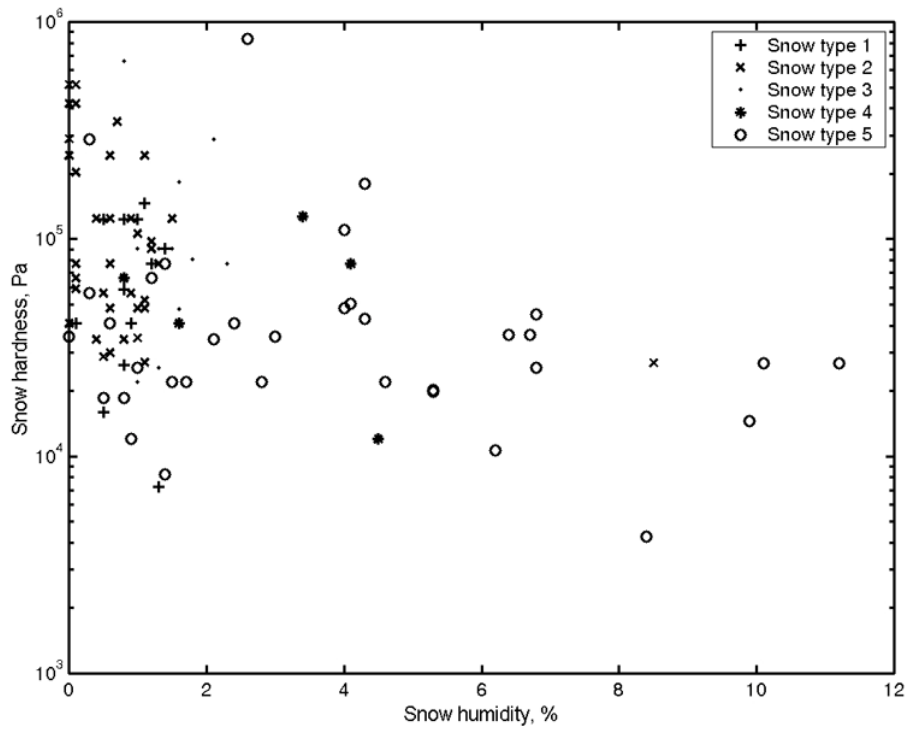


Fig. 5.6. Snow hardness as a function of snow humidity for different snow types.

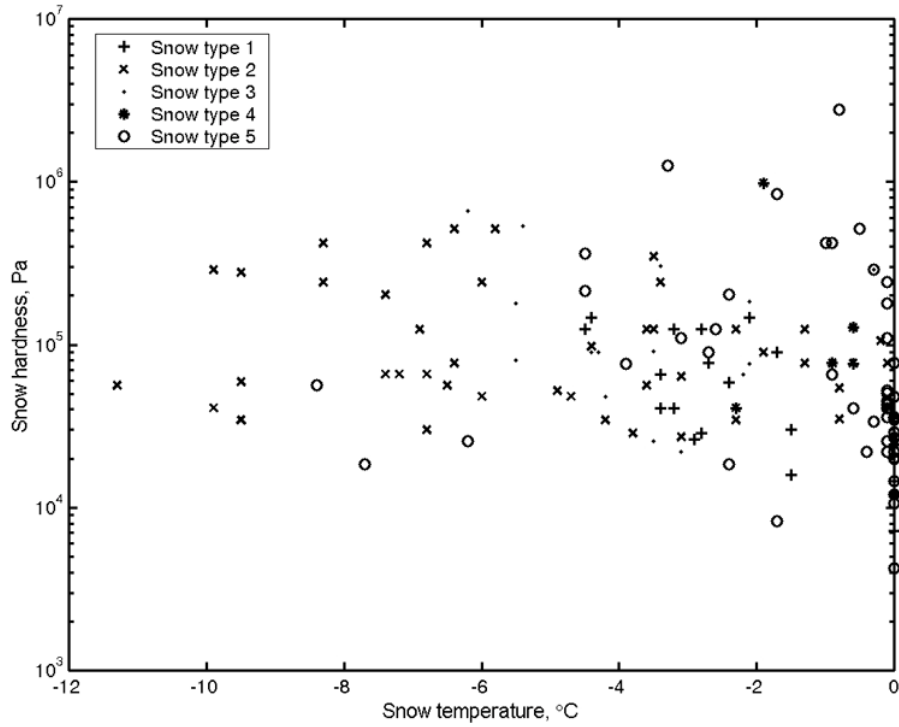


Fig. 5.7. Snow hardness as a function of snow temperature for different snow types.

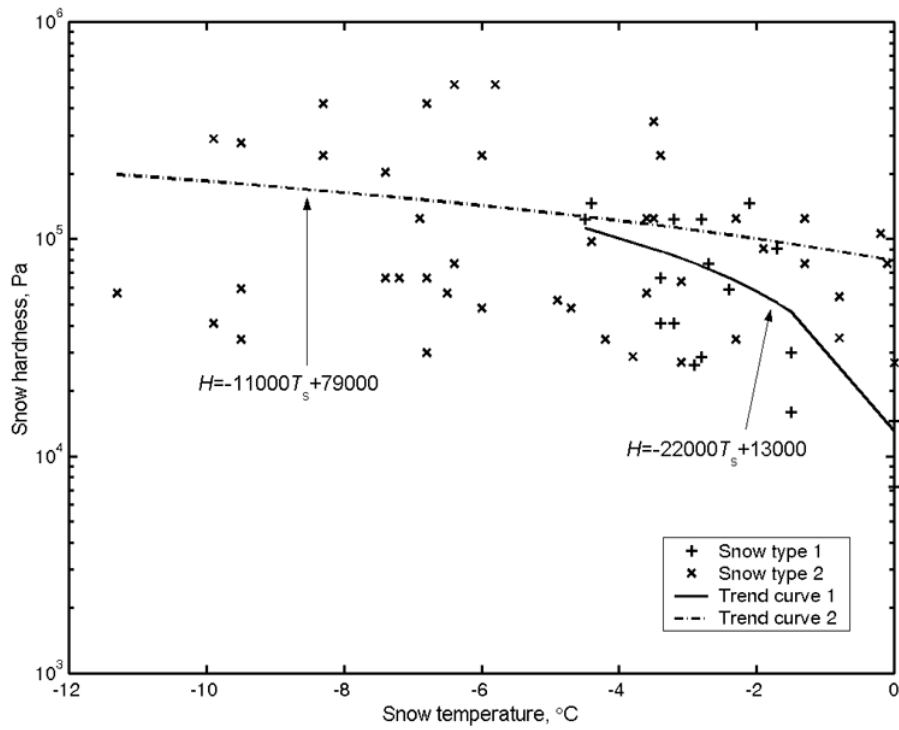


Fig. 5.8. Snow hardness as a function of snow temperature for Snow types 1 and 2.

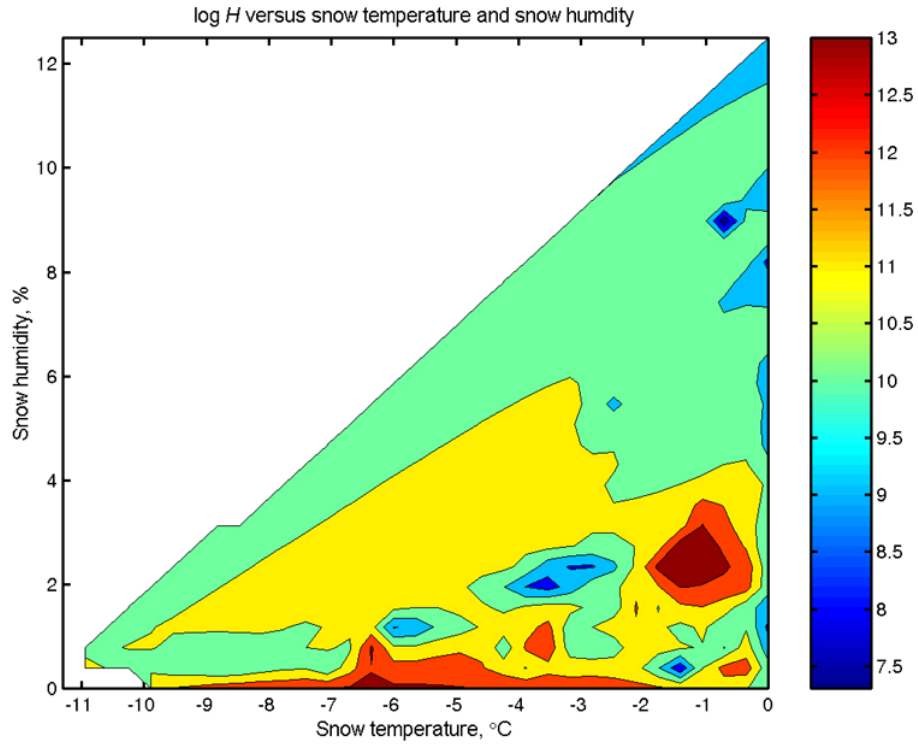


Fig. 5.9. Contour plot of log H versus snow humidity and snow temperature.

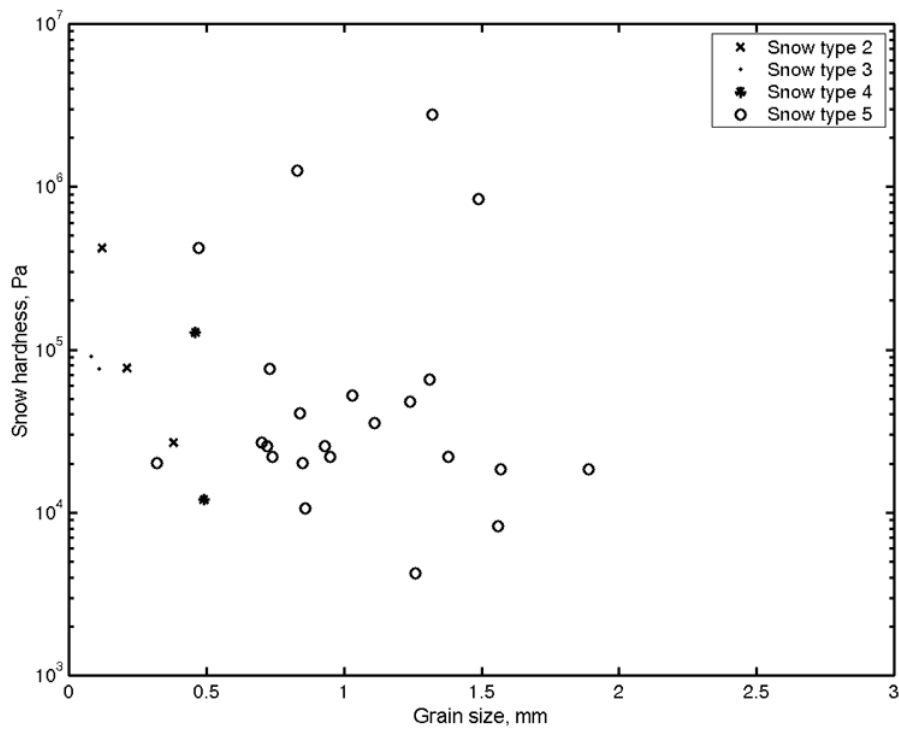


Fig. 5.10. Snow hardness as a function of grain size for different snow types.

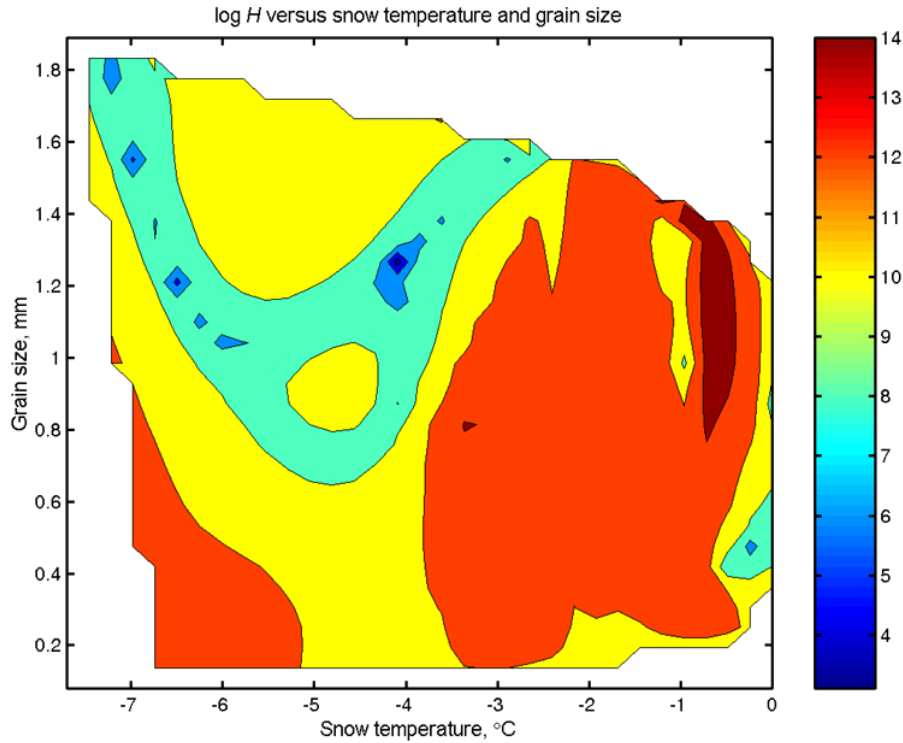


Fig. 5.11. Contour plot of $\log H$ versus grain size and snow temperature.

Table 5.6. Snow hardness statistics for different snow types in cross-country classic ski tracks and skating ski tracks. All the tests in the skating and classic tracks have been performed at the same time.

Snow type	Track (C = Classic, S = Skating)	\bar{H} (Pa)	δ_H (Pa)	H_{\max} (Pa)	H_{\min} (Pa)	H_{50} (Pa)	n_H
All	C	1.8×10^5	1.3×10^5	5.1×10^5	3.0×10^4	1.2×10^5	25
		High	High	High	Medium	High	
All	S	8.0×10^4	7.8×10^4	3.6×10^5	1.6×10^4	5.6×10^4	25
		Medium	High	Medium	Medium	Medium	
1	C	8.6×10^4	4.6×10^4	1.2×10^5	3.0×10^4	9.5×10^4	4
		Medium	High	Medium	Medium	Medium	
1	S	3.2×10^4	1.2×10^4	4.1×10^4	1.6×10^4	3.5×10^4	4
		Medium	Medium	Medium	Medium	Medium	
2	C	2.3×10^5	1.6×10^5	5.1×10^5	3.0×10^4	2.2×10^5	14
		High	High	High	Medium	High	
2	S	7.2×10^4	5.5×10^4	2.4×10^5	2.7×10^4	5.8×10^4	14
		Medium	High	Medium	Medium	Medium	
3	C	1.2×10^5	5.6×10^4	1.8×10^5	7.7×10^4	9.1×10^4	3
		High	High	High	Medium	Medium	
3	S	9.6×10^4	8.0×10^4	1.8×10^5	2.6×10^4	8.1×10^4	3
		Medium	High	High	Medium	Medium	
5	C	1.2×10^5	8.3×10^4	2.1×10^5	4.8×10^4	1.1×10^5	3
		High	High	High	Medium	High	
5	S	1.7×10^5	1.7×10^5	3.6×10^5	3.5×10^4	1.1×10^5	3
		High	High	High	Medium	High	

5.3.2. Snow humidity and snow density

Histograms for snow density measurements of different snow types in cross-country race ski tracks are shown in Fig. 5.12, while snow density statistics are given in Table 5.7. The following definitions are used in Table 5.7:

- $\bar{\rho}$ mean snow density for a snow type, g/cm^3
- δ_{ρ} standard deviation of $\bar{\rho}$, g/cm^3
- ρ_{\max} maximum snow density for a snow type, g/cm^3
- ρ_{\min} minimum snow density for a snow type, g/cm^3
- ρ_{50} median snow density for a snow type, g/cm^3
- n_{ρ} number of density measurements for a given snow type

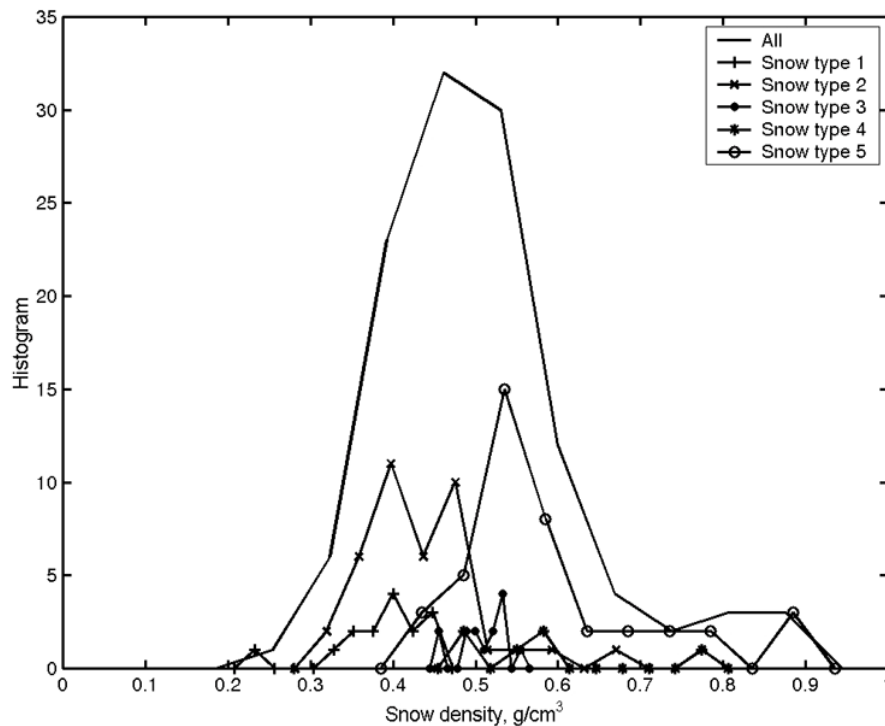


Fig. 5.12. Histograms for snow density measurements of different snow types in cross-country race ski tracks.

The snow density values in the 117 measurements have ranged between 0.22 and 0.92 g/cm^3 , i.e. the density of ice. The minimum density was registered for Snow type 1 in Granåsen, 27.03.1996. The highest measured density value was obtained for wet snow ($W_{\text{vol},\%} = 5.4\%$) in Sundance, 27.02.1999. The accuracy of this value can be questioned since the *Snow Fork*, although usable also for measuring higher snow densities, is primarily designed for measuring snow density below 0.6 g/cm^3 . The highest measured snow density for new snow types, 0.69 g/cm^3 , was registered on a warm day ($T_a = +5.1^\circ\text{C}$) in Lillehammer in April 1998. The lowest snow density value for transformed snow types, 0.41 g/cm^3 ,

was obtained in Granåsen 24.02.1997, immediately after the 10 km classic race for men in the Nordic World Ski Championships'97.

Table 5.7. Snow density statistics for different snow types in cross-country race ski tracks.

Snow type	$\bar{\rho}$ (g/cm ³)	δ_{ρ} (g/cm ³)	ρ_{\max} (g/cm ³)	ρ_{\min} (g/cm ³)	ρ_{50} (g/cm ³)	n_{ρ}
All	0.50	0.13	0.92	0.22	0.49	117
1	0.39	0.06	0.46	0.22	0.39	15
2	0.43	0.08	0.69	0.30	0.43	39
3	0.51	0.03	0.56	0.45	0.52	14
4	0.57	0.12	0.79	0.47	0.56	6
5	0.59	0.12	0.91	0.41	0.56	42

It can be seen from both Table 5.7 and the histograms in Fig. 5.12 that the mean snow density is higher for transformed snow types than new snow types. While Snow types 1 and 2 have mean snow densities of 0.39 and 0.43 g/cm³ respectively, the mean snow densities of Snow types 3, 4 and 5 are 0.51, 0.57 and 0.59 g/cm³.

Fig. 5.13 shows snow density plotted as a function of snow humidity for different snow types in 116 ski tracks. It is easy to see that the snow density increases with increased snow humidity, at least for snow humidities up to 8-10 %.

The liquid water content of snow or snow humidity has ranged from 0 to 12.5 % in the 117 measurements in ski tracks. No liquid water content ($W_{\text{vol},\%} = 0.0$ %) has been found at snow temperatures below approximately -6°C. The highest value was measured 21 April 1998 at Lillehammer on a warm, sunny day ($T_a = +5.8^\circ\text{C}$ and $q_{\text{net}} = 753 \text{ W/m}^2$). At this day the snow humidity increased from 0.6 % at 9:40 to 12.5 % at 11:59. Large variations in snow humidity have also been measured during ski competitions in winter. During the Nordic Combined competition in the Nordic World Ski Championships'97 in Granåsen (24.02.1997), the snow humidity changed from 2.4 % at 11:40 to 6.8 % at 14:17.

Fig. 5.14 shows snow humidity plotted as a function of snow temperature for different snow types in ski tracks. In the present experiments it is found that the snow humidity is less than 2 % for snow temperatures below -2°C and less than 1 % for snow temperatures below -7°C. Furthermore, the snow humidity is found to be less than 2 % for new snow types and below zero snow temperatures.

Fig. 5.15 depicts snow humidity versus air temperature for various snow types in ski tracks. It can be seen from the figure that the snow humidity is less than 1 % for air temperatures below -4°C and less than 2 % for air temperatures below -2°C. Snow humidities exceeding 4 % have only been registered at air temperatures above +1°C.

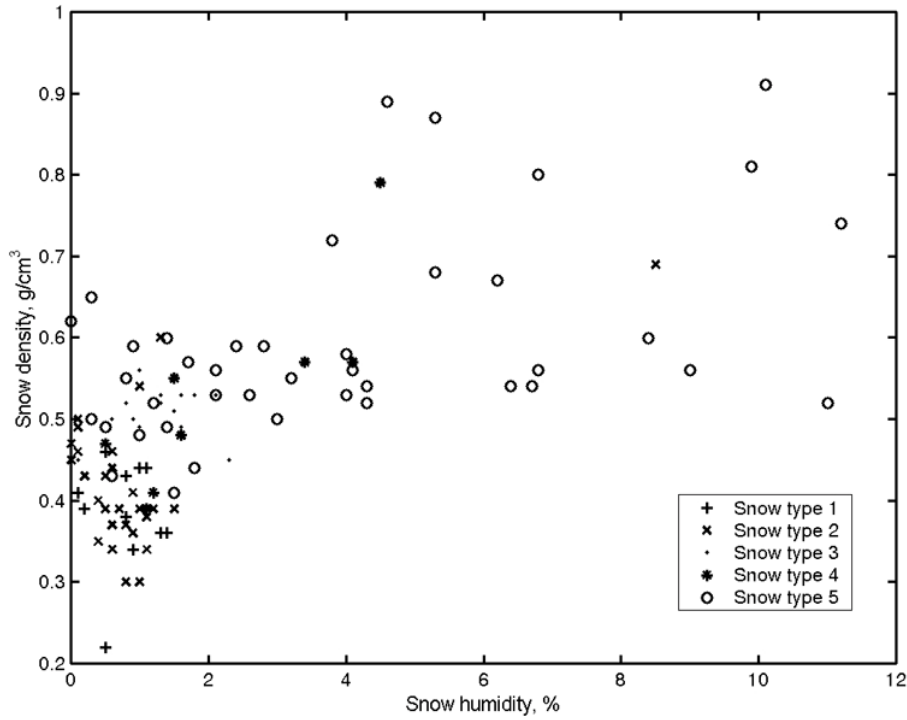


Fig. 5.13. Snow density plotted as a function of snow humidity for different snow types in ski tracks.

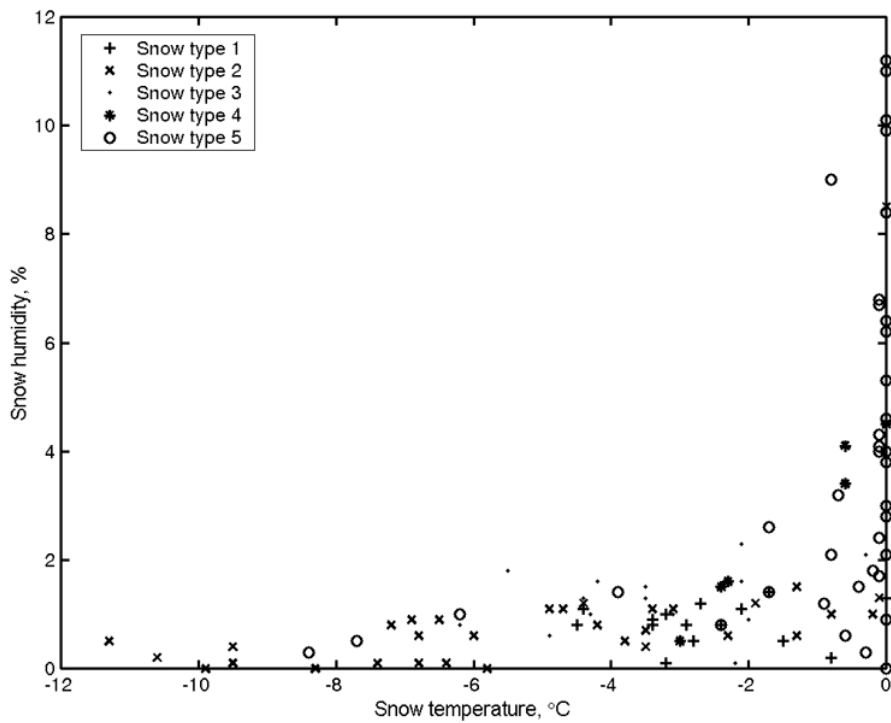


Fig. 5.14. Snow humidity versus snow temperature for different snow types in ski tracks.

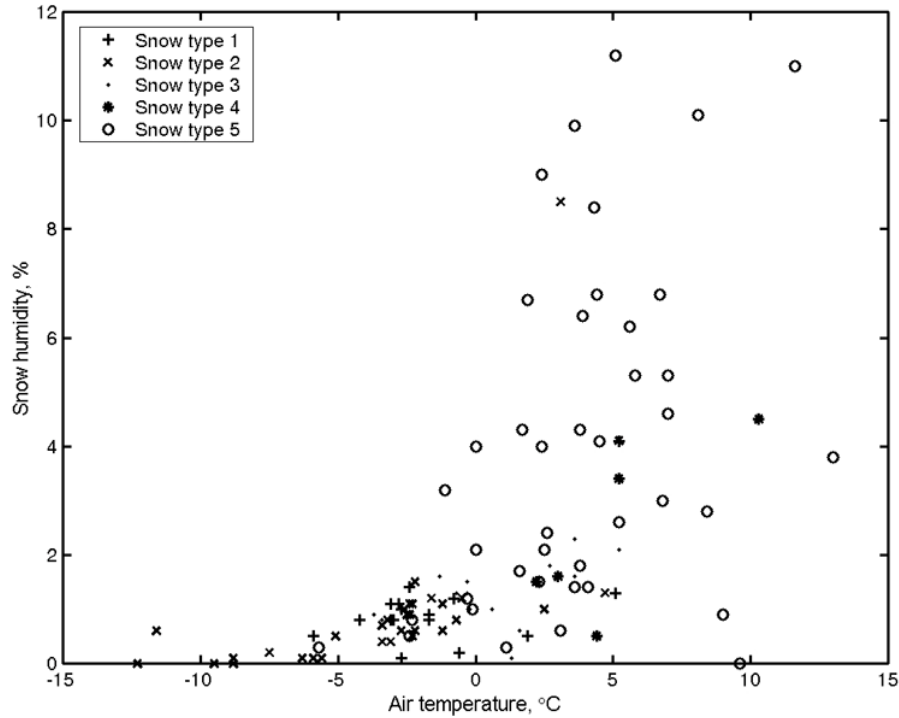


Fig. 5.15. Snow humidity plotted as a function of air temperature for different snow types in ski tracks.

Fig. 5.16 shows a contour plot of the measured snow humidity in ski tracks as a function of relative humidity and air temperature. A C/E line (Condensation/Evaporation line) based on Petterssen (1956) has been added to the plot. This line indicates the limiting value of relative humidity. If the relative humidity in the air above the snow is higher than that indicated by the line, water vapour condenses on the snow, otherwise it evaporates. It can be seen from the figure that the highest snow humidities are registered on clear, warm days with relative humidities between 40 and 60 % and air temperatures above +5°C. The snow humidity is relatively lower at relative humidities between 60 and 80 %, probably due to less efficient solar radiation compared to lower relative humidities. At relative humidities above 80 % the snow humidity shows an increasing tendency again when condensation processes start to be efficient. For relative humidities exceeding 65 %, the snow humidity is highest to the right of the C/E line, i.e. when condensation on the snow dominates over evaporation from the snow.

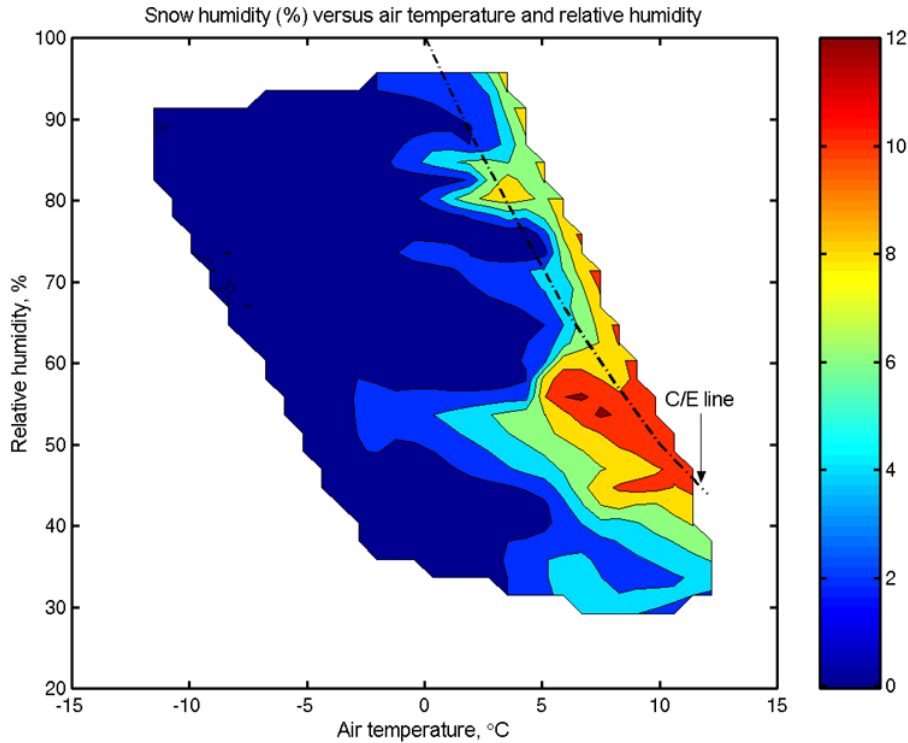


Fig. 5.16. Contour plot of the measured snow humidity in ski tracks as a function of relative humidity and air temperature. A C/E line (Condensation/Evaporation line) based on Petterssen (1956) has been added to the plot.

5.3.3. Snow type and snow grain structure

The mean snow grain diameter, \bar{d} , and the standard deviation of grain diameters, δ_d , have been calculated for 34 snow surface microscope images of ski tracks. These results are presented in Table 5.8 together with information of time, location, snow type, grain shape, snow humidity $W_{\text{vol},\%}$, snow density ρ , snow hardness H and snow temperature T_s . Ionic content of Cl^- , Na^+ , K^+ , Ca^{2+} , SO_4^{2-} , Mg^{2+} , NO_3^- and F^- and electrolytic conductivity σ_{mss} of collected and melted samples from the snow surfaces are shown in Table 5.9 for 22 of the images. Table 5.10 presents data on air temperature T_a , relative humidity Rh , cloudiness C and net radiation q_{net} at the time of snow microscope image registration.

Table 5.8. Table of snow measurements for snow surface microscope images.

Image No.	Date (Time)	Location	Snow type	Grain shape	$\bar{d} \pm \delta_d$ (mm)	$W_{vol,\%}$ (%)	ρ (g/cm ³)	H (Pa)	T_s (°C)
1	21.02.97 (12:54)	Granåsen cross-country	5	□	0.93±0.33 Medium	1 Moist	0.48	2.6×10 ⁴ Medium	-6.2
2	23.02.97 (8:46)	Granåsen cross-country	5	○	0.74±0.33 Medium	1.7 Moist	0.57	2.2×10 ⁴ Medium	-0.1
3	23.02.97 (11:40)	Granåsen cross-country	5	○	0.84±0.29 Medium	2.4 Moist	0.59	4.1×10 ⁴ Medium	-0.1
4	23.02.97 (14:17)	Granåsen cross-country	5	○	0.72±0.20 Medium	6.8 Wet	0.8	2.6×10 ⁴ Medium	-0.1
5	24.02.97 (8:52)	Granåsen cross-country	5	○	1.31±0.49 Coarse	1.2 Moist	0.52	6.6×10 ⁴ Medium	-0.9
6	24.02.97 (11:45)	Granåsen cross-country	5	○	1.38±0.44 Coarse	1.5 Moist	0.41	2.2×10 ⁴ Medium	-0.4
7	24.02.97 (13:49)	Granåsen cross-country	5	○	1.43±0.35 Coarse	1.8 Moist	0.44		-0.2
8	25.02.97 (8:36)	Granåsen cross-country	5	○	1.57±0.50 Coarse	0.8 Moist	0.55	1.9×10 ⁴ Medium	-2.4
9	25.02.97 (11:38)	Granåsen cross-country	5	○	1.56±0.53 Coarse	1.4 Moist	0.49	8.3×10 ³ Low	-1.7
10	26.02.97 (10:45)	Granåsen cross-country	5	□	1.89±0.52 Coarse	0.5 Moist	0.49	1.9×10 ⁴ Medium	-7.7
11	27.02.97 (11:42)	Granåsen cross-country	3	/	0.08±0.02 Very fine	1.5 Moist	0.51	9.1×10 ⁴ Medium	-3.5
12	28.02.97 (8:40)	Granåsen cross-country	3	/	0.11±0.03 Very fine	2.3 Moist	0.45	7.7×10 ⁴ Medium	-2.1
13	28.02.97 (12:35)	Granåsen cross-country	4	○	0.46±0.34 Fine	3.4 Wet	0.57	1.3×10 ⁵ High	-0.6
14	01.03.97 (8:47)	Granåsen cross-country	5	□	0.73±0.03 Medium	1.4 Moist	0.6	7.7×10 ⁴ Medium	-3.9
15	01.03.97 (12:34)	Granåsen cross-country	5	○	1.49±0.64 Coarse	2.6 Moist	0.53	8.4×10 ⁵ High	-1.7
16	02.03.97 (8:37)	Granåsen cross-country	5	○	1.03±0.39 Coarse			5.2×10 ⁴ Medium	-0.1
17	16.12.97 (19:28)	Granåsen jumping hill	5	○	0.47±0.28 Fine			4.2×10 ⁵ High	-0.9
18	27.12.97 (11:48)	Granåsen jumping hill	4	● (/)	0.26±0.09 Fine				-9.4
19	28.12.97 (10:15)	Granåsen jumping hill	4	□	2.59±0.71 Very coarse				-5.4
20	13.01.98 (14:49)	Granåsen jumping hill	5	○	1.32±0.44 Coarse			2.8×10 ⁶ Very high	-0.8
21	25.03.98 (12:15)	Granåsen cross-country	2	/	0.21±0.07 Fine	1.3 Moist	0.6	7.7×10 ⁴ Medium	-0.1
22	31.03.98 (13:49)	Granåsen jumping hill	5	○	1.26±0.36 Coarse	8.4 Very wet	0.6	4.3×10 ³ Low	0.0
23	01.04.98 (13:44)	Meråker cross-country	5	○	1.24±0.48 Coarse	4 Wet	0.53	4.8×10 ⁴ Medium	0.0
24	17.04.98 (12:35)	Lillehammer cross-country	2	○ (/)	0.38±0.13 Fine	8.5 Very wet	0.69	2.7×10 ⁴ Medium	0.0
25	20.04.98 (13:34)	Lillehammer cross-country	5	○	0.70±0.24 Medium	11.2 Very wet	0.74	2.7×10 ⁴ Medium	0.0

26	21.04.98 (11:59)	Lillehammer cross-country	5	○	0.86±0.29 Medium	12.5 Very wet	0.61	1.1×10 ⁴ Medium	0.0
27	07.11.98 (11:07)	Golå cross-country	2	/	0.12±0.07 Very fine	0.1 Dry	0.49	4.2×10 ⁵ High	-6.8
28	28.02.99 (11:15)	Sundance cross-country	5	○	0.32±0.16 Fine			2.0×10 ⁴ Medium	0.0
29	28.02.99 (12:46)	Sundance cross-country	5	○	0.40±0.16 Fine	3.8 Wet	0.72	<2×10 ⁴	0.0
30	01.03.99 (11:30)	Sundance cross-country	4	○	0.49±0.22 Fine	4.5 Wet	0.79	1.2×10 ⁴ Medium	0.0
31	02.03.99 (9:40)	Sundance cross-country	5	□	0.83±0.21 Medium			1.3×10 ⁶ Very high	-3.3
32	02.03.99 (13:00)	Sundance cross-country	5	○	0.85±0.38 Medium	5.3 Wet	0.87	2.0×10 ⁴ Medium	0.0
33	02.03.99 (13:43)	Sundance cross-country	5	○	0.95±0.34 Medium	4.6 Wet	0.89	2.2×10 ⁴ Medium	0.0
34	03.03.99 (10:55)	Sundance cross-country	5	○	1.11±0.54 Coarse	0 Dry	0.62	3.6×10 ⁴ Medium	0.0

Table 5.9. Electrolytic conductivity and chemical water properties for collected and melted samples from the snow surfaces described in Table 5.8.

Image No.	σ_{mss} ($\mu\text{S}/\text{cm}$)	Cl^- (mg/l)	Na^+ (mg/l)	K^+ (mg/l)	Ca^{2+} (mg/l)	SO_4^{2-} (mg/l)	Mg^{2+} (mg/l)	NO_3^- (mg/l)	F^- (mg/l)
1	25.4	3.73	1.06	0.17	0.16	<0.01	0.26	0.54	<0.01
2	17.2	1.52	0.64	0.13	0.16	<0.01	0.05	0.01	0.01
5	13.5	1.2	0.66	0.06	0.02	<0.1	0.05	<0.1	<0.1
8	14.9	1.4	0.71	0.09	0.02	<0.1	0.06	0.8	<0.1
10	17.3	1.4	0.72	0.15	0.045	<0.1	0.06	<0.1	<0.1
11	46.8	9.1	5.12	0.295	0.155	1.1	0.625	<0.1	<0.1
12	61.7	14.4	7.18	0.345	0.245	2.6	0.835	<0.1	<0.1
14	12.9	1.6	0.76	0.065	0.01	<0.1	0.05	<0.1	<0.1
16	12.1	1.2	0.62	0.06	0.01	<0.1	0.04	<0.1	<0.1
17	8.7								
21	16.6	3.08	1.32	0.08	0.09	0.12	0.2	<0.01	<0.01
22	3.8								
23	4								
24	21.6	0.3	0.05	0.02	0.01	1.6	0.01	1.9	<0.1
25	8.5	0.4	0.05	0.01	0.01	0.5	0.01	1	<0.1
26	3.8	0.3	0.02	<0.1	0.01	0.4	0.01	0.7	<0.1
27	4.1								
28	28.8	1.52	1.2	0.2	2.63	1.47	0.5	1.13	<0.01
30	18.7	1.07	0.61	0.18	2.16	<0.01	0.51	0.24	0.01
31	16.9	1.37	0.72	0.77	1.34	<0.01	0.33	0.2	<0.01
33	15.4	0.76	0.45	0.08	1.56	<0.01	0.41	<0.01	0.01
34	8.3	0.65	0.29	0.09	1.26	<0.01	0.37	<0.01	<0.01

Table 5.10. Table of weather measurements for the snow surface microscope images described in the snow measurements in Table 5.8 and the electrolytic conductivity and chemical water measurements in Table 5.9.

Image No.	T_a (°C)	Rh (%)	C (octoparts)	q_{net} (W/m ²)
1	-0.1	58	3	243
2	1.6	89	8	0
3	2.6	87	8	131
4	6.7	64	8	103
5	-0.3	72	8	0
6	2.3	61	8	0
7	3.8	64	8	33
8	-2.3	61	8	0
9	4.1	57	8	250
10	-2.4	71	4	217
11	-0.3	79	0	74
12	3.6	60	7	57
13	5.2	60	8	152
14	3.6	60	2	0
15	5.2	64	4	119
16	5.7	80	8	0
17	1.3	96	0	-21
18	-5.1	57		
19	-3.2	72	7	
20	3.7	60	2	-33
21	4.7	43	4	415
22	4.3	80	5	415
23	0.0	74	8	312
24	3.1	83	7	164
25	5.1	57	8	205
26	5.8	53	0	753
27	-5.9	64	0	79
28	9.4	32	0	580
29	13.0	31	0	596
30	10.3	32	6	
31	1.6	48	0	
32	7.0	35	1	480
33	7.0	29	1	440
34	9.6	23	8	94

Examples of registered snow microscope images are given in Figs. 5.17-5.30. In particular Figs. 5.17-5.23 focus on snow surfaces with different grain sizes and snow types. Snow surfaces with coarse ($\bar{d} = 1.89$ mm), medium ($\bar{d} = 0.85$ mm) and fine ($\bar{d} = 0.40$ mm) snow grains of Snow type 5 are presented in Figs. 5.17, 5.18 and 5.19, respectively. Figs. 5.20 and 5.21 show surfaces with very coarse ($\bar{d} = 2.59$ mm) and fine ($\bar{d} = 0.49$ mm) snow grains of Snow type 4, while a surface with very fine ($\bar{d} = 0.11$ mm) snow grains of Snow type 3 is given in Fig. 5.22. An example of a snow surface with Snow type 2 and fine ($\bar{d} = 0.21$ mm) snow grains is depicted in Fig. 5.23.

Wet grains, rounded grains, faceted crystals and decomposing and fragmented precipitation particles are the most common grain shapes on snow surfaces in ski tracks. Faceted crystals on a ski track surface are shown in Fig. 5.24.

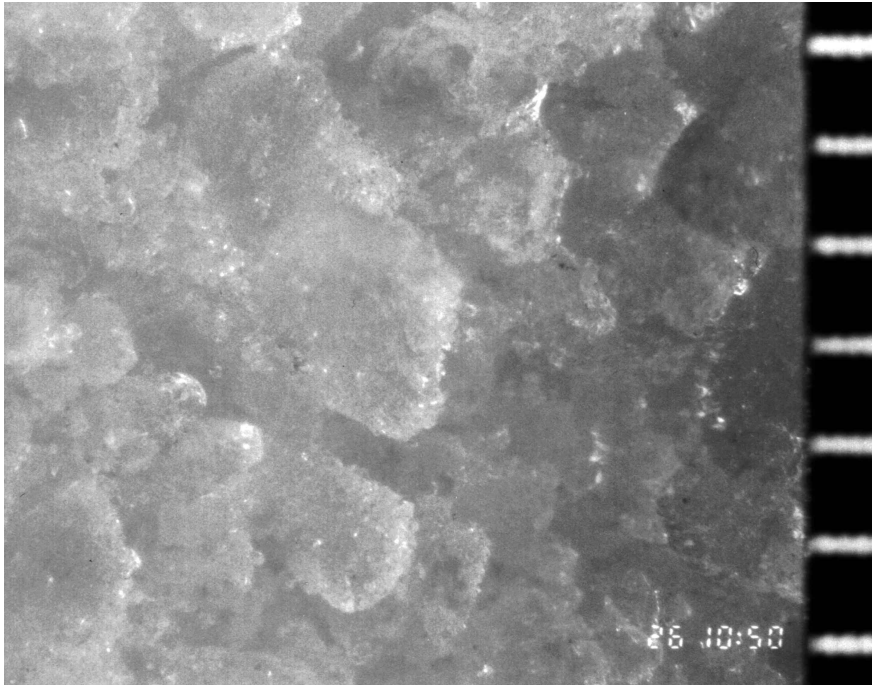


Fig. 5.17. Example of a snow surface with Snow type 5 and coarse snow grains ($\bar{d} = 1.89$ mm and $\delta_d = 0.52$ mm): Image No. 10. The distance between the tick marks on the ruler in the image is 1 mm.

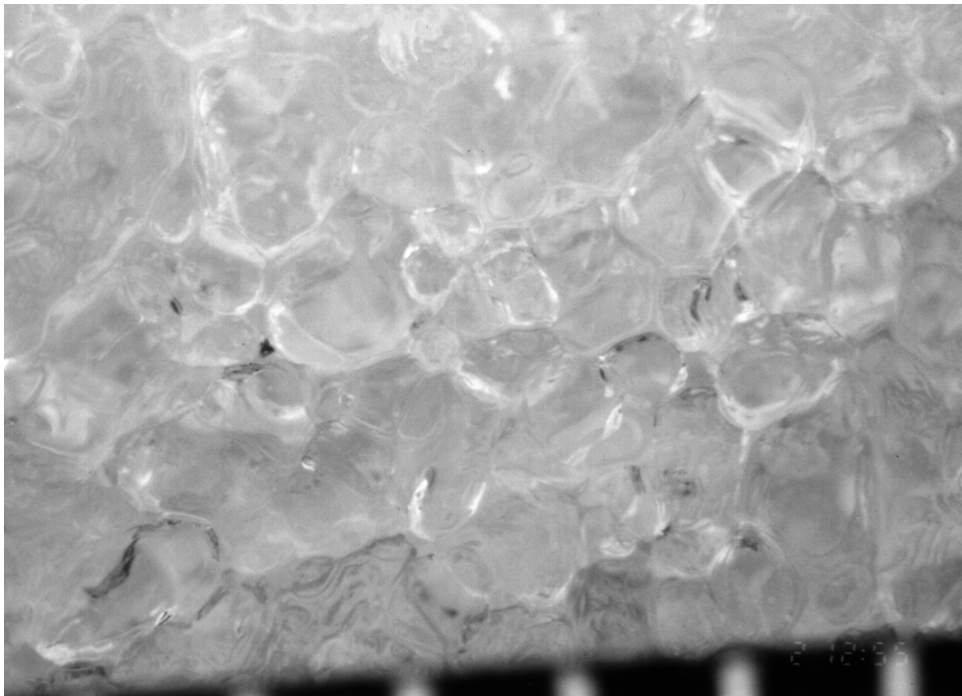


Fig. 5.18. Example of a snow surface with Snow type 5 and medium snow grains ($\bar{d} = 0.85$ mm and $\delta_d = 0.38$ mm): Image No. 32. The distance between the tick marks is 1 mm.

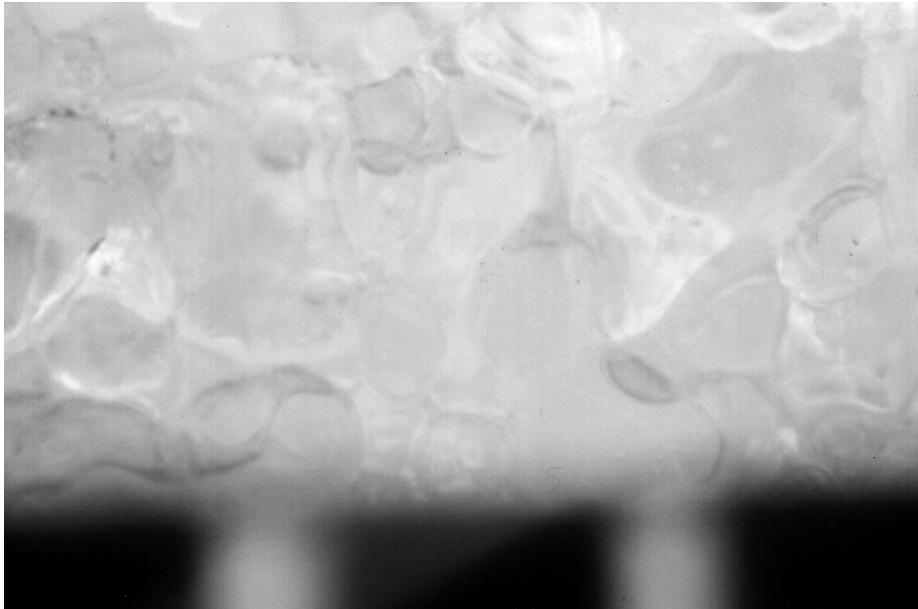


Fig. 5.19. Example of a snow surface with Snow type 5 and fine snow grains ($\bar{d} = 0.40$ mm and $\delta_d = 0.16$ mm): Image No. 29. The distance between the two tick marks is 1 mm.

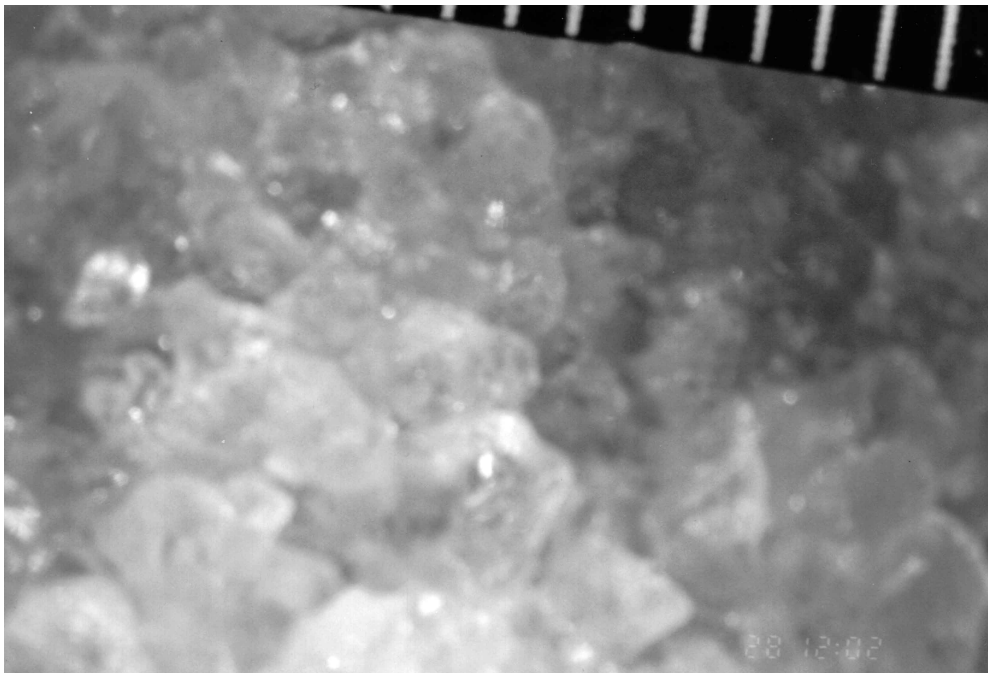


Fig. 5.20. Example of a snow surface with Snow type 4 and very coarse snow grains ($\bar{d} = 2.59$ mm and $\delta_d = 0.71$ mm): Image No. 19. The distance between the tick marks is 1 mm.

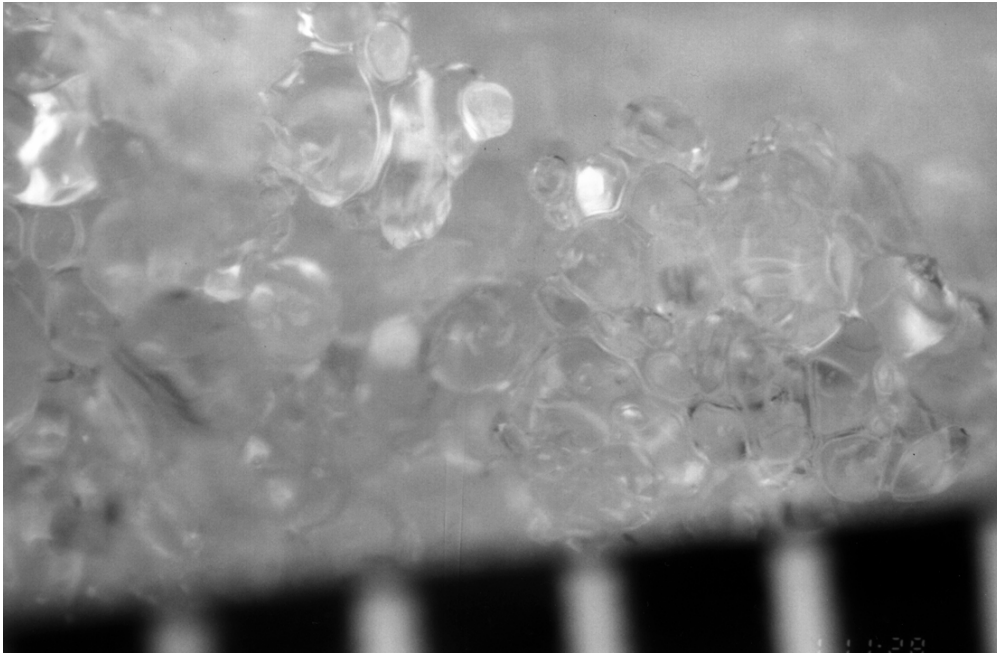


Fig. 5.21. Example of a snow surface with Snow type 4 and fine snow grains ($\bar{d} = 0.49$ mm and $\delta_d = 0.22$ mm): Image No. 30. The distance between the tick marks is 1 mm.

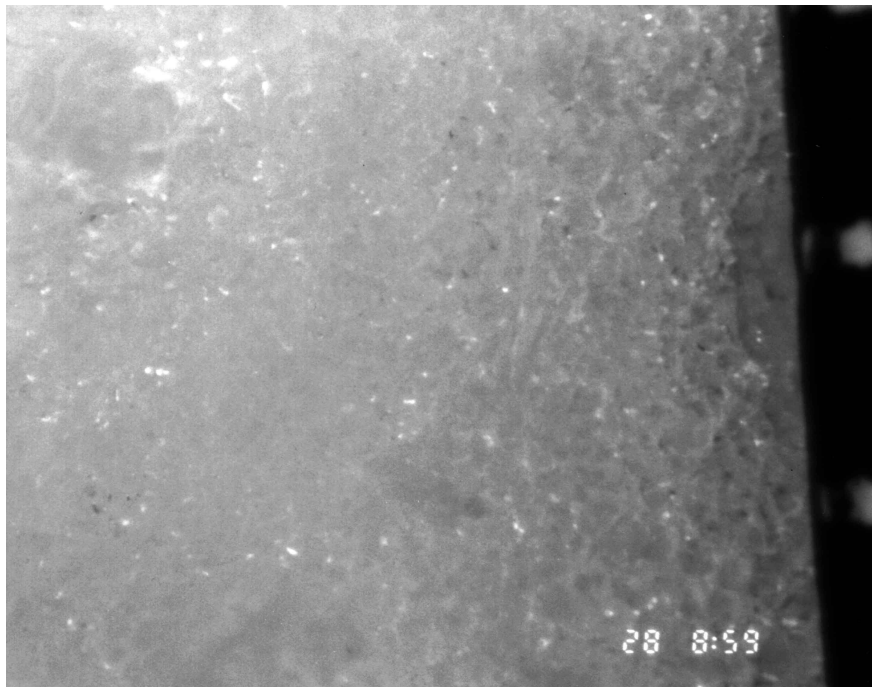


Fig. 5.22. Example of a snow surface with Snow type 3 and very fine snow grains ($\bar{d} = 0.11$ mm and $\delta_d = 0.03$ mm): Image No. 12. The distance between the tick marks is 1 mm.

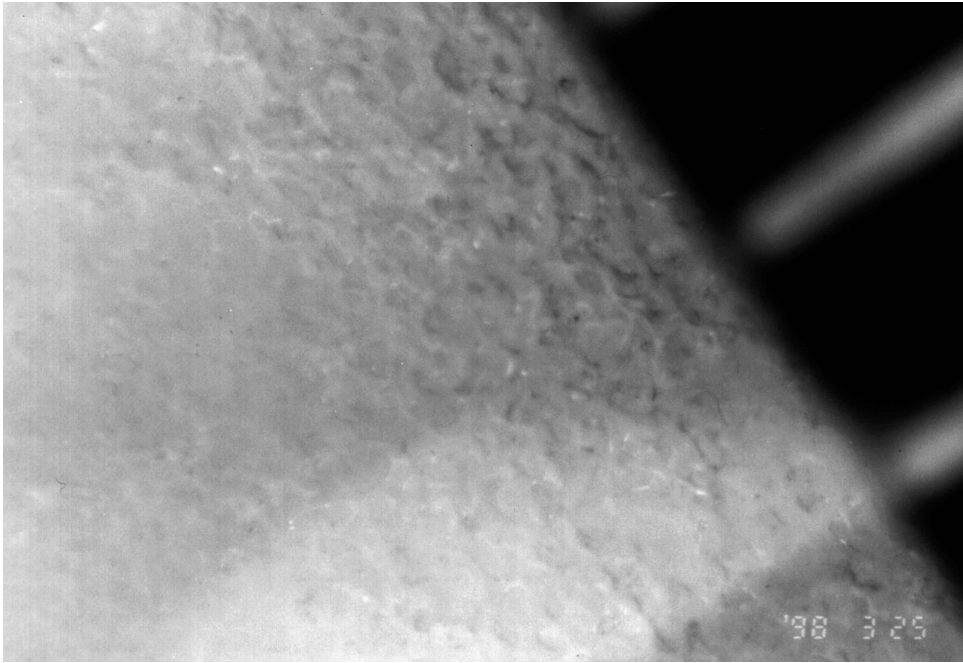


Fig. 5.23. Example of a snow surface with Snow type 2 and fine snow grains ($\bar{d} = 0.21$ mm and $\delta_d = 0.07$ mm): Image No. 21. The distance between the tick marks is 1 mm.

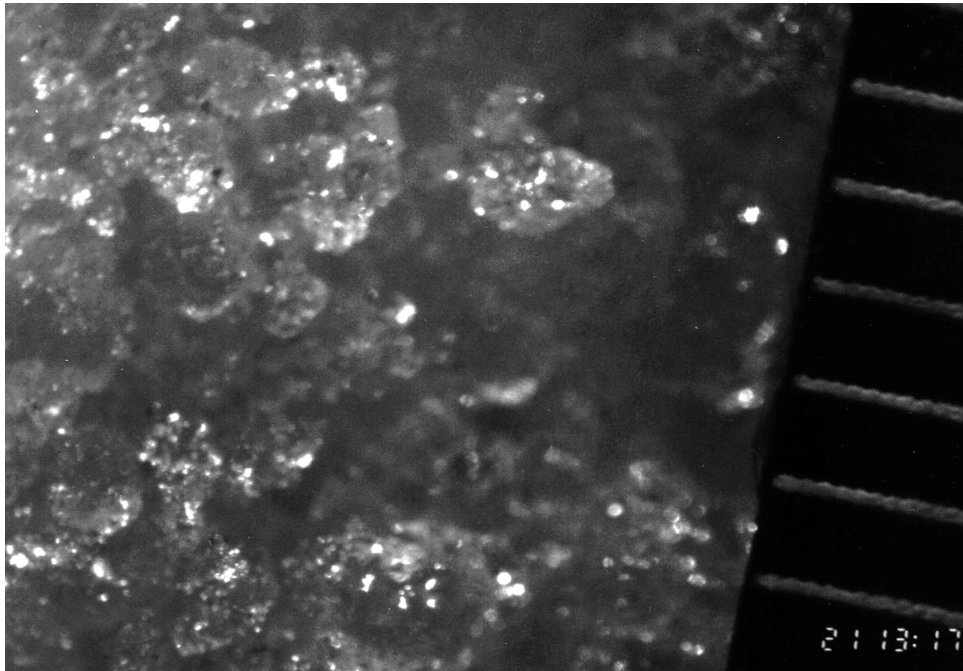


Fig. 5.24. Example of a snow surface with faceted crystals ($\bar{d} = 0.93$ mm and $\delta_d = 0.33$ mm): Image No. 1. The distance between the tick marks is 1 mm.

Figs. 5.25-5.28 depict snow humidity of snow surfaces. Examples of very wet ($W_{vol,\%} = 12.5$ %), wet ($W_{vol,\%} = 6.8$ %), moist ($W_{vol,\%} = 2.4$ %) and dry ($W_{vol,\%} = 0$ %) snow surfaces are presented in Figs.

5.25, 5.26, 5.27 and 5.28, respectively. Figs. 5.29 and 5.30 show examples of snow surfaces of Snow type 5 with high ($\rho = 0.89 \text{ g/cm}^3$) and low ($\rho = 0.41 \text{ g/cm}^3$) densities.

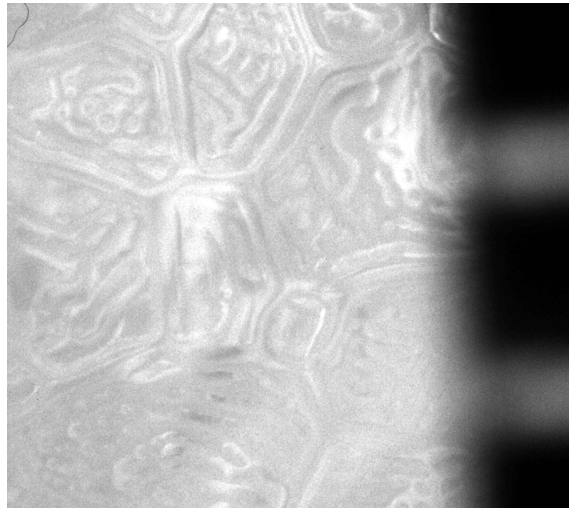


Fig. 5.25. Example of a very wet snow surface ($W_{\text{vol},\%} = 12.5 \%$, $\bar{d} = 0.86 \text{ mm}$ and $\delta_d = 0.29 \text{ mm}$): Image No. 26. The distance between the tick marks is 1 mm.

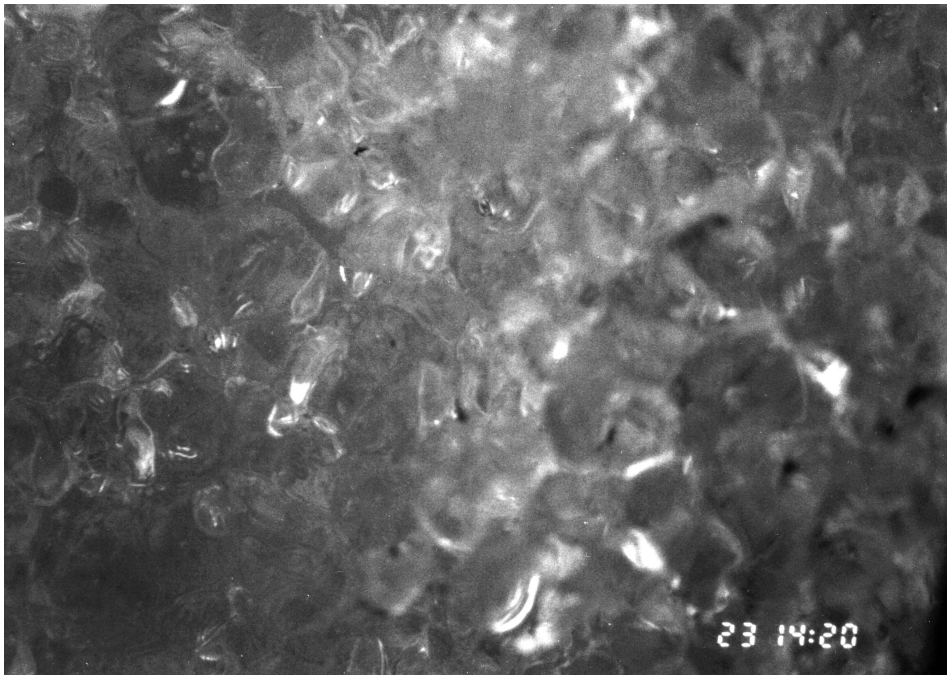


Fig. 5.26. Example of a wet snow surface ($W_{\text{vol},\%} = 6.8 \%$, $\bar{d} = 0.72 \text{ mm}$ and $\delta_d = 0.2 \text{ mm}$): Image No. 4.

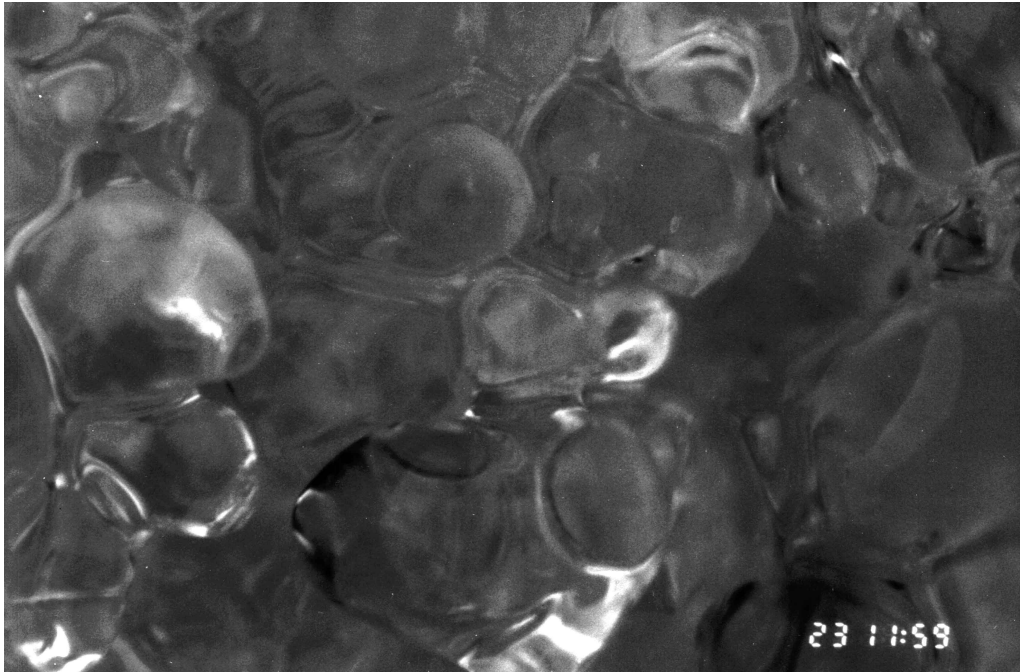


Fig. 5.27. Example of a moist snow surface ($W_{\text{vol},\%} = 2.4\%$, $\bar{d} = 0.84$ mm and $\delta_d = 0.29$ mm): Image No. 3.

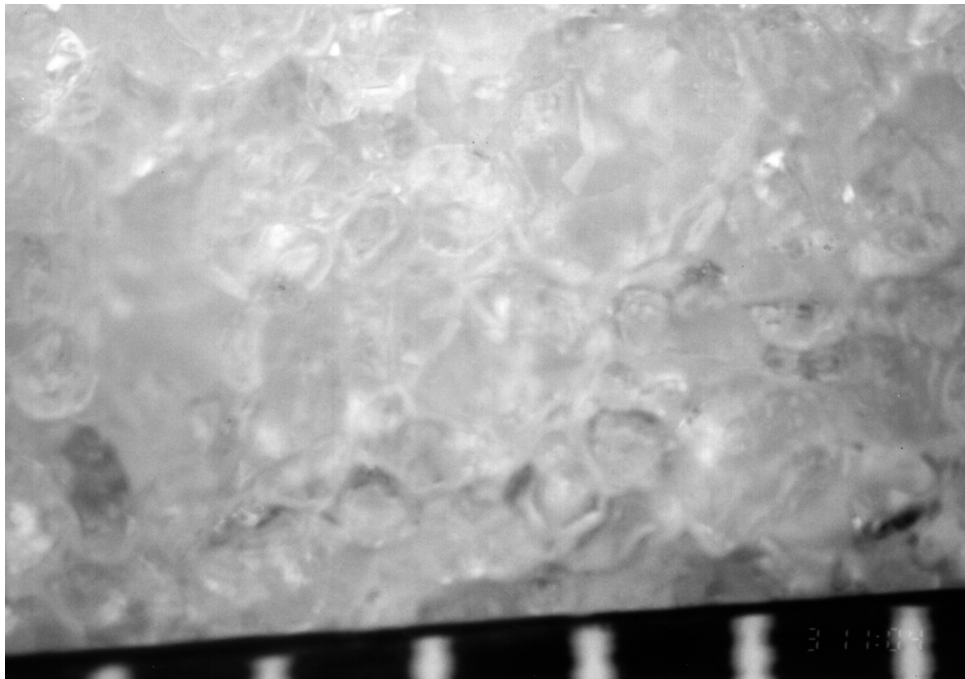


Fig. 5.28. Example of a dry snow surface ($W_{\text{vol},\%} = 0\%$, $\bar{d} = 1.11$ mm and $\delta_d = 0.54$ mm): Image No. 34. The distance between the tick marks is 1 mm.

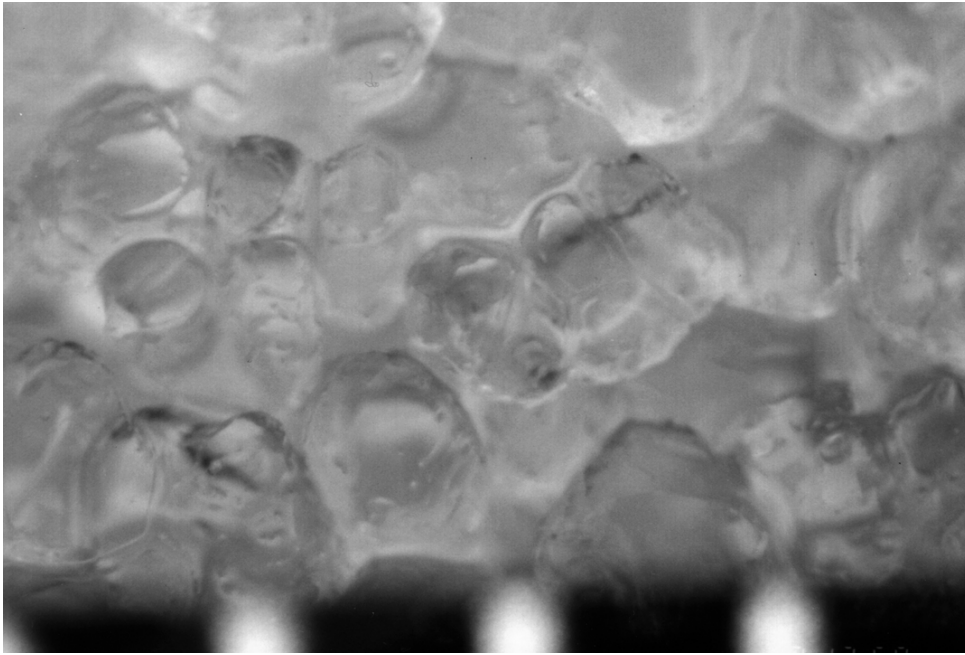


Fig. 5.29. Example of a snow surface with high density ($\rho = 0.89 \text{ g/cm}^3$, $\bar{d} = 0.95 \text{ mm}$ and $\delta_d = 0.34 \text{ mm}$): Image No. 33. The distance between the tick marks is 1 mm.

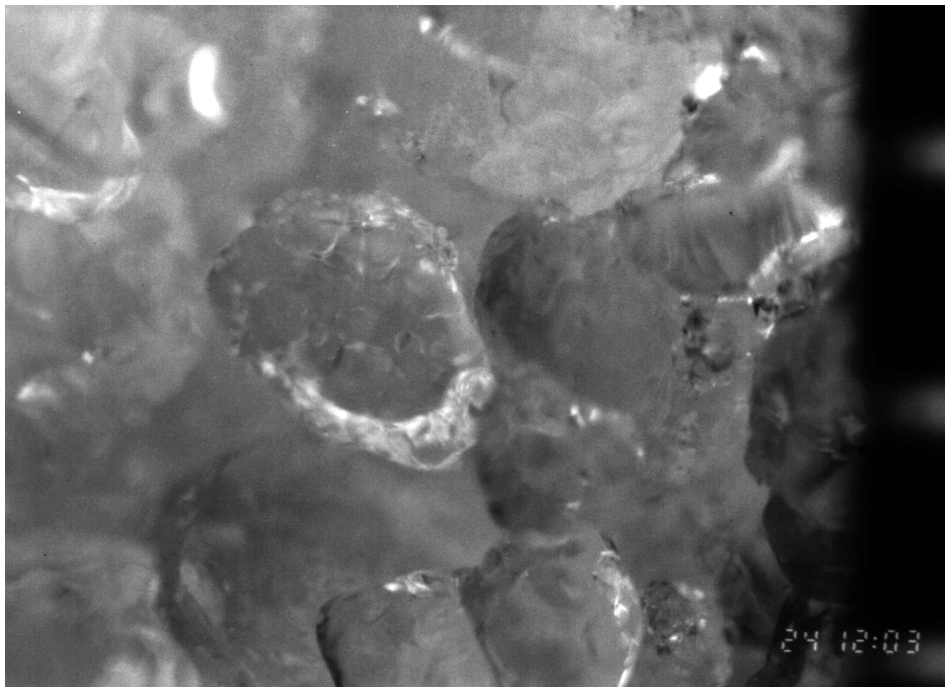


Fig. 5.30. Example of a snow surface with low density ($\rho = 0.41 \text{ g/cm}^3$, $\bar{d} = 1.38 \text{ mm}$ and $\delta_d = 0.44 \text{ mm}$): Image No. 6. The distance between the tick marks is 1 mm.

Fig. 5.31 presents a histogram of the grain size, i.e. \bar{d} , in 23 microscope images of ski tracks containing Snow type 5. The grain size in the microscope images has ranged from 0.32 to 1.88 mm with a mean value of 1.06 mm.

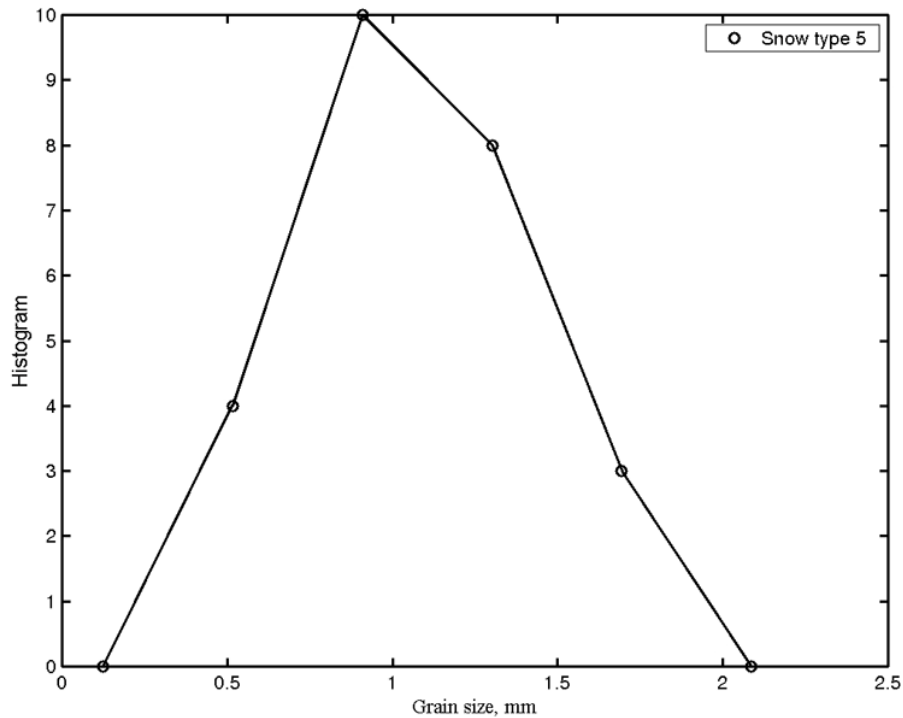


Fig. 5.31. Histogram of the grain size, i.e. \bar{d} , in 23 microscope images of ski tracks containing Snow type 5.

In the four analysed microscope images of Snow type 4, the grain size varied from 0.26 to 2.59 mm with a median value of 0.41 mm. The highest value was obtained in a jumping ski track with below zero snow temperature after a night where a thin veil of new snow had settled on very transformed snow. When 10 ski jumpers had slid down the track, the new snow grains had either blown away or fallen between the old transformed grains. The old snow grains therefore dominated the microscope image of the surface, thus indicating that larger grain size than 1.88 mm also should be possible to register for Snow type 5.

The five analysed microscope images of Snow types 2 and 3 have ranged in grain size from 0.08 to 0.38 mm with a mean grain size of 0.18 mm. Snow microscope images of Snow type 1 have at present not been registered.

5.3.4. Electrolytic conductivity

The development of electrolytic conductivity σ_{mss} , and grain size \bar{d} for various snow types in three different test campaigns is shown in Figs. 5.32-5.34. The snow in the ski courses was prepared with a trail groomer each morning during the test campaigns.

Fig. 5.32 presents results from the period 23 February to 2 March 1997 during the Nordic World Ski Championships'97 in Trondheim, Norway. We see that the electrolytic conductivity is increased and the grain size decreased when precipitation is introduced to the snow surface. It was also experienced during this campaign that the electrolytic conductivity could increase with snow density. After a warm day with snow melt (20.02.1997: $T_a = +3.0^\circ\text{C}$ and $W_{\text{vol},\%} = 1.6\%$), the snow was compacted and increased its density from 0.48 to 0.65 g/cm^3 and the electrolytic conductivity from 17.2 to $25.4 \mu\text{S/cm}$ during a cold, clear night with no snow precipitation (21.02.1997: $T_a = -5.7^\circ\text{C}$ and $W_{\text{vol},\%} = 0.3\%$).

Figs. 5.33 and 5.34 show results from test campaigns in Lillehammer and Sundance/USA, respectively. The electrolytic conductivity in the figures decreases as the snow goes through melt-freeze cycles and the grain size increases.

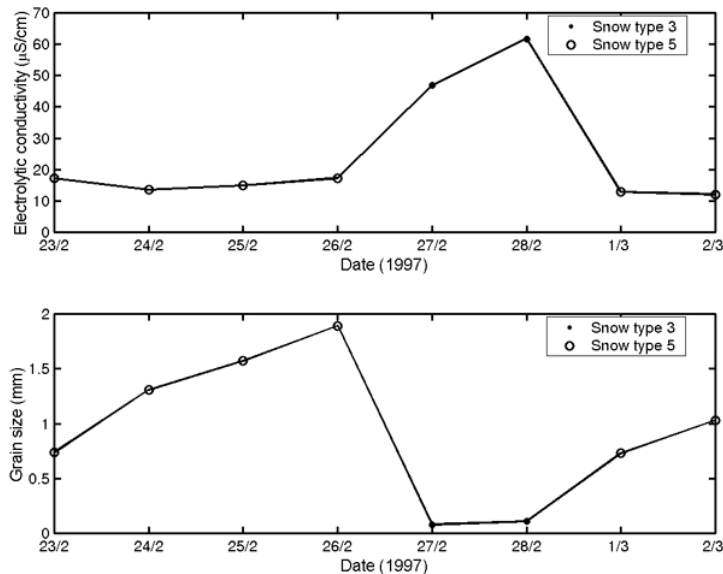


Fig. 5.32. Development of electrolytic conductivity σ_{mss} , and grain size \bar{d} for Snow types 3 and 5 in the period 23 February to 2 March 1997 during the Nordic World Ski Championships'97 in Trondheim, Norway.

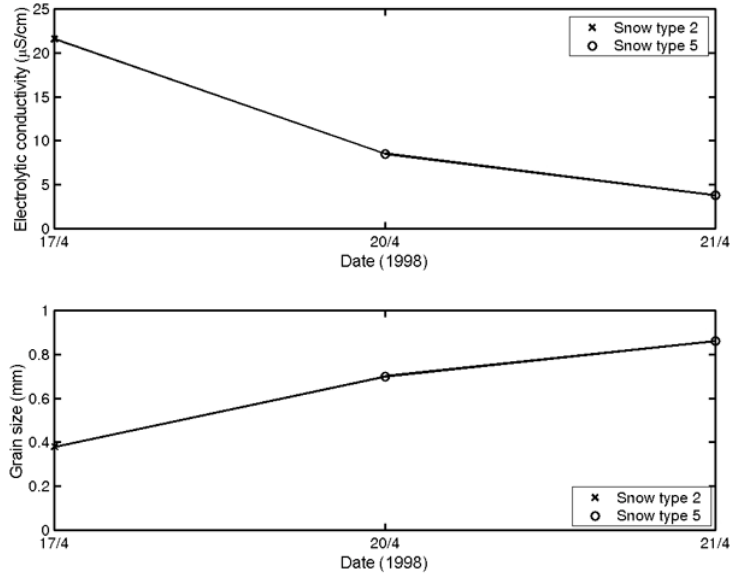


Fig. 5.33. Development of electrolytic conductivity σ_{mss} , and grain size \bar{d} for Snow types 2 and 5 in the period 17 to 21 April 1998 during ski base structure tests in Lillehammer, Norway.

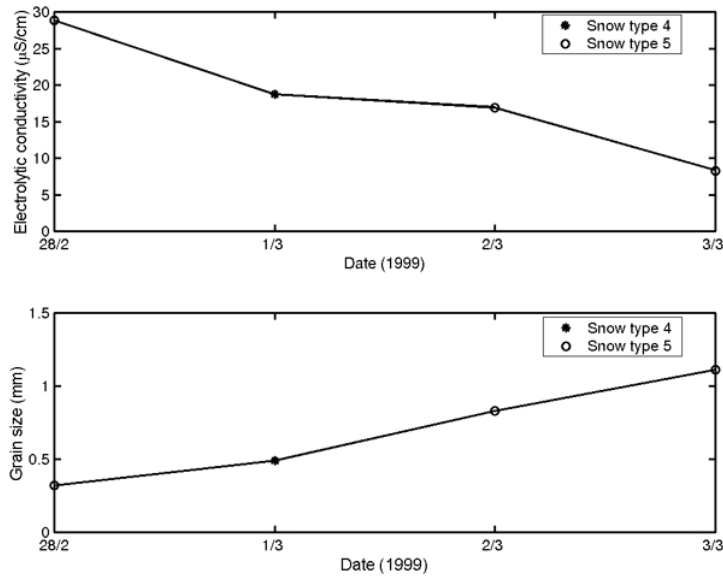


Fig. 5.34. Development of electrolytic conductivity σ_{mss} , and grain size \bar{d} for Snow types 4 and 5 in the period 28 February to 3 March 1999 during a test campaign in Sundance, USA.

Figs. 5.35-5.37 shows the development of ionic content in melted snow samples from the ski track for three different test campaigns. The development of electrolytic conductivity σ_{mss} , grain size \bar{d} and snow type in the test campaigns was given in Figs. 5.32-5.34, respectively.

Fig. 5.35 depicts ionic content of melted snow samples from the ski track in the period 28 February to 2 March 1997 during the Nordic World Championships'97 in Trondheim. The electrolytic conductivity decreased in the period from 61.7 $\mu\text{S}/\text{cm}$ for Snow type 3 on 28 February to 12.9 and 12.1 $\mu\text{S}/\text{cm}$ for Snow type 5 on 1 and 2 March, respectively. It can be seen from 5.35a that Cl^- and Na^+ -ions dominated the snow precipitation introduced to the snow pack on 27 and 28 February (see Fig. 5.32 for data on 27 February), thus indicating that sea salt was the major agent during snow nucleation. Further, Cl^- and Na^+ -ions were the only ions in the melted snow samples with non-negligible content after the snow had been through melt-freeze and restructured, i.e. on 1 and 2 March 1997. The SO_4^{2-} -ions had for instance been completely removed from the snow samples, i.e. the upper part of the snow pack.

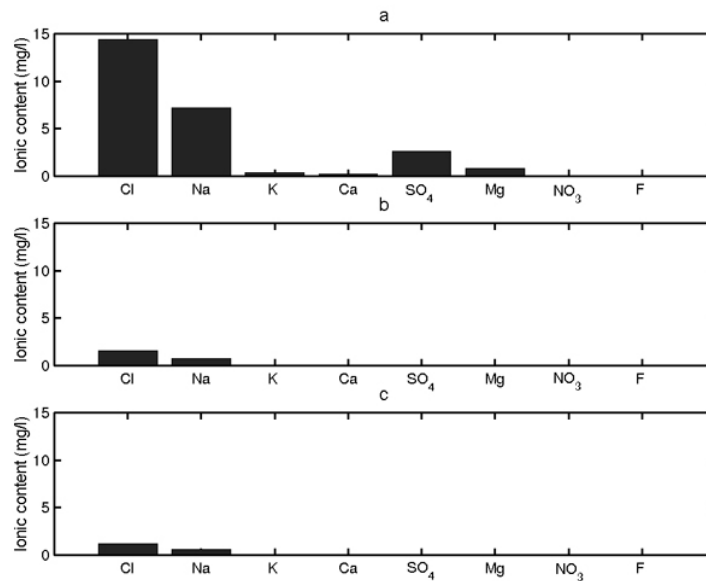


Fig. 5.35. Development in the ionic content of melted snow samples from the ski track in the period 28 February to 2 March 1997 during the Nordic World Ski Championships'97 in Trondheim, Norway. a) 28 February 1997: Snow type 3 and $\sigma_{\text{mss}} = 61.7 \mu\text{S}/\text{cm}$. b) 1 March 1997: Snow type 5 and $\sigma_{\text{mss}} = 12.9 \mu\text{S}/\text{cm}$. c) 2 March 1997: Snow type 5 and $\sigma_{\text{mss}} = 12.1 \mu\text{S}/\text{cm}$.

Fig. 5.36 shows the ionic content of melted snow samples from the ski track in the period 17 to 21 April 1998 during ski base structure tests in Lillehammer. The electrolytic conductivity decreased in the period from 21.6 $\mu\text{S}/\text{cm}$ for Snow type 2 on 17 April to 8.5 and 3.8 $\mu\text{S}/\text{cm}$ for Snow type 5 on 20 and 21 April, respectively. It can be seen from Fig. 5.36a that sulphur and nitrate dominated the snow precipitation at Lillehammer on 17 April. Further, the development of the ionic content of SO_4^{2-} , NO_3^- and Cl^- in the melted snow samples in the period indicated the anion elution order:



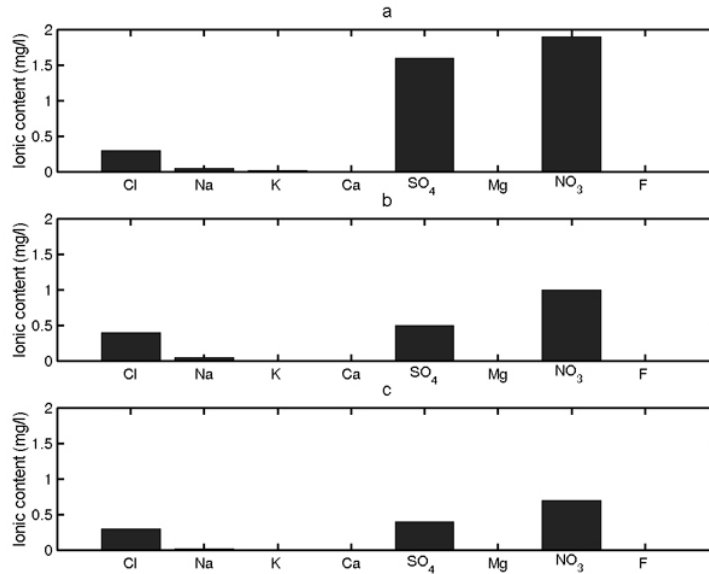


Fig. 5.36. Development in the ionic content of melted snow samples from the ski track in the period 17 to 21 April 1998 during ski base structure tests in Lillehammer, Norway. a) 17 April 1998: Snow type 2 and $\sigma_{\text{mss}} = 21.6 \mu\text{S/cm}$. b) 20 April 1998: Snow type 5 and $\sigma_{\text{mss}} = 8.5 \mu\text{S/cm}$. c) 21 April 1998: Snow type 5 and $\sigma_{\text{mss}} = 3.8 \mu\text{S/cm}$.

Fig. 5.37 depicts the ionic content of melted snow samples from the ski track in the period 28 February to 3 March 1999 during a test campaign in Sundance, USA. The electrolytic conductivity decreased in the period from $28.8 \mu\text{S/cm}$ on 28 February to $8.3 \mu\text{S/cm}$ on 3 March. The melted snow sample from the start of the period (28 February) contained Cl^- , Na^+ , K^+ , Ca^{2+} , SO_4^{2-} , Mg^{2+} and NO_3^- -ions. Ca^{2+} was the dominating ion (2.63 mg/l), while the contributions from Mg^{2+} - and K^+ -ions were rather small (0.5 and 0.2 mg/l , respectively). At the end of the period (3 March) the SO_4^{2-} - and NO_3^- -ions had been eluted completely from the top of the snow pack and no such ions were found in the melted snow samples. The Na^+ -content of the melted snow samples had decreased by 76% from 1.2 mg/l on 28 February to 0.29 mg/l on 3 March. The Ca^{2+} -, K^+ - and Cl^- -content showed a decrease of 52 to 57 % from 2.63 to 1.26 mg/l , 0.2 to 0.09 mg/l and 1.52 to 0.65 mg/l , respectively. The ionic content of Mg^{2+} had decreased by only 26 % from 0.5 mg/l to 0.37 mg/l .

Electrolytic conductivity σ_{mss} of melted snow samples from Trondheim, Hakuba, Lillehammer, Golå (Norway), Sundance/Heber and Toblach (Italy) is tabulated in Table 5.11, while the ionic content of melted snow samples from the same places is depicted in Fig. 5.38. The registered electrolytic conductivities have ranged from 3.8 to $169.7 \mu\text{S/cm}$. A sample of artificial snow from Toblach has given the highest value. The ionic content of this sample is shown in Fig. 5.38f. It can be seen from the figure that the sample contained high levels of Mg^{2+} -, Ca^{2+} -, SO_4^{2-} -, NO_3^- - and K^+ -ions; 13.6 , 8.71 , 5.56 , 3.91 and 2.26 mg/l , respectively. The lowest electrolytic conductivity value has been registered in snow samples from Lillehammer (Snow type 5) and Golå/Norway (Snow type 2).

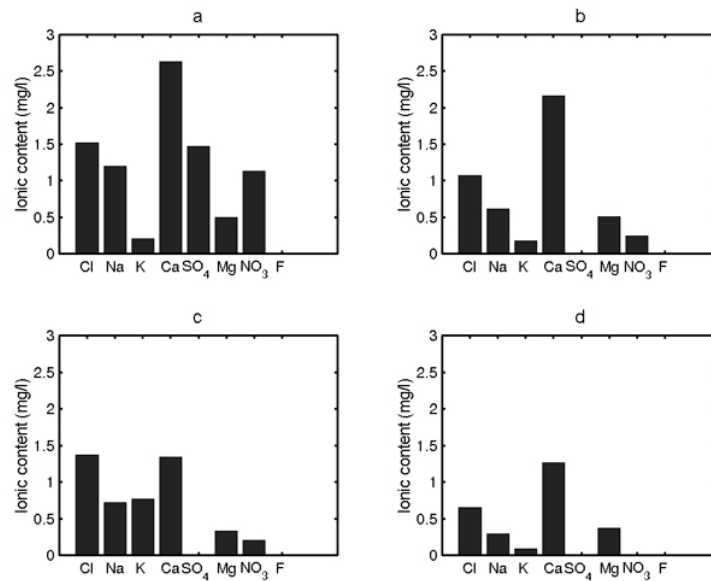


Fig. 5.37. Development in the ionic content of melted snow samples from the ski track in the period 28 February to 3 March 1999 during a test campaign in Sundance, USA. a) 28 February 1999: Snow type 5 and $\sigma_{\text{mss}} = 28.8 \mu\text{S/cm}$. b) 1 March 1999: Snow type 4 and $\sigma_{\text{mss}} = 18.7 \mu\text{S/cm}$. c) 2 March 1999: Snow type 5 and $\sigma_{\text{mss}} = 16.9 \mu\text{S/cm}$. d) 3 March 1999: Snow type 5 and $\sigma_{\text{mss}} = 8.3 \mu\text{S/cm}$.

Table 5.11. Electrolytic conductivity σ_{mss} of melted snow samples from some ski tracks in different parts of the world.

Location	σ_{mss} ($\mu\text{S/cm}$)	Snow type	n_{σ}
Trondheim, Norway (cross-country)	11.8 to 61.7	1 to 5	19
Hakuba, Japan	4.7 to 21.9	1 to 5	16
Lillehammer, Norway	3.8 to 21.6	2 and 5	3
Golå, Norway	3.8 to 4.1	2	4
Sundance/Heber, USA	8.3 to 94.5	1 to 5	13
Toblach, Italy	169.7	6	1

The snow samples from Trondheim and Sundance/Heber gave the highest conductivities for new snow types, 61.7 and 94.5 $\mu\text{S/cm}$, respectively. These values are approximately 3 to 5 times higher than the maximum values found for snow samples from Hakuba and Lillehammer (21.9 and 21.6 $\mu\text{S/cm}$, respectively). The reason for the high conductivities in Trondheim and Sundance/Heber is the high levels of Na^+ - and Cl^- -ions in the melted snow samples as depicted in Figs. 5.38a and 5.38e. The ionic content of Cl^- and Na^+ was 14.4 and 7.2 mg/l in Trondheim, and 25.1 and 14.4 mg/l in Sundance/Heber, respectively. High ionic content of Cl^- and Na^+ is due to salt being the major agent during snow nucleation in the snowfalls. Figs. 5.38b and 5.38c show that the ionic content of Cl^- and Na^+ in melted snow samples is relatively small in Hakuba (1.6 and 0.84 mg/l of Cl^- - and Na^+ -ions, respectively) and negligible at Lillehammer (0.3 and 0.05 mg/l of Cl^- - and Na^+ -ions, respectively). SO_4^{2-} and NO_3^- are the dominant ions at Lillehammer (1.6 and 1.9 mg/l of SO_4^{2-} - and NO_3^- -ions,

respectively). These ions do also give a significant contribution to the total ionic content in Hakuba (1.5 and 0.9 mg/l of SO_4^{2-} - and NO_3^- -ions, respectively). The lowest conductivities for new snow types, 3.8 to 4.1 $\mu\text{S}/\text{cm}$, were registered in melted snow samples from Golå. This snow is extremely pure as can be seen in Fig. 5.38e.

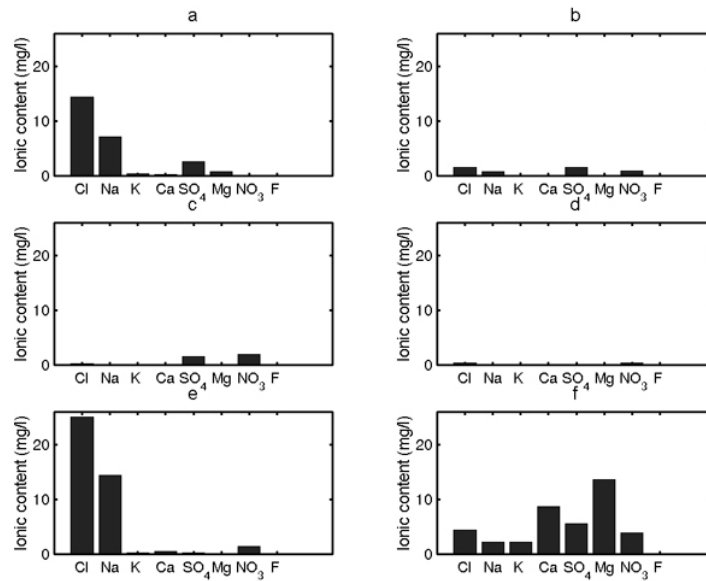


Fig. 5.38. Ionic content of melted snow samples from different parts of the world: a) Trondheim, Norway: Snow type 3 and $\sigma_{\text{mss}} = 61.7 \mu\text{S}/\text{cm}$. b) Hakuba, Japan: Snow type 1 and $\sigma_{\text{mss}} = 21.9 \mu\text{S}/\text{cm}$. c) Lillehammer, Norway: Snow type 2 and $\sigma_{\text{mss}} = 21.6 \mu\text{S}/\text{cm}$. d) Golå, Norway: Snow type 2 and $\sigma_{\text{mss}} = 3.8 \mu\text{S}/\text{cm}$. e) Sundance/Heber, USA: Snow type 1 and $\sigma_{\text{mss}} = 94.5 \mu\text{S}/\text{cm}$. f) Toblach, Italy: Snow type 6 and $\sigma_{\text{mss}} = 169.7 \mu\text{S}/\text{cm}$.

5.4. Discussion

5.4.1. Snow hardness

It was shown in Section 5.3.1 that hardness values between 10^4 and 10^6 Pa are the most common in ski tracks. This is considerably lower than the average compressive strength of freshwater ice at -10°C . Kovacs (1993) reports typical values for ice between 5.7×10^6 and 1.0×10^7 Pa. According to Yosida (1971) the ideal snow hardness for slalom and giant slalom races should be between 7 and 10 kg/cm^2 , i.e. approximately $7\text{-}10 \times 10^5$ Pa. Approximately 90 % of the measurements performed in ski tracks have been below this hardness. Hämäläinen and Spring (1986) performed ski friction tests in laboratory with snow hardness varying from approximately 1×10^5 to 3×10^6 Pa. Friction tests were not performed on medium and low hardness snow conditions which are likely to be present 60 % of the time in ski tracks according to our measurements. In the future more attention needs to be paid to the snow hardness range between 10^4 and 10^5 Pa in friction tests. Empirical experiences indicate that the macroscopic impact and compaction resistances are important for ski base sliding friction when the snow hardness is below approximately 7×10^4 Pa.

Except for snow conditions with Snow type 1 where the snow hardness tended to increase with snow density, no apparent relationship has been found between snow hardness and snow density in our measurements. This is not a new experience. Several authors e.g. Yosida (1956), Voitkovsky et al. (1975), Fukue (1979) and Armstrong (1980) have argued that the snow density is not a reliable indicator of the mechanical properties of snow e.g. compressive strength or hardness. Shapiro et al. (1997) stated that the bonding between snow grains is the critical factor in determining response of snow to applied loads. They further claimed that the reason why an apparent relationship between density and mechanical properties often seems to exist is that both the density and the mechanical properties depend on the nature of the bonding/grain contacts.

It was shown in Section 5.3.1 that ski tracks tend to have lower mean snow hardness when the snow humidity is above 5 %, and that moist snow with snow temperature between -1 and -4°C can have high snow hardness. Colbeck (1997) has also done similar experiences. He stated that wet snow is well bonded at low liquid contents, but cohesionless and slushy at high liquid contents because the grain boundaries then are unstable against pressure melting. Lower snow hardness at high snow humidities causes higher macroscopic impact and compaction resistances during ski base sliding friction. Moist snow with high hardness can ease the development of water film during skiing. These aspects must be accounted for when choice of optimum skis and ski base structures are made under the respective conditions.

It has also been experienced in our measurements that the minimum snow hardness tends to increase with decreasing snow temperature. Perla and Glenne (1981) have stated that the snow hardness correlates inversely with temperature, all other factors held constant. This means that macroscopic impact and compaction resistances in average should be less dominant at lower snow temperatures. Microscopic impact and compaction resistances are still important due to the thin water film present under such conditions.

It was established in Section 5.3.1 that the average snow hardness for new snow types in our measurements was approximately three times higher in classic ski tracks than in skating ski tracks. More measurements are needed in order to establish reliable trends for transformed snow types, but so far the differences between classic and skating ski tracks have been small for transformed snow types compared to new snow types. These results indicate that macroscopic impact and compaction resistances are much more important for skating skis than classic skis under new snow conditions. This must be accounted for when performing sliding tests of skating skis and ski base structures, and when choosing skis and ski base structures for skating competitions on new snow.

In future research it might be advantageous to use a ball with less mass in the measurement setup, e.g. an aluminium ball instead of a steel ball, when performing measurements on soft snow. In this way the accuracy for snow with low or very low hardness can be increased. Perla and Glenne (1981) have recommended to use a heavy-weight Rammsonde (1 kg) for hardness measurements in hard snow and a light-weight Rammsonde (0.1 kg) in soft snow.

5.4.2. Snow humidity and density

The snow density has ranged between 0.22 and 0.92 g/cm³ in our measurements. It was commented in Section 5.3.2 that the accuracy of the highest value can be questioned since the measurement equipment, although usable also for measuring higher snow densities, is primarily designed for measuring snow density below 0.6 g/cm³. In spite of this it can not be excluded that snow density close to the density of ice (0.92 g/cm³) might occur in groomed compressed wet ski trails. Yosida (1963) showed that a snow pillar with initial density of 0.35 g/cm³ could be deformed with a compression machine until the density of ice was reached. This typically occurred when the snow pillar was compressed to approximately one-hundredth of its initial height. Sommerfeld and LaChapelle (1970) referred a typical density range of 0.8 to 0.83 g/cm³ for "firnification" induced by advanced pressure metamorphism in their classification of snow by metamorphic state. Anyhow, the mean density of snow in ski tracks (0.50 g/cm³) is considerably higher than typical densities of seasonal snow covers. Sturm et al. (1995) referred bulk densities of 0.38 g/cm³ for tundra, 0.26 g/cm³ for taiga and 0.35 g/cm³ for maritime snow covers in their seasonal snow cover classification system. Yosida (1971) concluded that the ideal snow density for slalom and giant slalom races should not be much less than 0.5 g/cm³. This corresponds to the mean snow density in our measurements in ski tracks.

The snow density is important for the permeability of the snow and the potential drainage of frictional water film down in the snow during skiing. In Section 5.3.2 it was found that the mean snow densities were higher for transformed snow types than new snow types. Although fine-grained compact snow can have lower permeability than coarse-grained snow in spite of lower density (Shimizu, 1970), this might indicate higher frictional water film thickness in average during skiing on transformed snow. Higher frictional water film thickness means that coarser ski base structures have to be used in order to attain optimum sliding properties. See Chapter 2 for more details.

The snow humidity can be viewed as an indicator of the initial water film thickness in the ski track and the frictional water film thickness that is possible to attain during skiing. This makes it a very

important parameter for optimum choices of ski base structure, glide wax/powder and kick wax in a ski competition. Shimbo (1961) has also pointed out the importance of snow humidity on snow friction. The typical distribution of snow humidity with relative humidity and air temperature was shown for our measurements in Fig. 5.16. This figure indicates under which weather conditions the snow humidity (and thereby the initial water film thickness) is significant and needs to be measured. For instance is it sufficient to perform snow humidity measurements at air temperatures above -3°C when the relative humidity is 40 %, while it has to be considered for temperatures down to -10°C when the relative humidity is 80 %.

5.4.3. Snow type and snow grain structure

Throughout this text we have applied a simple classification system for snow types on snow surfaces. This system has been used quite extensively in practice by ski technicians due to its ease to use when no measurement equipment is accessible. It is for instance easy to interpret Snow type 5 in this system as snow where klistor wax ought to be applied as kick wax, and Snow type 2 as snow where hard wax should be applied. The grain shape and grain size classification system presented by Colbeck et al. (1990) should be used in addition when a microscope or hand lens is accessible for inspection of the snow surface.

The maximum value of \bar{d} for Snow type 4 in our measurements (2.59 mm) was higher than the maximum value registered for Snow type 5 (1.88 mm). This indicates that higher values of \bar{d} also should be possible to obtain for Snow type 5. Schemenauer et al. (1981) have stated that individual snow crystals observed at the surface of the earth range in maximum dimension from approximately 0.05 mm to 5 mm. Wiesmann et al. (1998) found that grain sizes in snow covers ranged from less than 0.1 mm to 3 mm. In our few analysed microscope images of new snow types in ski tracks grain sizes have ranged from 0.08 to 0.38 mm. Smaller grain sizes would probably also have been obtained if we had been able to register more snow microscope images of new snow types. In-situ microscope imaging of ski tracks is very difficult for new snow types with snow surface grains below 0.2 mm.

More microscope images of ski tracks need to be registered in order to find typical distributions of grain sizes for different snow types. The sizes of the snow surface grains are essential for the contact configuration between the ski base structure and the snow surface, and the design of optimum ski base structures for different snow conditions.

5.4.4. Electrolytic conductivity

It was established in Section 5.3.4 that electrolytic conductivity increases and the grain size decreases when precipitation is introduced to the snow surface. Further, the electrolytic conductivity decreases as the snow goes through melt-freeze cycles and the grain size increases. It was also experienced that electrolytic conductivity can increase with snow density. Kopp (1962) has also found similar trends for the electrical conductivity of snow, although the conductivity then is several orders of magnitude less than the electrolytic conductivity of melted snow samples. In Fig. 5.39 the electrical conductivity

of snow is depicted as a function of temperature for fresh snow compressed to various densities. It is easy to see from the figure that the electrical conductivity of snow increase with snow density and temperature. At temperatures above -5°C the electrical conductivity increases more steeply than for lower temperatures. It is interesting whether this is due to increased snow humidity or not. Fig. 5.40 shows electrical conductivity as a function of temperature for various states of snow metamorphism. Kopp found as can be seen in the figure, that snow samples that had previously reached the melting point showed significantly lower electrical conductivity values than samples that had not reached the melting point. He explained this with washout of trace quantities of contaminants rather than metamorphism. This corresponds very well with the electrolytic conductivity results. The electrical conductivity of snow and electrolytic conductivity of melted snow might be very important for electrical discharge between ski and snow during skiing.

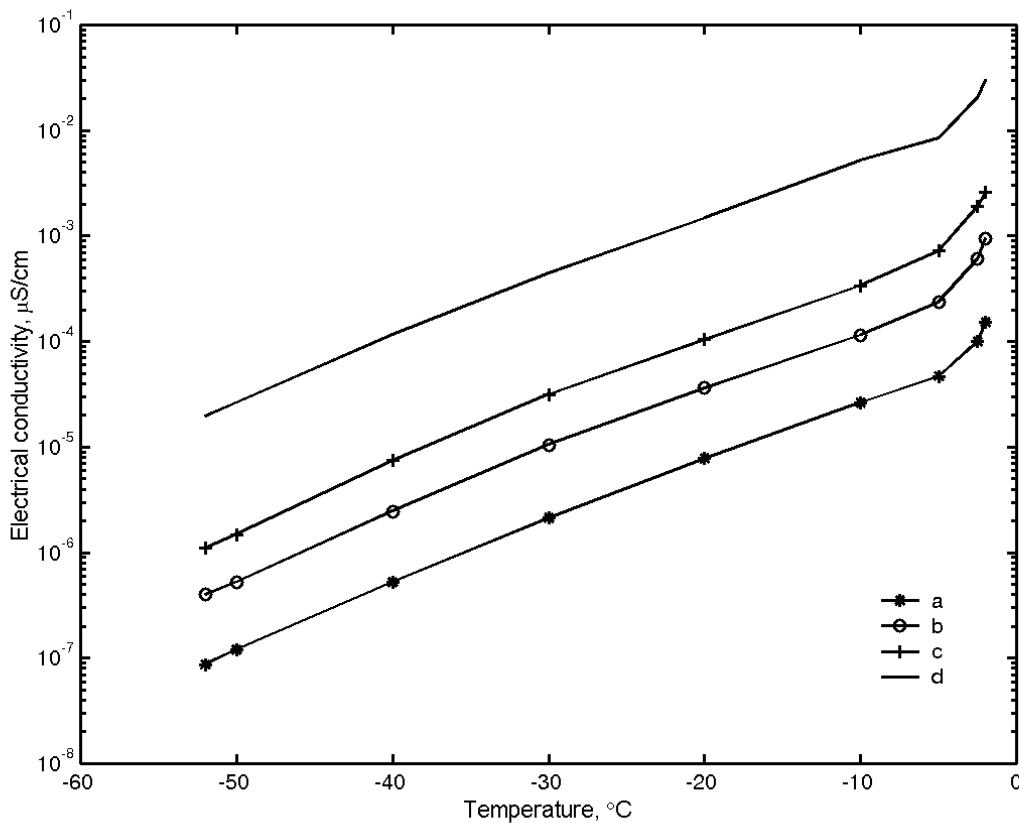


Fig. 5.39. Electrical conductivity versus temperature for fresh snow compressed to various densities (after Kopp, 1962): a) $\rho = 0.175 \text{ g/cm}^3$. b) $\rho = 0.29 \text{ g/cm}^3$. c) $\rho = 0.39 \text{ g/cm}^3$. d) $\rho = 0.57 \text{ g/cm}^3$.

High electrolytic conductivities and high levels of Na^+ - and Cl^- -ions have been registered in our melted snow samples from Trondheim and Sundance/Heber due to salt being a major agent during snow nucleation in the snowfalls. The maximum ionic content of Cl^- and Na^+ has been 14.4 and 7.2 mg/l in Trondheim, and 25.1 and 14.4 mg/l in Sundance/Heber, respectively. The maximum electrolytic conductivity of the melted snow samples from Trondheim was $61.7 \mu\text{S/cm}$, while the samples from Sundance/Heber had a maximum conductivity value of $94.5 \mu\text{S/cm}$. The values for

Trondheim correspond well with registrations of precipitation in Kaldvellfeltet near Trondheim in 1988 described by Storrø (1990). He found a maximum electrolytic conductivity of 72.2 $\mu\text{S}/\text{cm}$ and maximum Cl^- - and Na^+ -contents of 13.2 and 7.4 mg/l, respectively. Proximity to the Atlantic Ocean is known to result in relatively high inputs of sea-salt ions (Na^+ , Mg^{2+} , Cl^-) as either wet or dry deposition to the snowpack (Raben and Theakstone, 1997). Mean Na^+ -concentrations (mg/l) in precipitation in Norway in 1997 is shown in Fig. 5.41. It is easy to see from the figure that Na^+ -concentrations are higher in coastal areas e.g. Trondheim, than in interior parts of Norway, e.g. Golå and Lillehammer. The proximity to the Great Salt Lake causes the high inputs of salt ions to the snowpack in Sundance/Heber.

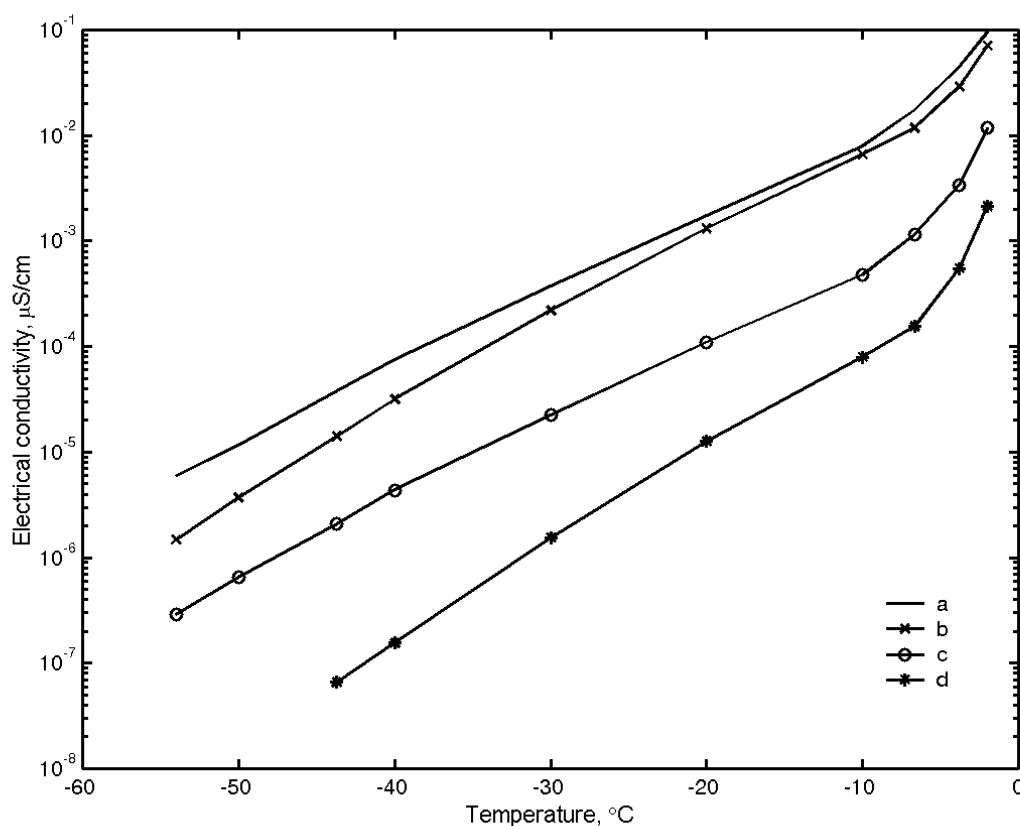


Fig. 5.40. Electrical conductivity versus temperature for various states of metamorphism (after Kopp, 1962): a) Untransformed snow, $\rho = 0.68 \text{ g}/\text{cm}^3$. b) After temperature gradient metamorphism, $\rho = 0.66 \text{ g}/\text{cm}^3$. c) Large grained neve (firn i.e. grains that have been through melt-freeze metamorphism), $\rho = 0.56 \text{ g}/\text{cm}^3$. d) Fresh snow equitemperature metamorphosed to granular form, $\rho = 0.24 \text{ g}/\text{cm}^3$. Different metamorphic states have different conductivities with similar densities.

Ca^{2+} has been the dominating ion (2.63 mg/l) in some snowfalls, e.g. the snowfall in Sundance prior to the period 28 February to 3 March 1999 shown in Fig. 5.37. The relatively high Ca^{2+} -content in Sundance can for instance be due to calcareous dust from bedrock of limestone in the area.

SO_4^{2-} and NO_3^- have been the dominant ions in melted snow samples from Lillehammer and have also given a significant contribution to the total ionic content in Hakuba. Langham (1981) have stated that gases like sulphur dioxide (SO_2) and nitrogen oxides (e.g. NO_3) can be adsorbed on the surface of snow crystals and that high sulphur contents in a snowpack are due to industrial sources. Mean nitrate-concentrations in precipitation in Norway in 1998 are shown in Fig. 5.42. It can be seen from the figure that nitrate pollution is higher in the southern part of Norway e.g. Lillehammer than further north e.g. in Trondheim. This corresponds well with our results, although our highest nitrate concentration in Trondheim (0.8 mg/l) has been higher than the nitrate concentration registered in Golå (0.34 mg/l). Snow precipitation in Trondheim has most often been registered with no nitrate content, see e.g. Fig. 5.38e.

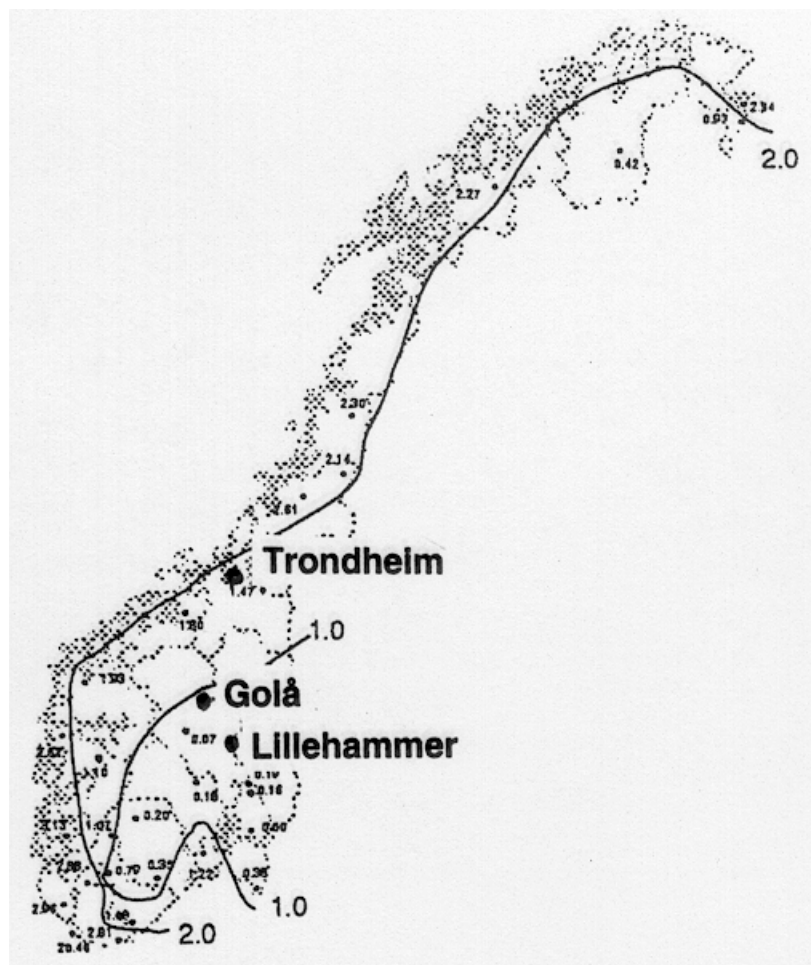


Fig. 5.41. Mean Na-concentrations (mg/l) in precipitation in Norway in 1997 (Lükeville et al., 1998).

The development of ionic content of SO_4^{2-} , NO_3^- and Cl^- in the melted snow samples from Lillehammer indicated the anion elution sequence:



This anion elution sequence was first proposed by Tranter et al. (1986). The sequence can be explained by chloride being more likely to find in the interior regions of snow crystal and sulphate on the outside (Davis, 1991).

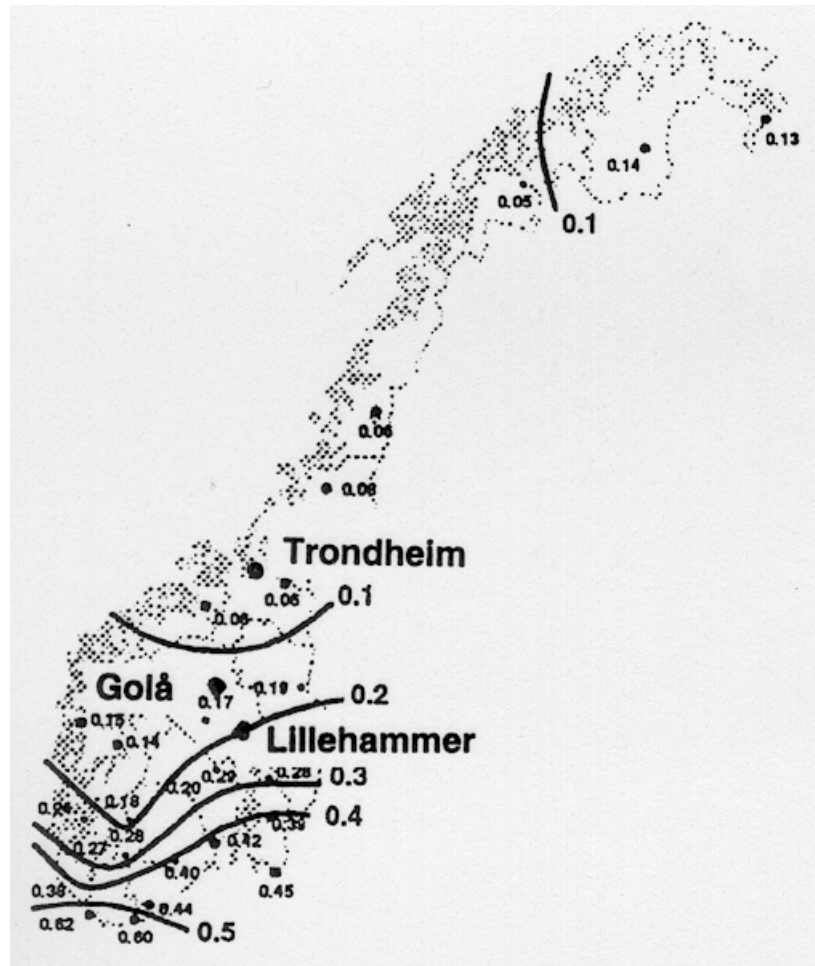


Fig. 5.42. Mean nitrate-concentrations (mg/l) in precipitation in Norway in 1998 (Tørseth et al., 1999).

A sample of artificial snow from Toblach has given the highest measured electrical conductivity value to present ($169.7 \mu\text{S}/\text{cm}$). The high value is probably due to pollution in the water applied in the snow production. The high conductivity value highlights that artificial snow has different chemical properties compared to normal snow and thereby can have other sliding properties. This influence optimum choice of ski wax and glide product on artificial snow compared to normal snow.

The varying electrolytic conductivity of melted snow samples with snow type, geography, grain size and density and the similarly varying electrical conductivity of snow with snow type and density are very interesting in connection with electrical discharge between ski and snow during skiing. The effect of electrical charging and electrostatic pressure on ski base sliding friction is further discussed in Chapter 7. Electrical charging and electrostatic pressure effects might be very important factors for making optimum choices of ski wax and glide product in different parts of the world. It might also have great impact on the understanding of ski base sliding friction, ski base structures and the frictional water film. Future research ought to be performed in this field.

5.5. Conclusions

During measurement campaigns in ski tracks in Norway (1995-98), Hakuba/Japan (1996-98) and Sundance/USA (1999) the following parameters have been registered: air temperature, relative humidity, net radiation, snow temperature, snow hardness, snow humidity, snow density, snow type, snow grain structure, electrolytic conductivity and ionic content of melted snow samples. Specific attention has been paid to snow hardness, snow humidity, snow density, snow grain structure and electrolytic conductivity in this text.

The measurements of snow hardness in ski tracks have given the following major results:

- Snow hardness between 10^4 and 10^6 Pa is most common in ski tracks, and snow hardness below 10^5 Pa is likely to be present 60 % of the time. Ski friction tests described in the literature have concentrated on snow with snow hardness above 10^5 Pa. More attention needs therefore to be paid on the snow hardness range between 10^4 and 10^5 Pa in friction tests in the future.
- Except for snow conditions with Snow type 1 where the snow hardness has tended to increase with snow density, no apparent relationship has been found between snow hardness and snow density.
- Ski tracks tend to have lower mean snow hardness when the snow humidity is above 5 %. This causes higher macroscopic impact and compaction resistances during ski base sliding friction and must be accounted for when choice of optimum skis and ski base structures are made under such conditions.
- The minimum snow hardness tends to increase with decreasing snow temperature.
- The snow hardness and the bonding of the snow grains seem to be dependent on both the snow temperature and the snow humidity.
- The average snow hardness for new snow types has been approximately three times higher in classic ski tracks than in skating ski tracks, thus implying that macroscopic impact and compaction resistances are much more important for skating skis than classic skis under such conditions. It is important to consider this when performing sliding tests of skating skis and ski base structures, and when choosing skis and ski base structures for skating competitions on new snow.

The measurements of snow density in ski tracks have shown that:

- The snow density typically ranges between 0.2 and 0.9 g/cm³.
- The mean density of snow in ski tracks (0.50 g/cm³) is considerably higher than typical densities of seasonal snow covers (0.26-0.38 g/cm³).
- The mean snow densities are higher for transformed snow types (0.51-0.59 g/cm³) than new snow types (0.39-0.43 g/cm³).

The measurements of snow humidities in ski tracks have resulted in the following findings:

- The snow humidity typically ranges between 0 and 12.5 %. It has been measured an increase in the snow humidity from 0.6 % to 12.5 % during two hours on a warm, sunny day in April at Lillehammer ($T_a = +5.8^\circ\text{C}$ and $q_{\text{net}} = 753 \text{ W/m}^2$). The snow humidity can be viewed as an indicator of the initial water film thickness in the ski track and the frictional water film thickness that is possible to attain during skiing. It is thus a very important parameter for optimum choices of ski base structure, glide wax/powder and kick wax in a ski competition.
- The snow humidity is typically less than 2 % for snow temperatures below -2°C and less than 1 % for snow temperatures below -7°C .
- Snow humidities exceeding 4 % have only been registered at air temperatures above $+1^\circ\text{C}$.
- The highest snow humidities have been registered on clear, warm days with relative humidities between 40 and 60 %, and an air temperature above $+5^\circ\text{C}$. Due to condensation processes being more efficient, the snow humidity has shown an increasing tendency at relative humidities above 80 % and air temperatures between $+1$ and $+6^\circ\text{C}$ compared to relative humidities between 60 and 80 %.

The mean snow grain diameter and the standard deviation of grain diameters have been calculated for 34 snow surface microscope images of ski tracks. Fourteen of the analysed snow microscope images have been depicted in this chapter. The analysis of snow surface grains in ski tracks have shown that:

- The typical grain size has ranged from 0.26 to 2.59 mm for Snow types 4 and 5.
- The five analysed microscope images of Snow types 2 and 3 have ranged in typical grain size from 0.08 to 0.38 mm.
- In-situ microscope imaging of ski tracks is very difficult for new snow types with snow surface grains below 0.2 mm. Thus, snow microscope images of Snow type 1 have not been registered at present.
- More microscope images of ski tracks need to be registered in order to find typical distributions of grain sizes for different snow types. The sizes of the snow surface grains are essential for the contact configuration between the ski base structure and the snow surface, and the design of optimum ski base structures for different snow conditions.

The measurements of electrolytic conductivity and ionic content of melted snow samples from ski tracks have given the following major results:

- The electrolytic conductivity increases and the grain size decreases when precipitation is introduced to the snow surface. The electrolytic conductivity can also increase with snow density.
- The electrolytic conductivity decreases as the snow goes through melt-freeze cycles and the grain size increases.
- The electrolytic conductivity of melted snow samples follows similar trends with respect to snow metamorphosis and snow density as the results referred by Kopp (1962) for the electrical conductivity of snow, but the electrical conductivity of snow is several orders of magnitude less than the electrolytic conductivity of melted snow samples. The electrical conductivity of snow and electrolytic conductivity of melted snow might be very important for the electrical discharge between ski and snow during skiing. The effect of electrical charging and electrostatic pressure on ski base sliding friction is further discussed in Chapter 7.

- In melted snow samples from Trondheim and Sundance/Heber high electrolytic conductivities (61.7 $\mu\text{S}/\text{cm}$ and 94.5 $\mu\text{S}/\text{cm}$, respectively) and high levels of Na^+ - and Cl^- -ions have been registered due to salt being a major agent during snow nucleation in the snowfalls. These values are approximately 3 to 5 times higher than the maximum values found for snow samples from Hakuba and Lillehammer (21.9 and 21.6 $\mu\text{S}/\text{cm}$, respectively).
- SO_4^{2-} and NO_3^- have been the dominant ions in melted snow samples from Lillehammer and have also given a significant contribution to the total ionic content in Hakuba.
- Ca^{2+} has been the dominating ion in some snowfalls, e.g. one snowfall in Sundance.
- A sample of artificial snow from Toblach has given the highest measured electrical conductivity value to present (169.7 $\mu\text{S}/\text{cm}$).

5.6. References

- Abele, G. and A. Gow (1975): Compressibility characteristics of undisturbed snow. CRREL Research Report 336, 57 p.
- Abele, G. and A. Gow (1976): Compressibility characteristics of compacted snow. CRREL Report 76-21, 47 p.
- Adobe (1998): Adobe Photoshop 5.0 - User guide. Adobe Systems Incorporated, San Jose, California, 390 p.
- Aebischer, H. and C. Mätzler (1983): A microwave sensor for the measurement of the liquid water content on the surface of the snow cover. In *Proceedings of the 13th European Microwave Conference (Nürnberg)*, Microwave Exhibition and Publishers, Ltd., pp. 483-487.
- Akitaya, E. (1974): Studies of depth hoar. *Low Temperature Science, Series A*, Vol. 26, pp. 1-67.
- Alley, R. B. (1987): Firm densification by grain-boundary sliding: A first model. *Journal de Physique, Supplement 3*, Vol. 48, pp. 249-256.
- Ambach, W. and A. Denoth (1975): On the dielectric constant of wet snow. In *The International Symposium on Snow Mechanics, Grindelwald, Switzerland, April 1-5, 1974*, IAHS-AISH Publication No. 114, pp. 136-142.
- Anderson, D. L. and C. S. Benson (1963): The densification and diagenesis of snow. In *Ice and Snow* (W. D. Kingery, Ed.), MIT Press, Cambridge, Massachusetts, pp. 391-411.
- Armstrong, R. L. (1980): An analysis of compressive strain in adjacent temperature-gradient and equi-temperature layers in a natural snow cover. *Journal of Glaciology*, Vol. 26, No. 94, pp. 283-289.
- Arons, E. M. and S. C. Colbeck (1995): Geometry of heat and mass transfer in dry snow: A review of theory and experiment. *Reviews of Geophysics*, Vol. 33, No. 4, pp. 463-493.
- Bader, H., R. Haefeli, E. Bucher, I. Neher, O. Eckel and C. Thams (1939): *Der Schnee und seine Metamorphose*. Beitrag zur Geologie der Schweiz, Geotechnische Serie, Hydrologie, Vol. 3, (in German), 340 p.
- Bader, H. and D. Kuroiwa (1962): The physics and mechanics of snow as a material. CRREL Monograph II-B, 79 p.
- Bales, R. C., R. E. Davis and D. A. Stanley (1989): Ionic elution through shallow, homogeneous snow. *Water Resources Research*, Vol. 25, pp. 1869-1877.
- Bales, R. C. and R. F. Harrington (1995): Recent progress in snow hydrology. *Reviews of geophysics*, Vol. 33, pp. 1011-1020.

- Bergman, J. A. (1986): In situ electrical measurements of snow wetness in a deep snowpack in the Sierra Nevada snow zone of California. In *Proceedings of the Symposium on Cold Regions Hydrology, Fairbanks, Alaska*, American Water Resources Association, pp. 367-375.
- Bergman, J. A. (1987): Accuracy and repeatability of in situ snow wetness measurements using the newly developed twin-disc capacitance sensor. In *Proceedings of the Western Snow Conference*, Vol. 57, pp. 142-145.
- Boyne, H. S. and D. Fisk (1987): A comparison of snow cover liquid water measurement techniques. *Water Resources Research*, Vol. 23, No. 10, pp. 1833-1836.
- Brimblecombe, P., M. Tranter, P. W. Abrahams, I. Blackwood, T. D. Davies and C. E. Vincent (1985): Relocation and preferential elution of acidic solute through the snowpack of small, remote high-altitude Scottish catchment. *Annals of Glaciology*, Vol. 7, pp. 141-147.
- Brimblecombe, P., S. L. Clegg, T. D. Davies, D. Shooter and M. Tranter (1987): Observations of the preferential loss of major ions from melting snow and laboratory ice. *Water Resources Research*, Vol. 21, pp. 1279-1286.
- Brown, R. L. (1989): Perspective on mechanical properties of snow. In *Proceedings of the 1st International Conference on Snow Engineering, Santa Barbara, California, July 1988*, CRREL Special Report 89-6, pp. 502-503.
- Brun, E., F. Touvier and G. Bregnot (1987): Experimental study on thermal convection and grains picture analysis. In *Seasonal snowcovers: physics, chemistry, hydrology* (H. G. Jones and W. J. Orville-Thomas, Ed.). NATO ASI Series, Vol. C 211, D. Reidel Publishing Co., Dordrecht, pp. 75-94.
- Buser, O. and W. Good (1987): Acoustic, geometric and mechanical parameters of snow, IAHS Publication No. 162, pp. 61-71.
- Colbeck, S. C. (1978): The compression of wet snow. CRREL Report 78-10, 23 p.
- Colbeck, S. C. (1986): Statistics of coarsening in water-saturated snow. *Acta Metallurgica*, Vol. 34, No. 3, pp. 347-352.
- Colbeck, S. C. (1987): A review of the metamorphism and classification of seasonal snow cover crystals. In *Proceedings of Avalanche Formation, Movement and Effects*, Vol. 162, pp. 1-34.
- Colbeck, S. C., E. Akitaya, R. Armstrong, H. Gubler, J. Lafeuille, K. Lied, D. McClung and E. Morris (1990): International classification for seasonal snow on the ground. International Commission for Snow and Ice, World Data Center for Glaciology, University of Colorado, Boulder, Colorado, 23 p.
- Colbeck, S. C. (1996): The basic ideas behind snow metamorphism. In *Snow as a Physical, Ecological and Economic Factor*, Davis, California, 1996.
- Colbeck, S. C. (1997): A review of sintering in seasonal snow. CRREL Report 97-10, 11 p.
- Coléou, C. and B. Lesaffre (1998): Irreducible water saturation in snow: experimental results in a cold laboratory. *Annals of Glaciology*, Vol. 26, pp. 64-68.
- Cragin, J. H., A. D. Hewitt and S. C. Colbeck (1993): Elution of ions from melting snow: Chromatographic versus metamorphic mechanisms. CRREL Report 93-8, 20 p.
- Davies, T. D., C. E. Vincent and P. Brimblecombe (1982): Preferential elution of strong acids from Norwegian ice cap. *Nature*, Vol. 300, pp. 161-163.
- Davies, T. D., P. Brimblecombe, M. Tranter, S. Tsiouris, C. E. Vincent, P. W. Abrahams and I. L. Blackwood (1987): The removal of soluble ions from melting snowpacks. In *Seasonal snowcovers: physics, chemistry, hydrology* (H. G. Jones and W. J. Orville-Thomas, Ed.). NATO ASI Series, Vol. C 211, D. Reidel Publishing Co., Dordrecht, Holland, pp. 337-392.
- Davidson, C. I., M. H. Bergin and H. D. Kuhns (1996): Atmospheric deposition of chemical species to polar snow. *Chemical Engineering Communications*, Vol. 151, pp. 227-249.

- Davis, R. E., J. Dozier, E. R. LaChapelle and R. Perla (1985): Field and laboratory measurements of snow liquid water by dilution. *Water Resources Research*, Vol. 21, No. 9, pp. 1415-1420.
- Davis, R. E. (1991): Links between snowpack physics and snowpack chemistry. In *Seasonal Snowpacks: Processes of compositional change* (T. D. Davies, M. Tranter and H. G. Jones, Ed.). NATO ASI Series, Vol. G 28, Springer Verlag, Berlin Heidelberg, pp. 115-138.
- Davis, R. E., C. E. Petersen and R. C. Bales (1995): Ion flux through a shallow snowpack: effects of initial conditions and melt sequences. In *Proceedings of the International Symposium on Biogeochemistry of Seasonally Snow-covered Catchments, Boulder, Colorado, July 1-14, 1995*, IAHS Publication No.228, pp. 115-126.
- Denoth, A., A. Foglar, P. Weiland, C. Mätzler, H. Aebischer, M. Tiuri and A. Sihvola (1984): A comparative study of instruments for measuring the liquid water content of snow. *Journal of Applied Physics*, Vol. 56, No. 7, pp. 2154-2160.
- Denoth, A. (1997): The monopole-antenna: A practical snow and soil wetness sensor. *IEEE Transactions on Geoscience and Remote Sensing*, Vol. 35, No. 5, pp. 1371-1375.
- de Quervain, M. (1948): Das Korngefüge von Schnee. *Mitteilungen von Eidgenössisches Institut für Schnee- und Lawinenforschung*, No. 6, (in German), pp. 1-12.
- de Quervain, M. (1958): On metamorphism and hardening of snow under constant pressure and temperature gradient. *IAHS-AISH Publication No. 46*, pp. 225-239.
- Dozier, J., R. E. Davis and R. Perla (1987): On the objective analysis of snow microstructure. In *Proceedings of Avalanche Formation, Movement and Effects*, Vol. 162, pp. 49-59.
- Ebinuma, T. and N. Maeno (1987): Particle rearrangement and dislocation creep in a snow-densification process. *Journal de Physique, Supplement 3*, Vol. 48, pp. 263-269.
- Edens, M. Q. and R. L. Brown (1991): Changes in microstructure of snow under large deformations. *Journal of Glaciology*, Vol. 37, No. 126, pp. 193-202.
- Elgmork, K., A. Hagen and A. Langeland (1973): Polluted snow in southern Norway during the winter 1968-1971. *Environmental Pollution*, Vol. 4, pp. 41-52.
- Eugster, H. P. (1952): Beitrag zu einer Gefügeanalyse des Schnees. *Beitrag zur Geologie der Schweiz, Geotechnische Serie, Hydrologie*, Vol. 5, (in German), 64 p.
- Fisk, D. (1986): Method of measuring liquid water mass fraction of snow by alcohol solution. *Journal of Glaciology*, Vol. 32, pp. 538-540.
- Frolov, A. D. and I. V. Fedyukin (1998): Elastic properties of snow-ice formations in their whole density range. *Annals of Glaciology*, Vol. 26, pp. 55-58.
- Fuchs, A. (1956): Preparation of plastic replicas of thin sections of snow. *CRREL Technical Report No. 41*, 6 p.
- Fukue, M. (1979): Mechanical performance of snow under loading. University Press, Tokai, Japan, (In Japanese with French summary), 136 p.
- Good, W. (1975): Numerical parameters to identify snow structure, *IAHS-AISH Publication No. 114*, pp. 91-102.
- Good, W. (1980): Structural investigations of snow. A comparison of different parameter sets. In *Pattern Recognition in Practice* (E. S. Gelsema and L. N. Kanal, Ed.), North-Holland, New York, pp. 161-174.
- Good, W. (1982): Structural investigations of snow and ice on core III from the drilling on Vernagt Ferner Austria in 1979. *Zeitschrift für Gletscherkunde und Glazialgeologie*, Vol. 18, No. 1, pp. 53-64.
- Good, W. (1987): Thin sections, serial cuts and 3-D analysis of snow, *IAHS Publication No. 162*, pp. 35-48.

- Good, W. (1989): Laboratory techniques for the characterisation of snow structures. In *Proceedings of the International Workshop on Physics and Mechanics of Cometary Materials*. European Space Agency, Noordwijk, The Netherlands, pp. 147-151.
- Good, W., G. Krüsi, J. von Niederhäusern and A. Roth (1991): Preparation and analysis of high contrast stratigraphic profiles. In *Proceedings of the International Symposium on Avalanches, Chamonix, France, June 4-8, 1991*, pp. 40-45.
- Goodison, B. E., H. L. Ferguson and G. A. McKay (1981): Measurement and data analysis. In *Handbook of Snow. Principles, Processes, Management and Use* (D. M. Gray and D. H. Male, Ed.), Pergamon press, Toronto, pp. 191-274.
- Gow, A. (1968): Deep core studies of the accumulation and densification of snow at Byrd Station and Little America V, Antarctica. CRREL Research Report 197, 48 p.
- Grant, L. O. and J. O. Rhea (1974): Elevation and meteorological controls on the density of new snow. In *Interdisciplinary Symposium on Advanced Concepts and Techniques in the Study of Snow and Ice Resources, Monterey, California, 1973*, U. S. National Academy of Science, Washington, D. C., pp. 169-181.
- Gray, D. M., D. I. Norum, G. E. Dyck (1970): Densities of prairie snowpacks. In *Proceedings of the Western Snow Conference*, pp. 24-30.
- Gray, D. M. and D. H. Male (1981): Handbook of snow. Principles, processes, management and use. Pergamon press, Toronto, 776 p.
- Gubler, H. (1975): On the Rammsonde hardness equation: A review of basic snow mechanics. In *The International Symposium on Snow Mechanics, Grindelwald, Switzerland, April 1-5, 1974*, IAHS-AISH Publication No. 114, pp. 110-121.
- Gubler, H. (1978): Determination of the mean number of bonds per snow grain and of the dependence of the tensile strength on snow on stereological parameters. *Journal of Glaciology*, Vol. 20, pp. 329-341.
- Hagen, A. and A. Langeland (1973): Polluted snow in southern Norway and the effect of the meltwater on freshwater and aquatic organisms. *Environmental Pollution*, Vol. 5, pp. 45-57.
- Hämäläinen, T. and E. Spring (1986): Influence of snow hardness on ski friction. *Commentationes Physico-Mathematicae*, Vol. 76, 17 p.
- Hansen, A. C. and R. L. Brown (1986): The granular structure of snow: An internal state variable approach. *Journal of Glaciology*, Vol. 32, No. 112, pp. 434-438.
- Hansen, B. L. and H. H. G. Jellenik (1957): A portable adiabatic calorimeter. SIPRE Technical Report 49, 6 p.
- He, Y. and W. H. Theakstone (1994): Climatic influence on the composition of snow cover at Austre Okstindbreen, Norway, 1989 and 1990. *Annals of Glaciology*, Vol. 19, pp. 1-6.
- Hewitt, A. D., J. H. Cragin and S. C. Colbeck (1989): Does snow have ion chromatographic properties? In *Proceedings of the Forty-Sixth Annual Eastern Snow Conference, June 8-9, Quebec City, Quebec*, pp. 165-171.
- Hewitt, A. D., J. H. Cragin and S. C. Colbeck (1991): Effect of crystal metamorphosis on the elution of chemical species. In *Proceedings of the Eastern Snow Conference*, pp. 1-10.
- Hewitt, A. D. and J. H. Cragin (1994): Determination of anion concentrations in individual snow crystals and snowflakes. *Atmospheric environment*, Vol. 28, No. 15, pp. 2545-2547.
- Johannessen, M., T. Dale, E. T. Gjessing, A. Henriksen and R. F. Wright (1975): Acid precipitation in Norway: The regional distribution of contaminants in snow and chemical processes during snowmelt. In *Proceedings of the International Symposium on Isotopes and Impurities in Snow and Ice, Grenoble, Aug. 28-30*, IASH Publication No. 118, pp. 116-120.

- Johannessen, M. and A. Henriksen (1978): Chemistry of snow meltwater; Changes in concentrations during melting. *Water Resources Research*, Vol. 14, pp. 615-619.
- Johnson, J. B., D. J. Solie, J. A. Brown and E. S. Gaffney (1993): Shock response of snow. *Journal of Applied Physics*, Vol. 73, No. 10, pp. 4852-4861.
- Johnson, J. B. (1998): A preliminary numerical investigation of the micromechanics of snow compaction. *Annals of Glaciology*, Vol. 26, pp. 51-54.
- Jones, E. B., A. Rango and S. M. Howell (1983): Snowpack liquid water determinations using freezing calorimetry. *Nordic Hydrology*, Vol. 14, pp. 113-126.
- Kendra, J. R., F. T. Ulaby and K. Sarabandi (1994): Snow probe for *in situ* determination of wetness and density. *IEEE Transactions on Geoscience and Remote Sensing*, Vol. 32, No. 6, pp. 1152-1159.
- Kinosita, S. (1960a): Natural changes in the microscopic texture of snow. *Low Temperature Science, Series A*, Vol. 19, (in Japanese with English summary), pp. 111-119.
- Kinosita, S. (1960b): The hardness of snow. I. *Low Temperature Science, Series A*, Vol. 19 (In Japanese with English summary), pp. 119-134.
- Kinosita, S. and G. Wakahama (1960): Thin sections of deposited snow made by the use of aniline. *Contributions from the Institute of Low Temperature Science, Hokkaido University, Series A*, Vol. 15, pp. 35-45.
- Kojima, K. (1967): Densification of seasonal snow cover. In *Proceedings of the International Conference on Low Temperature Science, Sapporo, Aug. 14-19, 1966*, Institute of Low Temperature Science, Hokkaido University, Vol. 1, Part 2, pp. 929-952.
- Kopp, M. (1962): Conductivité électrique de la neige, au courant continu. *Z. Math. Phys.*, Vol. 13 (In French), pp. 431-441.
- Kovacs, A. (1993): Comparison of axial double-ball and uniaxial unconfined compression tests on freshwater and sea ice samples. In *Proceedings of the 12th International Conference on Port and Ocean Engineering under Arctic Conditions, Hamburg, 17.-20. August 1993*, Vol. 1, pp. 72-84.
- Kragelski, I. V. (1949): Method of determining hardness and density of a snow surface. In *The Physico-Mechanical Properties of Snow and Their Application in the Construction of Airfields and Roads, Collected Papers of the Soviet Commission for Airfields and Roads, Academy of Sciences, Moscow*. Translation by Bureau of Yards and Docks, Department of the Navy, Washington, D. C., pp. 6-9.
- Kry, P. R. (1975): Quantitative stereological analysis of grain bonds in snow. *Journal of Glaciology*, Vol. 14, pp. 467-477.
- Kuroda, M. and I. Hurokawa (1954): Measurement of water content of snow. In *Proceedings of the Rome Symposium, Rome*. IAHS-AISH Publication No. 39, pp. 38-41.
- Kuroiwa, D. (1954): The dielectric property of snow. In *Proceedings of the Rome Symposium, Rome*. IAHS-AISH Publication No. 39, pp. 52-63.
- Kuroiwa, D. and E. R. LaChapelle (1972): Preparation of artificial snow and ice surface for XI Olympic Winter Games. In *The Role of Snow and Ice in Hydrology, Proceedings of the Banff Symposium, September 1972*, Unesco-WMO-IAHS, Geneva-Budapest-Paris, Vol. 2, pp. 1350-1361.
- LaChapelle, E. R. (1969): *Field Guide to Snow Crystals*. University of Washington Press, Seattle, 101 p.
- Langham, E. J. (1981): Physics and properties of snowcover. In *Handbook of Snow. Principles, Processes, Management and Use* (D. M. Gray and D. H. Male, Ed.), Pergamon press, Toronto, pp. 275-337.
- Lesaffre, B., E. Pougatch, E. Martin (1998): Objective determination of snow-grain characteristics from images. *Annals of Glaciology*, Vol. 26, pp. 112-118.

- Lukeville, A., S. Manø and K. Tørseth (1998): Monitoring of long-range transported air pollutants, Annual report for 1997. Norwegian Institute for Air Research, Report No. OR 33/98 (in Norwegian with English summary), 181 p.
- Løset, S. (1992): Heat exchange at the air exposed surface of icebergs. In *Proceedings of the 11th International Symposium on Ice, IAHR 92*, Banff, Alberta, Canada, Vol. 2, pp. 735-746.
- Maeno, N. and T. Ebinuma (1983): Pressure sintering of ice and its implication to the densification of snow at polar glaciers and ice sheets. *Journal of Physical Chemistry*, Vol. 87, No. 21, pp. 4103-4110.
- Magano, C. and C. W. Lee (1966): Meteorological classification of natural snow crystals. *J. Faculty Science*, Hokkaido University, Vol. 2, pp. 321-335.
- Male, D. H. and D. M. Gray (1981): Snowcover ablation and runoff. In *Handbook of Snow. Principles, Processes, Management and Use* (D. M. Gray and D. H. Male, Ed.). Pergamon press, Toronto, pp. 360-436.
- Mellor, M. (1964): Properties of snow. CRREL Monograph III-A1, 105 p.
- Mellor, M. (1975): A review of basic snow mechanics. In *The International Symposium on Snow Mechanics, Grindelwald, Switzerland, April 1-5, 1974*, IAHS-AISH Publication No. 114, pp. 251-291.
- Mellor, M. (1977): Engineering properties of snow. *Journal of Glaciology*, Vol. 19, No. 81, pp. 15-66.
- Nakaya, U. (1954): *Snow crystals, Natural and Artificial*. Harvard University Press, 510 p.
- Narita, H. (1969): Specific surface of deposited snow I. *Low Temperature Science, Series A*, Vol. 27, pp. 77-86.
- Narita, H. (1971): Specific surface of deposited snow II. *Low Temperature Science, Series A*, Vol. 29, pp. 69-79.
- Perla, R. and B. Glenne (1981): Skiing. In *Handbook of Snow. Principles, Processes, Management and Use* (D. M. Gray and D. H. Male, Ed.), Pergamon press, Toronto, pp. 709-740.
- Perla, R. (1985): Snow in strong or weak temperature gradients, II, Section-plane Analysis. *Cold Regions Science and Technology*, Vol. 11, pp. 181-186.
- Perla, R. and C. S. L. Ommanney (1985): Snow in strong or weak temperature gradients, I, Experiments and qualitative analysis. *Cold Regions Science and Technology*, Vol. 11, pp. 23-35.
- Perla, R., J. Dozier and R. E. Davis (1986): Preparation of serial sections in dry snow specimens, *Journal of Microscopy*, Vol. 114, pp. 111-114.
- Petrenko, V. F. (1994): The effect of static electric fields on ice friction. *Journal of Applied Physics*, Vol. 76, No. 2, pp. 1216-1219.
- Petterssen, S. (1956): *Weather forecasting and analysis*. Vol. 2, McGraw-Hill, New York, Toronto, London, 266 p.
- Raben, P. and W. H. Theakstone (1994): Isotopic and ionic changes in a snow cover at different altitudes: observations at Austre Okstindbreen, Norway in 1991. *Nordic Hydrology*, Vol. 29, pp. 1-20.
- Raben, P. and W. H. Theakstone (1997): Use of total input and output of ions to measure meltwater runoff time through a glacier's accumulation area. *Annals of Glaciology*, Vol. 24, pp. 148-151.
- Raben, P. and W. H. Theakstone (1998): Changes of ionic and oxygen isotopic composition of the snow pack at the glacier Austre Okstindbreen, Norway, 1995. *Nordic Hydrology*, Vol. 29, pp. 1-20.
- Raymond, C. F. and K. Tusima (1979): Grain coarsening of water-saturated snow. *Journal of Glaciology*, Vol. 22, No. 86, pp. 83-105.
- Reimann, C., H. Niskavaara, P. de Caritat, T. E. Finne, M. Äyräs and V. Chekushin (1996): Regional variation of snowpack chemistry in the vicinity of Nikel and Zapoljarnij, Russia, northern Finland and Norway. *The Science of the total environment*, Vol. 182, No. 1-3, pp. 147-158.
- Richter-Menge, J. A., S. C. Colbeck and K. C. Jezek (1991): Recent progress in snow and ice research. *Reviews of Geophysics, Supplement*, April 1991, pp. 218-226.

- Salm, B. (1982): Mechanical properties of snow. In *Proceedings of a Workshop on the Properties of Snow, Snowbird, Utah, April 8-10, 1981*; Reviews of Geophysics and Space Physics, Vol. 20, No. 1, pp. 1-19.
- Schaerer, P. A. (1981): Avalanches. In *Handbook of Snow. Principles, Processes, Management and Use* (D. M. Gray and D. H. Male, Ed.). Pergamon press, Toronto, pp. 475-518.
- Schemenauer, R. S., M. O. Berry and J. B. Maxwell (1981): Snowfall formation. In *Handbook of Snow. Principles, Processes, Management and Use* (D. M. Gray and D. H. Male, Ed.), Pergamon press, Toronto, pp. 129-152.
- Seligman, G. (1936): Snow structure and ski fields. Macmillan, New York, 555 p.
- Shapiro, L. H., J. B. Johnson, M. Sturm and G. L. Blaisdell (1997): Snow mechanics: Review of the state of knowledge and applications. CRREL Report 97-3, 43 p.
- Shimbo, M. (1961): Mechanism of sliding on snow. In *General Assembly of Helsinki*, International Association of Scientific Hydrology Publication No. 54, Gentbrugge, Belgium, pp. 101-106.
- Shimizu, H. (1970): Air permeability of deposited snow. Contributions from the Institute of Low Temperature Science, Hokkaido University, Series A, Vol. 22, pp. 1-32.
- Sihvola, A. and M. Tiuri (1986): Snow fork for field determination of the density and wetness profiles of a snow pack. IEEE Transactions on Geoscience and Remote Sensing, Vol. GE-24, No. 5, pp. 717-720.
- Skartveit, A. and Y. T. Gjessing (1979): Chemical quality of snow and runoff during snowmelt. Nordic Hydrology, Vol. 10, pp. 141-154.
- Slotfeldt-Ellingsen, D. and L. Torgersen (1983): Water in ice: influence on friction. Journal of Physics D: Applied Physics, Vol. 16, pp. 1715-1719.
- Sommerfeld, R. A. and E. LaChapelle (1970): Classification of snow metamorphism. Journal of Glaciology, Vol. 9, No. 55, pp. 3-17.
- Spring, E. (1988): A method for testing the gliding quality of skis. Tribologia, Vol. 7, No. 1, pp. 9-14.
- STAR (1995): STAR HD 8901 Multifunction Digital Microprocessor Hygrometer-Thermometer, instruction manual, 23 p.
- Stein, J., G. Laberge and D. Lévesque (1997): Monitoring the dry density and the liquid water content of snow using time domain reflectometry (TDR). Cold Regions Science and Technology, Vol. 25, pp. 123-136.
- Storrø, G. (1990): Hydrokjemi, hydrologi og geologi i Kaldvellfeltet; Et feltstudium med hovedvekt på grunnvannskjemi. The Norwegian Institute of Technology, Department of Geology and Mineral Resources Engineering, Dr. thesis (in Norwegian with English Summary), 194 p.
- Sturm, M., J. Holmgren and G. E. Liston (1995): A seasonal snow cover classification system for local to global applications. Journal of Climate, Vol. 8, No. 5, pp. 1261-1283.
- Takahashi, T., T. Endoh, K. Muramoto, C. Nakagawa and I. Noguchi (1996): Influence of the growth mechanism of snow particles on their chemical composition. Atmospheric Environment, Vol. 30, No. 10-11, pp. 1683-1692.
- Takeuchi, Y., Y. Nohguchi, K. Kawashima and K. Izumi (1998): Measurement of snow-hardness distribution. Annals of Glaciology, Vol. 26, pp. 27-30.
- Toikka, M. (1992): Field tests with the Snow fork in determining the density and wetness profiles of a snow pack. In *Microwave Signature - 92, IGLS - Innsbruck, July 1-3, Austria, The International URSI-Conference on Microwave Terrestrial Remote Sensing*, pp. 2D-13-2D-16.
- Toikka (1996): Snow fork measures the density and the liquid water content of snow. Folder, Ins. tsto Toikka Oy, Espoo, Finland, 4 p.
- Toikka (1998): Snow fork manual, model LG 97002. Ins. tsto Toikka Oy, Espoo, Finland, 17 p.

- Tranter, M., P. Brimblecombe, T. D. Davies, C. E. Vincent, P. W. Abrahams and I. Blackwood (1986): The composition of snowfall, snowpack, and meltwater in the Scottish Highlands evidence for preferential elution. *Atmospheric Environment*, Vol. 20, pp. 517-525.
- Tsiouris, S., C. E. Vincent, T. D. Davies and P. Brimblecombe (1985): The elution of ions through field and laboratory snowpacks. *Annals of Glaciology*, Vol. 7, pp. 196-201.
- Tørseth, K., T. Berg, J. E. Hanssen and S. Manø (1999): Monitoring of long-range transported air pollutants, Annual report for 1998. Norwegian Institute for Air Research, Report No. OR 27/99 (in Norwegian with English summary), 145 p.
- Voitkovsky, K. F., A. N. Bozhinsky, V. N. Golubev, M. N. Laptev, A. A. Zhigulsky, Yu. Ye. Slesarenko (1975): Creep induced changes in structure and density of snow. In *The International Symposium on Snow Mechanics, Grindelwald, Switzerland, April 1-5, 1974*, IAHS-AISH Publication No. 114, pp. 171-179.
- Wakahama, G. (1968): Metamorphism of wet snow. IASH Publication No. 79, pp.370-379.
- Wakahama, G. (1975): The role of melt-water in densification processes of snow and firn. In *The International Symposium on Snow Mechanics, Grindelwald, Switzerland, April 1-5, 1974*, IAHS-AISH Publication No. 114, pp. 66-72.
- Warren, G. C., S. C. Colbeck and F. E. Kennedy (1989): Thermal response of downhill skis. CRREL Report 89-23, 43 p.
- Wiesmann, A., C. Mätzler and T. Weise (1998): Radiometric and structural measurements of snow samples. *Radio Science*, Vol. 33, No. 2, pp. 273-289.
- Wilkinson, D. S. (1988): A pressure-sintering model for the densification of polar firn and glacier ice. *Journal of Glaciology*, Vol. 34, No. 116, pp. 40-45.
- Wright, R. F. and H. Dovland (1978): Regional surveys of the chemistry of the snowpack in Norway, late winter 1973, 1974, 1975 and 1976. *Atmospheric Environment*, Vol. 12, pp. 1755-1768.
- Yosida, Z. (1940): A method of determining thaw water content in snow layers. *Journal of Faculty of Science, Series 2, Hokkaido Imperial University*, Vol. 3, No. 4, pp. 91-112.
- Yosida, Z. (1956): Physical studies on deposited snow. II, Mechanical properties. (I). Contributions from the Institute of Low Temperature Science, No. 9, pp. 1-81.
- Yosida, Z. (1960): A calorimeter for measuring the free water content of wet snow. *Journal of Glaciology*, Vol. 3, pp. 574-576.
- Yosida, Z. (1963): Physical properties of snow. In *Ice and Snow* (W. D. Kingery, Ed.), MIT Press, Cambridge, Massachusetts, pp. 485-525.
- Yosida, Z. (1971): Investigations on snow conditioning for the XI Olympic Winter Games, Sapporo, February, 3-13, 1972. In *Scientific Study of Skiing in Japan* (The Society of Ski Science, Ed.). Tokyo: Hitachi, Ltd., pp. 113-125.

6. Searching for the optimum cross-country ski base structure

Notation

C	cloudiness in octoparts, $C = 0 \Rightarrow$ clear sky, $C = 8 \Rightarrow$ complete cloud cover
\bar{d}	mean of d_j for the n_g snow grains with distinguishable boundaries in a microscope image of a snow surface, mm
d_j	length of the largest 2D diagonal for snow grain surface number j in a microscope image of a snow surface, mm
H	snow hardness, N/m^2 or Pa
$\bar{h}_{\text{min,wf}}$	approximate average minimum water film thickness for a ski in the structure test series under different snow conditions, μm
n_g	number of snow grains with distinguishable boundaries in a microscope image of a snow surface
p_y	typical period between grooves in the y -direction, i.e. across the ski
q_{net}	net radiation 50 cm above the snow surface, W/m^2
R_a	arithmetic mean surface roughness, μm
$\bar{R}_{a,y}$	mean of R_a of the columns in a measured surface image, i.e. across the ski, when each column has an individual reference line parallel to the y -axis, μm
$\bar{R}_{a,yas}$	mean of $\bar{R}_{a,ys}$ for the afterbody of the ski, μm
$\bar{R}_{a,yfs}$	mean of $\bar{R}_{a,ys}$ for the forebody of the ski, μm
$\bar{R}_{a,ys}$	mean of R_a of the columns in a measured surface image, i.e. across the ski, when each column has an individual possibly sloping reference line relative to the y -axis, μm
$\bar{R}_{a,yws}$	mean of $\bar{R}_{a,ys}$ for the whole ski, μm

$R_{q,sbs}$	root mean square roughness of the ski base structure surface in a specific area on the ski defined in Eq. (2.20), μm
$R_{q,sn}$	root mean square roughness of snow surface defined in Eq. (2.20), μm
Rh	relative humidity 50 cm above the snow surface, %
T_a	air temperature 50 cm above the snow surface, $^{\circ}\text{C}$
T_s	snow temperature 2 cm below the snow surface, $^{\circ}\text{C}$
x	co-ordinate along the ski, mm
y	co-ordinate across the ski, mm
z_i	surface height registrations on a surface profile, μm
$W_{vol,\%}$	volume per cent liquid water content in the snow, %
δ_d	standard deviation of d_j for the n_g snow grains with distinguishable boundaries in a microscope image of a snow surface, mm
δ_{Rayas}	standard deviation of $\bar{R}_{a,yas}$, μm
δ_{Rayfs}	standard deviation of $\bar{R}_{a,yfs}$, μm
δ_{Rayws}	standard deviation of $\bar{R}_{a,yws}$, μm
Λ	film parameter defined in Eq. (2.20)
Λ_{opt}	optimum film parameter for cross-country skiing
ρ	density of snow, g/cm^3
σ_{mss}	electrolytic conductivity of snow collected from the snow surface, i.e. electrolytic conductivity of a melted snow sample from the snow surface, $\mu\text{S}/\text{cm}$

6.1. Introduction

Competition skiers and ski technicians have experienced that the optimum ski base structure depends on the skier speed and varies under different snow conditions. The large speed differences under some snow conditions make choice of the best structure an important issue for competition skiers and an interesting angle of incidence to understand the physical processes that control friction against snow. The effect of ski base structure on ski base sliding friction can be quantified by performing accurate sliding tests of ski pairs with various ski base structures, but otherwise equal qualities, i.e. the same pressure distribution, base material quality and ski wax.

This chapter describes and discusses the results from nine ski base structure sliding tests performed under various snow conditions. The tests have been performed using a structure test series consisting of ten ski pairs. The ten ski pairs have been ground with eight different ski base structures in order to test various hypothesis for low ski base sliding friction and ski base structures. Apart from two tests that took place at 25 and 50 km/h, the sliding tests have been performed with skier speeds between 30 and 40 km/h. The weight of the test skiers has been from 75 to 80 kg. The test results ought to be interpreted as valid only for such skier weight and skier speed conditions.

6.2. Hypotheses of low ski base sliding friction and ski base structures

Ski base sliding friction can to some extent be described and explained by:

- Tribology
- Impact and compaction resistances
- Electrostatic charging effects

A tribological approach was presented in Chapter 2 using Eq. (2.20) and Fig. 2.10. This theoretic framework postulated that the optimum ski base structure roughness varies under different snow conditions according to the generated frictional water film thickness under the ski and the roughness of the snow surface. Thick water films correspond to coarse ski base structures, while it is advantageous to use finer ski base structures and increase the water film thickness when the water film is thin. Possible increase of water film thickness along the ski implies increase of the ski base structure roughness along the ski. Measurement of snow humidity can be viewed as an indicator of the initial water film thickness in the ski track and the frictional water film thickness that is possible to attain during skiing. The structure pattern affects the dilution of the water film, the contact configuration between the ski base structure and the snow grains, and the bearing, pressure and drag area of the ski base structure during skiing.

Impact and compaction resistances are important when the snow hardness is below a certain limit. It has been found empirically that this limit is approximately 7×10^4 Pa for cross-country skis on snow. Microscopic impact and compaction resistances are also important when the water film thickness is low relative to the roughness of the ski base structure and the snow surface.

Electrostatic charging and pressure effects interact with the tribological framework. This interaction is further discussed in Chapter 7.

The purpose of the development and accurate sliding tests of the structure test series has been:

- To find the optimum and least optimum ski base structure roughness and patterns under different snow conditions for the given skier speed and skier weight conditions.
- To investigate the effect of different ski base structure roughness and patterns along the ski under different snow conditions for the given skier speed and skier weight conditions.
- To study the relation between optimum ski base structure roughness and snow humidity for the given skier speed and skier weight conditions.
- To study the effect of different ski base structures on different snow types with various snow grain sizes for the given skier speed and skier weight conditions.

6.3. Experimental setup

A structure test series consisting of ten *Madshus TXC 234H Skate Hard Packed Dry* ski pairs with 195-cm length and similar pressure distributions and ski base qualities has been made. A typical pressure distribution for a ski in the structure test series is shown in Fig. 6.1. All the ski pairs were prepared in the same way with *SWIX CH10*, *CH4* and *LF10* after stone grinding.

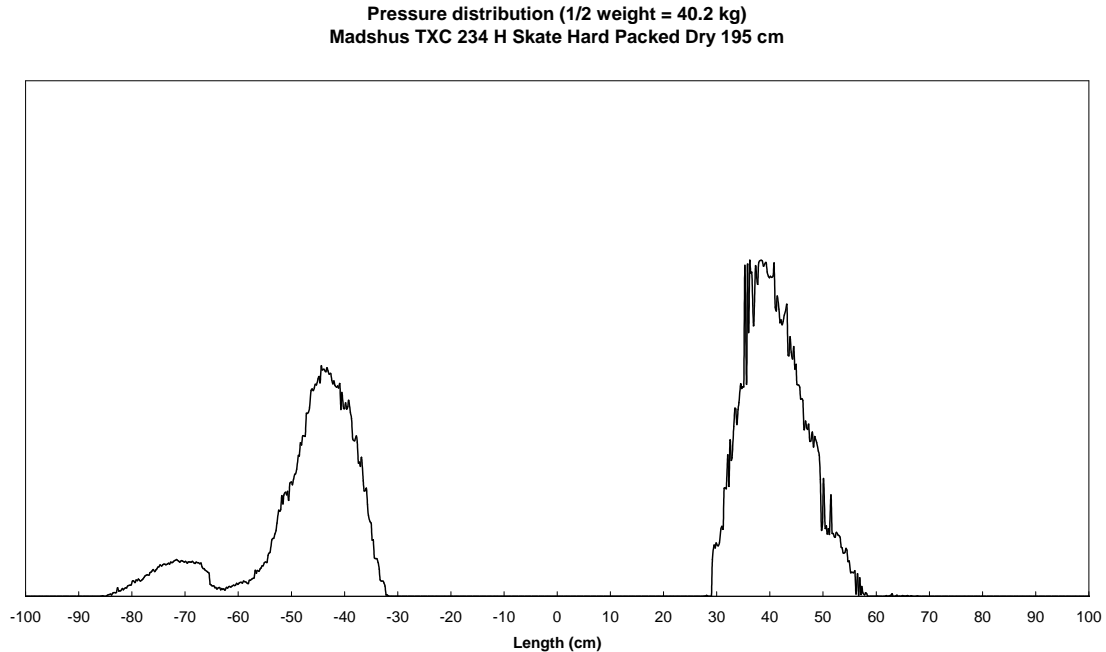


Fig. 6.1. Typical pressure (or load) distribution for a *Madshus TXC 234H Skate Hard Packed Dry* ski in the structure test series.

The structures on the forebody and the afterbody of the ski pairs in the test series, SP1 - SP10, are listed in Table 6.1. Four ski base structures named A, B, C and D were used to make the structure test series. The six ski pairs SP1, SP2, SP3, SP4, SP9 and SP10 were ground with the same structure on the forebody and the afterbody of the ski. Ski pair SP9 was ground as a replica of SP2, while SP10 was ground as a replica of SP3. The four ski pairs SP5, SP6, SP7 and SP8 were ground with different structures along the ski. Ski pair SP5 and SP7 were intended to have coarser structure on the afterbody than the forebody of the ski, while SP 6 and SP8 should have finer structure on the afterbody relative to the forebody.

Specifications for the ski base structures A, B, C and D are listed in Table 6.2. The different parameters in the table were defined in Chapter 4. The roughness parameter $\bar{R}_{a,ys}$ can be assumed to be equal to $\bar{R}_{a,y}$ for all four structures, i.e. the surface profiles do not contain any significant error of form. Notice that the period p_y increase with roughness when standard stone grinding is used to set the ski base structure, and that the two coarsest structures (C and D) are continuous, while the two finer structures (A and B) are discontinuous.

Table 6.1. Structures on the ski pairs in the test series.

Ski pair No.	Structure forebody	Structure afterbody
SP1	A	A
SP2	B	B
SP3	C	C
SP4	D	D
SP5	B	C
SP6	C	B
SP7	C	D
SP8	D	C
SP9	B	B
SP10	C	C

Table 6.2. Ski base structure specifications.

Structure	$\bar{R}_{a,ys}$ (μm)	p_y (mm)	Continuity
A	≈ 3.2	0.23	Discontinuous
B	≈ 4.0	0.31	„
C	≈ 5.3	0.39	Continuous
D	≈ 12.7	0.55	„

Prior to the grinding of a specific structure on a ski pair in the test series, the grindstone was setup and tested with other skis. According to the results from the SSA measurement and characterisation of the structure on the forebody and the afterbody of these skis, the grindstone was adjusted until the desired structure was attained. The respective ski pairs in the test series were then ground with the specific structure directly afterwards. Although this procedure mainly gave ski base structures with outstanding qualities, we were unlucky with the structure on the afterbody of one ski pair, namely SP5. The $\bar{R}_{a,ys}$ parameter for ski base structure C on the afterbody of this ski pair was $0.8 \mu\text{m}$ less (i.e. $4.5 \mu\text{m}$) than the desired value ($5.3 \mu\text{m}$), thus giving less roughness difference than desired between the forebody and the afterbody of the ski pair. Further structure roughness statistics for the ski pairs in the test series are given in Table 6.3 in Section 6.4.

Nine sliding tests were executed with the structure test series under different snow conditions in Trondheim, Meråker, Lillehammer and Golå in Norway. As mentioned in Section 6.1, the sliding tests were performed with skier speeds between 30 and 40 km/h apart from two tests at 25 and 50 km/h, while the weight of the test skiers varied between 75 and 80 kg. Skier speeds were calculated from sliding time measurements in downhill slopes and flats in the different classic cross-country tracks. An electronic device called *Ski Time Test mod. STN 94 M* that contains both a stopwatch and a photocell, was attached round the ankle of the test skier and registered the sliding time of the test skier between two reflectors set up at the start and end of the test distance. The skier speed at the start of the test distance was never below 20 km/h in any of the tests. The time resolution of the stopwatch of the *Ski Time Test mod. STN 94 M* was 0.01 seconds. Fortunately no cabling was necessary with this measurement setup. The length of the test distances could therefore be increased compared to standard sliding tests where the test distances normally vary between 10 to 40 m. In our sliding tests the test distances varied between 55 and 180 m, thus giving variations in sliding time between approximately

4 and 18 seconds. The long duration of the test runs increased our confidence in the test results. Four to six test runs were performed on each ski pair during a sliding test. Mean speeds from these test runs are presented for each sliding test in Section 6.4, together with results from snow and weather measurements before, during and after the tests. Snow and weather measurements were executed using the methods and procedures described in Chapter 5.

It would have been advantageous also to register the sliding friction coefficients during the sliding tests in the way described in Section 2.1.2. In order to do this at the time being different measurement equipment would have to be used. This would have involved more photocells and cabling, and resulted in shorter test distances. Preference was therefore rather given to have measurement equipment that was quick and easy to use, and that gave no restrictions on the test distance length. Measurement of the sliding friction coefficient during sliding tests might be given preference in future research.

6.4. Results

All the skis in the structure test series have been measured and characterised with the SSA. Examples of typical surface profiles across the ski for the ski base structures A, B, C and D are shown in Figs. 6.2, 6.4, 6.6 and 6.8, respectively. Contour plots of the surface topography of the different ski base structures are depicted in Figs. 6.3, 6.5, 6.7 and 6.9.

Table 6.3 lists the structure roughness statistics for the ten ski pairs in the structure test series. All the roughness parameters used in Table 6.3 have been defined earlier in Chapter 4. Six areas on each ski, i.e. twelve areas on each ski pair, have been measured and characterised with the SSA in order to find mean structure roughness values for the forebody and the afterbody of the ski pairs. The ski pairs in the structure test series can be divided into three structure roughness classes:

1. $3.2 \mu\text{m} < \bar{R}_{a,yws} < 5.4 \mu\text{m}$, i.e. SP1, SP2, SP3; SP5, SP6, SP9 and SP10
2. Coarse: $8.9 \mu\text{m} < \bar{R}_{a,yws} < 9.3 \mu\text{m}$, i.e. SP7 and SP8
3. Very coarse: $\bar{R}_{a,yws} = 12.7 \mu\text{m}$, i.e. SP4

As mentioned in Section 6.3, the grinding of ski pair SP5 was not optimal. From Table 6.3 it can be seen that the mean structure roughness on the forebody of ski pair SP5, $\bar{R}_{a,yfs}$, is $3.8 \mu\text{m}$, while the mean structure roughness on the afterbody of the ski pair, $\bar{R}_{a,yas}$, is $4.5 \mu\text{m}$. $\bar{R}_{a,yas}$ was intended to be equal to $5.4 \mu\text{m}$ in order to have a significant difference in structure roughness between the forebody and the afterbody of the ski.

Mean speeds in the different sliding tests are listed for the ski pairs in the structure test series in Table 6.4. The mean speed of all sliding tests is given for each ski pair in the last row of Table 6.4. Measurements at two different speeds were performed during the same test run in Test 1. The measurements at low speed ($\approx 30 \text{ km/h}$) are listed in Table 6.4 as Test 1A, while the measurements at high speed ($\approx 49\text{-}50 \text{ km/h}$) are listed as Test 1B. For Test 6 the results from the start of the test, Test

6A, and the end of the test, Test 6B, are presented together with the results from the whole test. The reason why this has been done is that the snow humidity increased from 0.6 to 12.5 % during this test, thus changing the behaviour of the different structures considerably. Test 8 has also been listed as two subtests, namely Test 8A and 8B, in addition to the whole test. This has been done since the four ski pairs with poorest glide only took part in the first half of Test 8. The same four pairs were not tested under relatively similar snow and weather conditions in Test 9.

Tables of snow and weather measurements for the ski base structure tests are given in Tables 6.5 and 6.6, respectively. The electrolytic conductivity and chemical water properties for collected and melted samples from the snow surfaces in the different ski base structure tests are listed in Table 6.7. All the parameters used in Tables 6.5-6.7 has been defined in Chapter 5.

The best structures and ski pairs in the sliding tests listed in Table 6.4 can be summarised as follows:

- Ski pairs with $\bar{R}_{a,yws} \leq 5.4 \mu\text{m}$ have except for ski pair SP6, been best under snow conditions with snow humidity $W_{vol,\%} \leq 0.6 \%$, snow temperatures below zero and Snow type 2, i.e. in Tests 7, 8 and 9. An average skier speed difference of approximately 3.4 % has been registered between the structure with best (C) and poorest (D) glide under these conditions.
- Structure C with $\bar{R}_{a,yws} = 5.3\text{-}5.4 \mu\text{m}$ has in average been best under snow conditions with snow humidity $W_{vol,\%} \leq 1.3 \%$, snow grain size \bar{d} less than approximately 0.25 mm and Snow type 2, i.e. in Tests 2, 7, 8 and 9.
- Ski pair SP7 with $\bar{R}_{a,yws}$ equal to 9.3 μm , $\bar{R}_{a,yfs} = 6.0 \mu\text{m}$ and $\bar{R}_{a,yas} = 12.6 \mu\text{m}$, has been best under snow conditions with snow humidity $W_{vol,\%}$ between approximately 0.3 and 4.0 %, snow hardness H higher than 4.1×10^4 Pa, and Snow types 4 and 5, i.e. in Tests 1 and 3. Average skier speed differences between 1.3 and 3.0 % have been registered between the ski pair with best (SP7) and poorest (SP5) glide under these conditions.
- Structure D with $\bar{R}_{a,yws} = 12.7 \mu\text{m}$ has been best under snow conditions with snow humidity $W_{vol,\%}$ higher than approximately 4 %, and Snow types 2 and 5, i.e. in Tests 4, 5, and 6B. Average skier speed differences between 3.0 and 6.3 % have been registered between the best (SP4) and the poorest (SP6 and SP9) ski pairs in the tests under these conditions. Structure D had 2.5 % higher average sliding speed than the second best structure in Test 6B.

Notice also that ski pair SP5 was the second best ski pair in Tests 4 and 5 under snow conditions with wet and very wet snow and average snow grain size \bar{d} equal to or below 0.70 mm. Typical relations between optimum structure roughness, snow humidity and snow type in the sliding tests of the structure test series are summarised in Table 6.8.

The highest average skier speed difference between two ski pairs in the structure test series, 2.5 km/h (6.3 %), was registered on very wet snow in Test 6B. The smallest average skier speed difference, 0.5 km/h (1.2-1.6 %), was found under snow conditions with dry and moist snow, snow hardness $H \geq 4.1 \times 10^4$ Pa, and Snow types 4 and 5, i.e. in Tests 1, 3 and 6A.

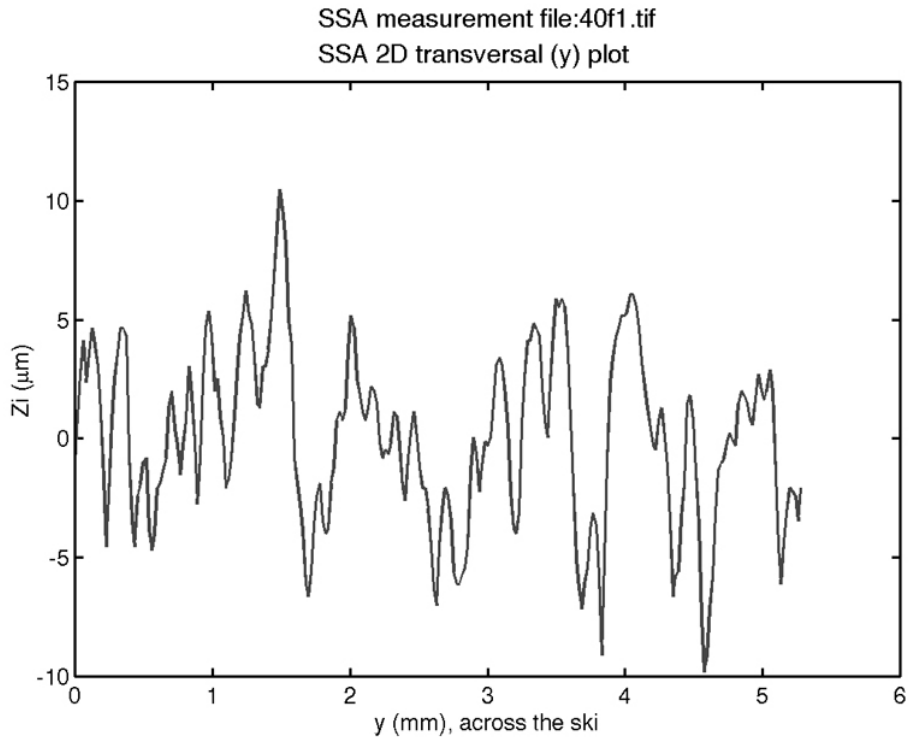


Fig. 6.2. Example of a surface profile across the ski for ski base structure A.

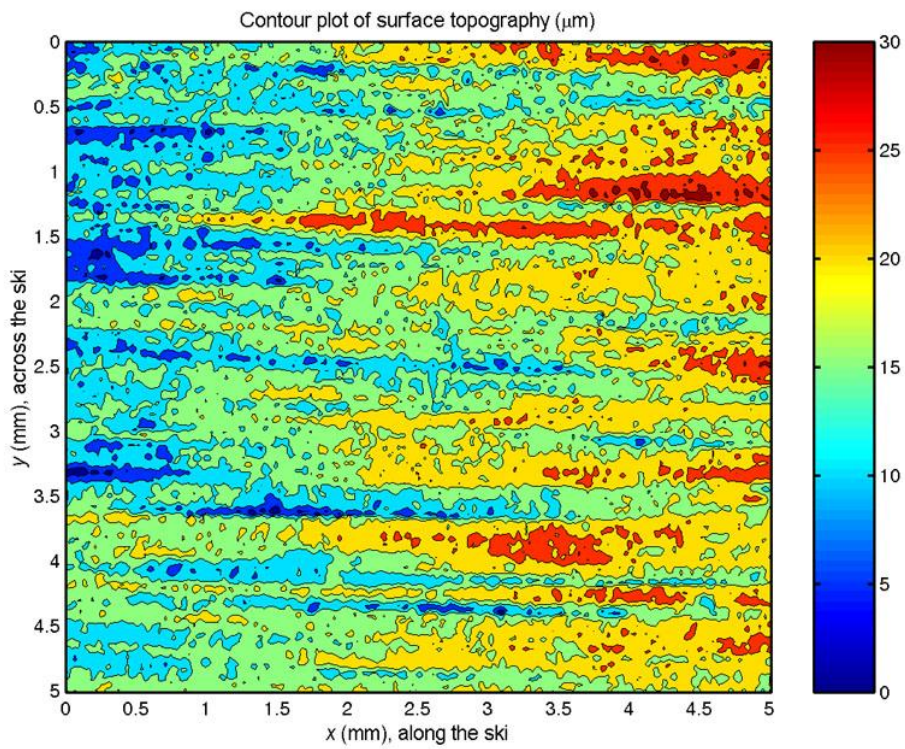


Fig. 6.3. Contour plot of the surface topography of ski base structure A.

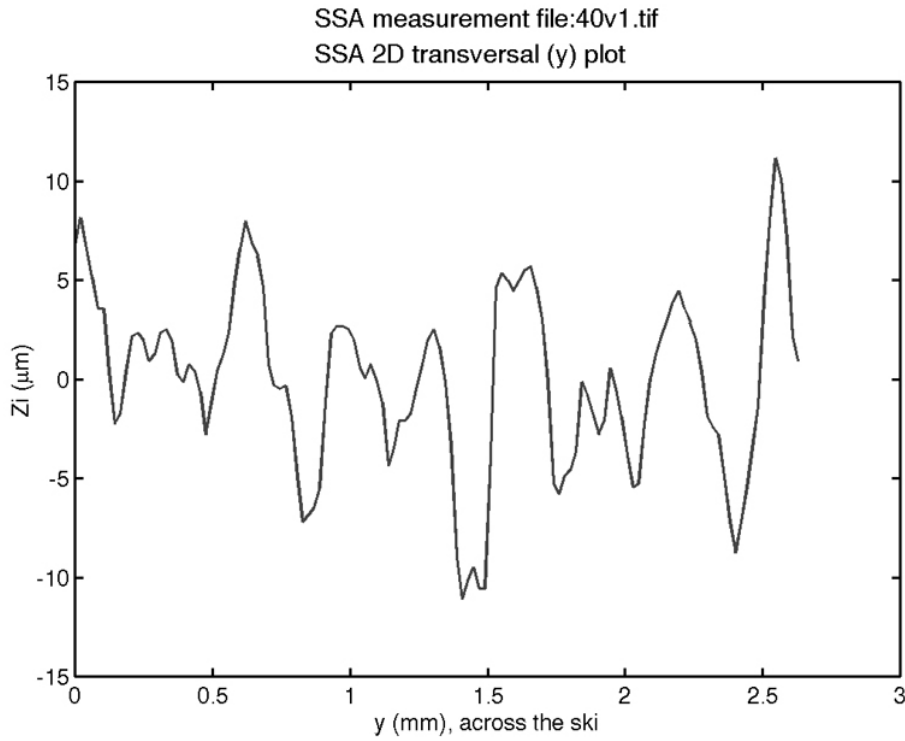


Fig. 6.4. Example of a surface profile across the ski for ski base structure B.

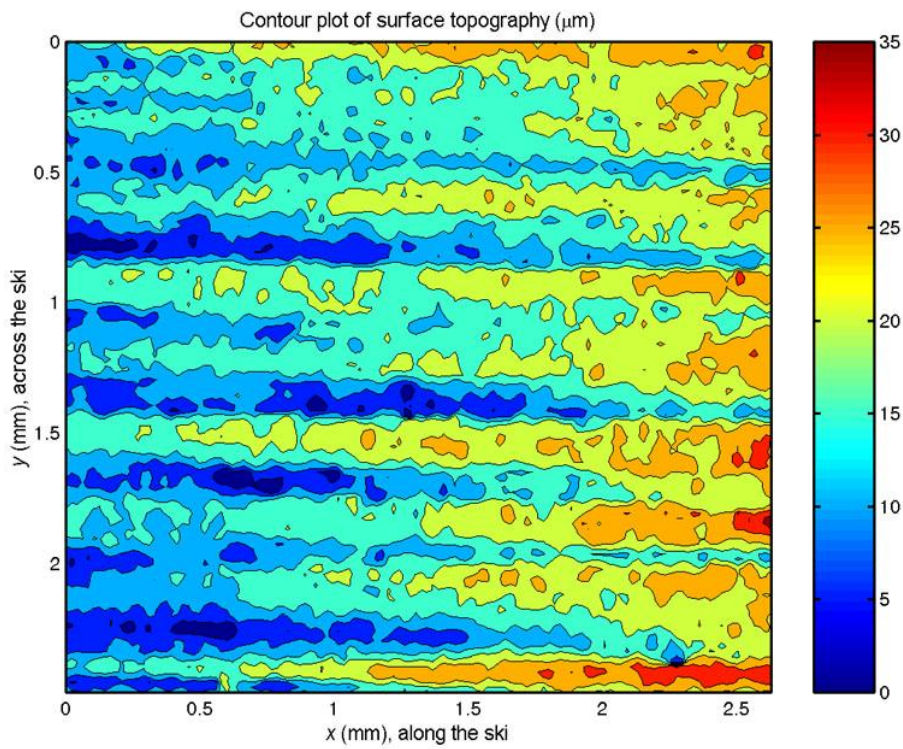


Fig. 6.5. Contour plot of the surface topography of ski base structure B.

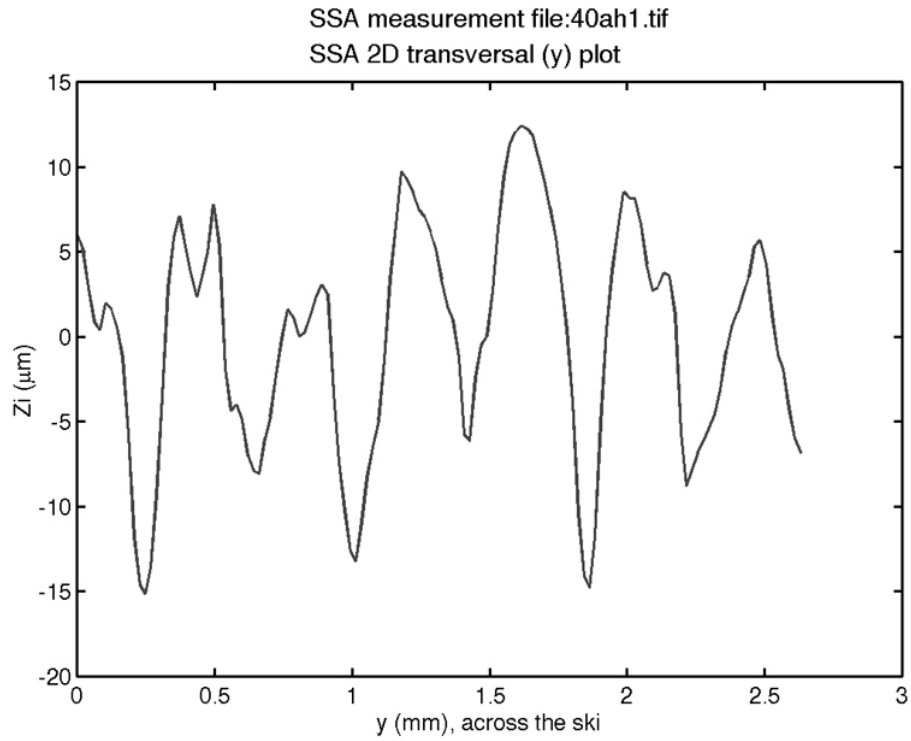


Fig. 6.6. Example of a surface profile across the ski for ski base structure C.

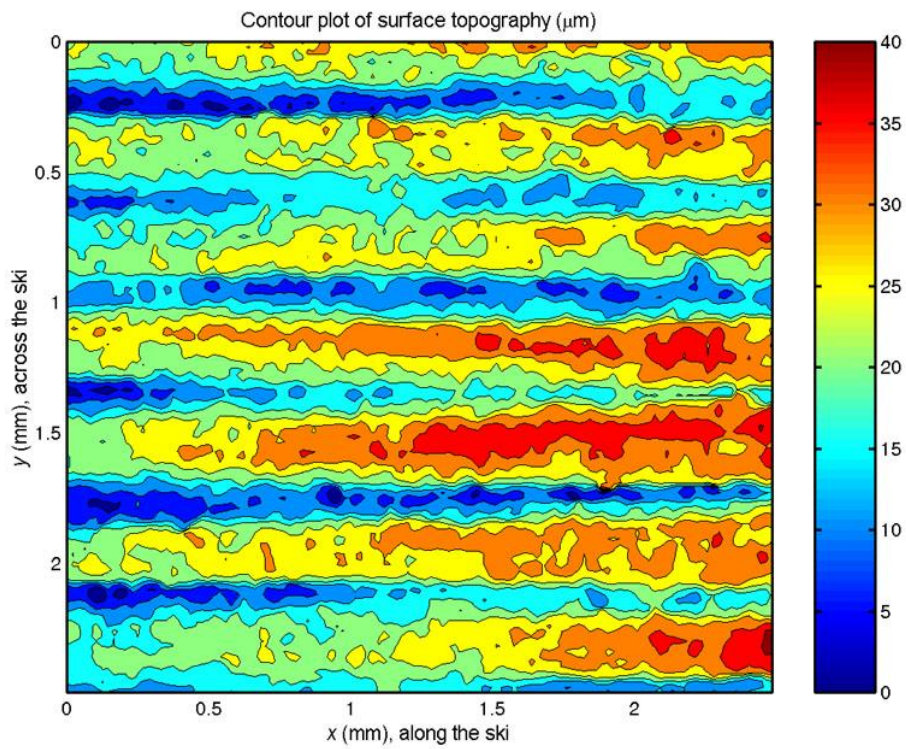


Fig. 6.7. Contour plot of the surface topography of ski base structure C.

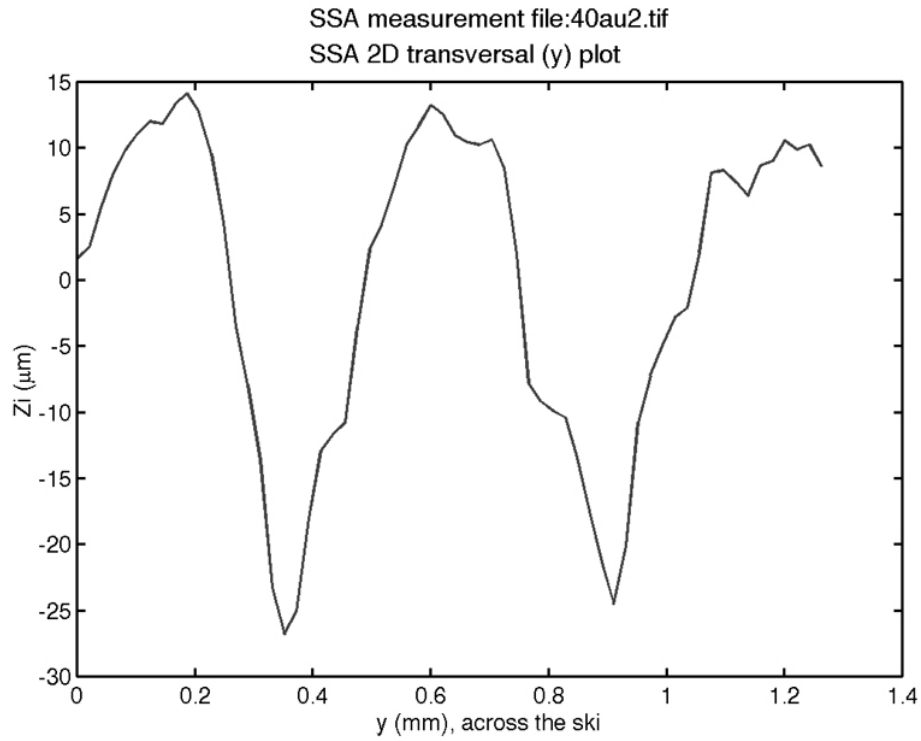


Fig. 6.8. Example of a surface profile across the ski for ski base structure D.

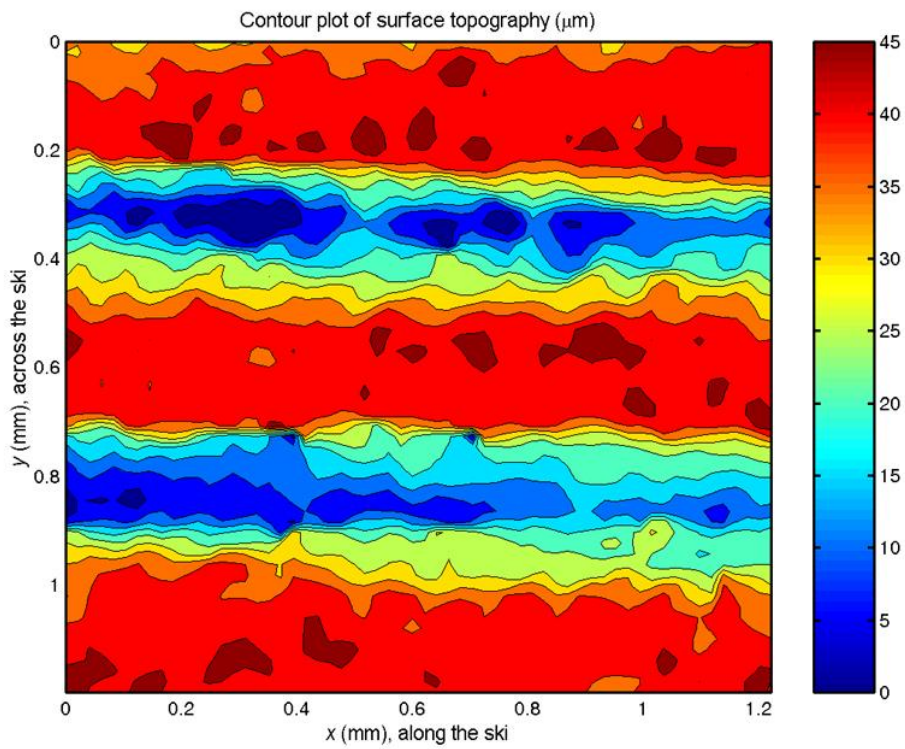


Fig. 6.9. Contour plot of the surface topography of ski base structure D.

Table 6.3. Structure roughness statistics for the ski pairs in the test series.

Ski pair No.	$\bar{R}_{a,yws} \pm \delta_{Rayws}$ (μm)	$\bar{R}_{a,yfs} \pm \delta_{Rayfs}$ (μm)	$\bar{R}_{a,yas} \pm \delta_{Rayas}$ (μm)
SP1	3.2 ± 0.3	3.3 ± 0.3	3.0 ± 0.1
SP2	4.0 ± 0.3	4.2 ± 0.1	3.7 ± 0.2
SP3	5.4 ± 0.4	5.4 ± 0.3	5.4 ± 0.5
SP4	12.7 ± 1.2	13.2 ± 1.4	12.3 ± 1.0
SP5	4.2 ± 0.5	3.8 ± 0.2	4.5 ± 0.5
SP6	4.4 ± 1.0	5.3 ± 0.2	3.5 ± 0.2
SP7	9.3 ± 3.5	6.0 ± 0.7	12.6 ± 0.6
SP8	8.9 ± 4.0	12.7 ± 0.4	5.1 ± 0.4
SP9	4.1 ± 0.4	4.1 ± 0.4	4.1 ± 0.4
SP10	5.3 ± 0.4	5.1 ± 0.3	5.6 ± 0.3

Table 6.4. Ski base structure test results.

Test No.	SP1 (km/h)	SP2 (km/h)	SP3 (km/h)	SP4 (km/h)	SP5 (km/h)	SP6 (km/h)	SP7 (km/h)	SP8 (km/h)	SP9 (km/h)	SP10 (km/h)
1A	30.1 (9)	30.3 (4)	30.5 (2)	30.2 (6)	30.1 (9)	30.2 (6)	30.6 (1)	30.3 (4)	30.2 (6)	30.4 (3)
1B	48.8 (9)	49.3 (4)	49.1 (6)	49.4 (3)	48.6 (10)	48.9 (8)	50.1 (1)	49.0 (7)	49.3 (4)	49.9 (2)
2	32.5 (7)	32.6 (3)	32.7 (2)	31.5 (10)	32.5 (7)	32.6 (3)	32.6 (3)	32.1 (9)	32.6 (3)	32.9 (1)
3	30.2 (5)	30.3 (2)	30.3 (2)	30.3 (2)	30.0 (8)	30.1 (6)	30.4 (1)	30.1 (6)	29.9 (10)	30.0 (8)
4	37.3 (9)	37.8 (7)	38.3 (3)	38.5 (1)	38.4 (2)	37.2 (10)	37.9 (5)	37.9 (5)	37.7 (8)	38.1 (4)
5	35.9 (6)	35.6 (9)	36.0 (4)	36.5 (1)	36.4 (2)	35.4 (10)	36.4 (2)	36.0 (4)	35.8 (8)	35.9 (6)
6	39.9 (2)	39.9 (2)	39.8 (4)	40.2 (1)	39.6 (6)	39.2 (8)	39.7 (5)	39.6 (6)	38.9 (10)	39.1 (9)
6A	40.8 (1)	40.8 (1)	40.7 (3)	40.6 (5)	40.4 (7)	40.4 (7)	40.7 (3)	40.5 (6)	40.4 (7)	40.3 (10)
6B	38.6 (2)	38.5 (3)	38.5 (3)	39.6 (1)	38.4 (5)	37.7 (8)	38.3 (6)	38.3 (6)	37.1 (10)	37.6 (9)
7	36.5 (3)	36.6 (2)	36.7 (1)	35.5 (10)	36.3 (6)	36.2 (7)	36.1 (8)	35.9 (9)	36.5 (3)	36.5 (3)
8	37.9 (4)	37.8 (6)	38.0 (1)		38.0 (1)				37.9 (4)	38.0 (1)
8A	37.8 (6)	37.9 (3)	38.1 (1)	36.8 (10)	38.0 (2)	37.8 (6)	37.3 (8)	37.3 (8)	37.9 (3)	37.9 (3)
8B	37.8 (5)	37.7 (6)	37.9 (4)		38.0 (3)				38.1 (2)	38.2 (1)
9	24.8 (3)	24.8 (3)	24.9 (1)		24.8 (3)				24.9 (1)	24.8 (3)
Mean	37.1 (5)	37.2 (3)	37.3 (1)	37.2 (3)	37.1 (5)	36.9 (9)	37.3 (1)	37.0 (8)	36.9 (9)	37.1 (5)

Table 6.5. Table of snow measurements for the ski base structure tests.

Test No.	Date (Time)	Place	Snow type	Grain shape	$\bar{d} \pm \delta_d$ (mm)	$W_{vol,\%}$ (%)	ρ (g/cm ³)	H (Pa)	T_s (°C)
1	24.03.98 (15:39)	Trondheim classic	4					4.09E+04 Medium	-0.1
1	24.03.98 (16:45)	Trondheim classic	5					7.71E+04 Medium	0.0
1	24.03.98 (17:49)	Trondheim classic	5			0.3 Dry	0.5	2.89E+05 High	-0.3
2	25.03.98 (10:19)	Trondheim classic	2			1 Moist	0.54	1.06E+05 High	-0.2
2	25.03.98 (12:15)	Trondheim classic	2	/	0.21±0.07 Fine	1.3 Moist	0.6	7.71E+04 Medium	-0.1
3	01.04.98 (10:15)	Meråker classic	5					2.03E+05 High	-2.4
3	01.04.98 (11:40)	Meråker classic	5					2.42E+05 High	-0.1
3	01.04.98 (13:44)	Meråker classic	5	○	1.24±0.48 Coarse	4 Wet	0.53	4.81E+04 Medium	0.0
3	01.04.98 (13:44)	Meråker skating	5			2.1 Moist	0.53	3.45E+04 Medium	0.0
4	17.04.98 (10:18)	Lillehammer classic	1			1.3 Moist	0.36	7.22E+03 Low	0.0
4	17.04.98 (11:40)	Lillehammer classic	1					1.46E+04 Medium	0.0
4	17.04.98 (12:35)	Lillehammer classic	2	○ (/)	0.38±0.13 Fine	8.5 Very wet	0.69	2.69E+04 Medium	0.0
5	20.04.98 (11:15)	Lillehammer classic	5			6.2 Wet	0.67	1.06E+04 Medium	0.0
5	20.04.98 (12:01)	Lillehammer classic	5			10.1 Very wet	0.91	2.69E+04 Medium	0.0
5	20.04.98 (12:40)	Lillehammer classic	5					2.91E+04 Medium	0.0
5	20.04.98 (13:34)	Lillehammer classic	5	○	0.70±0.24 Medium	11.2 Very wet	0.74	2.69E+04 Medium	0.0
6	21.04.98 (09:40)	Lillehammer classic	5			0.6 Moist	0.43	4.09E+04 Medium	-0.6
6	21.04.98 (11:59)	Lillehammer cl., shadow	5			5.3 Wet	0.68	1.98E+04 Medium	0.0
6	21.04.98 (11:59)	Lillehammer cl., sun	5	○	0.86±0.29 Medium	12.5 Very wet	0.61	1.06E+04 Medium	0.0
7	05.11.98 (09:24)	Golå classic	2			0 Dry	0.45	5.14E+05 High	-5.8
7	05.11.98 (11:43)	Golå classic	2			0.6 Moist	0.46	2.42E+05 High	-6.0
7	05.11.98 (11:43)	Golå skating	2			0.6 Moist	0.46	4.81E+04 Medium	-6.0
8	06.11.98 (09:02)	Golå classic	2			0.1 Dry	0.46	2.03E+05 High	-7.4
8	06.11.98 (09:02)	Golå skating	2			0.1 Dry	0.46	6.60E+04 Medium	-7.4
8	06.11.98 (10:47)	Golå classic	2			0.1 Dry	0.49	5.14E+05 High	-6.4

8	06.11.98 (10:47)	Golå skating	2	0.1 Dry	0.49	7.71E+04 Medium	-6.4
9	08.11.98 (09:15)	Golå classic	2	0.0 Dry	0.45	4.21E+05 High	-8.3
9	08.11.98 (09:15)	Golå skating	2	0.0 Dry	0.45	2.42E+05 High	-8.3

Table 6.6. Table of weather measurements for the ski base structure tests.

Test No.	Date (Time)	Place	T_a (°C)	Rh (%)	C (octoparts)	q_{net} (W/m ²)
1	24.03.98 (15:39)	Trondheim classic	4.4	67	7	258
1	24.03.98 (16:45)	Trondheim classic	4.4	46	0	
1	24.03.98 (17:49)	Trondheim classic	1.1	63	2	-70
2	25.03.98 (10:19)	Trondheim classic	2.5	57	8	254
2	25.03.98 (12:15)	Trondheim classic	4.7	43	4	415
3	01.04.98 (10:15)	Meråker classic	-2.4	74	8	
3	01.04.98 (11:40)	Meråker classic	-0.1		8	
3	01.04.98 (13:44)	Meråker classic	0.0	74	8	312
3	01.04.98 (13:44)	Meråker skating	0.0	74	8	312
4	17.04.98 (10:18)	Lillehammer classic	5.1	73	8	110
4	17.04.98 (11:40)	Lillehammer classic	1.7	92	8	
4	17.04.98 (12:35)	Lillehammer classic	3.1	83	7	164
5	20.04.98 (11:15)	Lillehammer classic	5.6	48	7	325
5	20.04.98 (12:01)	Lillehammer classic	8.1	44	8	526
5	20.04.98 (12:40)	Lillehammer classic	8.5			
5	20.04.98 (13:34)	Lillehammer classic	5.1	57	8	205
6	21.04.98 (09:40)	Lillehammer classic	3.1	64	0	431
6	21.04.98 (11:59)	Lillehammer cl., shadow	5.8	53	0	753
6	21.04.98 (11:59)	Lillehammer cl., sun	5.8	53	0	753
7	05.11.98 (09:24)	Golå classic	-12.3	91	8	-20
7	05.11.98 (11:43)	Golå classic	-11.6	81	8	17
7	05.11.98 (11:43)	Golå skating	-11.6	81	8	17

8	06.11.98 (09:02)	Golå classic	-8.8	75	8	-386
8	06.11.98 (09:02)	Golå skating	-8.8	75	8	-386
8	06.11.98 (10:47)	Golå classic	-6.3	73	8	-89
8	06.11.98 (10:47)	Golå skating	-6.3	73	8	-89
9	08.11.98 (09:15)	Golå classic	-8.8	71	7	-490
9	08.11.98 (09:15)	Golå skating	-8.8	71	7	-490

Table 6.7. Electrolytic conductivity and chemical water properties for collected and melted samples from the snow surfaces in the ski base structure tests described in Table 6.5.

Test No.	σ_{mss} ($\mu\text{S/cm}$)	Cl^- (mg/l)	Na^+ (mg/l)	K^+ (mg/l)	Ca^{2+} (mg/l)	SO_4^{2-} (mg/l)	Mg^{2+} (mg/l)	NO_3^- (mg/l)	F (mg/l)
1	22.4	4.79	2	0.12	0.08	0.34	0.31	<0,01	<0,01
2	16.6	3.08	1.32	0.08	0.09	0.12	0.2	<0,01	<0,01
3	4								
4	21.6	0.3	0.05	0.02	0.01	1.6	0.01	1.9	<0,1
5	8.5	0.4	0.05	0.01	0.01	0.5	0.01	1	<0,1
6	3.8	0.3	0.02	<0,1	0.01	0.4	0.01	0.7	<0,1
7	3.8	0.42	0.08	0.06	<0,01	<0,01	<0,1	0.34	0.01
8	4.1								
9	3.8								

Table 6.8. Typical relations between optimum structure roughness, snow humidity and snow type in the sliding tests of the structure test series.

Optimum structure roughness $\bar{R}_{a,\text{yws}}$ (μm)	Snow humidity $W_{\text{vol},\%}$ (%)	Snow type
$\leq 5-6$	≤ 0.6	2
$\approx 5-6$	≤ 1.3	2
≈ 9	$\approx 0.3-4$	4 and 5
≈ 13	> 4	2 and 5

The least optimum structures and ski pairs in the sliding tests have been:

- Structure D under snow conditions with snow humidity $W_{\text{vol},\%}$ below approximately 1.3 % and Snow type 2, i.e. in Tests 2, 7, 8 and 9.
- Ski pair SP6 under snow conditions with snow humidity $W_{\text{vol},\%}$ above approximately 1.3 %, for instance in Tests 4, 5 and 6.

The sliding tests with different structures along the ski have resulted in the following findings:

- The mean speeds of all the nine sliding tests are 0.5 and 0.8 % higher for the ski pairs SP5 and SP7 that have coarser structure on the afterbody relative to the forebody of the ski, than for the ski pairs SP6 and SP8 that have finer structure on the afterbody relative to the forebody of the ski.
- Decrease of the structure roughness along the ski is unfortunate at snow temperatures below zero. It has for instance been registered 0.8 and 1.4 % higher average sliding speeds for SP3 than SP6 under such conditions in Tests 8A and 7, respectively.
- Decrease of the structure roughness along the ski is unfortunate under snow conditions with snow humidity $W_{vol,\%}$ above approximately 1.3 %. It has been registered 0.7 to 3.3 % higher average sliding speeds for SP4 than SP8 under such conditions in Tests 3, 4, 5 and 6B.
- The largest speed differences between ski pair SP5 and SP6 have been measured under snow conditions with snow humidity $W_{vol,\%}$ above approximately 1.3 %, i.e. under snow conditions where the structure roughness $\bar{R}_{a,yws}$ of the ski pairs have been lower than the optimum roughness. It has been registered 1.8 to 3.1 % higher average sliding speeds for SP5 relative to SP6 under such conditions in Tests 4, 5 and 6B.

Tests 1A and 1B showed a rather large speed difference between ski pair SP3 and SP10 at high speed (≈ 49 -50 km/h) compared to low speed (≈ 30 km/h) during the same test runs. SP3 had 0.3 % (0.1 km/h) higher average sliding speed than SP10 at about 30 km/h, while SP10 had 1.6 % (0.8 km/h) higher average sliding speed than SP3 at about 49-50 km/h. The reason for this is probably a slight difference in the pressure distribution of ski pair SP3 relative to the other ski pairs. It was also found in Tests 1A and 1B that the coarsest structure D was relatively better than the finest structure A at high speeds compared to at low speeds. Structure D had only 0.3 % (0.1 km/h) higher average sliding speed than structure A at about 30 km/h, while the difference was 1.2 % (0.6 km/h) at about 49-50 km/h.

At the end of Test 3 some snowflakes with 1-mm diameter fell on the glazed test track and increased the snow humidity of the track. This led to an average decrease in sliding speed of 2.6 % (0.8 km/h), thus highlighting the importance of the snow humidity on the sliding properties of the ski track.

In spite of equal structures had ski pair SP2 2.5 % higher average sliding speed than SP9 in Test 6, while SP3 had 1.8 % higher average sliding speed than SP10. The main reason for this was the large increase in snow humidity from 0.6 to 12.5 % during this test. This led to deterioration of the sliding conditions for the ski pairs that were tested late in the test rounds compared to the ski pairs that were tested early.

6.5. Discussion

The sliding tests presented in Section 6.4 showed that the optimum ski base structure roughness of the best structures and ski pairs $\bar{R}_{a,yws}$ increased with snow humidity $W_{vol,\%}$, thus indicating that the optimum ski base structure roughness increases with water film thickness. This corresponds very well with the tribological theories deduced from Eq. (2.20) and Fig. 2.10 in Chapter 2. It also highlights the importance of measurement of snow humidity as an indicator of the initial water film thickness in the ski track and the frictional water film thickness that is possible to attain during skiing.

The water film thickness developed under the ski under different snow conditions can be postulated for the given skier speed and skier weight in the sliding tests by applying Eq. (2.20) and Fig. 2.10. By setting $R_{q,sn}$ in Eq. (2.20) equal to zero and letting $R_{q,sbs}$ in Eq. (2.20) be transformed from the $\bar{R}_{a,yws}$ - values in Table 6.8, the approximate average water film thickness $\bar{h}_{min,wf}$ under different snow conditions is found from Eq. (2.20) as:

$$\bar{h}_{min,wf} \approx \Lambda_{opt} R_{q,sbs} \quad (6.1)$$

where:

Λ_{opt} - optimum film parameter for cross-country skiing

The optimum film parameter for cross-country skiing Λ_{opt} is not known at present, but probably lies somewhere between 5 and 8. By letting Λ_{opt} be equal to 6, values of the approximate average water film thickness $\bar{h}_{min,wf}$ can be deduced for the structure tests series under different snow conditions as shown in Table 6.9. It is quite clear that the water film thickness values given in Table 6.9 are very speculative, and the values may be overestimated.

Table 6.9. Approximate average water film thickness $\bar{h}_{min,wf}$ for the structure tests series under different snow conditions.

$\bar{h}_{min,wf}$ (μm)	$W_{vol,\%}$ (%)	Snow type
≤ 40	≤ 0.6	2
≈ 40	0.6-1.3	2
≈ 60	$\approx 0.3-4$	4 and 5
≈ 80	>4	2 and 5

Tests 1A and 1B showed that the coarsest structure D was relatively better than the finest structure A at high speeds compared to low speeds. This can be explained by increased water film thickness at higher speeds, and thus increase in optimum structure roughness according to Eq. (2.20) and Fig. 2.10.

It was also found in Section 6.4 that structure D was the least optimum structure under snow conditions with Snow type 2 and snow humidity $W_{vol,\%}$ below approximately 1.3 %. This can be explained from the fact that:

- Structure D has an average structure roughness ($\bar{R}_{a,yws} = 12.7 \mu\text{m}$) that is too high to give an optimum Λ in Eq. (2.20) under such conditions. It can therefore be assumed that the frictional situation under the ski lies in the dry friction area (the left part) of Fig. 2.10, thus implying a higher sliding friction coefficient for structure D than for a structure with lower structure roughness under such conditions.
- The groove widths of structure D that typically vary between 0.3 and 0.4 mm (See for instance Figs. 6.8 and 6.9), lead to a contact configuration between ski and snow that is not efficient under snow conditions with typical snow grain sizes below 0.3 mm. This might be due to e.g.

enlargement of the dry friction contact surface between ski and snow and increased carving compared to structures with smaller groove widths and depths.

Further, ski pair SP6 was the least optimum ski pair under snow conditions with snow humidity $W_{vol,\%}$ above approximately 1.3 %. This can be elucidated from the fact that:

- Ski pair SP6 has an average structure roughness on the afterbody of the ski ($\bar{R}_{a,yas} = 3.5 \mu\text{m}$) that is too low to give an optimum Λ in Eq. (2.20) for the afterbody of the ski under such conditions. Thus, the frictional situation under the afterbody of the ski lies in the wet friction area (the right part) of Fig. 2.10, and suction may take place.

The sliding tests with different structures along the ski presented in Section 6.4 showed that it is unfortunate to decrease the structure roughness along the ski. This is very intuitive since it is not likely that the water film thickness decrease along the ski during skiing.

The effect of increasing the structure roughness along the ski relative to having the same structure roughness is more difficult to interpret at present. This is partly because the roughness difference between the forebody and the afterbody of ski pair SP5 was smaller than desired, and partly because no ski pair had structure roughness $\bar{R}_{a,yws} \approx 9 \mu\text{m}$ along the whole ski. Thus, it is difficult to state how an optimally made ski pair SP5 would have performed relative to the other ski pairs and structures, and how a ski pair with structure roughness $\bar{R}_{a,yws} \approx 9 \mu\text{m}$ along the whole ski would have performed under the snow conditions where SP7 showed the best structure test results (Tests 1 and 3).

Another aspect that is important to be aware of when testing the effect of increased structure roughness along the ski, is that the effect of a change in structure pattern might dominate over the effect of increased structure roughness. The structure pattern of structure C was for instance considerably better than the structure pattern of structure D under snow conditions with Snow type 2 and also better than the structure pattern of structure B under most snow conditions. This highlights the importance of testing ski pairs with equal structure patterns and increased structure roughness along the ski in future sliding tests.

Ski pair SP5 was the second best ski pair in Tests 4 and 5 under snow conditions with wet and very wet snow and average snow grain size \bar{d} equal to or below 0.70 mm. This was probably due to a combination of:

- Good "floating" (bearing) properties
- Small groove widths that were effective in reducing suction under snow conditions with such snow grain sizes
- Higher structure roughness on the afterbody relative to forebody of the ski

It would have been fortunate to perform more than nine tests with the structure test series and also to test other types of structures. The results described in this chapter should therefore be considered as only a starting point for research on ski base sliding friction and ski base structures. In spite of this the theoretical and experimental approach presented in this chapter and thesis ought to be interesting and

applicable also to increase understanding of other fields of snow tribology and sliding friction against snow and ice, e.g. studded tyres vs. normal tyres.

6.6. Conclusions and recommendations

6.6.1. Conclusions

A structure test series consisting of ten ski pairs have been ground with eight different ski base structures in order to:

- Find the optimum and least optimum ski base structure roughness and patterns under different snow conditions.
- Investigate the effect of different ski base structure roughness and patterns along the ski under different snow conditions.
- Study the relation between optimum ski base structure roughness and snow humidity.
- Study the effect of different ski base structures on different snow types with various snow grain sizes.

Sliding tests of the structure test series have been performed with skier speeds mainly between 30 and 40 km/h, and test skier weight between 75 and 80 kg. The experiments have resulted in the following findings:

- Ski pairs with $\bar{R}_{a,yws} \leq 5.4 \mu\text{m}$ have been best under snow conditions with snow humidity $W_{vol,\%} \leq 0.6 \%$, snow temperatures below zero and Snow type 2.
- A structure with $\bar{R}_{a,yws}$ equal to 5.3-5.4 μm has in average been best under snow conditions with snow humidity $W_{vol,\%} \leq 1.3 \%$, snow grain size \bar{d} less than approximately 0.25 mm and Snow type 2.
- A ski pair with $\bar{R}_{a,yws} = 9.3 \mu\text{m}$, $\bar{R}_{a,yfs} = 6.0 \mu\text{m}$ and $\bar{R}_{a,yas} = 12.6 \mu\text{m}$, has been best under snow conditions with snow humidity $W_{vol,\%}$ between approximately 0.3 and 4.0 %, snow hardness H higher than $4.1 \times 10^4 \text{ Pa}$, and Snow types 4 and 5.
- A structure with $\bar{R}_{a,yws} = 12.7 \mu\text{m}$ has been best under snow conditions with snow humidity $W_{vol,\%}$ higher than approximately 4 %, and Snow types 2 and 5. It was registered 2.5 % higher average sliding speed for this structure relative to the second best structure in one of the tests under very wet snow conditions. The same structure was the least optimum structure under snow conditions with snow humidity $W_{vol,\%}$ below approximately 1.3 % and Snow type 2.
- A ski pair with $\bar{R}_{a,yws} = 4.4 \mu\text{m}$, $\bar{R}_{a,yfs} = 5.3 \mu\text{m}$ and $\bar{R}_{a,yas} = 3.5 \mu\text{m}$, was the least optimum ski pair under snow conditions with snow humidity $W_{vol,\%}$ above approximately 1.3 %.
- The highest average skier speed differences between ski pairs in the structure test series (6.3 %) have been registered on very wet snow.

- The smallest average skier speed differences between ski pairs in the structure test series (1.2-1.6 %) have been found under snow conditions with dry and moist snow, snow hardness $H \geq 4.1 \times 10^4$ Pa, and Snow types 4 and 5.
- The optimum ski base structure roughness of the best structures and ski pairs has increased with snow humidity, thus indicating that the optimum ski base structure roughness increases with the water film thickness.
- Coarser structures have been relatively better than finer structures at high speeds compared to low speeds, thus implying increase in the water film thickness and optimum structure roughness with speed.
- Decrease of the structure roughness along the ski has been unfortunate under most snow conditions.
- The effect of increasing the structure roughness along the ski relative to having the same structure roughness is difficult to interpret at present. Accurate sliding tests of ski pairs with equal structure patterns and increased structure roughness along the ski is needed before conclusions can be drawn.

6.6.2. Recommendations

Many aspects regarding ski base structures and ski base sliding friction were not studied in detail in the experiments referred to in this chapter. More sliding tests with different structure test series and measurement of ski base structure, snow and weather parameters are therefore needed in order to further improve the present understanding of ski base sliding friction. Future research ought to investigate aspects such as the effect of the:

- Structure pressure contact area during skiing
- Structure capillary contact area during skiing under wet snow conditions
- Structure carving area during skiing under hard and dry snow conditions
- Structure bearing area during skiing under soft snow conditions
- Structure pattern on the dilution of water film during skiing under wet snow conditions
- Structure pattern on the minimisation of attachment of dirt during skiing
- Glide wax/powder and the pressure distribution of the ski on the optimum structure

It would also be interesting to perform measurement of the water film thickness along the ski and investigate the ski track with an infra red video camera during sliding tests of ski base structures under different snow conditions.

7. The effect of electrical charging and electrostatic pressure on ski base sliding friction

Notation

e	proton charge, 1.602×10^{-19} C
$e_{i,\text{ice}}$	charge of carrier given by defect i in ice, C
E	electric-field strength in dielectric gap, V/m
E_{ag}	electric-field strength in the air gap between the slider and snow/water film, V/m
$E_{z,\text{sk-wf}}(x, y, t)$	electric field-strength normal to the ski base (z -direction) at the interfacial contact between a point (x, y) on the ski and the frictional water film at time t , V/m
$E_{z,\text{sn-wf}}(x, y, t)$	electric field-strength normal to the ski (z -direction) under the ski base in the interfacial contact between snow and the frictional water film at time t , V/m
$E_{z,\text{wf}}(x, y, z, t)$	electric field-strength normal to the ski (z -direction), in the frictional water film at time t and at a point (x, y) under the ski base at a normal distance z from the ski base, V/m
$h_{\text{min,wf}}$	minimum water film thickness between a specific area on the ski and snow at a specific time during skiing, μm
i	type of charge carrier or defect in ice, $i = 1$ for H_3O^+ ions, $i = 2$ for OH^- -ions, $i = 3$ for D-defects and $i = 4$ for L-defects
k_{B}	Boltzmann constant, 1.381×10^{-23} JK ⁻¹
L	thickness of dielectric gap, m
L_{ag}	thickness of the air gap, m
$n_{i,\text{ice}}$	concentration in ice of defect i , m ⁻³

P_{el}	electrostatic pressure, N/m^2
$P_{el, ag}$	electrostatic pressure in an air gap between slider and snow/water film, N/m^2
$P_{el, sk-wf}(x, y, t)$	the electrostatic pressure at the interfacial contact between a point, (x, y) on the ski base and the frictional water film in a frictional ski base sliding situation at time t , N/m^2
$P_{el, sn-wf}(x, y, t)$	the electrostatic pressure at a point (x, y) under the ski base in the interfacial contact between snow and the frictional water film in a frictional ski base sliding situation at time t , N/m^2
$P_{el, wf}(x, y, z, t)$	the electrostatic pressure in the water film at a point (x, y) under the ski base at a normal distance, z , from the ski base in a frictional ski base sliding situation at time t
$1/R$	conductance, Ω^{-1}
R	resistance, Ω
$R_{q,sbs}$	root mean square roughness of the ski base structure surface in the specific area, μm
$R_{q,sn}$	root mean square roughness of snow surface, μm
r_{oo}	oxygen - oxygen distance in the ice lattice, 2.76 \AA ($1 \text{ \AA} = 10^{-10} \text{ m}$)
t	time, s
T	temperature, $^{\circ}C$ or K
V	potential difference in dielectric gap, V
V_{ag}	potential difference in the air gap between the slider and snow/water film, V
(x, y)	point on the ski base
z	direction normal to the ski and/or normal distance from the ski base, μm
ε	relative dielectric permittivity for a material between which a potential difference exists, $\varepsilon = 1$ for vacuum
ε_0	dielectric permittivity of vacuum, $8.854 \times 10^{-12} \text{ F/m}$
$\varepsilon_{s,ice}$	relative static dielectric permittivity of ice
$\varepsilon_{sk-wf}(x, y, t)$	relative dielectric permittivity at the interfacial contact between a point (x, y) on the ski base and the frictional water film at time t
$\varepsilon_{sn-wf}(x, y, t)$	relative dielectric permittivity at a point (x, y) under the ski base in the interfacial contact between snow and the frictional water film at time t
$\varepsilon_{wf}(x, y, z, t)$	relative dielectric permittivity in the frictional water film at time t and at a point (x, y) under the ski base at a normal distance z from the ski base
$\varepsilon_{\infty,ice}$	relative high-frequency dielectric permittivity of ice
Φ	factor defined in Eq. (7.10), Jm
Λ	non-dimensional film parameter
μ	sliding friction coefficient
$\mu_{i,ice}$	mobility in ice of charge carrier given by defect i , m^2/Vs
$\sigma_{\bullet,ice}$	H_3O^+ - and OH^- -ions conductivity in ice, $\Omega^{-1}m^{-1}=10^4 \mu S/cm$
$\sigma_{DL,ice}$	D- and L- defects conductivity in ice, $\Omega^{-1}m^{-1}=10^4 \mu S/cm$
$\sigma_{i,ice}$	partial conductivity given by defect i in ice, $\Omega^{-1}m^{-1}=10^4 \mu S/cm$
$\sigma_{s,ice}$	static electrical conductivity of ice, $\Omega^{-1}m^{-1}=10^4 \mu S/cm$
$\sigma_{\infty,ice}$	high frequency electrical conductivity of ice, $\Omega^{-1}m^{-1}=10^4 \mu S/cm$

7.1. Introduction

This section is based on the measurements and theories described in a report written by Petrenko (1993) and papers written by Petrenko (1994), Petrenko and Colbeck (1995) and Colbeck (1995). A comprehensive review of the electric properties of ice was given in the report by Petrenko (1993). Petrenko (1994) performed laboratory experiments on the effect of an electric dc bias applied between ice and sliders on static and dynamic ice friction. The effect of electric fields, electrostatic pressures and frictional self-electrification on ice friction was also discussed. Petrenko and Colbeck (1995) studied frictional ice electrification and generation of electric fields during ice friction in laboratory situations and snow friction in-situ for alpine skis. Electrical charging of alpine and cross-country skis gliding on in-situ snow were measured and discussed by Colbeck (1995).

Petrenko (1994) showed in laboratory experiments that a 3 kV bias applied between ice and a slider can increase the friction by 2/3 for polyethylene and by 2/5 for metal sliders on ice. Prior to this he had found that electric fields developed during ice friction due to frictional self-electrification. Electric fields with a strength in the order of 2×10^6 V/m had been induced by friction at an ice/polyethylene interface at a temperature of -31.5°C and sliding velocity of 8 m/s. Metal sliders (stainless-steel and aluminium foils) gliding on ice under the same conditions developed a potential difference of up to 1.6 kV between the ice and the sliders. These experimental results and basic electric field theory considerations showed that frictional self-electrification may play a significant role in forming ice and snow friction coefficients. The laboratory experiments were performed on pure polycrystalline ice with grain sizes between 5 and 12 mm (Petrenko and Colbeck, 1995) and temperatures ranging from -5 to -30°C and sliding velocities from 0.5 to 8 m/s. The static electrical conductivity of ice, $\sigma_{s,ice}$, was measured to $10^{-9} \Omega^{-1}\text{m}^{-1}$ ($10^{-5} \mu\text{S/cm}$) at $T = -30^\circ\text{C}$ and $10^{-7} \Omega^{-1}\text{m}^{-1}$ ($10^{-3} \mu\text{S/cm}$) at $T = -10^\circ\text{C}$. These figures are close to the electrical conductivity found in pure single crystalline ice (Petrenko, 1993, and Petrenko and Schulson, 1992), but much smaller than the electrolytic conductivity values for melted snow samples measured by the author (3.8 - 169.7 $\mu\text{S/cm}$). Notice that this indicates a difference in electrical conductivity of three to seven orders of magnitude between ice or the solid phase of snow and melted ice or snow, i.e. water.

7.2. The effect of electrical charging and electrostatic pressure on ski base sliding friction

The electrical conductivity of ice is known to have a characteristic frequency dependence (Petrenko, 1993). High frequency electrical conductivity, $\sigma_{\infty,ice}$, which Petrenko has given as $(1.8 \pm 0.2) \times 10^{-5} \Omega^{-1}\text{m}^{-1} = (0.18 \pm 0.02) \mu\text{S/cm}$ at -10°C , is approximately three orders of magnitude higher than static electrical conductivity, $\sigma_{s,ice}$. Measured values of $\sigma_{s,ice}$ (-10°C) in literature vary from 6×10^{-10} to $10^{-6} \Omega^{-1}\text{m}^{-1}$. Petrenko has explained this with the difficulty of purifying ice to a level where intrinsic ions dominate over ions supplied by impurities. The temperature dependence of bulk and surface conductance of pure ice is given in Fig. 7.1. Notice that conductance has the unit Ω^{-1} , while conductivity is given in $\Omega^{-1}\text{m}^{-1}$.

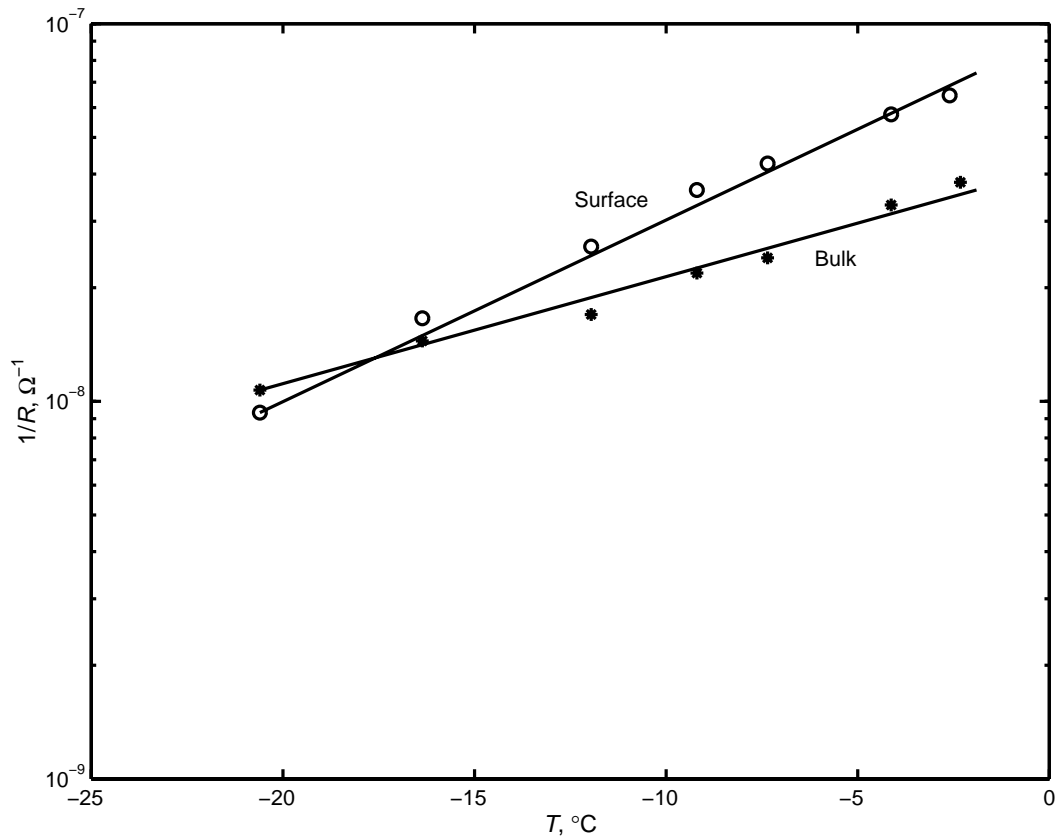


Fig. 7.1. Temperature dependence of bulk and surface conductance of pure ice. Temperature, T , is given in °C. Conductance, $1/R$ is given in Ω^{-1} (after Bullemer and Riehl, 1966).

It has been shown that the electrical conductivity of pure ice is entirely determined by proton motion within the temperature range of 0 to -42°C (Petrenko and Chesnakov, 1990). Three sources of protonic motion in ice are known (Petrenko, 1993):

1. Thermal generation of carriers
2. Atoms and molecules of impurities
3. Various types of external excitation such as strong electric fields, ultraviolet radiation or high-energy particle beams

The two first sources exist in a state of thermal equilibrium. Although liquid water (and thereby presumably a significantly thick water film generated during skiing by frictional melting of snow and containing pollution in form of the original snow nucleating agents) is a very good solvent for many substances, ice dissolves to almost nothing. Most of the impurities dissolved in water either get repelled from ice back into water or precipitate as a second phase inside the ice bulk in the form of segregations and clusters during the process of ice growth. Some exceptions exist, such as:

- A few acids: HF, HCl
- Ammonia: NH_3
- Some alkalises: KOH, NaOH
- Derivatives such as NH_4F or KCl

These substances can be included properly into the ice crystal lattice and drastically change the protonic carrier concentration in ice.

Protons can not be transferred sizeable distances in a defect-free ice structure. They must either move along hydrogen bonds, thereby creating H_3O^+ - and OH^- -ions, or from bond to bond, thereby causing a pair of Bjerrum defects:

- D-defect (Dobbelt-effect): O-O bond in ice crystal lattice with two protons close to or on it.
- L-defect (Leer-defect): O-O bond in ice crystal lattice with no protons close to or on it.

The motion of an L-defect causes the same reorientation of hydrogen bonds in a water molecule chain as H_3O^+ -ions. OH^- -ions and D-defects cause the opposite reorientation.

Jaccard (1959, 1964) has described the electric properties of ice assuming that charge carriers in ice are protons. Petrenko (1993) has defined the static electrical conductivity of ice, $\sigma_{s,ice}$, using the theoretical model given by Jaccard (be aware that the nature of surface conductivity of ice/snow will differ considerably from Jaccard's model):

$$\sigma_{s,ice} = \frac{e^2}{\frac{e_{1,ice}^2}{\sigma_{1,ice}^2 + \sigma_{2,ice}^2} + \frac{e_{3,ice}^2}{\sigma_{3,ice}^2 + \sigma_{4,ice}^2}} \quad (7.1)$$

where:

- e - proton charge, 1.602×10^{-19} C
- i - type of charge carrier or defect in ice, $i = 1$ for H_3O^+ ions, $i = 2$ for OH^- -ions, $i = 3$ for D-defects and $i = 4$ for L-defects
- $e_{i,ice}$ - charge of carrier given by defect i in ice, C
- $\sigma_{i,ice}$ - partial conductivity given by defect i in ice, $\Omega^{-1}\text{m}^{-1}=10^4\mu\text{S}/\text{cm}$

The sum of charge of a H_3O^+ ion and a D-defect is defined by Petrenko as:

$$e_{1,ice} + e_{3,ice} = e \quad (7.2)$$

Hubman (1979a, b) has found experimentally that:

$$e_{3,ice} = (0.38 \pm 0.01)e \quad (7.3a)$$

while Scheiner and Nagle (1983) theoretically has analysed that:

$$e_{3,ice} = (0.36 \pm 0.03)e \quad (7.3b)$$

The partial conductivities of the charge carriers in ice, $\sigma_{i,ice}$, are given as:

$$\sigma_{i,ice} = |e_{i,ice}| \mu_{i,ice} n_{i,ice} \quad (7.4)$$

where:

- $\mu_{i,ice}$ - mobility in ice of charge carrier given by defect i , m^2/Vs
 $n_{i,ice}$ - concentration in ice of defect i , m^{-3}

The high-frequency electrical conductivity of ice, $\sigma_{\infty,ice}$, is defined by Petrenko (1993) as:

$$\sigma_{\infty,ice} = \sum_{i=1}^4 \sigma_{i,ice} \quad (7.5)$$

The temperature dependencies of H_3O^+ - and OH^- -ions conductivity, $\sigma_{\bullet,ice}$:

$$\sigma_{\bullet,ice} = \sigma_{1,ice} + \sigma_{2,ice} \quad (7.6)$$

and D- and L- defects conductivity, $\sigma_{DL,ice}$:

$$\sigma_{DL,ice} = \sigma_{3,ice} + \sigma_{4,ice} \quad (7.7)$$

calculated from experimental results using best-fit method for ice doped with a small amount of HF in the concentration of $(1.3 \pm 0.1) \times 10^{20}$ molecules/ m^3 (Camplin et al., 1978) are shown in Fig. 7.2. The figure shows that $\sigma_{DL,ice}$ exceeds by about two orders of magnitude the value of $\sigma_{\bullet,ice}$ (ionic conductivity) at high temperatures (0 to $-10^\circ C$) indicating that normally at these temperatures $\sigma_{s,ice}$ is dominated by $\sigma_{\bullet,ice}$ and $\sigma_{\infty,ice}$ by $\sigma_{DL,ice}$ according to Eqs. (7.1) and (7.5).

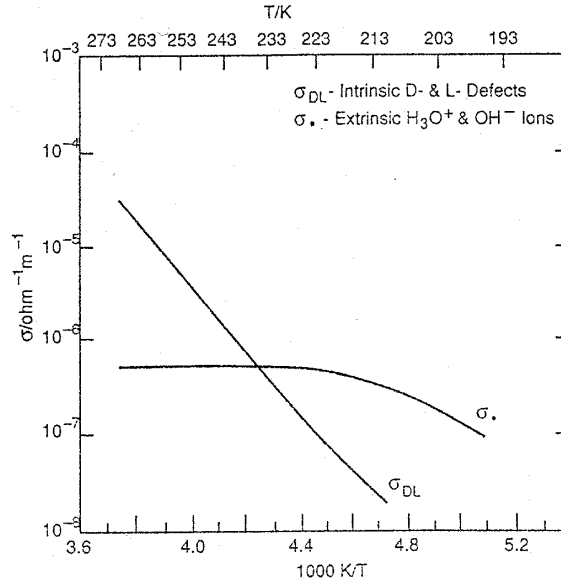


Fig. 7.2. The temperature dependencies of H_3O^+ - and OH^- -ions conductivity, $\sigma_{\bullet,ice}$, and D- and L- defects conductivity, $\sigma_{DL,ice}$, calculated from experimental results, using best-fit method, for ice doped with a small amount of HF in the concentration of $(1.3 \pm 0.1) \times 10^{20}$ molecules/ m^3 (Camplin et al., 1978). Temperature, T , is given in K. The conductivity, σ , is given in $\Omega^{-1}m^{-1}$.

Petrenko (1993) states that the most efficient impurities for the increase of H_3O^+ ion and L-defect concentrations in ice appear to be the acids HF and HCl. He also explains that the equilibrium concentrations of D-defects and OH^- -ions in pure ice are determined by a balance between the rate of their thermoactivated production and the rate of recombination: D- with L-defects and H_3O^+ with OH^- -ions. Increased H_3O^+ ion and L-defect concentrations, increase the rate of recombination, which result in lowered D-defect and OH^- -concentrations. He further explains that D-defects and OH^- -ions are less mobile carriers than H_3O^+ ions and L-defects thus indicating higher values for the electrical conductivities in Eqs. (7.1) and (7.5), when H_3O^+ ion and L-defect concentrations increase, like efficiently done by HF and HCl. The influence in terms of electrical conductivity of HF doping of ice is termed by Petrenko as "efficient" compared to NH_3 . He has explained this with the sizeable activation energies for release of D-defects and OH^- -ions from the NH_3 -molecule in ice and D-defects and OH^- -ions in ice being less mobile carriers.

Ski waxes based on fluorocarbons are highly appreciated by skiers. For warmer conditions, ski waxes contain less synthetic wax and increased amounts of fluorocarbon additives (SWIX, 1996). Waxes for cold man-made snow contain higher amounts of hard, brittle and synthetic paraffins. Haltenorth and Klinger (1969) have reported an extremely large mobility of fluorine ions in ice. This implies that fluorine ions possibly introduced by a fluorocarbon glide product during skiing should be effective for electrical discharge between ski and snow. The extent of introduction of fluorine ions by a fluorocarbon glide product during skiing can be questioned due to the chemical inertness of a fluorocarbon. Hamrock (1994) has stated that although not strictly fluorocarbons, the chlorotrifluorethylene polymers have found some applications and are better lubricants than fluorocarbons because chlorine is more reactive with metals than fluorine.

High electrolytic conductivity values due to high Cl^- -concentrations have been measured in freshwater mountain lakes situated close to the sea in the European multidisciplinary, multinational AL:PE project (Wathne et al., 1997). Cl^- was in most cases related to Na^+ -concentrations, indicating that they mainly derived from atmospheric deposition. Sea salt (Junge, 1963) and clay minerals (Kumai and Francis, 1962) are known as good snow nucleating agents. Hewitt and Cragin (1994) found in their measurements of anion (negatively charged ion) concentrations in individual snow crystals and snowflakes that Cl^- was frequently the dominant anion in stellar (planar dendrite) crystals. It was shown in Chapter 5 that:

- The electrolytic conductivity increases and the grain size decreases when precipitation is introduced to the snow surface. The electrolytic conductivity can also increase with snow density.
- The electrolytic conductivity decreases as the snow goes through melt-freeze cycles and the grain size increases.
- The electrolytic conductivity of melted snow samples follows similar trends with respect to snow metamorphosis and snow density as the results referred by Kopp (1962) for the electrical conductivity of snow, but the electrical conductivity of snow is several orders of magnitude less than the electrolytic conductivity of melted snow samples.

Decreased values for transformed snow types are natural due to drainage of free ions/impurities through the snowpack by melt waves during melt sequences of melt-freeze-cycles of the snowpack. Ion flux through a shallow snowpack and the effects of initial conditions and melt sequences on ion

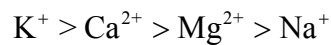
flux was investigated using tracers under controlled laboratory conditions by Davis et al. (1995). Hewitt et al. (1989) proposed that preferential chemical elution in snowpack meltwater is caused by preferential ion exclusion from snow grains during snow metamorphosis. Hewitt et al. (1991) concluded that less soluble chemical impurities, such as sulphates:

- are excluded more efficiently during snow crystal growth
- appear sooner and in higher concentrations in the meltwater during snowpack melting

than more soluble species such as chloride. Tranter et al. (1986) have proposed the anion elution sequence:



while Brimblecombe et al. (1987) suggested the cation elution order:



In the measurements referred in Chapter 5 the input to the snowpack of pollutants, which increased the ion level and electrolytic conductivity values of the melted snow samples collected at the top of the snowpack (ski track), were mainly introduced by snow precipitation. Davidson et al. (1996) have stated that particle and gases can deposit from the atmosphere to polar snow by several mechanisms:

1. Dry deposition considered to consist of three steps:

- aerodynamic transport from the free atmosphere to the viscous sublayer near the surface
- boundary layer transport across the sublayer
- interactions with the surface

2. Wet deposition:

- in-cloud scavenging:
 - uptake of particles during nucleation of cloud water
 - scavenging of particles and gases by existing droplets and ice crystals
- below-cloud scavenging

3. Incorporation of particles and gases into fog droplets and subsequent settling of the fog to the snow surface

In a study of the area surrounding the Nickel industries in Nikel and Zapoljarnij, Russia, and the iron ore mine and mill in Kirkenes, Norway, snow pack samples taken at the end of the 1991-1992 winter distinguished four different sources of element input (Reimann et al., 1996):

1. Industrial emissions
2. Sea spray
3. Geogenic dust
4. Anthropogenic dust

In the measurement campaigns prior to the 1998 Olympics in Japan and prior to and during the 1997 World Championship in cross-country skiing in Trondheim, two to three times higher electrolytic conductivity values were registered for melted snow samples of new-fallen snow from ski tracks in Trondheim than in Hakuba, Japan (See Section 5.3.4 for more details). Colbeck (1995) has pointed out that ionic charge can be introduced with the meltwater (water film) during friction. He explained this with the preferential separation of ions during freezing and therefore preferential production of ions during melting. Measurement of the electrolytic conductivity of a melted snow sample might be a good indicator of:

1. The electrolytic conductivity in the water film developed by frictional melting during skiing under a specific snow condition.
2. Possible sizes of potential differences that:
 - exists between ski and snow, ski and water film, water film and snow and in the water film under a specific snow condition
 - are generated by frictional electrification during skiing under a specific snow condition at a given time, where the friction situation in an area under the ski from a tribological point of view can be approached by using Eq. (2.20) and Fig. 2.10 in Chapter 2.

It was shown in Fig. 2.10 that the sliding friction coefficient, μ , between two interacting surfaces in relative motion, depends characteristically on a non-dimensional film parameter, Λ . The film parameter Λ is a function of:

- | | | |
|----------------|---|--|
| $h_{\min, wf}$ | - | minimum water film thickness between a specific area on the ski and snow at a specific time during skiing, μm |
| $R_{q, sbs}$ | - | root mean square roughness of the ski base structure surface in the specific area, μm |
| $R_{q, sn}$ | - | root mean square roughness of snow surface, μm |

The friction situation in an area under the ski is possible to approach at a given time during skiing by exploiting the knowledge of Fig. 2.10. At least this is true when impact and compaction resistances between ski and snow are negligible or small.

Petrenko and Colbeck (1995) found that frictional electrification during ice friction increased with decreasing temperature and increasing sliding velocity. The maximum voltage (1.6 kV) was found at the lowest temperature (-35°C) and the highest sliding velocity (8 m/s). The increased electrification at low temperatures is natural to analyse using the knowledge of:

- the lower measured electrical conductivity for ice at low temperature (-30°C) compared to high temperature (-10°C) in the laboratory experiments of Petrenko and Colbeck (1995), thus indicating lower discharge at lower temperatures and initial electrical conductivities for ice.
- the measured grain sizes of ice of 5-12 mm in the laboratory experiments of Petrenko and Colbeck (1995), which indicate a high surface roughness for ice compared to the water film thicknesses developed under the slider in the experiments, thus indicating a small Λ in Eq. (2.20) and a position to the left in Fig. 2.10 (dry friction area).

It is very interesting that during this presumably low Λ , dry friction process, the process of charge pick-up by the slider dominated over the process of electric discharge through the water film to the ice surface at different speeds. The last process was probably difficult due to the low conformity (poor connection) in the contact between water film and ice due to the presumably high surface roughness of ice. Although less frictional melting at lower temperatures also might have had influence, it is very interesting that charge pick-up was relatively largest when the electrical conductivity of ice was smallest. This may indicate that high initial snow or ice conductivity gives lower potential differences between slider and snow during friction under otherwise equal frictional situations and snow conditions, at least for the dry friction regime. It also addresses the importance of the electrolytic conductivity in a developed frictional water film (and thereby presumably the electrolytic conductivity of a melted snow sample!) on the potential differences between slider and snow/ice. It is tempting to suggest from the above discussion that:

- Sliders on highly electrical conductive snow should discharge easier than sliders on snow with lower electrical conductivity, given otherwise equal snow conditions and frictional situations (thus shifting the graph in Fig. 2.10 downwards!).
- Larger frictional electrification should take place on snow with low electrical conductivity compared to snow with high electrical conductivity given otherwise equal snow conditions and frictional situations (thus shifting the graph in Fig. 2.10 upwards!).

Petrenko (1993) stated that the process of proton transfer in ice via the creation of defects by an electric field turns out to be possible only in extremely strong electric fields: $E \geq 3 \times 10^{10}$ V/m. Petrenko (1994) referred to electric fields with a strength of the order of 2×10^6 V/m being induced by friction at an ice/polyethylene interface at a temperature of -31.5°C and sliding velocity of 8 m/s. This indicates that the following assumptions can be made for the laboratory experiments of Petrenko (1994) and Petrenko and Colbeck (1995):

- The electric fields generated between slider and ice were too weak to cause proton transfer in solid ice and significant discharge between slider and ice when no water was present in a contact between slider and ice during friction (assumed pure dry friction contact).
- The developed frictional water films under the slider were thin compared to ice roughness (small Λ) at all speeds. The electrical conduction and discharge between slider and ice through

a water film was thereby difficult due to poor contact between water film and ice. This resulted in negligible electric discharge taking place even at high speeds.

According to Petrenko (1994) the change in frictional force due to electrification can be explained by means of electrostatic pressures on the slider, that increase the normal pressures of the slider on the ice or snow surface. It is known from electric field theory that the electrostatic pressure, P_{el} , in a gap, L , filled with a dielectric material between which a potential difference, V , exists, is given by:

$$P_{el} = \frac{\epsilon_0 \epsilon E^2}{2} = \frac{\epsilon_0 \epsilon V^2}{2L^2} \quad (7.8)$$

where:

- V - potential difference in the dielectric gap, V
- E - electric-field strength in the dielectric gap, V/m
- L - thickness of the dielectric gap, m
- ϵ_0 - dielectric permittivity of vacuum, 8.854×10^{-12} F/m
- ϵ - relative dielectric permittivity for the material between which a potential difference exists, $\epsilon = 1$ for vacuum

Petrenko (1993) has defined the relative static dielectric permittivity of ice, $\epsilon_{s,ice}$, theoretically according to Jaccard's (1959, 1964) model as:

$$\epsilon_{s,ice} = \epsilon_{\infty,ice} + \frac{1}{\epsilon_0 \Phi} \left[\frac{\left(\frac{\sigma_{1,ice} + \sigma_{2,ice}}{e_{1,ice}} - \frac{\sigma_{3,ice} + \sigma_{4,ice}}{e_{3,ice}} \right)^2}{\left(\frac{\sigma_{1,ice} + \sigma_{2,ice}}{e_{1,ice}^2} + \frac{\sigma_{3,ice} + \sigma_{4,ice}}{e_{3,ice}^2} \right)^2} \right] \quad (7.9)$$

where:

- $\epsilon_{\infty,ice}$ - relative high-frequency dielectric permittivity of ice

and Φ is given by:

$$\Phi = 3.85 k_B T r_{oo} \quad (7.10)$$

where:

- k_B - Boltzmann constant, 1.381×10^{-23} JK⁻¹
- T - temperature, K
- r_{oo} - oxygen - oxygen distance in the ice lattice, 2.76 Å (1 Å = 10⁻¹⁰ m)

Petrenko states that the theory in its present form has some problems. For example, the slight anisotropy of ϵ measured in some experiments, but at present Jaccard's theory describes well, both quantitatively and qualitatively different electrical properties of ice.

The relative dielectric permittivity values found in literature for ice, water, polyethylene, ethylene, paraffin, HCl, HF, chlorine and fluorine are given in Table 7.1. Fig. 7.3 shows the change of the relative static dielectric permittivity of ice and water with temperature. Ice doped with HF has lower relative dielectric permittivity than pure ice (Camplin and Glen, 1973). At particular temperatures and impurity concentrations the relative static dielectric permittivity of ice, $\epsilon_{s,ice}$, can decrease considerably, and small values comparable with those of relative high-frequency dielectric permittivity of ice, $\epsilon_{\infty,ice} = 3.2$, can be found. This phenomena happens when the values of $\sigma_{\bullet,ice}$ and $\sigma_{DL,ice}$ become comparable, see Eqs. (7.6), (7.7) and (7.9), and is named "crossover" (more details and physical interpretation in Petrenko, 1993). High HF-concentrations in HF-doped ice gave "crossover" and minimum relative static dielectric permittivity at a higher temperature compared to the case for low HF-concentrations in the experiments of Camplin and Glen (1973), see Fig. 7.4. Steinemann (1957) found two "crossover" points in HF-doped ice at -3°C . In Petrenko (1993) this was explained by changes in $\sigma_{\bullet,ice}$ being proportional to the HF-concentration while changes in $\sigma_{DL,ice}$ being proportional to the square root of the HF-concentration.

Table 7.1. Relative dielectric permittivity values found in literature for ice, water, polyethylene, ethylene, paraffin, HCl, HF, chlorine and fluorine.

Material/Fluid	Relative dielectric permittivity	Temperature, K	Reference
Ice, static	$\epsilon_{s,ice} = 100.8$	263.2	Petrenko (1993)
Ice, high-frequency	$\epsilon_{\infty,ice} = 3.2$	263.2	Petrenko (1993)
Water, static	$\epsilon_{s,water} = 87.9$	273.2	CRC (1997)
Water, high-frequency	$\epsilon_{\infty,water} = 5.7$	273.2	CRC (1997)
Polyethylene	2.37	258.2	Petrenko (1994)
Ethylene (C ₂ H ₄)	1.41	270.0	CRC (1997)
Paraffin	≈ 2	?	Van Pelt and Knol (1983)
Fluorine (F ₂)	1.20	144.3	After equation in CRC (1997)
Chlorine (Cl ₂)	2.05	240	After equation in CRC (1997)
Hydrogen Fluoride (HF)	83.6	273.2	CRC (1997)
Hydrogen Chloride (HCl)	6.3	258.2	After equation in CRC (1997)

Due to $\epsilon = 1$ for air, the electrostatic pressure, $P_{el,ag}$, in an air gap, L_{ag} , between a slider and ice/snow/water film is given as:

$$P_{el,ag} = \frac{\epsilon_0 E_{ag}^2}{2} = \frac{\epsilon_0 V_{ag}^2}{2L_{ag}^2} \quad (7.11)$$

where:

- V_{ag} - potential difference in the air gap between slider and snow/water film, V
- E_{ag} - electric-field strength in the air gap between slider and snow/water film, V/m

L_{ag} - thickness of the air gap, m

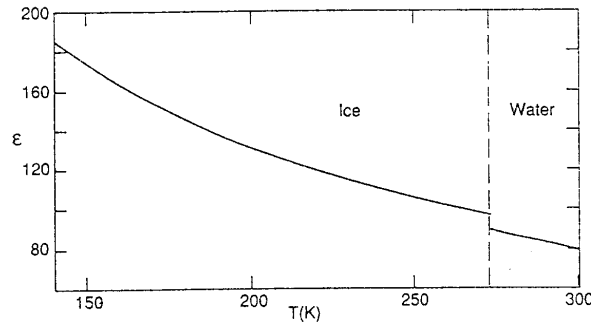


Fig. 7.3. Change of relative static dielectric permittivity of ice (Johari and Whalley, 1981) and water (Malmberg and Maryott, 1956) with temperature. Petrenko (1993) made the graph using extrapolations found in the referred papers. It is known that below a temperature of about 200 K the phenomena called "crossover" may exist.

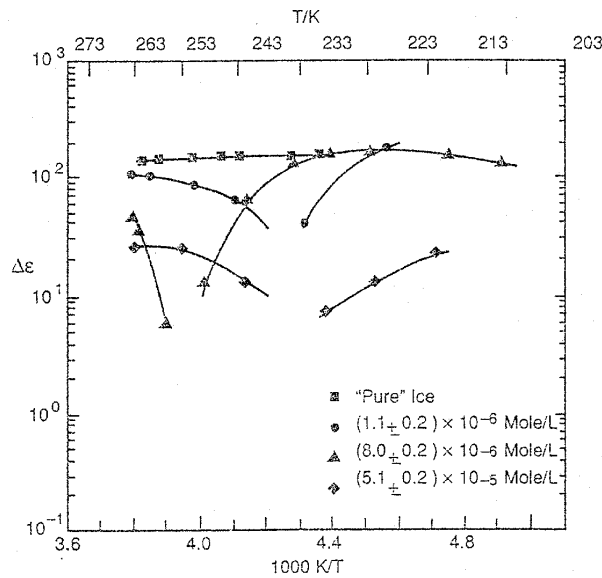


Fig. 7.4. $\Delta\epsilon = \epsilon_{s,ice} - \epsilon_{\infty,ice}$ as a function of temperature for ice doped with HF concentrations (Camplin and Glen, 1973). Temperature, T , is given in K, i.e. lower temperatures to the right in the figure.

In a frictional ski base sliding situation at time, t , the electrostatic pressure, $P_{el, sk-wf}(x, y, t)$, at the interfacial contact between a point, (x, y) , on the ski base and the frictional water film, can be defined as:

$$P_{el,sk-wf}(x, y, t) = \frac{\epsilon_0 \epsilon_{sk-wf}(x, y, t) (E_{z,sk-wf}(x, y, t))^2}{2} \quad (7.12)$$

where:

- $\varepsilon_{\text{sk-wf}}(x, y, t)$ - relative dielectric permittivity at the interfacial contact between a point (x, y) on the ski base and the frictional water film, at time t
- $E_{z,\text{sk-wf}}(x, y, t)$ - electric field-strength normal to the ski base (z -direction) at the interfacial contact between a point (x, y) on the ski and the frictional water film, at time t , V/m
- z - direction normal to the ski base, μm

In a frictional ski base sliding situation at time, t , the electrostatic pressure, $P_{\text{el,sn-wf}}(x, y, t)$, at a point (x, y) under the ski base in the interfacial contact between snow and the frictional water film, can be defined as:

$$P_{\text{el,sn-wf}}(x, y, t) = \frac{\varepsilon_0 \varepsilon_{\text{sn-wf}}(x, y, t) (E_{z,\text{sn-wf}}(x, y, t))^2}{2} \quad (7.13)$$

where:

- $\varepsilon_{\text{sn-wf}}(x, y, t)$ - relative dielectric permittivity at a point (x, y) under the ski base in the interfacial contact between snow and the frictional water film, at time t
- $E_{z,\text{sn-wf}}(x, y, t)$ - electric field-strength normal to the ski (z -direction) under the ski base in the interfacial contact between snow and the frictional water film, at time t , V/m

In a frictional ski base sliding situation at time, t , the electrostatic pressure in the water film, $P_{\text{el,wf}}(x, y, z, t)$, at a point (x, y) under the ski base at a normal distance z from the ski base, can be defined as:

$$P_{\text{el,wf}}(x, y, z, t) = \frac{\varepsilon_0 \varepsilon_{\text{wf}}(x, y, z, t) (E_{z,\text{wf}}(x, y, z, t))^2}{2} \quad (7.14)$$

where:

- $\varepsilon_{\text{wf}}(x, y, z, t)$ - relative dielectric permittivity in the frictional water film, at time t , at a point (x, y) under the ski base at a normal distance z from the ski base
- $E_{z,\text{wf}}(x, y, z, t)$ - electric field-strength normal to the ski (z -direction), in the frictional water film, at time t , at a point (x, y) under the ski base at a normal distance z from the ski base, V/m
- z - direction normal to the ski and normal distance from the ski base, μm

Petrenko and Colbeck (1995) found that an ice surface is not homogenous with respect to electrification. Along the 30 cm long ice cylinder they used in their laboratory experiments, it was possible to find two positions where the potential differed by two. Potential variations on the snow surface in a ski track are therefore natural to assume. It is also intuitive that different points on the ski base can have different potentials at a given time, t , during skiing, due to:

- Different frictional conditions along the ski in the length direction.
- Different contact conditions for different ski base structure points in an area, i.e. some ski base structure points are in contact with the frictional water film or snow, while others have no water film or snow contact (air pockets).
- The ski being a dielectric medium. When charges have been exchanged at the interface between two isolators and the materials afterwards are removed from each other, it is known from electrostatic charging theory that charges are not evenly distributed out in the materials like in metals. Graphite has very high electrical conductivity, $7.1 \times 10^8 \mu\text{S/cm}$ (CRC, 1978). The graphite content of the ski base is therefore very important for the electrical conductivity value of the ski base.

A glide product used on a ski has impact on several important ski base sliding friction aspects:

- It can decrease the surface tension of the ski base, thereby decreasing the surface wetted area and contact area between ski base structure and snow/frictional water film, thus implying larger air pocket volume between ski base structure and snow/frictional water film during skiing and influencing the friction coefficient.
- It can decrease/change the relative dielectric permittivity at the interfacial contact between a point on the ski base and the frictional water film or snow surface, thereby decreasing/changing the electrostatic (or capillary) pressure and the friction coefficient in the interfacial contact.
- It can introduce ions to the frictional water film or snow surface, thereby increasing the electrolytic/electrical conductivity in the frictional water film or snow surface, thus increasing electrical discharge and decreasing potential differences between ski and snow, thereby decreasing the electrostatic pressure and the friction coefficient in interfacial contacts between ski and water film or snow surface. One of the primary characteristics of a fluorocarbon wax is its inertness, and the extent of contribution of ions from the glide product can therefore be questioned.
- It can give less attachment of dirt to the ski base due to decreased electrostatic charging and relative dielectric permittivity for the glide product treated ski base. When the ski base is charged it will attract other substances and therefore function as a collector for dirt and dust.
- It can influence the thermal conductivity of the ski base and the development of frictional water film under the ski base.
- It can influence the hardness and wear of the ski base surface and microscopic impact and compaction resistances on the ski during skiing.
- It can influence "bleed" of electric charges (electrical conductivity) into the ski base from interfacial contact points between the ski base and the frictional water film or snow surface and thereby the distribution of electric potential on the ski base during skiing.

Colbeck (1995) has done field measurements of the potential difference between the ski base and the upper part of the ski during ski runs. The measured voltage was interpreted as an indicator of the accumulated electric charge on the ski base during the ski runs. A weakness in the experimental set-up was the introduction of a capacitor parallel with the ski to keep the induced voltages within acceptable

limits for the data acquisition system. This greatly increased the time constant of the system due to the low capacitance of the ski. It also gave 59 to 1180 times decrease in measured voltages.

Colbeck found that long ski runs with high speeds in deep, powder snow gave relatively steady rises in measured voltage during a ski run. It also produced the largest voltages. A great deal of variation in the measured voltage was found when skiing on wet, groomed runs or other hard or irregular surfaces due to frequent discharging. Icy surfaces produces even more noise and less accumulation of charge than wet, groomed snow. Skating in wet snow gave measured voltages that oscillated around zero. The glide parts of the cycle had positive peaks and were noisy when the gliding ski contacted obstacles. Charging mechanisms and induced voltages were different between wet and dry conditions. The voltage decayed much faster in wet snow than while resting on dry snow or suspending in air. This is natural due to the much higher electrical conductivity of water compared to snow (ice) and thereby better electrical connection between ski and snow when water is present. It also highlights:

- The importance of the water film introduced by frictional melting
- The electrolytic conductivity of the water film
- The aspect and effect of the glide product on the electrolytic conductivity of the water film
- The aspect of the measured electrolytic conductivity of a melted snow sample as an indicator of electrolytic conductivity of the water film

During the start period of a typical ski run when according to Colbeck the ski was warming and adjusting to heat generated by friction, a sudden decrease to a negative voltage was found in his measurements. He explained this with accumulation of negative charge on the sliding surface. According to Colbeck once the ski temperature and rate of meltwater generation stabilised, the voltage began to climb toward positive values i.e. zero voltage and lower absolute potential difference according to Fig. 5 in Colbeck (1995). Colbeck suggested in the discussion of this observation that charge may have changed sign after the ski surface reached its maximum wetting by meltwater. He referred to the Workman-Reynolds effect which are principled on ions being preferentially separated during freezing and thereby ions being preferentially produced during melting. This can cause introduction of ionic charges by the meltwater i.e. frictional water film under the ski. Colbeck thought it was questionable whether this effect always carried the same sign despite local differences in snow chemistry, although he referred to the fact that the observed pattern was registered at highly different geographical locations.

The author's suggestion is that this observation by Colbeck can be explained by using the knowledge of:

1. Higher electrical conductivity of water compared to ice or snow
2. From Point 1 it is intuitive that given approximately constant roughness for snow and ski base, $R_{q,sn}$ and $R_{q,sbs}$ in Eq. (2.20), a developed water film under the ski under dry conditions, i.e. a water film with larger water film thickness $h_{min,wf}$ and larger Λ in Eq. (2.20) compared to at the start time of the frictional situation and Λ still on the left side of the minimum point in the graph in Fig. 2.10 (dry friction area), at some time will introduce higher electrical conductivity between ski and snow compared to a situation where the water film thickness is lower or

almost non-present i.e. equal to the tiny liquid layer present on the dry snow surface when the observed frictional situation i.e. ski run started.

3. The higher electrical conductivity explained in Point 2 gives larger discharge from the ski to the snow.
4. Larger discharge from the ski to the snow gives the lower absolute voltages observed by Colbeck.

Snow compaction during the observed ski runs in soft snow may complicate the explanation given in Items 1 to 4. It can have lead to dynamic variations in $R_{q,sn}$ and water film thickness $h_{min,wf}$ and unstable contact situations between ski base and water film or snow during the ski runs. This surely would have influence on the observed voltages, but the essence in Point 1 to 4 should still be correct.

7.3. Summary and recommendations

7.3.1. Interpretation of friction

It is tempting from the theories and experiments cited in this section to suggest the following present interpretations of friction and the graph in Fig. 2.10 using ski base sliding friction as a case study:

1. The left hand side of the graph (dry friction area) in Fig. 2.10: Accumulation of electrostatic charges in the ski base contact points, the lubrication and discharge effect of the water film is still inefficient and insufficient. The friction process is dominated and characterised electrically by electrostatic charging behaviour.
2. The decrease in friction coefficient from the left hand side (dry friction area) to the minimum point in the graph in Fig. 2.10: The water film thickness $h_{min,wf}$ and the lubricate effect of the water film increase and the direct contact between ski and snow grains decreases. The water film introduces a resistance in the capacitor-dominated RC-"electrical circuit" under the ski, due to its much higher electrical conductivity compared to snow. This initiates discharge of potential differences between ski and snow. The friction coefficient decreases.
3. The increase in friction coefficient from the minimum point to the right hand side (wet friction area) of the graph in Fig. 2.10: The air gap volumes between the water film and the ski base structure, and the water film and the snow surface get smaller. Assuming relatively constant V_{ag} compared to L_{ag} , smaller L_{ag} cause the V_{ag}/L_{ag} ratio and thereby the electrostatic pressure in the air gap P_{ag} in Eq. (7.11) to increase. The surface wetted ski base structure area also increases. This increases the area directed towards water with high relative dielectric permittivity and decreases the area directed towards air with low relative dielectric permittivity. The phenomena of suction or drag may start occurring. This is commonly referred to as capillary forces.
4. The right hand side of the graph (wet friction): Electrolytic effects. The friction process is characterised electrically by electrolytic behaviour.
5. Ions can be introduced to the interface between snow and ski by melting or from the snow or ski base surfaces. The rate of ions introduced by melting depends on the snow. The electrolytic conductivity of a melted snow sample may indicate the rate of ions introduced by

melting and thereby the rate and ease of discharge between ski and snow through the water film during skiing. The glide product used under the ski is decisive for introduction of ions from the ski base surface. The extent of ions introduced by the glide product can be questioned, since chemical inertness is one of the primary characteristics of a glide product.

6. Fluid film lubrication has traditionally been modelled by continuum mechanics using mass and impulse balances and so-called Navier-Stokes equations that has been greatly simplified in order to solve them mathematically. In addition some have added energy considerations represented through energy balances and surface roughness considerations through surface roughness parameters to this framework, often introducing new assumptions. Whether the assumptions taken always have been sufficient for describing and understanding the true nature of the examined frictional process can be questioned. In order to evolve future understanding of friction processes it is necessary to increase the knowledge of the simultaneous processes of mass, impulse, energy, electrical and chemical balances between the two interacting surfaces in relative motion during friction. Knowledge of measured topography or structure of the two interacting surfaces and accurately measured test conditions during friction tests are important aspects in achieving this goal. Theory has to exploit and be able to verify repeated results found in experiments of frictional processes.
7. Small potential differences between upper and lower surface or low dielectric permittivities in the interfacial contacts between slider and lubricator during friction, shift the graph in Fig. 2.10 and thereby the sliding friction coefficient downwards.
8. Large potential differences between upper and lower surface or high dielectric permittivities in the interfacial contacts between slider and lubricator during friction, shift the graph in Fig. 2.10 and thereby the sliding friction coefficient upwards.
9. The relative humidity of air has several important aspects during friction :
 - The relative humidity may affect different snow properties that affect the development of water film and conformity between snow and ski during friction
 - High relative humidity may increase the relative dielectric permittivity in the air gaps between the water film and ski base structure and between the water film and snow, and thereby increase the electrostatic pressures between ski and water film, between snow and water film and in the water film.
 - High relative humidity may increase the electrical conductivity in the air gaps and thereby increase the electrical conductivity and discharge between ski and snow, thus decreasing the electrostatic pressures between the ski and the water film, between the snow and the water film and in the water film.

The approach and mechanisms cited above should also be possible to use to increase the understanding and knowledge of friction in general, although the electrical and chemical balances and reactions of course will be somewhat different in other friction processes due to other surfaces and lubricators being present. The approach and mechanisms might be interesting and useful when trying to understand different friction processes in the human body, for instance friction in blood veins. Concentrations of the most important electrolytes (anions and cations) in the human body are known to change during many diseases.

7.3.2. Minimisation of ski base sliding friction

To minimise friction between snow and ski when the frictional sliding situation in an area under the ski at a given time is on the left side of the minimum point of the graph in Fig. 2.10, i.e. dry friction area, the following aspects must be taken care of at the same time by means of structure, base, skier weight distribution given by the tension of the ski and glide product used on the ski:

- Creation of water film and increase of water film thickness under the ski in order to optimise the film parameter Λ given by Eq. (2.20) according to Fig. 2.10.
- Optimisation of structure roughness along the ski in order to optimise the film parameter Λ given by Eq. (2.20) according to Fig. 2.10.
- Minimisation of the electric fields and the potential differences between the ski and snow and water film, and minimisation of the electrostatic pressures in the contact points between the ski base and water film or snow, and in the air gaps between the ski base and water film or snow.
- Minimisation of macroscopic (mainly given by tension) and microscopic (mainly given by structure) impact and compaction resistances on the ski by optimisation of ski base bearing area.

To minimise friction between snow and ski when the frictional sliding situation in an area under the ski at a given time is on the right side of the minimum point of the graph in Fig. 2.10, i.e. wet friction area, the following aspects must be taken care of at the same time by means of structure, base, skier weight distribution given by the tension of the ski and the glide product used on the ski:

- Dilution of water film and decrease of water film thickness under the ski in order to optimise the film parameter Λ given by Eq. (2.20) according to Fig. 2.10.
- Optimisation of structure roughness along the ski in order to optimise the film parameter Λ given by Eq. (2.20) according to Fig. 2.10.
- Minimisation of the electric fields and the potential differences between the ski and snow and water film, and minimisation of the electrostatic pressures (capillary forces) in the contact points between the ski base and water film or snow, and in the air gaps between the ski base and water film or snow.
- Minimisation of macroscopic (mainly given by tension) and microscopic (mainly given by structure) impact and compaction resistances on the ski by optimisation of ski base bearing area.

The snow grain size has great impact on the frictional interface between snow and ski both at low and high snow hardness. The bearing or pressure areas and typical groove widths of the ski base structure are highly decisive for whether snow grains fill up the structure grooves or not when the snow hardness is low. Using structures with relatively sharp grooves with small widths can be favourable under such conditions, increasing the air gaps in non-contact areas at the same time as the total electrostatic contact area between ski base structure and snow or water film is decreased compared to a plane ski. The widths and depths of the grooves have to be optimised according to snow grain size, structure bearing area and lubrication under the ski. Relatively fine, so-called "sharp" structures were

highly appreciated by several Norwegian Olympic gold medal winners under new-fallen snow conditions during the 1998 Olympics in Japan. Further explanation and exploration of ski base sliding friction and structure is given in Chapter 6.

7.3.3. Epilogue

This section has been quite speculative due to the referred mechanisms not being fully understood nor examined at present. Colbeck (1995) stated in the introduction of the discussion of his observations that explanation of even laboratory experiments tend to be speculative in terms of known charging mechanisms. In spite of this the author has tried to describe interesting aspects and mechanisms using present available knowledge and personal experiences. The entire goal and motive for doing this has been that it might increase and evolve future understanding of the science of friction. Excuses is given in advance to future readers for possible erroneous suggestions and conclusions made in this text.

7.4. References

- Brimblecombe, P., S. L. Clegg, T. D. Davies, D. Shooter and M. Tranter (1987): Observations of the preferential loss of major ions from melting snow and laboratory ice. *Water Resources Research*, Vol. 21, pp. 1279-1286.
- Bullemer, B. and N. Riehl (1966): Bulk and surface conductivity of ice. *Solid State Com.*, Vol. 4, pp. 447-448.
- Camplin, G. C. and J. W. Glen (1973): The dielectric properties of HF-doped single crystals of ice. In *Physics and Chemistry of Ice* (E. Whalley, S. J. Jones and L. W. Gold, Ed.). Ottawa: Royal Society of Canada, pp. 256-261.
- Camplin, G. C., J. W. Glen and J. G. Paren (1978): Theoretical models for interpreting the dielectric behaviour of HF-doped ice. *Journal of Glaciology*, Vol. 21, No. 85, pp. 123-141.
- Colbeck, S. C. (1995): Electrical charging of skis gliding on snow. *Medicine and Science in Sports and Exercise*, Vol. 27, No. 1, pp. 136-141.
- CRC (1978): *CRC handbook of chemistry and physics* 58th edition, CRC Press, Cleveland, Ohio.
- CRC (1997): *CRC handbook of chemistry and physics* 78th edition 1997-1998, D. R. Lide (Editor-in-Chief), CRC Press, Boca Raton, New York, pp. 6-13, 6-139-6-187 and 13-12.
- Davidson, C. I., M. H. Bergin and H. D. Kuhns (1996): Atmospheric deposition of chemical species to polar snow. *Chemical Engineering Communications*, Vol. 151, pp. 227-249.
- Davis, R. E., C. E. Petersen and R. C. Bales (1995): Ion flux through a shallow snowpack: effects of initial conditions and melt sequences. In *Proceedings of the International Symposium on Biogeochemistry of Seasonally Snow-covered Catchments, Boulder, Colorado, July 1-14, 1995*, IAHS Publication No.228, pp. 115-126.
- Haltenorth, H. and J. Klinger (1969): Diffusion on hydrogen fluoride in ice. In *Physics of Ice* (N. Riehl, B. Bullemer and H. Engelhardt, Ed.). New York: Plenum Press, pp. 579.
- Hamrock, B.J. (1994): *Fundamentals of fluid film lubrication*. McGraw-Hill, New York, 690 p.

- Hewitt, A. D., J. H. Cragin and S. C. Colbeck (1989): Does snow have ion chromatographic properties? In Proceedings of the Forty-Sixth Annual Eastern Snow Conference, June 8-9, Quebec City, Quebec, pp. 165-171.
- Hewitt, A. D., J. H. Cragin and S. C. Colbeck (1991): Effect of crystal metamorphosis on the elution of chemical species. In *Proceedings of the Eastern Snow Conference*, pp. 1-10.
- Hewitt, A. D. and J. H. Cragin (1994): Determination of anion concentrations in individual snow crystals and snowflakes. *Atmospheric environment*, Vol. 28, No. 15, pp. 2545-2547.
- Hubman, M. (1979a): Polarization processes in the ice lattice, Part I. *Z. Physik B*, Vol. 32, pp. 127-139.
- Hubman, M. (1979b): Polarization processes in the ice lattice, Part II. *Z. Physik B*, Vol. 32, pp. 141-146.
- Jaccard, C. (1959): Étude théorique et expérimentale des propriétés électriques de la glace. *Helvetica Physica Acta*, Vol. 32, pp. 89-128.
- Jaccard, C. (1964): Thermodynamics of irreversible processes applied to ice. *Physik der Kondensierten Materie*, Vol. 3, pp. 99-118.
- Johari, G. P. and E. Whalley (1981): The dielectric properties of ice in the range 272-133 K. *Journal of chemical physics*, Vol. 75, 1333-1340.
- Junge, C. E. (1963): *Air chemistry and radioactivity*. Academic Press, New York, 382 p.
- Kopp, M. (1962): Conductivité électrique de la neige, au courant continu. *Z. Math. Phys.*, Vol. 13 (In French), pp. 431-441.
- Kumai, M. and K. E. Francis (1962): Nuclei in snow and ice crystals on the Greenland ice sheet under natural and artificially simulated conditions. *Journal of the atmospheric sciences*, Vol. 19, No. 6, pp. 474-481.
- Malmberg, C. G. and A. A. Maryott (1956): Dielectric constant of water from 0° to 100°. *Journal of Research of the National Bureau of Standards*, Vol. 56, pp. 1-8.
- Petrenko, V. F. and V. A. Chesnakov (1990): On a nature of charge carriers in ice. *Soviet Physics-Solid State*, Vol. 32, pp. 2368-2373.
- Petrenko, V. F. and E. M. Schulson (1992): Action of electric-fields on the plastic-deformation of pure and doped ice single-crystals. *Philosophical Magazine A*, Vol. 67, pp. 173-185.
- Petrenko, V. F. (1993): *Electric properties of ice*. Monograph, USA CRREL Special Report 1993-20, 80 p.
- Petrenko, V. F. (1994): The effect of static electric fields on ice friction. *Journal of Applied Physics*, Vol. 76, No. 2, pp. 1216-1219.
- Petrenko, V. F. and S. C. Colbeck (1995): Generation of electric fields by ice and snow friction. *Journal of Applied Physics*, Vol. 77, No. 9, pp. 4518-4521.
- Reimann, C., H. Niskavaara, P. de Caritat, T. E. Finne, M. Äyräs and V. Chekushin (1996): Regional variation of snowpack chemistry in the vicinity of Nikel and Zapoljarnij, Russia, northern Finland and Norway. *The Science of the total environment*, Vol. 182, No. 1-3, pp. 147-158.
- Scheiner, S. and J. Nagle (1983): Ab initio molecular orbital estimates of charge partitioning between Bjerrum and ionic defects in ice. *Journal of Physical Chemistry*, Vol. 87, pp. 4267-4272.
- Steinemann, S. (1957): Dielektrische Eigenschaften von Eiskristallen. *Helvetica Physica Acta*, Vol. 30, pp. 581-610.
- SWIX (1996): *Alpine ski preparation tech manual*, PR 952 N, SWIX SPORT, Lillehammer, Norway, 38 p.

- Tranter, M., P. Brimblecombe, T. D. Davies, C. E. Vincent, P. W. Abrahams and I. Blackwood (1986): The composition of snowfall, snowpack, and meltwater in the Scottish Highlands evidence for preferential elution. *Atmospheric Environment*, Vol. 20, pp. 517-525.
- Van Pelt, T. P. and E. H. Knol (1983): *Elektriciteitsleer 1*, B. V. Uitgeverij Nijgh & Van Ditmar, The Hague, The Netherlands (in Dutch), 220 p.
- Wathne, B. M., S. Patrick and N. Cameron (1997): AL:PE Acidification of mountain lakes: Palaeolimnology and Ecology. *Remote Mountain Lakes as Indicators of Air Pollution and Climate Change*. Norwegian Institute for Water Research, Norway, Report No. 3638-97, 213 p/10 app.

8. Summary, conclusions and recommendations for further work

8.1. Summary and conclusions

Basics of ski base sliding friction

The first part of this theoretical framework describes briefly the friction against a moving skier on the basis of air resistance and ski base sliding friction. The second extensive part emphasises ski base sliding friction and presents the most important ski and snow parameters for ski base sliding friction. Moreover, ski base sliding friction is discussed and explained by use of tribology, and impact and compaction resistances. The major conclusions are:

- The optimum ski base structure roughness varies under different snow conditions according to the generated frictional water film thickness under the ski and the roughness of the snow surface. Thick water films correspond to coarse ski base structures, while it is advantageous to use finer ski base structures and increase the water film thickness when the water film is thin.
- Possible increase of water film thickness along the ski implies an increase of the ski base structure roughness along the ski.
- Measurement of snow humidity can be viewed as an indicator of the initial water film thickness in the ski track and the frictional water film thickness that is possible to attain during skiing.
- Impact and compaction resistances are important when the snow hardness is below a certain limit, and when the water film thickness is low relative to the roughness of the ski base structure and the snow surface.

The ski base structure analyser (SSA) and ski base structure measurements

A Ski base Structure Analyser (SSA) utilising laser technology has been developed to analyse the detailed structure of a stone-ground ski base. The SSA displays the measured surface as an image with 739×570 pixels, where each pixel can have a grey level value from 0 to 255. The value of each pixel is proportional to the height at the corresponding point of the measured surface. Various roughness parameters can be calculated from the measured surface image in order to characterise the surface topography. In the period between 1995 and 1998 almost 1700 ski base structure measurements were performed on more than 350 skis. The major findings from these measurements are as follows:

- Ski pairs ground with the "same" structure at two different times are not necessarily equal if no quality control of the ski base structure and the stone grinding process has been performed.
- Ski base structure roughness can be divided into four categories: fine (arithmetic mean roughness 1-4 μm), medium (arithmetic mean roughness 4-7 μm), coarse (arithmetic mean roughness 7-10 μm) and very coarse (arithmetic mean roughness higher than 10 μm) that correspond to dry to moist, moist, moist to wet, and wet to very wet snow conditions, respectively.
- Higher structure roughness on the forebody than the afterbody of the ski (up to 84 %) has been revealed on several competition ski pairs and led to adjustment and regrinding of the ski pairs in order to attain constant or increased structure roughness along the ski.
- The assumption made by earlier investigators that the sliding friction coefficient remains constant in the range of bump heights from 10 to 30 μm is not valid.
- Properly plane ground test skis have shown up to 3 % higher sliding speeds than non-plane test skis with similar structure roughness under snow conditions with snow temperatures below zero.

The work has resulted in development of ski base structures with increased roughness along the ski, development and extreme optimisation of the best structures and improvement of the grinding diamonds used to set the grinding stone. Further, it has given ski technicians and competition skiers confidence that optimum structures and skis are used in competitions under different snow and weather conditions, and that the best structures can be reproduced.

Characterisation of snow structure in a cross-country race ski track

Various snow parameters have been registered during measurement campaigns in ski tracks in Norway (1995-98), Hakuba/Japan (1996-98) and Sundance/USA (1999). Specific attention has been paid to snow hardness, snow humidity, snow density, snow grain structure and electrolytic conductivity. The major results from this work are as follows:

- Snow hardness between 10^4 and 10^6 Pa is most common in ski tracks, and snow hardness below 10^5 Pa is likely to be present 60 % of the time. Ski tracks tend to have lower mean snow hardness when the snow humidity is above 5 %. The minimum snow hardness tends to increase with decreasing snow temperature. The average snow hardness for new snow types has been approximately three times higher in classic ski tracks than in skating ski tracks.

- The mean density of snow in ski tracks (0.50 g/cm^3) is considerably higher than typical densities of seasonal snow covers ($0.26\text{-}0.38 \text{ g/cm}^3$) and higher for transformed snow types ($0.51\text{-}0.59 \text{ g/cm}^3$) than new snow types ($0.39\text{-}0.43 \text{ g/cm}^3$).
- The snow humidity in a ski track typically ranges between 0 and 12.5 %. It is typically less than 2 % for snow temperatures below -2°C and less than 1 % for snow temperatures below -7°C . Snow humidities exceeding 4 % have only been registered at air temperatures above $+1^\circ\text{C}$.
- The mean snow grain diameter and the standard deviation of snow grain diameters have been calculated for 34 snow surface microscope images of ski tracks. The typical grain size has ranged from 0.26 to 2.59 mm for transformed snow types and from 0.08 to 0.38 mm for new snow types. In-situ microscope imaging of ski tracks is very difficult for new snow types with snow surface grains below 0.2 mm.
- The electrolytic conductivity increases and the grain size decreases when precipitation is introduced to the snow surface. The electrolytic conductivity can also increase with snow density. As the snow goes through melt-freeze cycles, the electrolytic conductivity decreases and the grain size increases. The electrical conductivity of snow is several orders of magnitude less than the electrolytic conductivity of melted snow samples, but follows similar trends with respect to snow metamorphosis and snow density.
- In melted snow samples from Trondheim and Sundance/Heber high electrolytic conductivities ($61.7 \text{ }\mu\text{S/cm}$ and $94.5 \text{ }\mu\text{S/cm}$, respectively) and high levels of Na^+ - and Cl^- -ions have been registered due to salt being a major agent during snow nucleation in the snowfalls. These values are approximately 3 times higher than the maximum values found for snow samples from Hakuba ($21.9 \text{ }\mu\text{S/cm}$). Artificial snow has given the highest measured electrical conductivity value to present ($169.7 \text{ }\mu\text{S/cm}$).

Searching for the optimum cross-country ski base structure

A structure test series consisting of ten ski pairs with eight different structures has been ground and quality-controlled. Accurate sliding tests have been executed with the series in order to test different hypotheses for low ski base sliding friction and ski base structure. This is the first time a proper examination has been performed on the effect of structure roughness on ski base sliding friction. The major results of the work are as follows:

- The optimum ski base structure roughness of the best structures and ski pairs increased with snow humidity, thus indicating that the optimum ski base structure roughness increases with the water film thickness. Ski pairs with arithmetic mean structure roughness $\leq 5.4 \text{ }\mu\text{m}$ were best under snow conditions with snow humidity $\leq 0.6 \text{ }\%$, snow temperatures below zero and new snow. A ski pair with arithmetic mean structure roughness equal to $9.3 \text{ }\mu\text{m}$ was best under snow conditions with snow humidity between approximately 0.3 and 4.0 %, snow hardness higher than $4.1 \times 10^4 \text{ Pa}$ and transformed snow types. Under snow conditions with snow humidity higher than approximately 4 %, a structure with arithmetic mean roughness $12.7 \text{ }\mu\text{m}$ was best.

- Coarser structures were relatively better than finer structures at high speeds compared to low speeds, thus implying an increase in the water film thickness and optimum structure roughness with speed.
- Decrease of the structure roughness along the ski was unfortunate under most snow conditions. The effect of increasing the structure roughness along the ski relative to having constant structure roughness is difficult to interpret at present.

The effect of electrical charging and electrostatic pressure on ski base sliding friction

This part of the study discusses the effect of electrical charging and electrostatic pressures on ski base sliding friction. A present interpretation of friction is suggested combining knowledge of tribology, electrical charging and electrostatic pressures. The major conclusions are as follows:

- The dry friction process is dominated and characterised electrically by accumulation of electrostatic charges in the ski base contact points. The frictional water film initiates discharge of potential differences between ski and snow due to the much higher electrical conductivity of water relative to snow.
- When the air gap volumes between the water film and the ski base structure, and the water film and the snow surface get small, the electrostatic pressures in the air gaps increase, and suction or drag may start occurring. The wet friction process is characterised electrically by electrolytic behaviour.
- The ski base structure topography and the snow surface topography is decisive for the electrical contact configuration between ski and snow.
- The electrolytic conductivity of a melted snow sample may indicate the rate of ions introduced to the interface between snow and ski by frictional melting and thereby the rate and ease of discharge between ski and snow through the frictional water film during skiing. Given otherwise equal snow conditions and frictional situations, sliders on highly electrical conductive snow should discharge easier than sliders on snow with lower electrical conductivity. Larger frictional electrification should take place on snow with low electrical conductivity compared to snow with high electrical conductivity.

In addition, a summary is given of the processes that must be accounted for in order to minimise the ski base sliding friction in different friction regimes.

8.2. Recommendations for further work

Many aspects seem interesting and promising to extend the present work. Future research is needed on topics such as the effect of:

- Structure pressure contact area during skiing
- Structure capillary contact area during skiing under wet snow conditions
- Structure carving area during skiing under hard and dry snow conditions
- Structure bearing area during skiing under soft snow conditions
- Structure pattern on dilution of water film during skiing
- Structure pattern on minimising attachment of dirt during skiing
- Glide wax/powder, kick wax and base material on electrical charging during skiing
- The pressure distribution of the ski on ski base sliding friction
- Electrolytic conductivity of snow on ski base sliding friction and electrical charging during skiing

It would be informative for the interpretation of friction to perform simultaneous measurements of water film thickness and electrical charging along the ski during sliding tests of ski base structure and glide wax/powder. Accurate measurement and characterisation of ski base structure and snow parameters are important in that respect. Further research is also necessary in order to increase the knowledge of the simultaneous processes of mass, impulse, energy, electrical and chemical balances between the two interacting surfaces in relative motion during friction.

The friction mechanisms cited and described in this thesis can also be exploited to increase the understanding of other microtribological processes. Interesting topics for further research are for instance friction between car tires and snow or ice, and friction in blood veins.

**DEPARTMENT OF STRUCTURAL ENGINEERING
NORWEGIAN UNIVERSITY OF SCIENCE AND TECHNOLOGY**

N-7491 TRONDHEIM, NORWAY
Telephone: +47 73 59 47 00 Telefax: +47 73 59 47 01

"Techniques for Static and Dynamic Solution for Nonlinear Finite Element Problems",
E. Mollestad - 1983, ISBN 82-90240-14-7.

"Flow-related Aspects of Hazard Area Prediction Following an Accidental Gas Release",
K. J. Eidsvik - 1983.

"Resonant Behaviour of Taut Cables Subjected to Deterministic and Stochastic Excitations",
T. Kjøberg - 1983.

"Sand Waves in Free Surface Flow. A Study with Emphasis on Hydrodynamic Aspects",
H. Moshagen - 1984.

"Free Span Vibrations of Submarine Pipelines in Steady and Wave Flows",
A. N. Mysore - 1985.

"An Experimental Study on Steel Column Behaviour at Elevated Temperatures",
B. Aasen - 1985.

"Nonlinear Analysis of Reinforced Concrete Structures Using Beam and Membrane Elements",
O. Strøm - 1986, ISBN 82-90240-15-5.

"The Free Formulation for Nonlinear Finite Elements with Applications to Shells",
M. K. Nygård - 1986, ISBN 82-90240-16-3.

"Hydrodynamic Force Coefficients in Random Wave Conditions",
T. Bostrøm - 1987.

"A Model for Oscillatory Turbulent Boundary Layers with Suspended Sediment",
K. Hagatun - 1987.

"Implementation of Tubular Joint Flexibility in Global Frame Analysis",
T. Holmås - 1987, ISBN 82-90240-17-1.

"Elasto-Plastic Material Models in the Nonlinear Finite Element Method",
K. E. Moen - 1987, ISBN 82-90240-19-8.

"Current Induced Vibrations and Scour of Pipeline on a Sandy Bottom",
Ø. Kristiansen, 1988:7, ISBN 82-7119-022-9.

"On the Dynamic Analysis of Large Floating Structures",
T. Lokna, 1988:21, ISBN 82-7119-038-5.

"Cyclic Plasticity Modelling in Force Space",
O. C. Astrup, 1988:23, ISBN 82-7119-040-7.

"Dropped Objects. Plugging Capacity of Steel Plates",
M. Langseth, 1988:25, ISBN 82-7119-042-3.

"Cyclic Plasticity and low Cycle Fatigue of Structural Steel and Buttwelded Components",
B. Skallerud, 1988:26, ISBN 82-7119-043-1.

"Nonlinear Static and Dynamic Analysis of Slender Structures Subjected to Hydrodynamic Loading",
H. T. Hansen, 1988:40, ISBN 82-7119-059-8.

"Pseudo-Dynamic Testing. Experimental Accuracy and Techniques",
K. A. Malo, 1988:56, ISBN 82-7119-077-6.

"The Pseudodynamic Test Method. Numerical Algorithms and Implementation",
E. Eberg, 1989:1, ISBN 82-7119-081-4.

"Wave and Current Forces on Pipelines at the Sea-bed",
O. A. Grytå, 1989:5, ISBN 82-7119-085-7.

"Passive Fire Protection subjected to Gas Explosion and Fire Loads",
T. A. Håverstad, 1989:24, ISBN 82-7119-106-3.

"Current Induced Vibrations of a Flexible Cylinder",
Zhi-Jie Wu, 1989:34, ISBN 82-7119-085-7.

"Dynamic Behaviour of Riser Systems Exposed to Internal Fluid Flow - An Analytical Approach",
K. C. Strømsem, 1989:55, ISBN 82-7119-141-1.

"Reliability Analysis of Structural Systems using Nonlinear Finite Element Methods",
C. A. Holm, 1990:23, ISBN 82-7119-178-0.

"Uniform Stratified Flow Interaction with a Submerged Horizontal Cylinder",
Ø. Arntsen, 1990:32, ISBN 82-7119-188-8.

"Large Displacement Analysis of Flexible and Rigid Systems Considering Displacement-Dependent Loads and Nonlinear Constraints",
K. M. Mathisen, 1990:33, ISBN 82-7119-189-6.

"Solid Mechanics and Material Models including Large Deformations",
E. Levold, 1990:56, ISBN 82-7119-214-0, ISSN 0802-3271.

"Inelastic Deformation Capacity of Flexurally-Loaded Aluminium Alloy Structures",
T. Welø, 1990:62, ISBN 82-7119-220-5, ISSN 0802-3271.

"Visualization of Results from Mechanical Engineering Analysis",
K. Aamnes, 1990:63, ISBN 82-7119-221-3, ISSN 0802-3271.

"Object-Oriented Product Modeling for Structural Design",
S. I. Dale, 1991:6, ISBN 82-7119-258-2, ISSN 0802-3271.

"Parallel Techniques for Solving Finite Element Problems on Transputer Networks",
T. H. Hansen, 1991:19, ISBN 82-7119-273-6, ISSN 0802-3271.

"Statistical Description and Estimation of Ocean Drift Ice Environments",
R. Korsnes, 1991:24, ISBN 82-7119-278-7, ISSN 0802-3271.

"Turbidity Current Modelling",
B. Brørs, 1991:38, ISBN 82-7119-293-0, ISSN 0802-3271.

"Zero-Slump Concrete: Rheology, Degree of Compaction and Strength. Effects of Fillers as Part Cement-
Replacement",
C. Sørensen, 1992:8, ISBN 82-7119-357-0, ISSN 0802-3271.

"Nonlinear Analysis of Reinforced Concrete Structures Exposed to Transient Loading",
K. V. Høiseth, 1992:15, ISBN 82-7119-364-3, ISSN 0802-3271.

"Finite Element Formulations and Solution Algorithms for Buckling and Collapse Analysis of Thin Shells",
R. O. Bjærum, 1992:30, ISBN 82-7119-380-5, ISSN 0802-3271.

"Response Statistics of Nonlinear Dynamic Systems",
J. M. Johnsen, 1992:42, ISBN 82-7119-393-7, ISSN 0802-3271.

"Digital Models in Engineering. A Study on why and how engineers build and operate digital models for decision support",
J. Høyte, 1992:75, ISBN 82-7119-429-1, ISSN 0802-3271.

"Sparse Solution of Finite Element Equations",
A. C. Damhaug, 1992:76, ISBN 82-7119-430-5, ISSN 0802-3271.

"Some Aspects of Floating Ice Related to Sea Surface Operations in the Barents Sea",
S. Løset, 1992:95, ISBN 82-7119-452-6, ISSN 0802-3271.

"Modelling of Cyclic Plasticity with Application to Steel and Aluminium Structures",
O. S. Hopperstad, 1993:7, ISBN 82-7119-461-5, ISSN 0802-3271.

"The Free Formulation: Linear Theory and Extensions with Applications to Tetrahedral Elements with Rotational Freedoms",
G. Skeie, 1993:17, ISBN 82-7119-472-0, ISSN 0802-3271.

"Høyfast betongs motstand mot piggdekkslitasje. Analyse av resultater fra prøving i Veisliter'n",
T. Tveter, 1993:62, ISBN 82-7119-522-0, ISSN 0802-3271.

"A Nonlinear Finite Element Based on Free Formulation Theory for Analysis of Sandwich Structures",
O. Aamlid, 1993:72, ISBN 82-7119-534-4, ISSN 0802-3271.

"The Effect of Curing Temperature and Silica Fume on Chloride Migration and Pore Structure of High Strength Concrete",
C. J. Hauck, 1993:90, ISBN 82-7119-553-0, ISSN 0802-3271.

"Failure of Concrete under Compressive Strain Gradients",
G. Markeset, 1993:110, ISBN 82-7119-575-1, ISSN 0802-3271.

"An experimental study of internal tidal amphidromes in Vestfjorden",
J. H. Nilsen, 1994:39, ISBN 82-7119-640-5, ISSN 0802-3271.

"Structural analysis of oil wells with emphasis on conductor design",
H. Larsen, 1994:46, ISBN 82-7119-648-0, ISSN 0802-3271.

"Adaptive methods for non-linear finite element analysis of shell structures",
K. M. Okstad, 1994:66, ISBN 82-7119-670-7, ISSN 0802-3271.

"On constitutive modelling in nonlinear analysis of concrete structures",
O. Fyrilev, 1994:115, ISBN 82-7119-725-8, ISSN 0802-3271.

"Fluctuating wind load and response of a line-like engineering structure with emphasis on motion-induced wind forces",
J. Bogunovic Jakobsen, 1995:62, ISBN 82-7119-809-2, ISSN 0802-3271.

"An experimental study of beam-columns subjected to combined torsion, bending and axial actions",
A. Aalberg, 1995:66, ISBN 82-7119-813-0, ISSN 0802-3271.

"Scaling and cracking in unsealed freeze/thaw testing of Portland cement and silica fume concretes",
S. Jacobsen, 1995:101, ISBN 82-7119-851-3, ISSN 0802-3271.

"Damping of water waves by submerged vegetation. A case study of laminaria hyperborea",
A. M. Dubi, 1995:108, ISBN 82-7119-859-9, ISSN 0802-3271.

"The dynamics of a slope current in the Barents Sea",
Sheng Li, 1995:109, ISBN 82-7119-860-2, ISSN 0802-3271.

"Modellering av delmaterialenes betydning for betongens konsistens",
Ernst Mørtsell, 1996:12, ISBN 82-7119-894-7, ISSN 0802-3271.

"Bending of thin-walled aluminium extrusions",
Birgit Sjøvik Opheim, 1996:60, ISBN 82-7119-947-1, ISSN 0802-3271.

"Material modelling of aluminium for crashworthiness analysis",
Torodd Berstad, 1996:89, ISBN 82-7119-980-3, ISSN 0802-3271.

"Estimation of structural parameters from response measurements on submerged floating tunnels",
Rolf Magne Larssen, 1996:119, ISBN 82-471-0014-2, ISSN 0802-3271.

"Numerical modelling of plain and reinforced concrete by damage mechanics",
Mario A. Polanco-Loria, 1997:20, ISBN 82-471-0049-5, ISSN 0802-3271.

"Nonlinear random vibrations - numerical analysis by path integration methods",
Vibeke Moe, 1997:26, ISBN 82-471-0056-8, ISSN 0802-3271.

"Numerical prediction of vortex-induced vibration by the finite element method",
Joar Martin Dalheim, 1997:63, ISBN 82-471-0096-7, ISSN 0802-3271.

"Time domain calculations of buffeting response for wind sensitive structures",
Ketil Aas-Jakobsen, 1997:148, ISBN 82-471-0189-0, ISSN 0802-3271

"Estimation of chloride penetration into concrete bridges in coastal areas",
Per Egil Steen, 1998:89, ISBN 82-471-0290-0, ISSN 0802-3271.

"Stress-resultant material models for reinforced concrete plates and shells",
Jan Arve Øverli, 1998:95, ISBN 82-471-0297-8, ISSN 0802-3271.

"Chloride binding in concrete. Effect of surrounding environment and concrete composition",
Claus Kenneth Larsen, 1998:101, ISBN 82-471-0337-0, ISSN 0802-3271.

"Rotational capacity of aluminium alloy beams",
Lars A. Moen, 1999:1, ISBN 82-471-0365-6, ISSN 0802-3271.

"Stretch Bending of Aluminium Extrusions",
Arild H. Clausen, 1999:29, ISBN 82-471-0396-6, ISSN 0802-3271.

"Aluminium and Steel Beams under Concentrated Loading",
Tore Tryland, 1999:30, ISBN 82-471-0397-4, ISSN 0802-3271.

"Engineering Models of Elastoplasticity and Fracture for Aluminium Alloys",
Odd-Geir Lademo, 1999:39, ISBN 82-471-0406-7, ISSN 0802-3271.

"Kapasitet og duktilitet av dybelforbindelser i trekonstruksjoner",
Jan Siem, 1999-46, ISBN 82-471-0414-8, ISSN 0802-3271.

“Etablering av distribuert ingeniørarbeid; Teknologiske og organisatoriske erfaringer fra en norsk ingeniørbedrift”, Lars Line, 1999:52, ISBN 82-471-0420-2, ISSN 0802-3271.

“Estimation of Earthquake-Induced Response”, Símon Ólafsson, 1999:73, ISBN 82-471-0443-1, ISSN 0802-3271.

“Coastal Concrete Bridges: Moisture State, Chloride Permeability and Aging Effects”
Ragnhild Holen Relling, 1999:74, ISBN 82-471-0445-8, ISSN 0802-3271.

“Validation of Numerical Collapse Behaviour of Thin-Walled Corrugated Panels”, Håvar Iltad, 1999:101, ISBN 82-471-0474-1, ISSN 0802-3271.

“Strength and Ductility of Welded Structures in Aluminium Alloys”, Mirosław Matusiak, 1999:113, ISBN 82-471-0487-3, ISSN 0802-3271.

“Thermal Dilation and Autogenous Deformation as Driving Forces to Self-Induced Stresses in High Performance Concrete”, Øyvind Bjøntegaard, 1999:121, ISBN 82-7984-002-8, ISSN 0802-3271.

“Some Aspects of Ski Base Sliding Friction and Ski Base Structure”, Dag Anders Moldestad, 1999:137, ISBN 82-7984-019-2, ISSN 0802-3271.